Thesis

Ultrafast processes in N_2 photoionization: implementation of the XCHEM code

Presented for a doctor in Quantum Chemistry and Computational Modelling

Author:
Markus Klinker
Supervisors:
Jesús González Vázquez
Fernando Martín García

June 2017

Abstract

This project studies the ultrafast photoionization (dissociative and non-dissociative) of molecular Nitrogen from a theoretical and computational point of view. Specifically, we present the implementation of the XCHEM approach; a set of tools which allows the study, including electronic correlation, of photoionization going beyond simple benchmark systems. In particular we focussed on the successful description of autoionizing states; quasi-boundstates (coupled to continuum states) with a finite life time after which the system ionizes. Molecular Hydrogen was studied as a simple test case, allowing for comparison with results from well established methods. Subsequently the photoionization of molecular Nitrogen was studied in between the first and third ionization threshold, i.e. where dissociation does not play a role. This is an important step establishing the XCHEM method's capability to handle complex multielectronic molecular systems.

From a mathematical point of view the XCHEM method relies on a close coupling expansion of the electronic wavefunction, which is fitted to the asymptotic behaviour seen in a Coulomb potential. The (ionic) scattering states are expanded in a novel hybrid Gaussian/B-Spline (GABS) basis set, whereas the (neutral) bound states are calculated using modified Quantum Chemistry Packages (QCP). As part of the development of this approach, this work focussed on the creation of original programs to be used in combination with modified and redesigned QCPs, allowing them to interface with the part of the XCHEM code dealing with scattering theory and involving GABS basis functions.

The dissociatiove photoionization of molecular Nitrogen was also studied in collaboration with experimental efforts. In this experiment, Nitrogen was ionized using a single attosecond XUV pump pules and the subsequent dissociation dynamics was probed by a femtosecond IR pules (XUV pump/IR probe). The dependence of the kinetic energy of the fragments was recorded as a function of the delay between the pulses, giving rise to a clearly visible interference pattern. A theoretical description of this experiment, including large numbers of potential energy surfaces and taking into account non-adiabatic couplings, is proposed in this thesis and used to reproduce these results. From this model an interpretation of the observed experimental features is extracted.

Resumen

Este proyecto investiga desde punto de vista teórico y computacional la foto ionización (disociativa y no disociativa) ultra rápida de la molécula de Nitrógeno. Para simularla, presentamos la implementación del método XCHEM : un conjunto de herramientas que permite estudiar la foto ionización de sistemas complejos teniendo en cuenta correlación electrónica. En concreto, nos centramos en la descripción de estados que experimentan autoionización: estados casi ligados acoplados con estados del continuo. Dado que estos estados están inmersos en el continuo, acaban decayendo a estados del catión. Como primer sistema, hemos estudiado la molécula de Hidrógeno lo que nos ha permitido comparar con resultados

obtenidos con otros métodos. Posteriormente hemos estudiado la foto ionización de la molécula de Nitrógeno entre el primer y el tercer umbral de ionización. Eso constituye un paso importante, ya que establece la capacidad del método XCHEM para describir sistemas complejos en moléculas poli-electrónicas.

Desde el punto de vista matemático el método XCHEM esta basado en una expansión close coupling, de la función de onda electrónica, que esta ajustada para describir el comportamiento asintótico observado en un potencial culombiano. Los estados del continuo (iónicos) se expanden en un nuevo conjunto de funciones de base que incluye una mezcla de funciones gausianas y B-Splines (GABS). Por otra parte, los estados ligados (neutros) se calculan con programas modificadas de estructura electrónica (QCP). Como parte del desarrollo de este método, en este trabajo se han programado una serie de programas originales que, en combinación con QCPs modificados y rediseñados al efecto, permiten construir un interfaz entre estados ligados y estados del continuo.

La foto ionización disociativa de la molécula de Nitrógeno se ha estudiado en colaboración con un grupo experimental. En el experimento, se empleó un pulso XUV de attosegundo para ionizar la molécula de Nitrógeno y la dinámica del proceso de disociación, provocada por este pulso, se siguió con un pulso IR de femtosegundos a través de un esquema bombeo-sonda. Se midió la dependencia de la energía cinética de los fragmentos molecular con el retraso entro los dos pulsos, dando lugar a un patrón de interferencia. En esta tesis, describimos este experimento usando un modelo teórico (que incluye cientos de superficies de energía potencial con sus correspondientes acoplamientos no adiabáticos) que es capaz de reproducir los resultados experimentales. Además, profundizando en el modelo hemos sido capaces de entender la naturaleza del patrón de interferencia.

Contents

1 Introduction

With the availability of laser pulses of increasingly short duration over the last few decades [1, 2], chemical processes of an evermore fleeting nature, touching on evermore fundamental concepts have shifted into the realm of what is open to observation, precise measurement and ultimately interpretation and even control. From the experimental side this trend has been driven by a few key innovations leading to technologies opening up entire fields of investigation. Among these, by no means independent, fields are the disciplines of femtochemistry, attochemistry[3] and quantum control[4]. Alongside mile stone breakthroughs, a continuous effort has been and is being undertaken to steadily refine these newly emerging techniques providing hitherto unobtainable precision in the control of ultra short pulses on the one hand, and in the methods used to measure the molecular processes induced by these pulses. It is the theoretical and computational study of these processes that forms the focus of our attention in this work.

Before providing a background on the theoretical aspects of the specific phenomena we set out to study, considering the recent history of the shortest available laser pulses used in the study of chemical processes is a good starting point, as this provides a fundamental limit on the time scale on which chemical processes may take place while still being subject to experimental scrutiny (and therefore warranting falsifiable theoretical curiosity). Furthermore this gives a natural progression to highlighting the ever faster processes whose investigation became possible with the advances in pulses generation. For much of the previous century, mode locked dye lasers provided the the fastest available light sources culminating in the creation of 27 fs pulses[5] and ultimately 6 fs second pulses[6] by means of external compression in 1992. This was not surpassed for a decade to come until the invention of Ti:Sapphire lasers (also in conjunction with external compression) lead to the creation of 3.8 fs pulses[7, 8, 9]. Atoms within a molecule typically move on a femto second time scale during a chemical reaction, and therefore these advances made attainable the study of reaction dynamics. The most notable contribution to femtochemistry was work by Zewail on nuclear reaction dynamics[10, 11] ultimately leading to his being awarded the Noble prize. Besides the application to the study of chemical bond breaking, an additional interesting aspect is the high intensity that may be achieved for femto second pulses, with up to 10^{15} W/cm^2[8, 12] having become available some twenty years ago. At these intensities effects which are associated with high-field lase physics become relevant [1].

For the 3.8 fs generated in a Ti:Sapphire laser, the pulses contain only two optical cycles, thus due to the limitations on the wavelength that can be achieved with a "conventional" Ti:Sapphire laser (650 nm to 1100 nm), a fundamentally different approach is necessary to improve upon few femto second laser pulses. The exploitation of one of the high field processes alluded to in the last paragraph paved the way for the production of sub femto second laser pulses. The process in question is high harmonic generation (HHG) in certain gases upon being subjected to strong laser fields, leading to generation of trains of attosecond pulses[1]. The attosecond pulse generation via HHG has been explained by the very successful Three-Step Model proposed by Corkum[14, 15]. Inherent to HHG generation of attosecond pulses is that the pulse producing process is repeated with every half cycle of the driving field, therefore leading to a train of attosecond pulses. While interesting in their own right, it has since become possible to generate single attosecond pulses, making use of the strong dependency of the efficiency of HHG on the ellipticity of the driving pulse[16, 17]. The generation of attosecond pulses was pioneered by

[1] An alternative means of creating pulses of a similarly ultra short nature is based on Free Electron Lasers [13], but as these are not relevant to this work we omit their discussion

a multiple works improving first on the 3.8 fs limit[18] and later penetrating deep into the attosecond regime[19, 20]. A variety of techniques exist to achieve not only achieve these short pulses, but also extend the parameters controllable in experiment to amplitude and phase. We mention among these the resolution of attosecond beating by interference of two-photon transitions (RABBITT [21, 22, 23]) and attosecond streaking[18, 24, 25]. Using these techniques a high degree of control can be exerted over the profile of attosecond pulses, which in effect means that is has become possible achieve control over electronic motion deep into the subfemto second regime.

In the past few years, this arsenal of atto second technologies has provided very powerful tools for studying and controlling the ultrafast electronic processes occurring in a molecule after sudden removal of an electron by the absorption of high energy photon [26, 27, 28, 29, 30], as these occur on a subfemtosecond time scale. As the electronic density is reponsible for bond formation and bond breaking, attosecond control of electronic motion should ultimately open the possibility to control photo chemical reactions. Photoionization by XUV attosecond pulses produces a coherent superposition of many excited states (due to the expansive bandwidth of several tens of eV for these pulses) of the remaining cation, thus inducing charge oscillations ultimately leading to charge localization on a particular molecular site [31, 32, 33]. By probing the system with a second ultrashort pulse (leading to what is commonly referred to as a pump/probe experiment), one can in principal follow the induced molecular dynamics with attosecond time resolution and potentially extract information of the potential energy surfaces (PES) involved in the process.

From the previous paragraph we infer therefore that two (closely related) processes in particular have sparked considerable interest. On the one hand the removal of an electron upon interaction with a laser pulse: photoionization; and on the other hand the subsequent behaviour of the ionized molecule, which depending on the electronic state of the cationic system, may break apart: photodissociation. The goal of this work is the design of theoretical tools to describe these processes in systems of such complexity, that existing models are incapable of working with. Taking into account the order of the ionization and dissociation event it is natural to consider photo ionization first.

The way in which photoionization takes places may be divided into a host of processes, depending on the precise nature of the way in which an electron ends up being ejected into the continuum. A subset of these processes is presented in figure 1.1, of which the one that is most relevant to this project is auto ionization. A correct description of auto ionization inherently depends on the inclusion of electron correlation to enable a qualitative or quantitative description. As a consequence it has proven to be a considerable theoretical challenge to successfully describe these processes. Autoionization refers to the excitation of an electron to a quasi bound state, which energetically lies above the ionization threshold of the atom or molecule. After some time characteristic to said bound state, the electron may escape into the continuum leaving behind the ionized system. This process competes with a direct ionization of the molecule. It was Fano [34, 35] who realized that it is the interference between these two different quantum paths, ultimately both leading to the removal of an electron from the system, that gives rise to the asymmetric resonance features appearing in the photoionization cross-section (also depicted in figure 1.1) in the vicinity of autoionizing states (experimentally this was well known, but poorly understood at this point). Due to the challenges in describing the interaction of the electron escaping into the continuum and the remaining cationic system, the successful computational reproduction of these Fano profiles has established itself as somewhat of a benchmark in gauging a method's capability of accurately describing photoionzation processes.

The accurate description of auto ionizing states, so far been mostly confined to small atomic system, such as Helium [36, 37, 38], Neon [39] and Argon [40] or diatomic systems with two electrons [41, 42, 43]. These works have been pioneering in the study of photoionization but their success is limited to small systems. The reliable theoretical study of photo ionization for larger systems, has been only possible in a reasonably straightforward way if the electron escapes the system with sufficiently high energy, so that the interaction with the cationic core can be seen as approximately Coulombic (allowing for the electron to be well approximated by Coulomb waves or even plane waves [44]), or if the coupling between autoionizing states and continuum states is disregarded [45]. The principal reasons for the failure of most methods, in going beyond very small systems, has its root the different and conflicting requirements to describe either the electronic wave function of the molecular or cationic bound system or the electron ejected into the continuum.

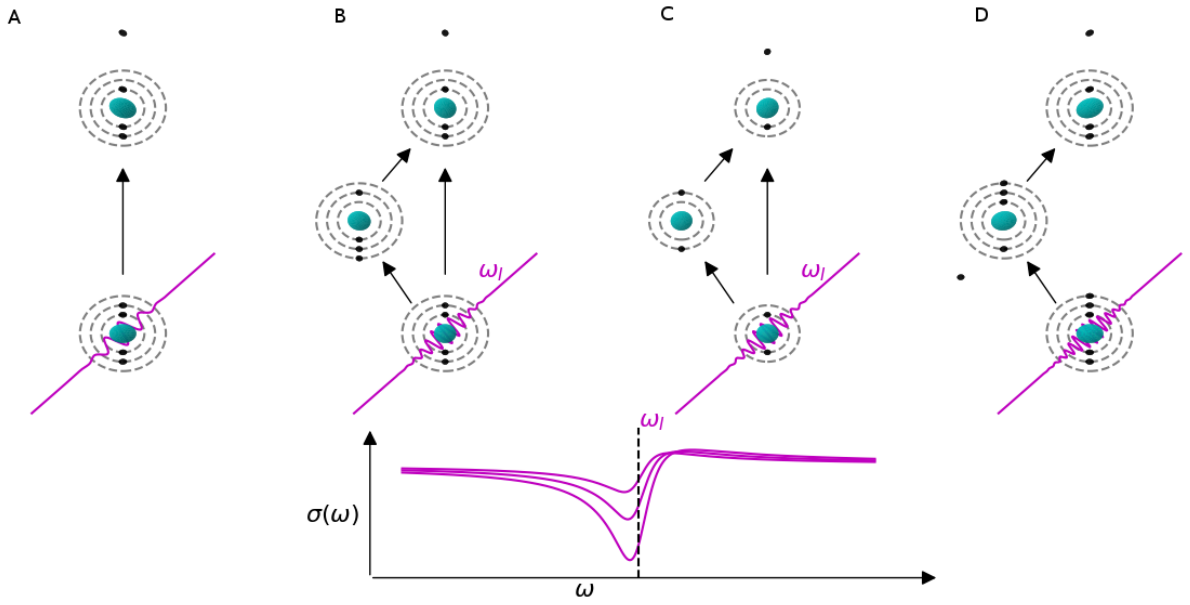

Figure 1.1: Different schematically depicted photo ionization processes. Cyan circles correspond to nuclei, black cicle to electrons; bound if on a dashed circle, unbound if otherwise. A) Ionization by removal of a valence electron B) Autoionization provides an alternative path to the ejection of the electron from the system, by intermediate excitation to an autoionizing state. Here the autoionizing state is a singly excited state achieved by promotion of a non-valence electron C) Equivalent to panel B), with in this instance the autoionizing state being a doubly excited state (all autoionizaing states are of this kind in Helium and molceular Hydrogen) D) Auger decay leading to double ionization via first removing a core electron. Subsequent relaxation ejects another electron, the Auger electron, into the continuum. Processes B) to D) are driven by electron correlation and as such it must be included in any model aimed at capturing any one of these processes. Other processes, not depicted here, include for example shake up processes and resonant X-Ray absorption. For panels B) and C) the lower panel displays sample Fano Resonance features, with their characteristic asymmetric shape, as they are obeserved in the photoionization spectrum in the vicinity of the autoionizing state.

The wave function of the bound system (before and after ionization), for cases going beyond the aforementioned most basic ones, is characterized by a very intricate nature, due to the presence of many electrons interacting with several nuclei as well as with each other and is guaranteed to exponential decay for large radii. Conversely an electron ejected into the continuum requires a good description of scattering states, that do not decay but rather oscillate throughout all space. The difficulties in merging these requirements have stifled the progress in the theoretical description of autoionizing states in even moderately complex systems such as molecular Nitrogen [46].

It should be pointed out that the study of autoionizing states, despite their short lifetimes, does not inherently put one in the real of atto or femtochemistry, and their Fano lineshapes have been seen experimentally since the early 20^{th} century. However the rapid advances in ultra short pulse generation now allow for the investigation of the dynamical behaviour of autoionizing states, manifesting itself in the temporally dependent build up of the Fano resonance, as the time since initiation of the ionization process approaches the characteristic life time of the auto ionizing states. References [47, 48] carried out an investigation of the dynamics of the same autoionizing, doubly excited state $2s2p$ in Helium, giving insight into the attosecond electron dynamics in this system during an ionization process. Experimentally this is achieved using the Atto Second Transient Absorption Spectrum (ATAS) method[49]. From the point of view of theoretical investigation of this process, Helium is, as mentioned before, sufficiently small to allow for an accurate, fully correlated description of this process. If any such time dependent studies are to be extended to larger, molecular systems, a necessary requirement is an equivalent, fully correlated treatment describing the autoionizing state (decaying due to their coupling to scattering states) of these

more complex systems. Once this has been achieved an extension of this to undertake time dependent studies is conceptually a simple step (though considerable computational resources should be expected to be necessary). Furthermore this would open up the intriguing possibility of studying the time dependent nature of other processes such as Auger decay[50].

The method presented here, which we hope will ultimately pave the way for the fully correlated theoretical investigation of time dependent photoionization problems in poly-atomic/poly-electronic systems, may be broken down into three key ingredients. The use of **a)** the novel hybrid Gaussian/B-Spline (GABS[51]) basis, combined with **b)** a Close Coupling approach to express the asymptotic behaviour of the ionized system, taking into account all short range interaction, where **c)** the bound neutral and ionic states are calculated using state of the art computational quantum chemistry packages (QCP). The sum of these components is what we shall interchangeably refer to as the XCHEM method or the XCHEM code [52, 53] and allows for the exploitation of the sophisticated methods that come with modern QCP and the tools of scattering theory to describe electrons ejected from the molecule into a scattering state. In reference to the problems that existing methods have in merging the different challenges posed by complicated bound states and scattering states with infinite spatial extension, the XCHEM method makes use of QCPs to address the former and the B-Spline part of the novel GABS basis to address the latter, with the technical details of the GABS basis making possible the fusion of these methodologies.

Turning now from photoionization to photodissocation, we are concerned with the dynamics a system may undergo once it has been stripped of an electron. So far the processes we mentioned were concerned with the electron dynamics of the ionization itself focussing especially on autoionization. However, as a rather natural second step arises the notion of investigating how this electronic rearrangement may drive chemical reactions [28]. We motivated studying photoionization in the presences of autoionizing states for small molecules, by it being the simplest process that cannot easily be studied given current methods. In much the same way we may regard photodissociation of small molecules (summarized in figure 1.2) as the simplest chemical reaction fulfilling the same criteria. The advances in ultra short pulses we mentioned have made possible to experimentally follow the photodissociation process in a pump/probe setup, by recording the dependence of the kinetic energy of the dissociated molecular fragments as a function of the time delay between the ionizing pump pulse and the probing pulse. This technique has established itself as a useful tool to study ultrafast nuclear dynamics, but has only been used to this end in a small number of systems. Again, much like for photoionzation, H_2 and D_2 (whose geometry, being a diatomic systems, is fully specified by the separation of the two nuclei and whose electronically simple structure make it an appealing candidate to test new methods) were the first systems whose dissociative photoionization was experimentally[54, 28] and theoretically [55] studied. For larger systems the results available theoretically or experimentally of comparable quality quickly thin out with increasing complexity of the molecules. While for O_2[56],CO [57], N_2[58, 59] and even IBr [60] (though not recording the kinetic energy of the fragments) experimental results of good quality exist, the situation drastically begins to deteriorate for larger systems. And even for these smaller cases, as a consequence of the large number of electronic states involved, the theoretical investigation of electronic and nuclear dynamics following ionization by attosecond pulses is still in its infancy.

Summarizing the preceding paragraphs we may state the aim of this project to be the theoretical description of the photoionization and dissociation of diatomic, polyelectronic molecules, with the intention of designing the models in way a that allows extension to systems (much) larger than what can currently be studied at a similar level of theory. Throughout this work, we almost entirely confine ourselves to the study the photoionization and photodissociation of molecular Nitrogen. Nitrogen is an appealing sample system for a variety of reasons. In the study of photoionization it is the smallest system that does not meet the requirements to make it accessible in any straightforward way to existing methods: it is a molecular, polyelectronic system. Therefore the structure of the molecular and cationic states leads to very complicated short range interaction with the ejected electron. Hence N_2 is the natural first step in testing the XCHEM methods viability on the path to ultimately applying it to more complex molecules of chemical or even biological interest. For the same reason literature exists on the performance of essentially any existing method attempting the same feat of accurately describing the N_2 continuum [61, 62, 63, 64, 46], allowing us to contrast the performance of the XCHEM methods with these existing approaches. Furthermore, besides the availability of theoretical results, N_2 is also an attractive system to study photoionization experimentally and thus the rich literature on the

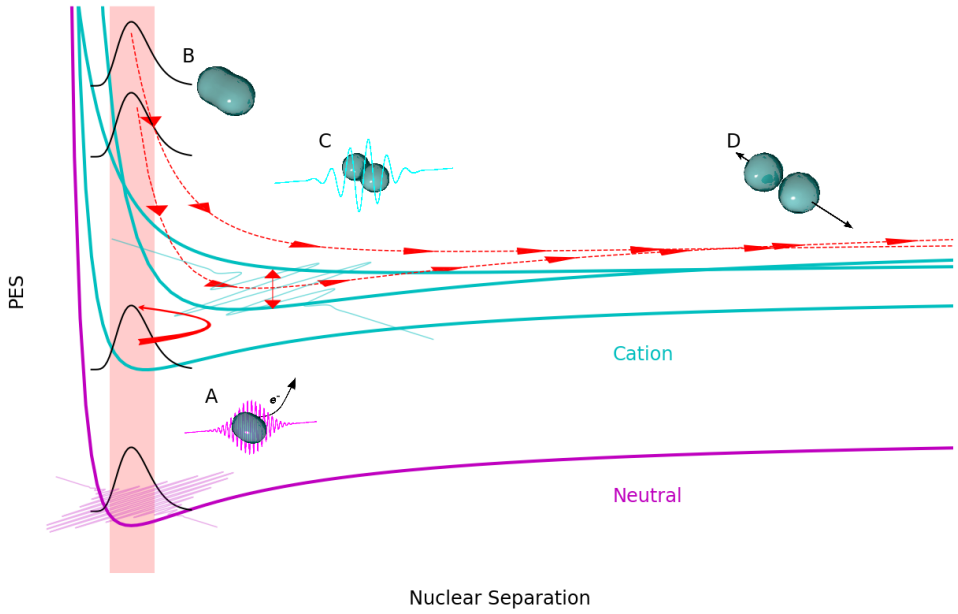

Figure 1.2: Schematically depicted photodissociation process. The lower (mangenta) curve represents the neutral systems's potential energy surface (PES) as a function of nucelar geometry. The upper three curves represent the PES of three ionic states. The black curve shows the nucelar wavefunction of the system before ionization. The transparent red region highlights the Franck Condon Region. The photodissociation as studied in an pump/probe type experiment takes places in four steps. A) Ionization induced by an attosecond XUV pulse (for details on the ionization see figure 1.1) leaving multiple ionic states populated, B) the nuclear wavefunction is not in an eigenfunction of the system and begins begins to evolve. The lowest ionic PES shows a bound state with the nuclei vibrating whitout dissociating. The upper two show dissociative states. C) the probe pulse may produce population transfere between different PES, if at the moment of probing, the dissociative PES carry population for nuclear separation where the energy difference between the PES falls within the bandwidth of the probe pulse. D) The molecular fragments break apart. Their kinetic energy possibly contains a signature of the interaction of the probe pulse with the system.

same [65, 66, 67, 68, 69, 70] will serve to compliment the theoretical data to give an accurate impression of the performance of the XCHEM method. Using N_2 as the system of choice also for the study of photodissociation is in part motivated by the possibility of providing a sense of continuity to this work, yielding a fairly complete picture of the processes induced in N_2 by attosecond XUV pulses. This was made possible by the availability of very high quality data obtained for the kinetic energy spectra in N_2 in a pump (attosecond XUV)/probe(femtosecond NIR/VIS) experiment[59].

1.1 Structure of this work

This work presents a new approach, the XCHEM approach, that enables the study of photoionization and subsequently occurring processes, while fully accounting for electron correlation. The problem is approached in three parts. The first part (chapters 2 to 7) divulges the theoretical background necessary for an appreciation of the method proposed here. The second part (chapters 8 and 9) introduces the XCHEM approach itself, while the last part (chapters 10 and 11) present results that were obtained throughout this creation of the development of the XCHEM approach.

Part I - Theory

As was mentioned in the previous section a key idea of the XCHEM approach is the relegation of different aspects of the photoionization process to different theoretical and computational machineries. In the first part chapters 2, 3 and 4 are concerned with the quantum chemical aspects relating to the poly electronic structure of the neutral and ionic system before and after ionization. Chapters 5 and 6 on the other hand are concerned with the electron that leaves the system during ionization, and consequently heavily draw from scattering theory. Chapter 7 falls outside either of these categories and is not part of the XCHEM approach but rather outlines how processes following ionization may be investigated, with the objective of providing the necessary background to present a computational model for photo dissociation.

Part II - Methodology

With the theoretical aspects in place, this part is dedicated purely to the XCHEM method. Chapter 8 presents the novel basis set that the scattering problem will be expressed in and outlines how the close coupling expansion is used to merge multi channel scattering theory with quantum chemistry from a theoretical point of view. Chapter 9 describes in considerable detail how the QCPs were exploited and modified to permit the use of their computational power in calculating bound states to a high level of theory in applying the XCHEM method to study photoionization.

Part III - Results

The results obtained from the various theoretical tools, as applied to molecular Nitrogen are presented in chapters 10 and 11. The first of these presents the result obtained in studying the photoionization of N_2 between the $^2\Pi_u$ and $^2\Sigma_u$ ionization thresholds. Chapter 11 presents results on the photodissociation of N_2, which were obtained in collaboration with the experimental efforts studying the same process. The scope of these two chapters is slightly different in nature. The photoionization is studied with a focus on attaining extremely high accuracy to assess the performance of the new method, without the ambition to investigate unknown or poorly understood phenomena. The photodissociation conversely places less emphasis on novel methods, but rather seeks to understand the origin of the physical processes that are seen to manifest themselves in the experimental data of our collaborators.

Part I

Theory

Overview

In the following chapters the theory underlying the various models we implemented, treating photo ionization and photo dissociation, will be outlined. Broadly speaking this will be divided into two parts treating different aspects of the mathematical and conceptual machinery that is required to fully understand the results and conclusions that we arrive at in this work; the bound state part and the scattering state part. As was stated in the introduction, in the most general of terms, this work seeks to computationally solve the Schrödinger Equation as applied to many electron system under the influence of laser pulses. Therefore in its essence the theory outlined in the pages to come, boils down to finding solutions to the Schrödinger Equation within the confines of different scenarios relating to the different aspects of bound and scattering states. Before the mathematical nuts and bolts will be examined in more detail said parameters shall be outlined to motivate the scope of the exploration of quantum theory given here.

As was said in the introduction we wish to provide an *ab initio* description of the ionization of small molecules by the absorption of a single photon (photoionization), as well as the dynamics of the resulting ionic molecule.

Here small molecules refers to multi electronic diatomic molecules. These although small compared to most molecules of chemical or even biological interest, provide a magnificent challenge in this context, due to the complex interplay of electrons being excited into continuum states, all the while interacting with the intricate electronic structure of the ionic parent molecule. This gives rise to resonance structures in observables such as the photo ionization cross section. The challenging nature of this problem is primarily due to three aspects: multiple atomic sites (molecules rather than atoms are the focus of this work), many electrons (molecules more complicated than H_2) and continuum states. The omission of any one of these leads to problems which have already been solved to varying, but all around convincing degrees of accuracy. Describing multi electronic molecules without the need to include continuum states leaves one in the field of traditional quantum chemistry (QC) dealing with bounds states of molecules. *ab initio* codes for the description of photoionization in multi electronic, atomic systems (that is letting an electron escape into continuum states) exist [40] and have been used as a benchmark in this project in the case of Neon. Finally the case of photoionization of molecular Hydrogen has also been studied extensively (multiple atoms, continuum states and ionic system with single electron) [42], once again providing results for benchmarking and testing the present work (the details of benchmarking and testing are outlined in chapters 8 and 9)

Thus we are to conclude that an *ab initio* description of photoionization of multi electronic, molecular systems requires on the one hand the methods of QC to accurately describe the molecule to be ionized as well as the ionic states of the molecule after ionization (parent ion) and on the other hand the machinery of scattering theory to account for the electron that is ejected into a continuum state. In contrast to most existing models and codes this will be accomplished by using a Gaussian and B-Spline hybrid (GABS) basis set [51], providing the flexibility to describe complex, multi atomic bound states as well as continuum states.

Another challenge posed by ultra short laser pulses used in conjunction with relatively complex molecules, is the large bandwidth of these pulses, yielding ionic states which are superpositions of large numbers of electronic eigenstates of the ion. Thus the resulting dissociation dynamics is complex and requires large number of potential energy surfaces and exhibits strong non-adiabatic behaviour. This time dependent treatment of the nuclear dynamics after ionization in the presence of non-adiabatic effect was, although only indirectly linked to the process of photoionization itself, presents an additional focus of this work.

With these theoretical objectives in mind, the outline of the theoretical discussion is structured as follows: chapter 2 will discuss Hartree Fock theory serving as a theoretical starting point and introducing the terms and notation which will be used throughout later chapters. Chapter 3 builds on this to introduce different methods to account for electron correlation beyond the Hartree Fock Level of theory. Chapter 4 contains a review of commonly used basis functions in quantum chemistry calculations as well as a more in depth exploration of the properties of Gaussian Basis functions. Chapter 5 explores the most relevant

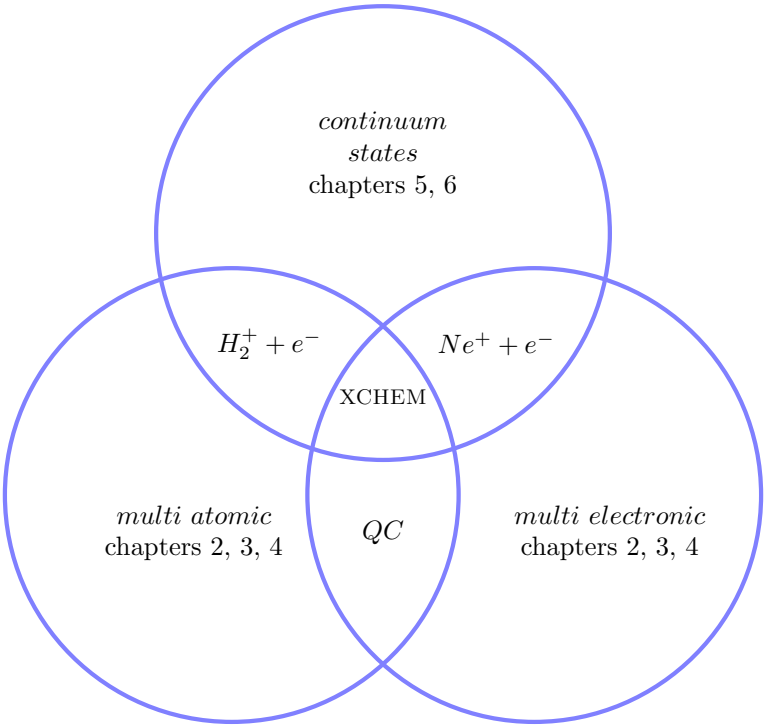

Figure 1.3: Diagrammatic summary of the conceptual relationship between the different aspects of theory that are applied in this work (with QC standing for quantum chemistry). For all but the central region of the Venn diagram ample resources are available for the description of physical phenomena that fall into these categories. A central goal of this work is the centre, relating to the ionization of polyelectronic molecules. These processes necessarily draw from all three disciplines represented by the individual circles. We achieve this with the XCHEM approach the details of which are given in chapters 8 and 9. As was said in the text, the chapters to follow divulge the relevant theoretical aspects on which the XCHEM approach rests.

aspects of scattering theory including a discussion of aforementioned resonance features. Chapter 6, equivalent to the purpose of chapter 4 in the discussion of QC calculations, explains the basic ideas behind B-Splines; the basis functions used to describe scattering states. Finally chapter 7 describes the time dependent aspects as we shall encounter them in our discussion of nuclear dynamics after ionization. This include methods used to solve the time dependent Schrödinger Equation, as well as a discussion of the method we developed to include non-adiabataic effects, i.e. effects the description of which cannot be describe within the confines of the Born-Oppenheimer Approximation.

It should be noted that as this work focuses on many different aspects (as diagrammatically indicated below) drawing on ideas from various disciplines, spanning a fairly wide range of mathematical tools. As such to provide an adequate understanding of all the concepts tying this work together necessarily quite a lot of ground will have to be covered. Therefore if a choice had to be made this works focus lies on understandability and conveying the tools of and connections between the various theories from Chemistry and Physics that will be encountered.

2 Hartree Fock Theory

In general we wish to find a solution for the Schrödinger equation for a system of N_e electrons (indexed by lower case letters starting from i) and N_n nuclei (indexed by upper case letter starting from A) to obtain the energy E and the wavefunction Ψ:

$$\hat{\mathcal{H}}\left|\Psi\right\rangle = E\left|\Psi\right\rangle \quad \text{where} \tag{2.1}$$

$$\hat{\mathcal{H}} = \hat{\mathcal{T}}_e + \hat{\mathcal{T}}_n + \hat{\mathcal{U}}_{ne} + \hat{\mathcal{U}}_{ee} + \hat{\mathcal{U}}_{nn} \tag{2.2}$$

$$\hat{\mathcal{H}} = -\sum_{i=1}^{N_e}\frac{1}{2}\nabla_i^2 - \sum_{A=1}^{N_n}\frac{1}{2M_A}\nabla_A^2 - \sum_{i=1}^{N_e}\sum_{A=1}^{N_n}\frac{Z_A}{r_{iA}} \tag{2.3}$$

$$+\sum_{i=1}^{N_e}\sum_{j>i}^{N_e}\frac{1}{r_{ij}} + \sum_{A=1}^{N_n}\sum_{B>A}^{N_n}\frac{Z_A Z_B}{R_{AB}}, \tag{2.4}$$

where the five terms correspond to electronic kinetic energy, nuclear kinetic energy, nucleus-electron potential energy, electron-electron potential energy, nucleus-nucleus potential energy. We shall for now focus on the electronic part of the Hamiltonian by assuming the nuclear kinetic energy to be negligible, which is to say assuming the fixed nuclei approximation, yielding the electronic Schrödinger equation (the nuclear part of the wavefunction will be studied in more detail in in chapter 7)

$$\hat{\mathcal{H}}_e\Phi(\{r_i\};\{R_A\}) = E_e\Phi(\{r_i\};\{R_A\}) \quad \text{where} \tag{2.5}$$

$$\hat{\mathcal{H}}_e = \hat{\mathcal{T}}_e + \hat{\mathcal{U}}_{ne} + \hat{\mathcal{U}}_{ee} + \hat{\mathcal{U}}_{nn}, \tag{2.6}$$

where the parametric dependence of electronic wavefunction Φ on the nuclear geometry accounts only for a constant nuclear potential energy term contribution to the total energy as $E = E_e + \sum_{A=1}^{N_n}\sum_{B>A}^{N_n}\frac{Z_A Z_B}{R_{AB}}$ the evaluation of which is trivial.

The goal of quantum chemistry is, in general, to find a solution Φ to equation 2.6, which is a function of the N_e electronic positions, that is $\Phi = \Phi(\mathbf{r_1}, \cdots, \mathbf{r_{N_e}})$.

The starting point of almost any quantum chemistry bound state calculation is by finding an orthonormal set of spin orbitals $\chi(\mathbf{x})$. The spin orbitals are functions of the coordinates of one electron, including the spatial variables as well as the spin variable, i.e. $\chi(\mathbf{x}) = \psi(\mathbf{r})\alpha(\omega)$. The ground state of the system $\Psi_0(\mathbf{x_1}, \cdots, \mathbf{x_{N_e}})$ shall be expressed in terms of these spin orbitals. Ψ_0 must respect the fermionic nature of the electron, and thus be antisymmetric under the exchange of any two electrons. The most straightforward way to achieve this is by constructing Ψ_0 as a single Slater determinant of N_e spin orbitals, given by

$$\left|\Psi_0\right\rangle = \frac{1}{\sqrt{N_e}}\begin{vmatrix} \chi_1(\mathbf{x_1}) & \cdots & \chi_{N_e}(\mathbf{x_1}) \\ \vdots & \ddots & \vdots \\ \chi_1(\mathbf{x_{N_e}}) & \cdots & \chi_{N_e}(\mathbf{x_{N_e}}) \end{vmatrix} = \left|\chi_1 \cdots \chi_{N_e}\right\rangle. \tag{2.7}$$

In general there is no reason to assume that the exact solution to equation 2.6 can be expressed as a single determinant. A weighted sum of Slater determinants over a set of spin orbitals larger than N_e, would be antisymmetric just as well. However for now we shall assume one determinant is sufficient; this assumption is known as the Hartree-Fock approximation. Within this approximation the N_e sought for

spin orbitals are those which, in accordance with the variational principle, minimize the ground state energy given by

$$
\begin{aligned}
E_0 &= \langle\Psi_0|\hat{\mathcal{H}}_e|\Psi_0\rangle && (2.8)\\
&= \langle\chi_i\cdots\chi_j| - \sum_{i=1}^{N_e}\frac{1}{2}\nabla_i^2 - \sum_{i=1}^{N_e}\sum_{A=1}^{N_n}\frac{Z_A}{r_{iA}} + \sum_{i=1}^{N_e}\sum_{j>i}^{N_e}\frac{1}{r_{ij}}|\chi_i\cdots\chi_j\rangle && (2.9)\\
&= \sum_{i=1}^{N_e}\langle\chi_i\cdots\chi_j|h_i|\chi_i\cdots\chi_j\rangle + \sum_{i=1}^{N_e}\sum_{A=1}^{N_n}\langle\chi_i\cdots\chi_j|\frac{1}{r_{ij}}|\chi_i\cdots\chi_j\rangle\,, && (2.10)
\end{aligned}
$$

where in the last line we have defined the operator $\hat{h}_i = -\nabla_i - \sum_{A=1}^{N_n}\frac{Z}{r_{iA}}$ acting on $\mathbf{x}_i$. The subscript shall be omitted if the operator appears in an equation where no ambiguity is possible.

The first step in obtaining an equation to find those χ that minimize E_0 is recasting the above equation in a form that does not involve Slater determinants but rather simple matrix elements in terms of the spin orbitals. The two operators appearing in the definition if $\hat{h}_i$ depend on the coordinate of only one electron (one electron operators), whereas the third operator in equation 2.9 depends on the coordinates of two electrons (two electron operator).

The Slater-Condon rules for matrix elements of two determinants $|D_1\rangle = |\chi_1\cdots\chi_{N_e}\rangle$ and $|D_2\rangle = |\chi'_1\cdots\chi'_{N_e}\rangle$ of orthonormal spin orbitals state that for a general one electron operator $\hat{\mathcal{O}}_1$ the following holds

$$
\langle D_1|\hat{\mathcal{O}}_1|D_2\rangle = \begin{cases} \sum_{i=1}^{N_e}\langle\chi_i|\mathcal{O}_1|\chi_i\rangle & \text{if} \quad D_1 = D_2 \\ \langle\chi_m|\hat{\mathcal{O}}_1|\chi'_m\rangle & \text{if} \quad D_1 \text{ and } D_2 \text{ differ in orbital } m:\ \chi_m \neq \chi'_m \\ 0 & \text{if} \quad D_1 \text{ and } D_2 \text{ differ in more than one orbital} \end{cases}, \tag{2.11}
$$

where $\langle\chi_i|\hat{\mathcal{O}}_1|\chi_j\rangle = \int \chi_i(\mathbf{x})\hat{\mathcal{O}}_1\chi_j(\mathbf{x})dx$. For a general two electron operator $\hat{\mathcal{O}}_2$ the following expressions hold

$$
\langle D_1|\hat{\mathcal{O}}_2|D_2\rangle = \begin{cases} \frac{1}{2}\sum_{i=1}^{N_e}\sum_{j=1}^{N_e}\langle\chi_i\chi_j||\chi_i\chi_j\rangle_{\mathcal{O}_2} & \text{if} \quad D_1 = D_2 \\ \frac{1}{2}\sum_{i=1}^{N_e}\langle\chi_m\chi_i||\chi'_m\chi_i\rangle_{\mathcal{O}_2} & \text{if} \quad D_1 \text{ and } D_2 \text{ differ in orbital } m \\ \langle\chi_m\chi_n||\chi'_m\chi'_n\rangle_{\mathcal{O}_2} & \text{if} \quad D_1 \text{ and } D_2 \text{ differ in orbitals } m \text{ and } n \\ 0 & \text{if} \quad D_1 \text{ and } D_2 \text{ differ in more than two orbital,} \end{cases} \tag{2.12}
$$

where $\langle\chi_i\chi_j||\chi_k\chi_k\rangle_{\mathcal{O}_2} = \int dx_1dx_2\chi_i(x_1)\chi_j(x_2)\mathcal{O}_2(1-\mathcal{P}_{12})\chi_k(x_1)\chi_l(x_2)$. When the subscript $\mathcal{O}_2$ is dropped this shall be default refer to $\mathcal{O}_2 = r_{12}^{-1}$ as this is the only two electron operator we will encounter.

Applying equations 2.11 and 2.12 (and the notations introduced in them) to equation 2.10, yields the ground state energy as a functional of the set of spin orbitals (note that as we are dealing with only one determinant, Ψ_0, only the $D_1 = D_2$ case in either equation applies. The cases in which the determinants differ in one or more spin orbital will however be relevant later.).

$$
E_0[\{\chi_i\}] = \sum_{i=1}^{N_e}\langle\chi_i|\hat{h}|\chi_i\rangle + \frac{1}{2}\sum_{i=1}^{N_e}\sum_{j=1}^{N_e}\langle\chi_i\chi_j||\chi_i\chi_j\rangle + \sum_{i=1}^{N_e}\sum_{j=1}^{N_e}\varepsilon_{ij}(\langle\chi_i|\chi_j\rangle - \delta_{ij}), \tag{2.13}
$$

where the last term was introduced to enforce orthonormality[1] of the spin orbital, by means of introducing the Lagrange multiplier ε_{ij}, thus imposing on the spin orbitals the condition $\langle\chi_i|\chi_j\rangle - \delta_{ij} = 0$.

[1] It is not in general necessary to impose this conditions, and not imposing orthonormality does in fact provide a freedom of choice in spin orbital which can be very useful under certain circumstances. This does however come with the considerable disadvantage of the Slater-Condon Rules no longer being applicable, resulting in substantial computational complications. We will refer back to this in later chapters discussing implementation.

We shall obtain those $\{\chi_i\}$ that minimize E_0 by varying them by $\{\delta\chi_i\}$ and solving for those spin orbital whose first order variation $\delta E_0[\{\delta\chi_i\}]$ vanishes.

$$\begin{aligned}
\delta E_0[\{\delta\chi_i\}] &= E_0[\{\chi_i+\delta\chi_i\}] - E_0[\{\chi_i\}] && (2.14)\\
&= \sum_{i=1}^{N_e} \langle \chi_i+\delta\chi_i|\hat{h}|\chi_i+\delta\chi_i\rangle + && (2.15)\\
&\quad \frac{1}{2}\sum_{i=1}^{N_e}\sum_{j=1}^{N_e} \langle (\chi_i+\delta\chi_i)(\chi_j+\delta\chi_j)||(\chi_i+\delta\chi_i)(\chi_j+\delta\chi_j)\rangle + && (2.16)\\
&\quad \sum_{i=1}^{N_e}\sum_{j=1}^{N_e} \varepsilon_{ij}(\langle \chi_i+\delta\chi_i|\chi_j+\delta\chi_j\rangle - \delta_{ij}) - E_0[\{\chi_i\}] && (2.17)\\
&= \sum_{i=1}^{N_e} \langle \delta\chi_i|\hat{h}_i|\chi_j\rangle + \sum_{i=1}^{N_e}\sum_{j=1}^{N_e} \langle \delta\chi_i\chi_j||\chi_i\chi_j\rangle - && (2.18)\\
&\quad \sum_{i=1}^{N_e}\sum_{j=1}^{N_e} \varepsilon_{ij}\,\langle \delta\chi_i|\chi_j\rangle + O(\{\delta\chi_i^2\}) + \text{complex conjugate} = 0 && (2.19)
\end{aligned}$$

Expanding this last expression in terms of integrals yields

$$\begin{aligned}
0 &= \sum_{i=1}^{N_e}\int d\mathbf{x}_1\delta\chi_i(\mathbf{x}_1)\left[h_1\chi_i(\mathbf{x}_1) + \sum_{j=1}^{N_e}\left[\int d\mathbf{x}_2\chi_j(\mathbf{x}_2)\frac{1}{r_{12}}\chi_j(\mathbf{x}_2)\chi_i(\mathbf{x}_1)\right] - \right. && (2.20)\\
&\quad \left. \sum_{j=1}^{N_e}\left[\int d\mathbf{x}_2\chi_j(\mathbf{x}_2)\frac{1}{r_{12}}\chi_i(\mathbf{x}_2)\chi_j(\mathbf{x}_1)\right] - \sum_{j=1}^{N_e}\varepsilon_{ij}\chi_j(\mathbf{x}_1)\right]. && (2.21)
\end{aligned}$$

To simplify this equation the Coulomb and Exchange operators, defined as

$$\begin{aligned}
\hat{\mathcal{J}}_{jm}\chi_i(\mathbf{x}) &= \int d\mathbf{x}'\chi_j(\mathbf{x}')\frac{1}{r_{12}}\chi_j(\mathbf{x}')\chi_i(\mathbf{x}_m) && (2.22)\\
\hat{\mathcal{K}}_{jm}\chi_i(\mathbf{x}) &= \int d\mathbf{x}'\chi_j(\mathbf{x}')\frac{1}{r_{12}}\chi_i(\mathbf{x}')\chi_j(\mathbf{x}_m) && (2.23)
\end{aligned}$$

respectively, are introduced where (analogous to the definition of h_i) the second subscript will be omitted whenever confusion is impossible. In terms of these operators and noting in equation 2.21 the expression in brackets has to vanish, as the equation must hold for any $\delta\chi_i$, gives:

$$\begin{aligned}
\hat{h}\chi_i(\mathbf{x}) + \sum_j\left[\hat{\mathcal{J}}_j - \hat{\mathcal{K}}_j\right]\chi_i(\mathbf{x}) &= \sum_{j=1}^{N_e}\varepsilon_{ij}\chi_j(\mathbf{x}) && (2.24)\\
\hat{f}\,|\chi_i\rangle &= \sum_{j=1}^{N_e}\varepsilon_{ij}\,|\chi_j\rangle\,, && (2.25)
\end{aligned}$$

where in the second line we introduced the Fock operator f_m defined as acting on a spin orbital $\chi_i(\mathbf{x}_m)$ in the following way:

$$\hat{f}_m\chi_i(\mathbf{x}_m) = \hat{h}_m\chi_i(\mathbf{x}_m) + \sum_j\left[\hat{\mathcal{J}}_j - \hat{\mathcal{K}}_j\right]\chi_i(\mathbf{x}_m). \quad (2.26)$$

Where, again, the subscript m will only be used when it is necessary to make explicit on which, of several $\mathbf{x}_i$, $\hat{f}$ acts. At this point it is important to note that any unitary transformation $\mathbf{U}$ of the spin orbitals χ_i to a new set of spin orbitals $\chi_i' = \sum_{j=1}^{N_e}U_{ij}\chi_j$, leaves determinants of spin orbitals unchanged up to a complex phase $e^{i\alpha}$, thereby not effecting any observables. Furthermore it is easy to show that the Fock operator is invariant under unitary transformation to the new set of spin orbitals. Therefore we are at

liberty to rotate the set of spin orbitals by a $\mathbf{U}$ satisfying

$$\varepsilon'_{ij} = \sum_{k=1}^{N_e}\sum_{l=1}^{N_e} U^*_{ik}\varepsilon_{kl}U_{lj}; \quad \text{such that } \varepsilon'_{ij} = \delta_{ij}\varepsilon'_i \tag{2.27}$$

Using this new set of spin orbitals defined by the transformation diagonalizing ε_{ij} and dropping the prime puts equation 2.25 into the form

$$\hat{f}\,|\chi_i\rangle = \varepsilon_i\,|\chi_i\rangle\,. \tag{2.28}$$

These are the well known Hartree-Fock equations whose solutions χ_i define the canonical Hartree-Fock orbitals. Note that the functional dependence of the Fock operator only extends to the first N_e eigenfunctions (that is spin orbitals) of f, not to the remaining infinitely many $\{\chi_{N_e+1}, ..\}$. The former set of spin orbitals is generally referred to as occupied orbitals (denoted by χ_i with eigenvalue ε_i) and the letter as virtual orbital (denoted by χ_ι with eigenvalue ε_ι). So far we have referred to ε as eigenvalue; the physical interpretation of the eigenvalues of the Fock operator is delivered by the Koopman theorem which states, that ε_i is the energy required to remove an electron from the occupied orbital χ_i and, conversely ε_ι the energy of adding an electron to the virtual orbital χ_ι. For this reasons the ε are generally referred to as the orbital energies of the orbitals $|\chi\rangle$.

Another important theorem relating to Hartree Fock Orbitals is the Brillouin Theorem, which we shall use in the upcoming discussion of Configuration Interaction. Assuming we have solved the Hartree Fock equations yielding the canonical Hartree Fock orbitals we may consider the Hamiltonian matrix elements between the Hartree Fock solution and a singly excited states obtained by removing one electron from an occupied orbital, placing it instate in a virtual orbital. The Brillouin Theorem then states, that for a singly excited state,

$$\langle\Psi_0|\hat{\mathcal{H}}|\Psi_{\text{exc}}\rangle = 0. \tag{2.29}$$

After the general considerations of the Koopman and Brillouin theorems, we shall now consider how to actually solve equations 2.28. As a consequence of the complicated structure of the Fock operator f, the Hartree Fock equations cannot be solved directly for the spin orbitals. What is in general done for molecules, to remedy this, is to expand the spatial part of the spin orbitals in terms of a set of basis functions $\{\phi_p\}$ (we shall from here onwards use the indeces $i, j, \cdots$ denoting orbitals and $p, q, \cdots$ denoting basis functions).

In principle these basis functions would have to be capable of representing all functions in the space $\mathcal{L}^2(\mathbb{R}^3)$, which would require an infinitely large number of basis functions. In practice a finite set is chosen, specifically designed to represent the spatial orbitals of the molecule in question as best possible. The theory of basis functions relevant to bound state calculations will be outlined in chapter 4. For now, however, we shall assume a suitable choice of set of basis functions of size N_b (leaving the equation 2.28 with N_b rather than infinitely many eigenfunctions to find), to expand the solutions in has been made, leaving the spatial part of the spin orbitals in the form

$$\psi_i = \sum_{p=1}^{N_b} c_{ip}\phi_p. \tag{2.30}$$

We will show how to thus turn the integro-differential Hartree-Fock equation into an (albeit self consistent) set of algebraic equations, which can be solved numerically for the expansion coefficients c_{ip}. We shall restrict the spin orbitals, so that for all χ_i the spatial component does not depend on the spin function. This is enforced by defining a set of spatial orbitals $\{\psi_i\}$ of size $N_e/2$ from each of which we construct two spin orbitals $\chi_i = \psi_j\alpha(\omega)$ and $\chi_{i'} = \psi_j\beta(\omega)$ yielding a set of N_e spin orbitals. In terms of this space-spin factorization of the spin orbitals the Fock equation 2.28 reads

$$\hat{f}\psi(\mathbf{r}_i)\alpha(\omega_i) = \varepsilon_i\psi(\mathbf{r}_i)\alpha(\omega_i). \tag{2.31}$$

In addition to the restriction of spin independent spatial orbitals, it as assumed that the all occupied orbitals are doubly occupied, (somewhat limiting the choice of treatable molecules). It is then possible

obtain a version of the Hartree-Fock equations yielding the spatial part of the spin orbitals. To do so one must eliminate spin from equation 2.31 by multiplying by $\alpha^*(\omega)$ and integrating over the spin variable. Exploiting the orthonormality of α and expanding χ into its spatial and spin components in the definition of f, the spatial Hartree-Fock equations are found to read,

$$\hat{f}^{\mathbb{R}}\psi_i(\mathbf{r}) = \varepsilon_i\psi_i(\mathbf{r}_i) \quad \text{where} \tag{2.32}$$

$$\hat{f}^{\mathbb{R}} = \int d\omega\alpha^*(\omega)f\alpha(\omega) = h + \sum_i^{\frac{1}{2}N_e} 2 * \hat{\mathcal{J}}_i^{\mathbb{R}} - \hat{\mathcal{K}}_i^{\mathbb{R}}. \tag{2.33}$$

The superscript-$\mathbb{R}$ indicates the operators as operators acting on spatial orbitals, where the definitions of $\hat{\mathcal{J}}_i^{\mathbb{R}}$ and $\hat{\mathcal{K}}_i^{\mathbb{R}}$ are exactly equivalent to those in 2.23 and 2.23 with the spin orbitals being replaced by spatial orbitals and the integration variable being $\mathbf{r}$. The superscript shall be omitted from now on, with the correct operator being implied by its acting on a spin or spatial orbital. The simple structure of 2.33, highly analogous to equation 2.28, is crucially dependent on the closed shell assumption of all occupied orbitals being doubly occupied. It is possible to relax both conditions (independently); that of restricting the spatial orbitals to spin independent ones (restricted Hartree-Fock) and that of treating only closed shell molecules (closed-shell Hartree-Fock), leading to somewhat more involved mathematical treatments. But as the restricted closed-shell formalism is satisfactory for our purposes (primarily because subsequent treatment using more advanced methods, outlined later on, renders void any potential gain of beginning with less restrictive Hartee-Fock formalism) and allows us to circumvent problems associated with the unrestricted open-shell formalism (wave function is not guaranteed to be an eigenfunction of the spin operator $\mathcal{S}$) or the restricted open-shell formalism (not implemented in all Quantum Chemistry Packages relevant in this project, e.g. MOLCAS), we shall not concern ourselves with these. Information on these methods can be found in reference [71].

Returning to equation 2.33 we shall substitute into it the basis expansion 2.30, so as to make progress towards obtaining an algebraic version of equation 2.33:

$$\hat{f}\sum_p c_{ip}\phi_p(\mathbf{r}) = \varepsilon\sum_p c_{ip}\phi_p(\mathbf{r}). \tag{2.34}$$

In order to convert this into a matrix equation, both sides of this equation are projected onto ϕ_q^* to yield

$$\sum_p c_{pi}F_{qp} = \varepsilon_i\sum_p c_{pi}S_{qp}, \tag{2.35}$$

where we have defined the following matrices: The overlap matrix $\mathbf{S}$ as

$$S_{pq} \equiv \int d\mathbf{r}\phi_p(\mathbf{r})\phi_q(\mathbf{r}), \tag{2.36}$$

and the Fock Matrix $\mathbf{F}$ as

$$F_{pq} \equiv \int d\mathbf{r}\phi_p(\mathrm{r})\hat{f}\phi_q(\mathbf{r}), \tag{2.37}$$

allowing us to write equation 2.34 in the desired matrix form as,

$$\mathbf{FC} = \mathbf{SC}\varepsilon, \tag{2.38}$$

where $\mathbf{C}$ is the matrix of expansion coefficients c_{pi}, the solving for which yields the Hartree-Fock orbitals within the basis set $\{\phi_p\}$. The equations in 2.38 are called the Roothaan equations. The matrices $\mathbf{S}$, $\mathbf{F}$ and the Roothaan equations, in which they appear, are clearly of great importance to Hartree-Fock theory. Thus we shall elaborate on each of them.

The overlap matrix is Hermitian, and in the case of real basis functions real symmetric. As we shall not encounter complex basis functions we shall assume the latter from now on. Furthermore it is a positive-definite matrix (i.e. real positive eigenvalues). The basis functions are usually assumed to be

normalized, which implies $0 \leq |S_{pq}| \leq 1$, though not usually orthogonal, leading to off diagonal elements. The overlap matrix is important in analysing the presence of linear dependencies between basis functions. Linear dependencies, if present, manifest themselves as eigenvalues being zero to within some sensibly defined threshold. The removal of linear dependencies from custom made basis sets required considerable attention, and shall be looked with more mathematical rigour later on.

It should be obvious from equation 2.38, that the Fock Matrix is a crucial object in Hartree-Fock theory, essentially determining the Hartree-Fock orbitals, such as they are given by $\mathbf{C}$ as linear combinations of basis functions. In writing a useful expression allowing the evaluation of the Fock Matrix, the so called charge density $\rho(\mathbf{r})$, shall prove to be a useful object. It is defined as

$$\rho(\mathbf{r}) \equiv 2 \sum_{i}^{\frac{1}{2}N_e} |\psi_i(\mathbf{r})|, \tag{2.39}$$

where the sum runs over the (doubly) occupied orbitals. It is to be interpreted as yielding the probability of finding an electron within $d\mathbf{r}$ around $\mathbf{r}$ to be $\rho(\mathbf{r})d\mathbf{r}$. In expanding the orbitals as basis functions equation 2.39 becomes:

$$\begin{aligned} \rho(\mathbf{r}) &= \sum_{pq} P_{pq}\phi_p(\mathbf{r})\phi_q(\mathbf{r}) \quad \text{where} & (2.40)\\ \mathbf{P} &\equiv 2\mathbf{C}\mathbf{C}^{\dagger}, & (2.41) \end{aligned}$$

where the second equation defines the density matrix $\mathbf{P}$. Obtaining values for $\mathbf{P}$ is equivalent to finding a solution of 2.38 for C. Returning now to the Fock matrix, by using the definition of the Fock operator 2.31 we find

$$\begin{aligned} F_{pq} &= \int d\mathbf{r}\phi_p(\mathbf{r})h\phi_q(\mathbf{r}) + \sum_{j}^{\frac{1}{2}N_e} \int d\mathbf{r}\phi_p(\mathbf{r}) \left[2 * \mathcal{J}_j - \mathcal{K}_j\right] \phi_q(\mathbf{r}) & (2.42)\\ &= H_{pq}^{\text{core}} + \sum_{j}^{\frac{1}{2}N_e} 2 * g_{pqii} - g_{piiq}. & (2.43) \end{aligned}$$

Where for some set of functions $\{\zeta_\alpha(\mathbf{r})\}$ we have defined the integrals

$$\begin{aligned} H_{\alpha\beta}^{\text{core}} &\equiv \int d\mathbf{r}\zeta_\alpha(\mathbf{r})h\zeta_\beta(\mathbf{r}) & (2.44)\\ g_{\alpha\beta\gamma\delta} &\equiv \int d\mathbf{r_1}d\mathbf{r_2}\zeta_\alpha(\mathbf{r_1})\zeta_\beta(\mathbf{r_1})r_{12}^{-1}\zeta_\gamma(\mathbf{r_2})\zeta_\delta(\mathbf{r_2}), & (2.45) \end{aligned}$$

with the indeces $i, j, \cdots$ and $p, q, \cdots$ in equation 2.43 specifying the appropriate orbitals and basis functions respectively. Expanding now also in terms of basis functions those orbitals appearing implicitly in equation 2.42 via the definition of the Exchange and Coulomb operators, allows for an expression of the Fock matrix purely in terms of integrals between basis functions:

$$\begin{aligned} F_{pq} &= H_{pq}^{\text{core}} + G_{pq} \quad \text{where} & (2.46)\\ G_{pq} &\equiv \sum_{rs} P_{rs} \left[g_{pqrs} - \frac{1}{2} g_{prqs} \right]. & (2.47) \end{aligned}$$

Thus, given a density matrix $\mathbf{P}$ (or equivalently coefficient matrix $\mathbf{C}$), finding the Fock matrix $\mathbf{F}$ is a matter of computing the one electron (H_{pq}^{core}) and two electron integrals (g_{pqrs}) appearing in equations 2.46 and 2.47. It should be noted that of these, only the expression for g_{pqrs} involves the density matrix $\mathbf{P}$. Therefore H_{pq}^{core} depends only on the chosen basis set and can be computed was little computational cost.

The Fock Matrix $\mathbf{F}$ presents more of a challenge for two reasons.

On the one hand due the presence of the two electron integral, of which there is a considerably larger number compared to one electron integrals. Specifically the number of necessary two electron integrals grows as N_b^4. This quartic growth however, may be reduced by considering symmetries present in this two electron integrals, somewhat reducing computational and memory requiring. These symmetries are given by

$$\begin{aligned} g_{\alpha\beta\gamma\delta} &= g_{\alpha\beta\delta\gamma} \\ &= g_{\beta\alpha\delta\gamma} \\ &= g_{\beta\alpha\gamma\delta} \\ &= g_{\gamma\delta\alpha\beta} \\ &= g_{\gamma\delta\beta\alpha} \\ &= g_{\delta\gamma\alpha\beta} \\ &= g_{\delta\gamma\beta\alpha}. \end{aligned} \tag{2.48}$$

This exploitation of these properties of $g_{\alpha\beta\gamma\delta}$ will be very important in the computational implementations which will be discussed in chapter 9. But even in light of this the evaluation two electron integrals takes up a considerable percentage of the computational resources.

The other reason making the Fock matrix a challenging object to deal with is its dependence on the charge density matrix $\mathbf{P}$. The charge density matrix in turn is found solving the Roothaan equations requiring in itself the Fock matrix, thus making apparent the self-consistent nature of the Roothann equations. Before addressing the self-consistency of the Roothan equations, progress is made by noting that if, in equation 2.38, $\mathbf{S}$ were the identity matrix, it would reduce to an, albeit still self consistent, standard eigenvalue equation. This is to say that, the first step must be orthogonalizing the set of basis functions $\{\phi_p\}$. One way to achieve orthogonality is canonical orthogonalization. To this end a transformation matrix $\mathbf{X}$ is defined as,

$$\mathbf{X} = \mathbf{U}\mathbf{s}^{-\frac{1}{2}}, \tag{2.49}$$

where $\mathbf{U}$ is the matrix that diagonalizes the overlap matrix, i.e $\mathbf{U}^\dagger\mathbf{S}\mathbf{U} = \mathbf{s}$, where $\mathbf{s}$ is diagonal (making the computation of $\mathbf{s}^{-\frac{1}{2}}$ trivial). Thus the basis set obtained by applying the transformation $\mathbf{X}$ to the initial basis set ϕ_p, has the desired property of an identity overlap matrix:

$$\mathbf{X}^\dagger\mathbf{S}\mathbf{X} = \left(\mathbf{U}\mathbf{s}^{-\frac{1}{2}}\right)^\dagger \mathbf{S}\mathbf{U}\mathbf{s}^{-\frac{1}{2}} = \mathbf{s}^{-\frac{1}{2}}\mathbf{U}^\dagger\mathbf{S}\mathbf{U}\mathbf{s}^{-\frac{1}{2}} \tag{2.50}$$

$$= \mathbf{s}^{-\frac{1}{2}}\mathbf{s}\mathbf{s}^{-\frac{1}{2}} = \mathbf{I}. \tag{2.51}$$

We make of use of this matrix, by, rather than explicitly transforming the basis and recalculating all integrals by defining

$$\tilde{\mathbf{C}} = \mathbf{X}^{-1}\mathbf{C}, \tag{2.52}$$

which upon substitution into equation 2.38 and left multiplying by $\mathbf{X}$ gives,

$$\mathbf{F}\mathbf{X}^{-1}\tilde{\mathbf{C}} = \mathbf{S}\mathbf{X}^{-1}\tilde{\mathbf{C}}\varepsilon \tag{2.53}$$

$$= \tilde{\mathbf{C}}\varepsilon. \tag{2.54}$$

Defining now

$$\tilde{\mathbf{F}} \equiv \mathbf{F}\mathbf{X}^{-1} \tag{2.55}$$

leaves the transformed Roothaan equations to the desired eigenvalue problem form:

$$\tilde{\mathbf{F}}\tilde{\mathbf{C}} = \tilde{\mathbf{C}}\varepsilon. \tag{2.56}$$

This, as mentioned before, despite having the appearance of a trivial eigenvalue problem, requires some more thought to solve due to the dependence of $\mathbf{F}$ on $\mathbf{C}$. Due to this self-consistency no closed form solution of this problem is possible and an iterative approach must be taken. This iterative approach is called self consistent field theory (SCF) and it is best explained by directly presenting the SCF algorithm to be carried out iteratively:

1. Define the problem be specifying the molecular geometry and the basis sets and set convergence threshold δ_{thr}
2. Calculate $\mathbf{S}$,$\mathbf{H}^{\text{core}}$ and g_{pqrs} (equations 2.36, 2.44 and 2.45)
3. Obtain $\mathbf{X}$ from $\mathbf{S}$ (equation 2.49)
4. Make initial guess for $\mathbf{P}$ labelled $\mathbf{P}_0$
5. Calculate $\mathbf{G}$ to find $\mathbf{F}$ (equations 2.46 and 2.47)
6. Use $\mathbf{X}$ to obtain $\tilde{\mathbf{F}}$ (equation 2.55)
7. Solve equation 2.56 for $\tilde{\mathbf{C}}$
8. Compute $\mathbf{C}$ (equation 2.52)
9. Compute $\mathbf{P}_{i+1}$ (equation 2.41)
10. If $|\mathbf{P}_{i+1} - \mathbf{P}_i| \geq \delta_{\text{thr}}$ return to step 5
11. Done. $\mathbf{C}$ defines Hartree Fock Orbitals and ε their orbital energies.

With this algorithm yielding the Hartree Fock orbitals we have reviewed the fundamentals of Hartee Fock theory. This has been but a superficial account of this theory, representing the starting point of a substantial subset of all Quantum Chemistry Calculations. It was already mentioned that extensions (in the form of unrestricted or open shell formalism) exist, but it should also be noted that the theory was outlined here with a focus on conciseness and comprehensibility rather than computational efficiency. It goes without saying that the importance of Hartree Fock Theory in Quantum Chemistry has sparked considerable effort in designing efficient algorithms. As however the objective of this thesis was not an investigation of the more arcane aspects of Hartree Fock theory, the reader is referred to the following references[72, 71].

Before continuing with the discussion of post Hartree Fock theories, a few conclusions shall be drawn from the preceding derivations. Specifically, it is instructive to mention situations under which Hartree Fock theory as presented here breaks down, to motivate the development of more complete methods. Qualitatively incorrect predictions by HF theory occur in:

1. Incorrect description of H_2 dissociation potential. This is due to the restrictions of the closed shell formalism not allowing the two separated H atoms to each have singly occupied orbitals. These can be remedied by relaxing the closed shell condition.
2. Incorrect ordering of the N_2 ionization potentials (crucial to this work). There is no easy remedy to this problem, as at its core lies the breakdown of the central approximation of HF theory: the wave function is incorrectly described by a single determinant. This is equivalent to saying that the electron correlation has be neglected, i.e. every electron only feels a mean field generated by the other electrons. Such is description is incomplete, as clearly the field every electron fields depends on the position of all other electrons. Theories incorporating electron correlation which in many theories boils down to allowing the wave function being expressed by many determinants. This we shall refer to as configuration interactions (CI). Theories including it will be introduced in the next chapter.

3 Configuration Interaction

Having discussed Hartree Fock Orbitals and their underlying theory, we shall now investigate some of the ways in which to build on top of Hartree Fock theory and allow us to overcome some of the shortcomings inherent to the treatment of a molecule at a Hartree Fock level of theory, such as they were mentioned at the end of the last chapter.

We recall that two assumptions were made in the development of Hartree Fock Theory: the fixed nuclei approximation (ignoring nuclear motion) and the Hartree-Fock approximation, assuming the wave function of a molecular system can be described by a single determinant. In this chapter we shall address the latter. First we shall consider the conceptually simple (though computationally very expensive for most interesting cases) CI theory, which serves as a useful introduction to the challenges presented by electron correlation. It exemplifies how inclusion of multiple determinants yields a better approximation, not only to the ground state, but further allows to find additional electronic states, that are eigenfunctions of the electronic Hamiltonian $\hat{\mathcal{H}}$, and therefore present equally valid solutions to the SE. Afterwards some more efficient methods are presented, allowing for the more economical inclusion of CI to obtain multiple electronic states.

For the development of CI methods it will be convenient in places to work in second quantization formalism. We shall begin the chapter by very briefly introducing the relevant aspects and notation, as they will be used throughout this chapter. For a comprehensive introduction we refer to chapter 1 of reference [71].

3.1 Second Quantization

In second quantization the wave function is no longer expressed only as a function, but is alternatively described as an operator acting on the vacuum state which is thought of as an "empty" Slater determinant over no electrons (the resulting function returns us to the familiar idea of the wave function). More specifically the anti symmetric wave function is generated by the repeated action of the creation or annihilation operators (creating or annihilating electrons in some orbitals, say for instance the Hartree Fock Orbitals of the previous section) on the vacuum state. Often times we may thus view the operator (built from creation and annihilation operators) generating some wave function as the central object in the second quantization formalism. The fundamental objects in this formalism are

1. The occupation number vector $|\mathbf{k}\rangle = |k_{1\alpha}, k_{1\beta}, \cdots, k_{N_b\alpha}, k_{N_b\beta}\rangle$, with each entry being 1 or 0. It denotes the Slater determinant created by distributing $\sum_{i,\sigma}^{N_b,\beta} k_{i\sigma}$ electrons over those spin orbitals whose entries in the occupation vector are 1. We let the subscript $\kappa, \lambda \cdots$ label the spin orbitals as in the order given in the expression for $|\mathbf{k}\rangle$.
2. The vacuum state $|\text{vac}\rangle$ given by $|0, \cdots, 0\rangle$

The operators acting on Slater determinants as we will encounter are

1. The Annihilation and Creation operators $a_{i\sigma}$ and $a^\dagger_{i\sigma}$ satisfying

$$a_\kappa |\mathbf{k}\rangle = \delta_{1k_\kappa} \left(\prod_{\nu=1}^{\kappa-1} (-1)^{k_\nu} \right) |k_1, \cdots, k_{\kappa-1}, 0, \cdots\rangle \tag{3.1}$$

$$a^\dagger_\kappa |\mathbf{k}\rangle = \delta_{0k_\kappa} \left(\prod_{\nu=1}^{\kappa-1} (-1)^{k_\nu} \right) |k_1, \cdots, k_{\kappa-1}, 1, \cdots\rangle \tag{3.2}$$

2. The operators for spin orbital occupation, orbital occupation number operators and spin occupation given by

$$N_\kappa = a^\dagger_\kappa a_\kappa, \quad \text{and} \tag{3.3}$$

$$N_i = a^\dagger_{i,\alpha} a_{i,\alpha} + a^\dagger_{i,\beta} a_{i,\beta}. \tag{3.4}$$

$$N_\alpha = \sum_i a^\dagger_{i,\alpha} a_{i,\alpha}. \tag{3.5}$$

   The first operator's eigenvalues are 1 and 0 if the orbital τ is occupied or unoccupied, respectively. The second operator's eigenvalues are 0,1 and 2 in an analogous. Finally, N_α has eigenvalues between 0 and N_e.

3. The Spin Operators

$$S_+ = \sum_i a^\dagger_{i\alpha} a_{i\alpha} \quad ; \quad S_- = \sum_i a^\dagger_{i\beta} a_{i\beta} \tag{3.6}$$

$$S_z = \frac{1}{2} \sum_i a^\dagger_{i\alpha} a_{i\alpha} - a^\dagger_{i\beta} a_{i\beta} = N_\alpha - N_\beta \tag{3.7}$$

$$\mathbf{S}^2 = S_+ S_- + S_z(S_z - 1), \tag{3.8}$$

   where the eigenvalues of the latter two are the projected and total spin, respectively. They fulfil the following commutator relation

$$\left[\mathbf{S}^2, S_z\right] = 0 \tag{3.9}$$

$$[S_z, N_{i\sigma}] = 0 \tag{3.10}$$

$$[S_z, N_i] = \left[\mathbf{S}^2, N_i\right] = 0 \tag{3.11}$$

$$[S_+, N_{i\sigma}] = a^\dagger_{i\alpha} a_{i\sigma} \delta_{\beta\sigma} - a^\dagger_{i\sigma} a_{i\beta} \delta_{\alpha\sigma} \tag{3.12}$$

$$[S_-, N_{i\sigma}] = a^\dagger_{i\beta} a_{i\sigma} \delta_{\alpha\sigma} - a^\dagger_{i\sigma} a_{i\alpha} \delta_{\beta\sigma} \tag{3.13}$$

4. General one electron operators h which may be written as

$$\sum_{\kappa\lambda} \langle \kappa | h | \lambda \rangle \, a^\dagger_\kappa a_\lambda \tag{3.14}$$

5. The two electron operator g may be written as

$$\sum_{\kappa\lambda\mu\eta} \langle \kappa\lambda || \mu\eta \rangle \, a^\dagger_\kappa a^\dagger_\mu a_\lambda a_\eta \tag{3.15}$$

6. For completeness we mention the Hamiltonian $\hat{\mathcal{H}}$. But its definition in terms of the creation and annihilation is not particularly enlightening, and as it will not be relevant we shall not state it here.

The Hartree Fock ground state of the previous section may then be written as $\prod_{i=1}^{N_e/2} a^\dagger_{i\alpha} a^\dagger_{i\beta}$.

3.2 Configuration Interaction

As we pointed out in chapter 2 the choice of representing Ψ_0 as single determinant (equation2.7) was the desire to ensure the antisymmetric nature of Ψ_0. From this we ultimately arrived at equation 2.28, the iterative solution of which yields a set of orbitals of size equivalent to the size of basis functions. The determinant constructed from the $N_e/2$ Hartree Fock orbitals with lowest orbital energy ε, was the solution for the ground state we arrived at. Starting now from the HF orbitals and relaxing the restriction of representation of Ψ_0 as a single determinant, we may write the most general antisymmetric wave function as

$$\Psi_{\mathrm{CI}} = \frac{1}{\sqrt{N_e}} \sum c_v \left|\mathbf{k}_v\right\rangle \tag{3.16}$$

where we may classify arbitrary determinants (indexed by v and w), specified by the occupation number vector $\mathbf{k}_v$, via their occupation of virtual orbitals relative to the Hartree Fock solution. Let this be denoted by $\Psi_{o_1\cdots o_n}^{v_1\cdots v_n}$ meaning the determinant with n excitations as given by the o_i^{th} occupied orbital of the Hartree Fock determinant being replace by the v_i^{th} virtual orbital. We may then write the solution including CI

$$\begin{aligned}
\left|\Psi\mathrm{ci}\right\rangle &= \sum_{n=0}^{N_e} \sum_{\substack{v_1<\cdots<v_n \\ o_1<\cdots<o_n}} c_{o_1\cdots o_n}^{v_1\cdots v_n} a_{o_1}\cdots a_{o_n} a_{v_1}^\dagger \cdots a_{v_n}^\dagger \left|\Psi_0\right\rangle \\
&= \sum_{n=0}^{N_e} \frac{1}{(n!)^2} \sum_{\substack{v_1,\cdots,v_n \\ o_1,\cdots,o_n}} c_{o_1\cdots o_n}^{v_1\cdots v_n} a_{o_1}\cdots a_{o_n} a_{v_1}^\dagger \cdots a_{v_n}^\dagger \left|\Psi_0\right\rangle \\
&= c_0\Psi_0 + \mathbf{C}_S\left|S\right\rangle + \mathbf{C}_D\left|D\right\rangle + \mathbf{C}_T\left|T\right\rangle + \cdots,
\end{aligned} \tag{3.17}$$

expressing the wavefunction as an expansion over the number of excitation with respect to the HF solution.

The task is to find those coefficient $c_{o_1\cdots o_n}^{v_1\cdots v_n}$ that minimize the energy of the wave function, referred to as the full CI solution. This quickly turns into a magnificent task with the number of possible Slater Determinants that may be constructed from N_e being distributed over $2N_b$ spin orbitals is

$$\binom{2N_b}{N_e}, \tag{3.18}$$

therefore limiting full CI treatment to small benchmark systems. Progress may be made by systematically decreasing the number of terms entering in the CI expansion. An obvious approach is truncating the first sum in equation 3.17, allowing only for up to single (CIS), double (CISD), triple (CISDT) etc. excitations, where in the last expression this was anticipated in the notation $\mathbf{C}_{\mathbf{X_i}}\left|X_i\right\rangle$, being the sum over all terms involving the same number of excitations (we also write $\left|X_0\right\rangle = \left|\Psi_0\right\rangle, \left|X_1\right\rangle = \left|S\right\rangle, \left|X_2\right\rangle = \left|D\right\rangle$ ...). Conceptually finding a solution for the vector of coefficient (CI vector) is independent of where we choose to truncate the sum. Writing

$$\left(\mathcal{H}_e - E_{\mathrm{HF}}\right)\left|\Psi_{\mathrm{ci}}\right\rangle = E_{\mathrm{ee}}\left|\Psi_{\mathrm{ci}}\right\rangle \tag{3.19}$$

$$\left(\mathcal{H}_e - E_{\mathrm{HF}}\right)(\Psi_0 + \mathbf{C}_S\left|S\right\rangle + \mathbf{C}_D\left|D\right\rangle + \cdots) = E_{\mathrm{ee}}(\Psi_0 + \mathbf{C}_S\left|S\right\rangle + \mathbf{C}_D\left|D\right\rangle + \cdots), \tag{3.20}$$

where E_{HF} and E_{ee} are the Hartree Fock ground state energy, and the correction introduced by CI, respectively. Successively projecting equation 3.20 onto $\left|S\right\rangle$,$\left|D\right\rangle$, etc. yields the matrix equation

$$\mathbf{Hc} = E_{\mathrm{ee}}\mathbf{c}, \tag{3.21}$$

where $\mathbf{c} = (C_0, \mathbf{C}_S, \mathbf{C}_D, \cdots)$ and $\mathbf{H}$ is block wise given by $\mathbf{H}_{i,j} = \langle X_i|\hat{\mathcal{H}} - E_{\mathrm{ee}}|X_i\rangle$. Evidently equation 3.21, if solved fully yields a set of eigenvectors $\mathbf{c}_I$ of which the one with the lowest eigenenergy

corresponds to the ground states, whereas the remaining CI-vectors yield the wavefunction of different (excited) electronic states. Some progress towards solving equation 3.21 may be made by exploiting the Brillouin Theorem as well as the Slater Condon rules of the previous section to realize this matrix has the following structure $\mathbf{H}_{i,j} = 0$ if $|i-j| > 2$ (Slater Condon rules) or $(i,j) \in \{(0,1),(1,0)\}$ (Brillouin Theorem). This sparse banded structure somewhat facilitates computations. In practice though, the gargantuan size of the CI vector means we are normally still confined to CIS,CID or CISD. And even in those cases (with the possible exception of CIS, though a CIS calculation based on the Hartree Fock wavefunction Ψ_0 will yield $E_{\rm cc} = 0$ as a consequence of the Brillouin Theorem. This is not true in general, when considering excitations based on state built already using multiple determinants, which will shall return to later, but even then the CIS contribution is generally too small to make CIS particularly useful), $\mathbf{H}$ quickly becomes to large to be stored in memory not to even speak of diagonalization. This however can be solved by noting that mostly we are only interest in the lowest few eigenvalues (correponding to the ground states and the lowest few excited states), and methods exist to numerical obtain these. Method routinely employed to this effect are the Newton method[73] based on Taylor expanding $E_{\rm ee}(\mathbf{c})$ to second order and setting its first derivative to zero yielding

$$\mathbf{c} = \frac{(\mathbf{H} - E_0\mathbb{I})^{-1}\mathbf{C_0}}{||(\mathbf{H} - E_0\mathbb{I})^{-1}\mathbf{C_0}||}, \tag{3.22}$$

which is to be solved iteratively. This converges rather quickly, but may be further sped up by replacing treatment of replacing $\mathbf{H}$ in $(\mathbf{H}-E_0\mathbb{I})^{-1}$ by an approximate $\mathbf{H}_0$, a common choice for which is the neglect of off diagonal elements in $\mathbf{H}$. This leads to the quasi Newton method[74], and the frequently used Davidson method[75]. In any of these methods at every step (outer iteration) in iteratively solving 3.22 the matrix inversion in equation 3.22 is in itself done iteratively (inner iteration), where every iteration requires the calculation of a matrix vector product involving the Hamiltonian. This makes it apparent why the quasi Newton or Davidson method result in a substantial speed of the inner iterations involved at each Newton step, requiring knowledge of far fewer Hamiltonian matrix element. This increase in efficiency normally outweighs the decreased rate of convergence in the outer iterations, induced by the approximations inherent to the quasi Newton or Davidson scheme.

3.3 Reduced Density Matrices

In this section we introduce the so called one and two electron reduced density matrix. The evaluation of these matrices will be of great importance when we discuss the implementation of the XCHEM code in chapter 9, and furthermore allows us to motivate a common method allowing for a more efficient implementation of the CI-method discussed in the previous section.

3.3.1 One Electron Reduced Density Matrix

We begin with the one electron reduced density matrix, by expressing two arbitrary multi determinantal states $|\Psi^I\rangle$ and $|\Psi^J\rangle$ in their CI expansions $|\Psi^I\rangle = \sum_v c_v^I |\mathbf{k}_v\rangle$, and now investigate the resulting operator matrix element of some one electron operator $\hat{h}$.

$$\begin{aligned}
h_{IJ} &= \sum_{vw} c_v^I c_w^J \langle \mathbf{k}_v|\hat{h}|\mathbf{k}_w\rangle && (3.23)\\
h_{IJ} &= \sum_{vw}\sum_{\kappa\lambda} \langle\kappa|\hat{h}|\lambda\rangle\, c_v^I c_w^J \langle \mathbf{k}_v|\hat{a}_\kappa^\dagger \hat{a}_\lambda|\mathbf{k}_w\rangle && (3.24)\\
&= \sum_{\kappa\lambda} h_{\kappa\lambda} \langle \Psi^I|\hat{a}_\kappa^\dagger \hat{a}_\lambda|\Psi^J\rangle \quad \text{where} && (3.25)\\
h_{\kappa\lambda} &= \langle\psi_\kappa|\hat{h}|\psi_\lambda\rangle\,, && (3.26)
\end{aligned}$$

where the second line is obtained using equation 3.14. Inspection of equation 3.25 suggests the following definition of the one electron reduced spin orbital density matrix,

$$\bar{D}_{\kappa\lambda} = \langle \Psi | \hat{a}^\dagger_\kappa \hat{a}_\lambda | \Psi \rangle \,, \tag{3.27}$$

simplifying equation 3.25 to

$$h_{IJ} = \sum_{\kappa\lambda} h_{\kappa\lambda} \bar{D}^{IJ}_{\kappa\lambda}. \tag{3.28}$$

Thus we have succeeded in splitting the evaluation of the matrix elements h_{IJ}, into two terms. On the one hand the evaluation of the operator matrix elements with respect to the spin orbitals and on the other hand the evaluation of the one electron reduced spin orbital density matrix. Therefore once $h_{\kappa\lambda}$ has been obtained the matrix operator elements h_{IJ} may easily be obtained from the, now in matrix notation, one electron reduced density matrices $\bar{\mathbf{D}}_{\lambda\kappa}$. The situation may be further simplified if we are not interested in the evaluation of matrix elements of spin dependent operators (as is the case in this project), allowing us to work with the smaller one electron reduced density matrix

$$\mathbf{D}_{ij} = \bar{\mathbf{D}}_{i\alpha,j\alpha} + \bar{\mathbf{D}}_{i\beta,j\alpha}. \tag{3.29}$$

Therefore we may use $\mathbf{D}_{ij}$ to efficiently evaluate, given a set of states $|\Psi^I\rangle$, the matrix elements of any one electron operator we are interested in, such as for instance dipole transition moments or kinetic energy. It is insightful to study a one electron reduced density matrix of the HF state $|\Psi_0\rangle$. The matrix is in this case a scalar as we consider only one state, and as this state contains only one determinant the elements $D_{\kappa\lambda}$ may easily be seen to obey

$$D_{\kappa\lambda} = 2\delta_{\kappa\lambda}. \tag{3.30}$$

3.3.2 Two Electron Reduced Density Matrix

Following, in a closely analogous way, the steps that lead to the definition of $\mathbf{D}_{\kappa\lambda}$, we shall arrive at a definition for the two electron reduced spin orbital density matrix by considering the operator matrix elements of the two electron operator $\hat{g}$. In this case we may write the operator matrix elements as

$$\begin{aligned}
g_{IJ} &= \sum_{vw} c_v c_w \langle \mathbf{k}_v | \hat{g} | \mathbf{k}_w \rangle && (3.31)\\
&= \sum_{vw} \sum_{\kappa\lambda\mu\eta} \langle \kappa\lambda | \hat{g} | \mu\eta \rangle \, c_v c_w \langle \mathbf{k}_v | \hat{a}^\dagger_\kappa \hat{a}^\dagger_\mu \hat{a}_\lambda \hat{a}_\eta | \mathbf{k}_w \rangle && (3.32)\\
&= \sum_{\kappa\lambda\mu\eta} g_{\kappa\lambda\mu\eta} \langle \Psi^I | \hat{a}^\dagger_\kappa \hat{a}^\dagger_\mu \hat{a}_\lambda \hat{a}_\eta | \Psi^J \rangle \,, && (3.33)\\
& && (3.34)
\end{aligned}$$

where we $g_{\kappa\lambda\mu\eta}$ is defined in equation 2.45. As was done for the one electron case we thus use equation 3.33 to motivate the definition of the equivalent two electron matrix

$$\bar{d}^{IJ}_{\kappa\lambda\mu\eta} = \langle \Psi^I | \hat{a}^\dagger_\kappa \hat{a}^\dagger_\mu \hat{a}_\lambda \hat{a}_\eta | \Psi^J \rangle \,, \tag{3.35}$$

turning equation 2.45 into

$$g_{IJ} = \sum_{\kappa\lambda\mu\eta} g_{\kappa\lambda\mu\eta} \bar{d}^{IJ}_{\kappa\lambda\mu\eta}. \tag{3.36}$$

As in the on electron case we may reduce the number of terms appearing in this sum by turning our attention only two spin independent Hamiltonian. To this end we define now the two electron reduced density matrix as (using now matrix notation, where $\mathbf{d}_{\kappa\lambda\mu\eta}$ is a square two dimensional matrix with the number rows corresponding to the number of states under consideration)

$$\mathbf{d}_{ijkl} = \bar{\mathbf{d}}_{i\alpha,j\alpha,k\alpha,l\alpha} + \bar{\mathbf{d}}_{i\beta,j\beta,k\beta,l\beta} + \bar{\mathbf{d}}_{i\alpha,j\alpha,k\beta,l\beta} + \bar{\mathbf{d}}_{i\beta,j\beta,k\alpha,l\alpha}, \tag{3.37}$$

drastically reducing the number of term that have to be considered in equations 3.36. The utility of the two electron reduced density is equivalent to that of the one electron case. That is, once having calculated the necessary orbital integrals g_{ijkl} the matrix elements of any two states may be computed fairly efficiently using $\mathbf{d}_{ijkl}$. We shall return to this point in chapter 9.

3.4 Natural Orbitals and Occupation Numbers

Equipped with the definition of the one electron reduced density matrix we may now present a useful concept which may be used (among other things) to achieve faster convergence in CI theory; the so called natural orbitals. Thus far we have assumed to be working with HF orbitals to carry out a CI calculation. While the occupied orbitals obtained from an HF calculation, represent fairly useful orbitals to work with, the same is often times not the case for the virtual HF orbitals, excitations to which we consider in CI theory (heuristically this can be motivated by noting, that the self consistent nature of the Fock operator in equation 2.28 only extends to the occupied orbitals). This results in the converged CI expansion likely containing a large number of determinants involving many virtual orbitals. We may thus naturally enquire, if there is a better set of orbitals to begin with, leading to faster convergence and smaller CI expansions. A valid way to modify the orbitals with which to work are unitary transformations among them. In fact we shall see later any unitary transformation of the set of HF orbitals will give the same result in CI theory. Thus the question is now to find such a unitary transformation improving on the HF case.

One such set of orbitals is given by the so called natural orbitals. The natural orbital of some state Ψ^I are defined as those orbitals ψ_{NO} that if the CI vector of Ψ^I is transformed to read $\Psi^I = \sum_v C^I_{v,\mathrm{NO}} |\mathbf{k}_{v,\mathrm{NO}}\rangle$, the matrix d^{II}_{ij} fulfils

$$D^{II}_{ij} = w_i \delta_{ij}. \tag{3.38}$$

The diagonal elements of ω_i of D^{II}_{ij} are then referred to as the occupation numbers of the natural orbitals of the state $|\Psi^I\rangle$, giving an indication of their relative importance in the the expansion of $|\Psi^I\rangle$ in terms of determinants over the set of natural orbitals. Therefore we may expect a CI expansion of some state to be more concise if expressed in the natural orbitals of that states. Note that this diagonalization via a unitary matrix of D^{II}_{ij} is only possible because $D^{II}_{ij} = D^{II}_{ji}$, which does not in general hold for D^{IJ}_{ij}.

Clearly the strategy of constructing the natural orbitals as a possible improved starting point for a CI calculation is beginning to look circular, requiring prior knowledge of the CI solution (a point made even more obious by recalling the properties of the one electron density matrix of the HF ground state, given in section 3.3.1). In practice what is therefore done is an iterative process, including a small number of configurations based on the HF orbitals. The natural orbitals of the resulting CI vector are then computed and the process is repeated iteratively starting from the natural orbitals of the previous step[76, 77, 78].

3.5 Multi Configuration Self Consistent Field Theory (MCSCF)

Truncating the expansion of Ψ_{CI} as we did so far, i.e. limiting the maximum number of excitations from a reference function, is by no means the only way to control the size of the CI vector. A natural

alternative would be to divide the orbitals into three categories according to the relevance we expect them to have in the final CI expansion; inactive orbitals, active orbitals and virtual orbitals. With in the (small) set of active orbitals we allow for all possible excitations (that is to say a full CI of manageable size), whereas the inactive orbitals are doubly occupied always, and the virtual orbitals empty always. This method is referred to as a complete active space (CAS) calculation[79, 80].

A crucial difference between an MCSCF and a CI calculation is that, unlike in the CI case, the particular set of orbitals we work with (obtainable through rotations among the HF orbitals) does now no longer only contribute to the speed of convergence, but instead the results change with the choice of orbitals contained in the active space. Therefore the main technical challenge of MCSCF, compared to CI(SDT$\cdots$) is how to incorporate the optimization of orbitals along side the optimization of the CI vector, to ensure converged results within the space of possible CI vectors and orbital rotations. Before addressing orbital rotations explicitly in second quantization formalism, we shall briefly review different approaches that may be used to divide the orbitals into inactive, active and virtual orbitals.

In addition to the CAS method, we may wish to provide a more refined approach for greater flexibility. This leads to the restricted active space (RAS) method[81, 82, 83], subdividing the orbitals into inactive,RAS1,RAS2,RAS3 and virtual orbitals. The RAS2 space is equivalent to the set of active orbitals in the CAS method, within which all excitations are permitted. The RAS1 space is constructed from orbitals whose occupation we suspect to be generally large but not necessarily large enough to be considered inactive. Therefore the RAS1 space is characterized by the number of holes we permit (for example along one hole in a RAS1 space of three orbitals forces all determinants in the CI expansion to contain at least a total of 5 electrons in these orbitals). Conversely the RAS3 space is constructed from orbitals whose occupation we expect to be small in general, but not small enough to consider them virtual. Therefore the RAS3 space is characterized by the maximum total number of electrons we allow to be excited to the orbitals, in any determinant of the CI expansion. For even greater flexibility one may wish to consider the generalized active space (GAS) method[84], allowing for more user defined subdivision of space, each possibly subjected to some limitation on excitations. Of these three methods we have used CASSCF and RASSCF extensively in this project. Figure 3.1 shows a schematic description of how the wave function is expanded in terms of determinants in these methodologies.

As we mentioned at the outset of introducing MCSCF theory, the primary motivation was to reduce the number of configurations to a manageable number (while also retaining the possibility of CI theory to yield electronic states other than the ground state). That being said it is clear that within an MCSCF implementation (CAS,RAS,GAS) the size of the active space and the number electrons we distribute in them limit the size of system we can treat. The CAS method such as presented starts running into problems beyond CAS(16,16) (that is 16 electron distributed among 16 active orbitals). More recently methods have been developed building on the CAS formalism to allow for the treatment of larger active space. Some of these methods are the density-matrix renormalization group (DMRG) [85, 86], the variational calculation of the two electron reduced density matrix (2-RDM) [87] or the graphical-contracted-function (GCF) MCSCF method [88]. None of these methods have established themselves as a standard but they do represent important advances in overcoming limitations of traditional MCSCF methods applied to large active spaces.

Due to the huge size of the CI vector in a full CI calculation, almost all wave functions based modern quantum chemistry incorporates electron correlation using some active space methodology. This leads to manageable CI vectors and allows for treatment of fairly complex molecules at a reasonable computational expense. Most QCPs furthermore allow to calculate the electronic states of a molecule reflecting the point group symmetry of the molecule. By therefore allowing in a certain CI expansion only those determinants that are in the same irreducible representation of the point group of the molecule leads to a further reduction in the size of the CI expansion. Naturally this is most drastic for very symmetric molecules, such as for example atoms or (homonuclear) diatomic molecules. For these specific, very symmetric examples one must take into account the infinite number of irreducible representations (diatomic $C_{\infty v}$, homonuclear diatomic $D_{\infty h}$). The most symmetric point group offered by QCPs tends to be D_{2h} with 8 irreducible representations.

After these general considerations of MCSCF we shall now turn our attention to the mathematical challenge of considering optimization in the much larger parameter space allowing also for orbital rota-

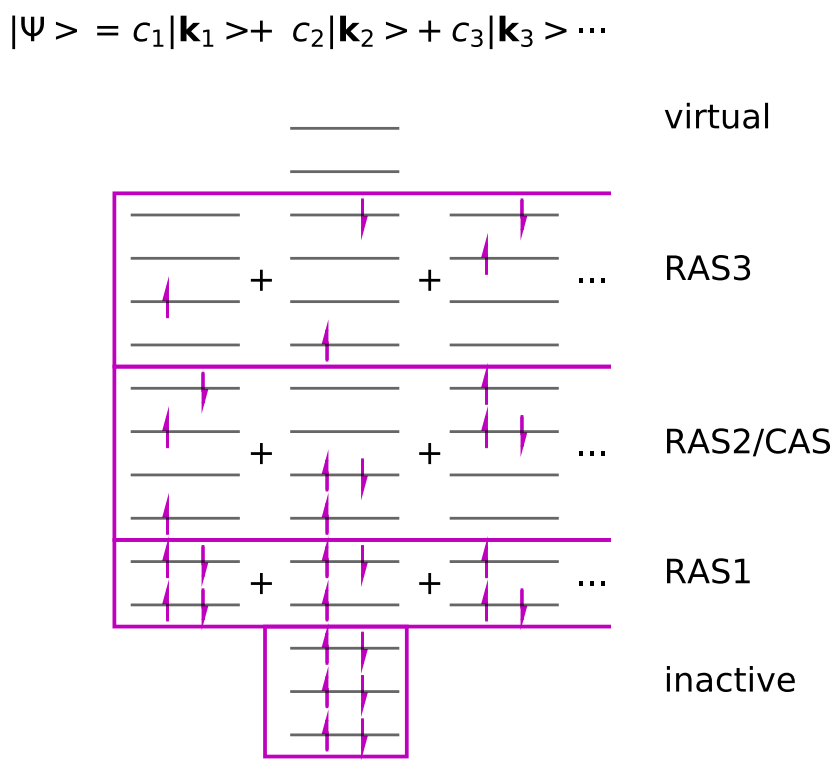

Figure 3.1: Schematic depiction of CAS/RAS methodologies, showing the different subset of orbitals. In the present case the RAS1 space contains two orbitals and allows for at most one hole ($n_{RAS1} = 1$). The RAS3 case contains four orbitals an allows for at most two electrons occupying these ($n_{RAS3} = 2$). The four RAS2 oribtals have at most five electrons distributed among them. The wavefunction of some state Ψ is then built as a linear combination of all possible determinants subject to these restrictions. This case is simplified to a CAS approach if we set $n_{RAS1} = 0$ and $n_{RAS3} = 0$.

tions.

3.5.1 Orbital Optimization

In MCSCF the set of orbitals is optimized by performing unitary rotations $\mathbf{U}$ among all orbitals (inactive,active,virtual), quantified by the rotational parameter $\boldsymbol{\kappa}$. To this end we make use of the fact, that any unitary matrix $\mathbf{U}$ may be written as the exponential of an anti Hermitian matrix, so that for some U

$$\mathbf{U} = e^{-\boldsymbol{\kappa}}. \tag{3.39}$$

Considering now some configuration $|\mathrm{k}'\rangle$ in the transformed orbitals, with corresponding creation and annihilation operators $a'_I = \sum_J a_J U_{IJ}$ and $a'^{\dagger}_I = \sum_J a_J U^*_{IJ}$, gives

$$|\mathbf{k}'\rangle = \left[\prod_\tau \left(a^{\dagger\prime}_\tau\right)^{k_\tau}\right] |\mathrm{vac}\rangle\,. \tag{3.40}$$

To make progress from here we consider the operator $\hat{\kappa} = \sum_{IJ} \kappa_{IJ} a^\dagger_I a_J$ and use the BCH expansion to

write

$$\begin{aligned} e^{-\hat{\kappa}}\hat{a}_i e^{\hat{\kappa}} &= \hat{a}_i + [\hat{a}_i, \hat{\kappa}] + \frac{1}{2}\left[[\hat{a}_i, \hat{\kappa}], \hat{\kappa}\right] + \cdots \\ &= \sum_{n=0}^{\infty} \frac{1}{n!}[\hat{a}_i, \hat{\kappa}]_n, \end{aligned} \tag{3.41}$$

where the second line introduces the notation $[\cdot,\cdot]_n$. We can prove (easily done by recursion), that

$$[\hat{a}_I, \hat{\kappa}]_n = \frac{1}{n!}\sum_J a_J \left(\boldsymbol{\kappa}^n\right)_{IJ}, \tag{3.42}$$

which allows to rewrite equation 3.41 as

$$e^{-\hat{\kappa}}\hat{a}_i e^{\hat{\kappa}} = \sum_J a_J e^{\boldsymbol{\kappa}}_{IJ} = \sum_J a_J U_{IJ} = a'_I \quad \text{and} \tag{3.43}$$

$$e^{-\hat{\kappa}}\hat{a}_i^\dagger e^{\hat{\kappa}} = \hat{a}_I'^\dagger, \tag{3.44}$$

the second line of which, can be obtained in close analogy to the first. Using this result in equation 3.40 yields,

$$|\mathbf{k}'\rangle = \left[\prod_I \left(e^{-\hat{\kappa}} a_I^\dagger e^{\hat{\kappa}}\right)^{k'_I}\right] |\text{vac}\rangle \tag{3.45}$$

$$= e^{-\hat{\kappa}}\left[\prod_I \left(a_I^\dagger\right)^{k'_I}\right] e^{\hat{\kappa}} |\text{vac}\rangle \tag{3.46}$$

$$= e^{-\hat{\kappa}} |\mathbf{k}\rangle, \tag{3.47}$$

where we have made use of the fact, that the vacuum state is not effected by a unitary transform. By restricting the possible rotations to those that do not alter the spin, we may reduce the number of parameters by writing $\hat{\kappa}$ as

$$\hat{\kappa} = \sum_{i,j} k_{ij} E_{ij} = \sum_{i,j} k_{ij}(a_{i\alpha}a_{j\alpha} + a_{i\beta}a_{j\beta}). \tag{3.48}$$

This, if we furthermore constrict ourselves to real orbitals, implies $\boldsymbol{\kappa}$ to be anti symmetric, reducing the number of independent parameters even further to give,

$$\hat{\kappa} = \sum_{i>j} k_{ij} E^-_{ij} = \sum_{i>j} k_{ij}(E_{ij} - E_{ji}), \tag{3.49}$$

where E_{ij} and E^-_{ij} are the excitation and antisymmetric excitation operators, respectively. These reductions of parameter space and equation 3.47 suggest the straightforward parametrized expression of the MCSCF wave function in terms of the to entities $\boldsymbol{\kappa}$ and $\mathbf{C}$, to be optimized:

$$|\boldsymbol{\kappa}, \mathbf{C}\rangle = e^{-\hat{\kappa}} \sum_i^{N_{\text{det}}} C_i |\text{det}_i\rangle \tag{3.50}$$

running over all configurations dictated by the active space. In a similar fashion as to what was done in the HF case we proceed by variationally optimizing the energy by finding those parameters that minimize

$$E = \min_{\boldsymbol{\kappa},\mathbf{C}} \frac{\langle \boldsymbol{\kappa}, \mathbf{C}|\mathcal{H}|\boldsymbol{\kappa}, \mathbf{C}\rangle}{\langle \boldsymbol{\kappa}, \mathbf{C}|\boldsymbol{\kappa}, \mathbf{C}\rangle}, \tag{3.51}$$

where it is convenient to parametrize the normalized $|\boldsymbol{\kappa}\rangle$ with respect to some normalized reference state $|0\rangle$ and $\hat{P} = 1 - |0\rangle\langle 0|$ being the operator that removes reference contributions from some state:

$$|\boldsymbol{\kappa}, \mathbf{C}\rangle = e^{-\hat{\kappa}} \frac{|0\rangle + \hat{P}|\mathbf{c}\rangle}{\sqrt{1 + \langle \mathbf{c}|\hat{P}|\mathbf{c}\rangle}}, . \tag{3.52}$$

This parametrization ensures normalization as well as facilitating the treatment of redundancies, as will be discussed in more detail below. Next we express the energy $E(\boldsymbol{\kappa}, \mathbf{c})$ in terms of this parametrization giving

$$\begin{aligned} E(\boldsymbol{\kappa}, \mathbf{c}) &= \frac{(\langle \mathbf{c}|\hat{P} + \langle 0|)e^{\hat{\boldsymbol{\kappa}}}\hat{\mathcal{H}}e^{-\hat{\boldsymbol{\kappa}}}(|0\rangle + \hat{P}|\mathbf{c}\rangle)}{1 + \langle \mathbf{c}|\hat{P}|\mathbf{c}\rangle} & (3.53) \\ &= \frac{N(\boldsymbol{\lambda})}{D(\mathbf{c})}, & (3.54) \end{aligned}$$

where we have introduced the vector $\boldsymbol{\lambda}$ of all variational parameters (orbital rotations and CI vector), given by $\boldsymbol{\lambda} = (\boldsymbol{\kappa}, \mathbf{C})^{\mathrm{T}}$. Although this problem is in appearance similar in idea to the HF approach, it is considerably more complex due to the additional freedom introduced by the parameter governing orbital rotations. We shall not endeavour a complete exposition of it here but outline in rather broad strokes of how the MCSCF wave function may be obtained from 3.51.

In HF theory it is possible to find solutions by expanding to first order in the variational parameter, leading to the Roothan equation solved by the SCF method. Similar approaches have been found to converge poorly for MCSCF theories; a second order expansion must be made yielding

$$\begin{aligned} Q(\boldsymbol{\lambda}) &= E_{\boldsymbol{\lambda}=0} + \sum_i \left(\frac{\partial E}{\partial \lambda_i}\right)_{\boldsymbol{\lambda}=0} \lambda_i + \frac{1}{2}\sum_{ij} \lambda_i \left(\frac{\partial^2 E}{\partial \lambda_i \partial \lambda_j}\right)_{\boldsymbol{\lambda}=0} \lambda_j & (3.55) \\ &= E_{\boldsymbol{\lambda}=0} + \mathbf{g}^{\mathrm{T}}\boldsymbol{\lambda} + \frac{1}{2}\boldsymbol{\lambda}^{\mathrm{T}}\mathbf{H}\boldsymbol{\lambda}, \end{aligned}$$

where we used the letter Q to denote the energy expanded in this way.

The aim must now be to find a strategy that allows for the determination of stationary points of 3.56. Broadly speaking any approach to this end can be split up into two steps closely analogouse to the CI method: an outer step and an inner step. The outer step will be the way in which we iteratively try to a approach a minimum of equation 3.56, whereas the inner step will be concerned with the calculation of the matrix elements and operations that are necessary for each outer step. We shall deal with the "inner part" of the algorithm first. From equation 3.56 it should be clear that the objects necessary to perform any kind of outer procedure bringing us closer to a minimum are the gradients $\mathbf{g}$ and the Hessian $\mathbf{H}$. These can be obtained from equation 3.54 by multiplication with $D(\mathbf{c})$ and subsequent differentiation (denoting $\partial/\partial\lambda_i$ by ∂_i)

$$\begin{aligned} g_i &= [\partial_i N - E\partial_i D]_{\boldsymbol{\lambda}=0} & (3.56) \\ h_{ij} &= [\partial_i\partial_j N - g_i\partial_j D - g_j\partial_i D - E\partial_i\partial_j D]_{\boldsymbol{\lambda}=0} & (3.57) \end{aligned}$$

We introduce now the notation ∂_i^c and ∂_{pq}^o dividing the differential operator into two groups. The former denote differentiation by a CI coefficient c_i and the latter by an element E_{pq} of the orbital rotation matrix. We note the following

$$\begin{aligned} [\partial_i D]_{\boldsymbol{\lambda}=0} &= 0 & (3.58) \\ [\partial_i^c N]_{\boldsymbol{\lambda}=0} &= 2\langle i|\hat{P}\hat{\mathcal{H}}|0\rangle & (3.59) \\ [\partial_i^o N]_{\boldsymbol{\lambda}=0} &= \langle 0|[E_{pq}^-, \hat{\mathcal{H}}]|0\rangle & (3.60) \\ \left[\partial_{pq}^o\partial_i D\right]_{\boldsymbol{\lambda}=0} &= 0 & (3.61) \\ \left[\partial_i^c\partial_j^c D\right]_{\boldsymbol{\lambda}=0} &= 2\langle i|j\rangle & (3.62) \\ \left[\partial_i^c\partial_j^c N\right]_{\boldsymbol{\lambda}=0} &= 2\langle i|\hat{P}\hat{\mathcal{H}}|j\rangle & (3.63) \\ \left[\partial_{pq}^o\partial_j^c N\right]_{\boldsymbol{\lambda}=0} &= 2\langle i|\hat{P}[E_{pq}^-, \hat{\mathcal{H}}]|0\rangle & (3.64) \\ \left[\partial_{pq}^o\partial_{rs}^o N\right]_{\boldsymbol{\lambda}=0} &= \langle 0|[E_{pq}^-, [E_{rs}^-, \hat{\mathcal{H}}]] + [E_{rs}^-, [E_{pq}^-, \hat{\mathcal{H}}]]|0\rangle\,. & (3.65) \end{aligned}$$

From these expression we may easily construct $\mathbf{g}$ and $\mathbf{H}$. It is insightful to consider the resulting expression for $\mathbf{g}$ explicitly. At a stationary point the gradient must therefore satisfy

$$g_i^c = 2\langle i|\hat{P}\mathcal{H}|0\rangle = 0 \tag{3.66}$$
$$g_i^o = \langle 0|[E_{pq}^-, \hat{\mathcal{H}}]|0\rangle = 0, \tag{3.67}$$

where $\mathbf{g}^c$ and $\mathbf{g}^o$ are the CI and orbital gradients, respectively. This result is referred to as the generalized Brillouin Theorem (GBT).

Thus expressions have been established in principal allowing for the calculation of all terms in equation 3.56. The next step must thus be to identify the energetic minima, as given by the condition $\partial_i Q = 0$ resulting in the eigenvalue problem

$$\mathbf{H}\boldsymbol{\lambda} = -\mathbf{g}. \tag{3.68}$$

While this appears to be a straightforward problem allowances must be made for several circumstances complicating the problem. The first issue (as we shall explore in more detail in the next section) is that given a solution $\boldsymbol{\lambda}$, any $\boldsymbol{\lambda} + \alpha|0\rangle$ is an equally valid solution. This is easily remedied by replacing $\boldsymbol{\lambda}$ by $\mathbf{P}\boldsymbol{\lambda}$ in equation 3.68, where we have introduced the matrix representation of the operator $\hat{P}$, given by $1 - \boldsymbol{\xi}_0\boldsymbol{\xi}_0^{\mathrm{T}}$, with $\boldsymbol{\xi}_0$ denoting the vector $(\mathbf{C}_0, 0)$, specifying the reference configuration $e^0|0\rangle$. The more serious issue is that the second order expansion is (as compared done with the CI case) done in the much more complex parameters space including the orbital rotations. Therefore the methods introduced in the CI sections are likely to produce serious issue in converging to the correct solution. Different methods exist to solve this problems, based on introducing a parameter. This parameter referred to as a trust radius restricts the correction to the CI vector of the previous $\boldsymbol{\xi}_0$ step to have a given length, thus defining a circle of some radius around ξ_0, within which we trust the surface $E(\boldsymbol{\lambda})$ to be very close to quadratic in $\boldsymbol{\lambda}$. Regardless of the details of how this is accomplished, at the end of every outer iteration stands a matrix eigenvalue problems requiring the inner iterations to find the next $\boldsymbol{\lambda}$. We consider as an example the Newton trust region method[89]. The eigenvalue problem in this case reads

$$(\mathbf{H} - \mu 1)\mathbf{P}\lambda = -\mathbf{g}., \tag{3.69}$$

introducing the so called level shift parameter μ, which must be determined at every step. The expensive part of the inner iteration in these method generally involves the repeated matrix vector multiplication involving in some form the Hessian $\mathbf{H}$.

3.5.2 State Average MCSCF

As we mentioned at the beginning of the sections, like CI theory, MCSCF is capable of simultaneously optimizing multiple electronic states (e.g. ground states and one or several excited states). As we shall later explore the properties of some highly excited states a comment is in order on how this is achieved. Naturally one may carry out independent MCSCF calculations for every state of interest, while ensuring that the system does not "variationally collapse" back to the ground state and ensuring that the resulting state are orthogonal (for applications see for example references [90, 91]). There are two difficulties associated with this approach; one of a more fundamental nature, the other of a computational nature. The fundamental disadvantage of separate orbital optimization is the problem of so called root flipping. Root flipping refers to a situation in which the orbitals are optimized with the aim of representing some particular non-ground state. In the course of this the orbitals may become increasingly ill-suited to represent the ground state. Under such circumstances the eigenvalues of two states may suddenly change change their energetic ordering, leading to convergence not to a minimum, but rather a saddle point in orbital space, no longer ensuring that the energy obtained represents an upper bound (see reference[92] and references therein). Furthermore it should be be clear that any such approach inevitably leads to a description of different states, in which each states is defined using its own set of orbitals, optimized for that state in particular. Thus the calculations of reduced density matrices (necessary for the calculation of operator matrix elements) is complicated by the fact that the CI vector belonging to different sets of orbitals are no longer orthogonal, meaning the Slater Condon rules are no

longer applicable. In principal this can problem can be solved by using a so called biorthonormalization procedure, but in the case of this project, as we shall see later this presents a substantial complications, the implementation of which was not undertaken in this work.

The alternative to individually optimizing the MCSCF states, is the method of State Averaged MCSCF[93] which circumvents both of these problems. As the name suggests, rather than minimizing the energy of an individual state we now wish to minimize the average energy

$$E(\boldsymbol{\lambda}) = \sum_I w_I \langle I|\hat{\mathcal{H}}|I\rangle \,, \tag{3.70}$$

weighted by w_I, where the weights are almost always chosen to be equal. We may expect the resulting states to be less optimal than the results as they would be yielded by completely independent optimization. And while this is the case, in all applications in this work the results prove satisfactory while providing significantly simplification by virtue of working with only one set of orbitals.

3.5.3 Redundancies

When changing the parameters $\boldsymbol{\lambda}$ in trying to find the optimal energy certain classes of changes are found to result in no change in the energy of $|\lambda\rangle$. These changes are referred to as redundancies and should be excluded in as far as possible for the sake of stability and efficiency. A general treatment of redundancies, would identify the minimal set $\boldsymbol{\lambda}_m$ of parameters necessary for the expansion of any $|\lambda\rangle$. We shall however content ourselves with identifying a set of sufficient conditions for redundancy leaving open the question of possible additional redundancies. To begin note that a redundancy must manifest itself as a non trivial solution for

$$\begin{aligned} \hat{\mathcal{H}}\,|0\rangle &= \hat{\mathcal{H}} e^{-\hat{\kappa}}(|0\rangle + \hat{P}\,|\mathbf{c}\rangle) && (3.71)\\ &= \hat{\mathcal{H}}(1-\hat{\kappa}\cdots)(|0\rangle + \hat{P}\,|\mathbf{c}\rangle), && (3.72) \end{aligned}$$

where in the second line we expanded to orbital rotation operator. This upon retaining terms in first order of parameters only yields a condition for redundancy given by

$$\hat{\kappa}\,|0\rangle = \hat{P}\,|\mathbf{c}\rangle \,. \tag{3.73}$$

Despite neglecting higher order terms this does in fact represent a condition for redundancy, albeit a sufficient and not necessary one. We may argue the sufficiency by noting that if sets of orbital rotations form a group (as is readily established) then their being disregarded from the set of parameters leaves the description of the wave function unaffected to any order in $\hat{\kappa}$. A trivial solution to equation 3.73 is $|\mathbf{c}\rangle = \alpha\,|0\rangle$, making now obvious the choice of parametrization of equation 3.52. A set of non trivial redundancies can thus be identified by looking for those orbital E^-_{ij} that may be expressed as a linear combination of all remaining parameters,

$$E^-_{ij}\,|0\rangle = \sum_i c_i \hat{P}\,|i\rangle + \sum_{i'j'\neq ij} \kappa_{i'j'} E^-_{i'j'}\,|0\rangle \tag{3.74}$$

where we shall further restrict ourselves by considering only redundancies expressible as

$$\begin{aligned} E^-_{ij}\,|0\rangle &= \sum_i c_i \hat{P}\,|i\rangle && (3.75)\\ &= \sum_i c_i\,|i\rangle \,, && (3.76) \end{aligned}$$

where in the second line we have used the orthogonality of $|0\rangle$ and $E^-_{ij}\,|0\rangle$ to omit the projection operator. We may now straightforwardly identify two classes of redundant rotations. If i and j both correspond to

inactive (that is doubly occupied orbitals), necessarily the creation operators contained in the definition of E^- imply $E^-_{ij}|0\rangle = 0 = \sum_i c_i \hat{P}|i\rangle$ which is trivially satisfied for $\mathbf{c} = 0$. An analogous argument can be made for i and j both being inactive (where now the annihilation operators in E^- render $E^-_{ij}|0\rangle$ zero). Therefore any rotation of the type inactive-inactive or virtual-virtual is redundant and should be excluded from the sum in equation 3.49. The situation is only slightly more complicate for active-active rotations. The left hand side of equation 3.76 is then no longer trivially zero, but any such rotation does leave virtual and inactive orbitals doubly occupied and empty, respectively. As all such configurations are included in the CI expansion a vector $\mathbf{c}$ satisfying equation 3.76 must exist. Analogous cases may easily be made for RAS1-RAS1 and RAS3-RAS3 rotations by arguing that the number of holes or electrons is preserved by E^-. Note also that by simple extension of the active space to all orbitals we have established what we eluded to in the discussion of configuration interactions, namely a full CI expansion will yield the correct energy for any set of orthonormal starting orbitals.

3.5.4 Configuration State Functions

One important aspect, which in working now with multiple determinants, rather than a single determinant closed shell expression is that different determinants may correspond to different spin states. As in this project we are not concerned with relativistic effects, the Hamiltonian does not couple states of different total or projected spin. Therefore it is enough to expand Ψ_{CI} in terms of eigenfunctions of the spin operators $\hat{\mathbf{S}}^2$ and $\hat{S}_z$, retaining only those eigenfunctions in the expansion antisymmetric functions corresponding to the same eigenvalues of these operators. The Slater determinants as we have used them so far are ill suited for this task as they are eigenfunctions of $\hat{S}_z$ only, but not of $\hat{\mathbf{S}}^{\mathbf{2}}$. This is easily understood by writing an arbitrary Slater determinant $|\mathbf{k}\rangle$ as a string of β creation operator and α creation operators:

$$|\mathbf{k}_\alpha \mathbf{k}_\beta\rangle = \left[\prod_{i=1} \left(a^\dagger_{i\alpha}\right)^{k_{i\alpha}}\right] \left[\prod_{i=1} \left(a^\dagger_{i\beta}\right)^{k_{i\beta}}\right] |\text{vac}\rangle\,, \tag{3.77}$$

acting on it with $\hat{S}_z$ and $\hat{\mathbf{S}}^2$ and applying equations 3.11, 3.8, 3.13 and 3.13. For the former we find

$$S_z |\mathbf{k}_\alpha \mathbf{k}_\beta\rangle = \frac{1}{2}(N_\alpha - N_\beta)|\mathbf{k}_\alpha \mathbf{k}_\beta\rangle = m_s |\mathbf{k}\rangle\,, \tag{3.78}$$

whereas as the latter satisfies the considerably more complicated expression

$$\mathbf{S}^2 |\mathbf{k}_\alpha \mathbf{k}_\beta\rangle = \frac{1}{4}\left[(N_\alpha - N_\beta)^2 + 2(N_\alpha - N_\beta)\right]|\mathbf{k}_\alpha \mathbf{k}_\beta\rangle + \tag{3.79}$$

$$\prod \left(a^\dagger_{i\alpha} a^\dagger_{i\beta}\right)^{k_{i\alpha}k_{i\beta}} \left[S_-, \prod \left(a^\dagger_{i\alpha}\right)^{k_{i\alpha}(1-k_{i\beta})}\right] \left[S_+, \prod \left(a^\dagger_{i\beta}\right)^{k_{i\beta}(1-k_{i\alpha})}\right] |\text{vac}\rangle\,, \tag{3.80}$$

which renders the Slater determinant an eigenfunction of $\mathbf{S}^2$ only if it consist just of α spins, just of β spins or equal numbers of both for the same spatial orbitals (which is the closed shell case). We therefore wish to construct from the determinants the spin adapted set of so called configuration state functions (CSFs), spanning the same space but each being an eigenfunction of both, S_z and $\mathbf{S}^2$. The root of the problem is that $N_{i\sigma}$ do not commute with $\mathbf{S}^2$. Equation 3.12, however, implies that we can construct simultaneous eigenfunctions of $\mathbf{S}^2$,S_z and N_i. These will be the CSFs. Note that by construction, unlike the determinants, these will no longer be eigenfunctions of the occupation number operator $\hat{N}_{i\sigma}$ (defined in equation 3.4).

There a several schemes for the construction of the CSFs. The genealogical coupling scheme[94], the graphical representation of model spaces (GRMS) and the graphical unitary group approach (GUGA)[95, 96], of which the last has established itself as the de facto standard.

3.5.5 Beyond MCSCF

Having presented MCSCF theory we shall now point out an inherent shortcoming and will conclude this section by commenting on a few widely used method not mentioned so far which may build on

CASSCF or RASSCF results. To understand the said shortcoming it is necessary to consider the nature of electron in some more detail. Electron correlation may be said to divide into static correlation and dynamic correlation. Static correlation is a consequence of a molecular state being describe by several degenerate configurations whereas dynamical correlation must be included to describe the correlated motion of the electrons in the system at hand. MCSCF methods are very successful in accounting for the former requiring for its description comparatively few configurations. Dynamical correlation on the other hand requires much large numbers of configurations to be taken into account. Therefore, while MCSCF by including static correlation tends to give qualitatively correct results, we must include also dynamical correlation if greater accuracy is required.

One common approach is two perform a CI calculation using as reference states, those that were obtained from a prior MCSCF calculation and allowing certain certain classes of excitations, leading to determinants (say all singles or doubles excitations) that were not not included in the MCSCF calculation. This approach is referred to as multi reference CI (MRCI). This combination of MCSCF and CISD(T$\cdots$) has proved a valuable tool in the calculation of accurate electronic structure calculations. An alternative approach which is routinely implemented in QCPs, and which we have not yet discussed is provided by Perturbation Theory applied to multi configuration states (CASPT). CASPT has the advantage that built on top a MCSCF calculation it is somewhat more efficient than a CI calculation while yielding comparably good results. A drawback however is that CASPT (like all perturbation theories) is not variational, meaning we can not relay on the resulting energies of the states being guaranteed to be higher in energy than the true eigen energies.

The methods presented in this and the previous chapter, represent much of what modern QC is based on, and we have used especially the MCSCF method extensively, modifying in place the standard MOLCAS implementation of it to suit our need. One aspect that we have addressed only in passing so far are the basis functions, in which to expand the the molecular orbitals and thus the wavefunction in. As this work was designated in no small part to the design and use of a novel type of basis set, the next chapter is dedicated to the kind of function used as basis function in QC calculations.

4 Basis Sets - Bound States

The previous two chapters have outlined the theoretical basics for solving within and beyond the Hartree Fock approximation, the Schröding Equation as applied to multi electronic molecules, demonstrating how, with a basis set and a nuclear geometry, sets of spin orbitals can be obtained to express the solution in terms of. It was seen that for all of these calculations the main ingredients are the integrals of the type: $\mathbf{S}$,$\mathbf{H}^{\text{core}}$ and g_{pqrs}; all of which integrals of two or more basis functions. Thus it should be apparent that the quality of any Hartree Fock calculation (and any subsequent calculation building on it) will always only be as good as the set of basis functions that was used in that calculation. It should come as no surprise that in general larger basis sets yield better results, but require more computational effort to deal with. Therefore one normally finds oneself engaged in compromising between computational efficiency and computational accuracy. However much can be gained be making an initially smart choice of basis function.

A few general considerations on the mathematical properties any set of basis functions should so a to stand a chance to give reasonable results, are in order:

1. Analyticity[1]: For the efficient evaluation of integrals in polyatomic molecules with potentially low symmetry the orbitals must be expanded in terms of basis functions with analytical expressions. Clearly, the more efficient the analytical evaluation is in a particular basis set, the more efficient the calculation will be.

2. Completeness: As mentioned before, for a complete description of the problem, the basis set should in principle be able to span the entire Hilbert space of square integrable functions in three dimensional space $\mathcal{L}^2(\mathbb{R}^3)$. Clearly we have to restrict ourselves to a finite basis set. But in the spirit of *ab initio* calculations it should be of such design so as to allow the systematic expansion yielding a complete basis set in the limit of infinitely many basis functions.

3. Convergence: Given some way to generate basis functions, it should be the case that only a reasonably small number of basis functions are necessary to yield satisfactory results.

The most obvious way to systematically produce a set of basis functions in accordance with these properties, is by generating them as solution to the Schrödinger Equation subject to a Hamiltonian with known solution. The (infinitely many) eigenfunctions of any Hermitian operator constitute a complete orthogonal (orthonormal in the case of bound states) set of basis functions. As previously mentioned we are interested in analytical functions, restricting the choice of Hamiltonian to but a few. Given such a set of analytically known eigenfunctions of some Hamiltonian, we therefore have a basis set in accordance with the first two of the three aforementioned properties.

In order to fulfil the third property it is intuitive that this is probably best achieved by generating basis functions from a Hamiltonian that mimics as best as possible the physics of the molecule whose solution we wish to obtain. From these considerations quite naturally emerges the idea to construct the basis set by viewing a molecule as a collection of atoms and centring a set of basis functions at each atomic site. To account for the difference in atomic structure of different elements it is to be expected that different basis sets are necessary for different atomic sets, depending on the elements comprising the molecule at hand. Given Hydrogen as the only element whose solution is available analytically, the Hydrogen orbitals

[1] An alternative approach to the algebraic expansion in a set of basis function is to use a numerical representation in a grid[97, 98]. These methods are only mentioned for completeness sake and we shall not concern ourselves with then.

are the most obvious candidate as a starting point for generating such basis sets serving for the different atoms in a molecule.

In addition to identifying a solvable reference problem to yield a first guess of basis functions, it is important to note that the kind of basis functions that will yield satisfactory results crucially depends on us being interested in bound states or scattering states. In order for the basis set to yield succinct expansions of the wave function, the basis functions should mirror the qualitative differences between the two situations. In this chapter we shall focus on bound states only.

In the interest of completeness we shall start here by providing an whistle stop tour of (historically) relevant basis functions on the way to introducing Gaussian type functions as the standard for basis sets in modern quantum chemistry bound state calculations. As we mentioned before, in the interest of the analyticity of the basis functions we begin by considering the single electron Hamiltonian of any central field:

$$-\frac{1}{2}\nabla^2\psi(\mathbf{r}) + V(r)\psi(\mathbf{r}) = E\psi(\mathbf{r}). \tag{4.1}$$

The isotropy of the Hamiltonian suggests the separability of the solution into radial and angular part: $\psi(r,\theta,\phi) = R(r)Y(\theta,\phi)$. Using this guess in equation 4.1 separates the Schrödinger equation into angular and radial part. The radial part satisfies

$$\left[-\frac{1}{2r}\frac{\mathrm{d}^2}{\mathrm{d}r^2}r + V(r) + \frac{l(l+1)}{2r^2}\right] R_{nl}(r) = E_{nl}R_{nl}(r). \tag{4.2}$$

Using the separability of the SE the next section treats the design of the angular part of basis functions, whereas the subsequent sections review different approaches for the radial part.

Angular Basis Functions

The angular part of equation 4.1 is solved by the the well known spherical harmonics; eigenfunctions of the total angular momentum operator $\mathbf{L}^2$ and the operator for the projected angular momentum L_z.

$$\begin{aligned} Y_{lm}(\theta,\phi) &= \sqrt{\frac{2l+1}{4\pi}\frac{(l-m)!}{(l+m)!}}P_l^m(\cos(\theta))e^{im\phi} && (4.3)\\ \mathbf{L}^2Y_{lm} &= l(l+1)Y_{lm} && (4.4)\\ L_zY_{lm} &= mY_{lm}, && (4.5) \end{aligned}$$

where P_l^m are the associated Legendre Polynomials given by the Rodrigues expression

$$P_l^m(y) = \frac{(-1)^m}{2^l l!}\left(1-y^2\right)^{m/2}\frac{\mathrm{d}^{l+m}}{\mathrm{d}y^{l+m}}(y^2-1)^l \tag{4.6}$$

Anticipating the polynomial part of the radial, it will prove convenient to absorb this term r^l into the definition of the spherical harmonics, yielding the so called solid harmonics given by

$$\mathcal{Y}_{lm}(\mathbf{r}) = \mathcal{Y}_{lm}(r,\theta,\phi) = r^l Y_{lm}(\theta,\phi) \tag{4.7}$$

Furthermore, as mentioned in section, we shall work exclusively with real basis functions. We therefore define an angular basis of real solid harmonics:

$$\begin{aligned} S_{l0} &= \sqrt{\frac{4\pi}{2l+1}}\mathcal{Y}_{l0} && (4.8)\\ S_{lm} &= (-1)^m\sqrt{\frac{4\pi}{2l+1}}\mathrm{Re}\mathcal{Y}_{lm} && (4.9)\\ S_{l,-m} &= (-1)^m\sqrt{\frac{4\pi}{2l+1}}\mathrm{Im}\mathcal{Y}_{lm}, && (4.10) \end{aligned}$$

and an equivalent definition based on the spherical (rather than solid spherical) harmonics leads to the so called real spherical harmonics X_{lm}.

Analytically the choice for working in spherical polar coordinates was clear: the isotropy of the Hamiltonian. Computationally the most relevant object are expressions involving integrals over spherical harmonics. This proves to be much easier working with Cartesian coordinates representation. By realizing that $r^l Y_{lm}(\theta,\phi)$ is a solution to the Laplace equation $\nabla^2 r^l Y_{lm} = 0$ and inserting a guess polynomial expression in terms of the Cartesian coordinates into it, we can obtain a Cartesian expression for the (real) solid harmonics:

$$S_{lm} = N_{lm} \sum_{t=0}^{(l-|m|)/2} \sum_{u=0}^{t} \sum_{v=v_m}^{|m|/2} C_{tuv}^{lm} x^{2y+|m|-1(u+v)} y^{2(u+v)} z^{l-2t-|m|} \tag{4.11}$$

$$C_{tuv}^{lm} = (-1)^{t+v-v_m} \left(\frac{1}{4}\right)^t \binom{l}{t} \binom{l-t}{|m|+t} \binom{t}{u} \binom{|m|}{2v} \tag{4.12}$$

$$N_{lm} = \frac{1}{2^{|m|} l!} \sqrt{\frac{s(l+|m|)!(l-|m|)!}{2^{\delta_{0m}}}} \quad \text{where} \tag{4.13}$$

$$v_m = \frac{1}{2}\theta_{\text{Heaviside}}(-m). \tag{4.14}$$

Hydrogenic Basis Functions

In the previous section addressing angular basis functions the only restriction imposed on the Hamiltonian was isotropy. In developing radial basis functions, we shall, as hinted at before, consider hydrogenic atoms as a natural starting point. Thus $V(r) = Zr^{-1}$. The solution to this can be found in any elementary text on quantum mechanics, giving the eigenfunctions as:

$$\psi_{nlm}(r,\theta,\phi) = R_{nl}(r) Y_{lm}(\theta,\phi) \tag{4.15}$$

$$R_{nl}(r) = \left(\frac{2Z}{n}\right)^{\frac{3}{2}} \sqrt{\frac{(n-l-1)!}{2n(n+1)!}} \left(\frac{2Zr}{n}\right)^l L_{n-l-1}^{2l+1}\left(\frac{2Zr}{n}\right) e^{-\frac{Zr}{n}}, \tag{4.16}$$

where L_n^α are the associated Laguerre polynomials given by the following Rogdrigues expression

$$L_n^\alpha = \frac{e^x x^{-\alpha}}{n!} \frac{\mathrm{d}^n}{\mathrm{d}x^n} \left[e^{-x} x^{n+\alpha}\right], \tag{4.17}$$

with the corresponding energies

$$E_n = -\frac{Z^2}{2n^2}. \tag{4.18}$$

The Hydrogenic basis function do serve as a useful starting point in understanding the necessary ingredients to design the structure of sets of basis functions. But without any modification the Hydrogenic basis functions are of limited utility as basis functions, for a couple of reasons that will become apparent in the following paragraphs.

Clearly the exponentially decaying nature of these functions is indispensable for the description of bound states requiring $\lim_{r\to 0} \psi(r,\theta,\phi) = 0$. Equally important is some kind of polynomial dependence on r to account for the expected nodal structure. The nodal structure such as it appears in equation 4.16 leads to very diffuse functions, which results in undesirably large basis sets necessary to describe complicated electronic structures at small radii. Furthermore inherent to the specific case of Hydrogen is the value of the $Z = 1$, thus to develop basis functions designed to describe different atoms, we should expect to need different values for Z. Due to its appearance in the exponential term we shall refer to this term as basis exponent(s) and denote them by ξ (taking the place of Z/n). Fixing a set of basis exponents ξ, is therefore tantamount to defining a basis set, which if used in equation 4.16 would yield a set of Hydrogenic basis functions $\psi_{nlm}(r,\theta,\phi;\xi)$.

Next it should be noted that the condition of completeness is not fulfilled by the eigenfunctions in equation 4.16. As mentioned the set of eigenfunctions of a Hamiltonian constitutes a complete basis set spanning $\mathbb{R}^3$. The presented eigenfunctions however do not include the positive energy continuum solutions and are therefore incomplete. But as this chapter's concern are boundstates, completeness is achieved by means of a structural modification of 4.16 rather than including the continuum eigenfunctions. It can be shown that, for a given α, the weighted associated Laguerre functions $\tilde{L}_n^\alpha$ do indeed form a complete basis[99]

$$\begin{aligned} \langle \tilde{L}_n^\alpha(x) | \tilde{L}_m^\alpha(x) \rangle &= \frac{\Gamma(n+\alpha+1)}{n!}\delta_{nm} \quad \text{where} && (4.19) \\ \tilde{L}_n^\alpha(x) &= e^{\frac{x}{2}} x^{\frac{\alpha}{2}} L_n^\alpha(x). && (4.20) \end{aligned}$$

Alternatively this may be stated as the Laguerre functions L_n^α being orthogonal with respect to the weight function $W(x) = x^\alpha e^{-x}$, expressed by

$$\int \mathrm{d}x L_n^\alpha(x) L_m^\alpha(x) W(x) = \frac{\Gamma(n+\alpha+1)}{n!}\delta_{nm}. \tag{4.21}$$

Hence, casting equation 4.16 into this form yields

$$\begin{aligned} R_{nl}^{\text{Laguerre}}(r) &= (2\xi)^{\frac{3}{2}} \sqrt{\frac{(n-l-1)!}{(n+l+1)!}} \tilde{L}_{n-l-1}^{2l+2}(2\xi r) && (4.22) \\ &= (2\xi)^{\frac{3}{2}} \sqrt{\frac{(n-l-1)!}{(n+l+1)!}} (2\xi r)^l L_{n-l-1}^{2l+2}(2\xi r) e^{-\xi r} && (4.23) \end{aligned}$$

which guarantees completeness, where the expression in the square root was modified to ensure normality in accordance with equation 4.19. (The missing factor of r in this equation, to achieve the form of equation 4.19 is introduced via the Jacobian upon integration in spherical polar coordinates). This maintains the essential structure of equation 4.16 with the notable exception of not containing a n^{-1}-term in neither the exponential nor the polynomial expression, changing the expectation value of r from

$$\begin{aligned} \langle R_{nl} | r | R_{nl} \rangle &= \frac{3n^2 - l(l+1)}{2Z} \quad \text{to} && (4.24) \\ \langle R_{nl}^{\text{Laguerre}} | r | R_{nl}^{\text{Laguerre}} \rangle &= \frac{2n+1}{2\xi}. && (4.25) \end{aligned}$$

This turns out not to be a disadvantage, for the more slowly expanding nature R_{nl}^{Laguerre} with increasing n is capable of better representing the richer structure of polyatomic/polyelectronic molecules at small radii.

In summary, we may write the following expressions for Laguerre-type basis functions

$$\begin{aligned} \chi_{nlm}^{\text{Laguerre}} &= R_{nlm}^{\text{Laguerre}} Y_{lm}(\theta, \phi) && (4.26) \\ &= (2\xi)^{\frac{3}{2}} \sqrt{\frac{(n-l-1)!}{(n+l+1)!}} (2\xi r)^l L_{n-l-1}^{2l+2}(2\xi r) e^{-\xi r} Y_{lm}(r, \theta, \phi). && (4.27) \end{aligned}$$

While these basis functions incorporate the key properties necessary for a useful basis set, it still provides insufficient flexibility for the complicated electronic structure for even simple systems such as a Nitrogen atom[2]. To equip a basis set with the potential to represent complicated structures at a wider range of

[2] insufficient flexibility is here meant in the sense of insufficient flexibility for a reasonably small number of basis functions. Given the preceding discussion about completeness this basis set would be perfectly adequate given unlimited (or at least immense) computational resources.

radii we return to equation 4.25. This expression suggests that a basis set containing functions $\chi^{\text{Laguerre}}_{nlm;\xi_p}$ obtained from sets of exponents $\{\xi\}_{nl}$ may result in an improvement of the basis (the reason for nl as the choice of subscript we become apparent shortly).

While the effect of including different exponents does make for more compact expansions of the molecular wave function, this comes at the price of relinquishing orthogonality of the basis. While this may sound like an important property to give up, we did in fact anticipate this in chapter 2 when providing a method in dealing with basis sets with whose overlap matrices contain non-zero off-diagonal elements.

In view of this and by further realizing that any polynomial may be constructed as a linear combination of monomials, we may significantly simplify the structure of the Laguerre functions by retaining only the highest power in the polynomial part of equation 4.23. Inspection of $(2\xi r)^l L^{2l+2}_{n-l-1}(2\xi r)$ tells us the sought for monomial version of the Laguerre Functions must be of degree $l+n-l-1=n-1$. Therefore we obtain the following radial basis function, giving rise to what is commonly referred to as Slater Type Orbitals (STOs):

$$R^{\text{STO}}(r) = \frac{(2\xi)^{\frac{3}{2}}}{\sqrt{(2n+1)!}}(2\xi r)^{n-1}e^{-\xi r}. \tag{4.28}$$

We now return to the idea which which motivated the construction of STOs, namely introducing a basis set comprised of functions containing more than one exponent. The result of equation 4.25 carries over to STOs and we may furthermore note that $R^{\text{STO}}(r)$ takes its maximum at $r^{\text{STO}}_{\text{max}} = n\xi^{-1}$. Thus we can choose the exponents to endow the set of basis functions with a desired radial structure by identifying exponents appropriately.

Again progress as to how to do this is made by following the most natural path, which is to say it may seem like a decent first guess to include STOs for n and l according to the occupied Hartree Fock Orbitals in the molecule in question and then choose some set of exponents $\{\xi\}_{nl}$ for each. In this fashion a so called minimal basis set is obtained if the each set $\{\xi\}_{nl}$ contains only one exponent, leading to a description where each Hartree Fock Orbital is represented by one STO only[100] . Extended basis sets are obtained by including larger sets of exponents $\{\xi\}_{nl}$, where the exponents are obtained by minimizing the Hartree Fock Energy[101]. It should be noted that these STOs with variable exponents still constitute eigenfunctions of a Hydrogen type Hamiltonian (albeit one with non-integer charge) by virtue of being linear combinations of the Laguerre Functions.

One important theoretical aspect is that we must be careful in our choice of ξ_{nl}, so as to ensure completeness of the resulting basis set. Suffice it to say for now that it is possible to find sets of coefficients that ensure completeness[102]. This point will be addressed in more detail when Gaussian basis functions are discussed, as these play a more important role in this project.

The development of the STOs as it was presented here was chiefly motivated by the case of atomic systems, therefore bestowing on the STOs the symmetries inherent to an atomic system. In moving to molecular systems of lower symmetries this is most naturally addressed by employing multiple basis functions centred at the different atomic site of the molecule in question, which will allow the description of the complicated charge distributions found in molecules. It is at this point that we begin to encounter disadvantages of STOs which will eventually lead to them all but falling out of use for molecular systems. STO based basis sets are still routinely available in libraries of basis functions[103][104] and have been quite successful in the description of atoms and diatomic molecules. It is however in going beyond diatomic systems, that we find that using STOs the computation of the large number of two electron integrals necessary, cannot be done efficiently in cases with basis sets at positioned at many different origins. This difficulty motivates the final structural change that shall be made on the path to a basis set that is useful for describing multi atomic molecules.

4.1 Gaussian Basis Functions

Having progressed from Laguerre Functions to STOs by changing the structure of the polynomial part (and allowing for variable exponents), the only useful remaining term left to modify, in order to obtain a set of basis functions with analytically more accessible integrals, is the exponential term. As the name of this section suggests the STOs exponential behaviour is modified from $e^{-\zeta r}$ to a Gaussian type distribution of the form $e^{-\zeta r^2}$. In modern day basis expansion based quantum chemistry (including also entirely different non-wavefunction basis such as density functional theory) basis sets based on these functions have been (and continue to be) the work horse since the late 1980. Thus they will be exposed here in some more detail compared to the preceding basis sets, which were included mainly for completeness sake and to motivate the discussion on Gaussian basis functions. Before elaborating on disadvantages and advantages introduced by working with Gaussian basis functions, we shall comment on their compliance with the fundamental requirement of completeness.

We can verify completeness by recalling that the Harmonic Oscillator Hamiltonian $H_{HO} = -\frac{1}{2}\nabla^2 + \frac{1}{2}(2\alpha)^2 r^2$ has the following eigenfunctions (which we shall refer to as HOFs):

$$\chi^{HO}_{nlm}(r,\theta,\phi) = R^{HO}_{nl}(r)Y_{lm}(\theta,\phi) \quad \text{where} \tag{4.29}$$

$$R^{HO}_{nl}(r) = \frac{(2\alpha)^{\frac{3}{4}}}{\pi^{\frac{1}{4}}}\sqrt{\frac{2^{n+1}(n-l-1)!}{(2n-1)!!}}\left(\sqrt{2\alpha}r\right)^l L^{l+\frac{1}{2}}_{n-l-1}e^{-\alpha r^2}. \tag{4.30}$$

Note that unlike in the case of eigenfunctions considered for Hydrogen in equation 4.1 this is the complete set eigenfunctions of H^{HO} (this is true since we have not neglected a continuum part, which in fact does not exist here as $H^{HO} \to \infty$ as $r \to \infty$). Therefore completeness is guaranteed and the eigenfunctions possess the sought for Gaussian nature.

The main disadvantage in transitioning to a quadratic exponential decay is that convergence is slower, requiring larger basis sets for a good description of the electronic structure. This should not come as a surprise as the Hamiltonian which these functions are eigenfunctions of less closely resembles the Hamiltonian of the system we aim to model, specifically in its harmonic rather then Coulombic structure. The slower convergence is however far outweighed by the speed up obtainable in having to evaluate integrals of Gaussian type functions.

Rather than working directly with the eigenfunctions of the harmonic oscillator, we modify them analogous to the way we proceeded in obtaining STOs from Laguerre functions. That is we retain only the highest power of r and introduce variable exponents. The former naturally yields the so called Gaussian Type Orbitals (GTO):

$$\chi^{GTO}_{nlm}(r,\theta,\phi) = R^{GTO}_{nl}(r)Y_{lm}(\theta,\phi) \quad \text{where} \tag{4.31}$$

$$R^{GTO}_{nl}(r) = \frac{2(2\alpha)^{\frac{3}{4}}}{\pi^{\frac{1}{4}}}\sqrt{\frac{2^{2n-l-2}}{(4n-2l-3)!!}}\left(\sqrt{2\zeta}r\right)^{2n-l-2}e^{-\zeta r^2}. \tag{4.32}$$

Just as for STOs, completeness is ensured by the possibility to reconstruct the HOFs as linear combinations of GTOs, implying that HOFs and GTOs span the same space. In practice, all GTOs found in modern basis sets are made up entirely of functions with n=l+1. Thus the degree of the polynomial part is completely determined by the angular momenta included in the basis set. Inspection of the expectation and maximum value of r shows how fixing n in the GTOs still allows for a flexible description of the radial structure:

$$\langle \chi^{\text{GTO}}_{nlm}|r|\chi^{\text{GTO}}_{nlm}\rangle \approx \sqrt{\frac{2n-l-2}{2\zeta}} =_{n=l+1} \sqrt{\frac{l}{2\zeta}} \tag{4.33}$$

$$r^{\text{GTO}}_{\max} = \sqrt{\frac{2n-l-1}{2\zeta}} =_{n=l+1} \sqrt{\frac{l-1}{2\zeta}} \tag{4.34}$$

Thus we construct the final expression of GTOs is given in term of l,m and ζ_{nl} where here the index n now relates to the different exponents associated with some given l:

$$\chi^{GTO}_{\zeta_{nl},l,m} = R_{\zeta,l}(r)^{GTO} Y_{lm}(\theta,\phi) \quad \text{where} \tag{4.35}$$

$$R_{\zeta_{nl},l}(r)^{GTO} = \frac{2(2\alpha)^{\frac{3}{4}}}{\pi^{\frac{1}{4}}} \sqrt{\frac{2^l}{(2l+1)!!}} \left(\sqrt{2\zeta} r\right)^l e^{-\zeta_{nl} r^2}, \tag{4.36}$$

or in terms of real solid harmonics

$$\chi^{GTO}_{\zeta_{nl},l,m} = \frac{2(2\alpha)^{\frac{3}{4}}}{\pi^{\frac{1}{4}}} \sqrt{\frac{2^{l-\delta_{m0}}}{2l!!}} \left(\sqrt{\frac{2\zeta}{8\pi}}\right)^l S_{lm}(r,\theta,\phi) e^{-\zeta_{nl} r^2} \tag{4.37}$$

As alluded to in the discussion of STOs, we shall now make a few comments about how to identify a suitable set of exponents, that may allow us to create a more flexible but still complete set of basis functions.

Naturally the choice of exponents must be such that the resulting basis function can be systematically extended to give an (infinite) basis that is complete. There are a several sufficient criteria for this, fulfilment of any one of which yields a complete basis:

1. For some fixed l the sequence a_{nl} has a finite non-zero accumulation point a_l
2. For some fixed l the sequence a_{nl} is monotonically decreasing and satisfies $\sum_n a_{nl} = \infty$ as $n \to \infty$

While it is easy to come up with any number of sequences of exponents that satisfy one of these conditions, in practice not all such series are useful. Thus for now these conditions merely serve as a theoretical way to convince oneself that the search for GTOs with variables exponents is not in vain. We shall look into the exact way of obtaining suitable sets of basis functions in the following sections. Having defined the analytical structure of the GTOs and established the theoretical suitability, we shall now look at the specific tailoring of such as basis set, so as for it to yield the best results for some given atom.

4.1.1 Determination of Exponents

The first attempts to use GTOs were largely guided by the previously gained experience with STOs. Which is to say that the fundamental object continued to be STOs and, to exploit their computational advantages, the attempt is made to expand the STOs in terms of some number of GTOs. This leads to the so called STO-kG basis sets[105, 106, 107], where each STO is expanded in terms of k Gaussian Type functions. In the (practically fairly useless case) of $k = 1$ we may obtain a straightforward expression for the coefficient ζ for each GTO that best represents one STO via the variational principle with ζ being the variational parameter[108] minimizing the following expression

$$\langle \chi^{\mathrm{GTO}}_{\zeta_i lm} | \mathcal{H}^{\mathrm{STO}} | \chi^{\mathrm{GTO}}_{\zeta_i lm} \rangle = \left[(2l+3) \frac{\zeta_i \zeta_j}{\zeta_i + \zeta_j} + \frac{l'(l'+1) + l(l+1)}{2l+1} (\zeta_i + \zeta_j) - \right. \tag{4.38}$$

$$\left. \frac{l! 2^{l+1}}{(2l+1)!! \sqrt{\frac{(\zeta_i+\zeta_j)}{\pi}}} \right] \langle \chi^{\mathrm{GTO}}_{\zeta_i lm} | \chi^{\mathrm{GTO}}_{\zeta_i lm} \rangle \,, \tag{4.39}$$

where $\mathcal{H}^{\mathrm{STO}}$ is the hydrogenic Hamiltonian whose eigenfunction is an STO according to equation 4.28 with $n - 1 = l'$ and the GTO overlap is given by

$$\langle \chi^{\mathrm{GTO}}_{\zeta_i lm} | \chi^{\mathrm{GTO}}_{\zeta_i lm} \rangle = \left[\frac{2\sqrt{\zeta_i \zeta_j}}{\zeta_i + \zeta_j} \right]^{l+\frac{3}{2}} . \tag{4.40}$$

Finding thus the optimal value for ζ representing a single STO yields

$$\zeta_{\mathrm{opt}} = \left[\frac{l! 2^{l+1} \sqrt{2}}{(2l-1)!! \sqrt{\pi}} \frac{1}{4(l+1) + 4l'(l'+1) - 1} \right]^2 \tag{4.41}$$

.

This method can be extended to cases where $k > 1$, yielding so called double zeta (DZ), triple zeta (TZ) (and so forth) basis sets. This introduces multiple variational parameters making the search for a minimum much less trivial, as a result of the possible existence of multiple minima, leading to nevertheless useful double zeta basis sets[109]. Alternatively one may find a set of suitable exponent by fitting a set of Gaussian functions of size k to some STO via a least square method[105].

Up to this point the discussion has been, despite the introduction of GTOs, been very much moved by STOs which, as previously mentioned has at its core the idea of representing molecular systems as eigenfunctions of a Hamiltonian very closely related to the hydrogenic Hamiltonian. The move to considering GTOs as the fundamental basis functions of quantum chemistry, represented somewhat of a paradigm shift, which took some years to reach maturity from first proposals[110, 111, 112] to acceptance as what is by now a ubiquitously used tool in quantum chemistry.

While as was mentioned already GTOs are much nicer to work with than STOs due to the simplicity with which integrals between GTOs (centred at different origins) can be evaluated. We do find that to obtained comparable accurate results we must use significantly larger sets of basis functions. For example, for first row atoms six s and four p STOs are sufficient to provide accuracy to within 7 digits for first row atoms[101] while a similar number of GTOs provides accuracy worse by more than an order of magnitude[109]. Qualitatively this can be in large part understood by turning to the main structural difference we have introduced in passing from STOs (motivated directly by the bound state eigenfunctions of the Hydrogenic Hamiltonian) to GTOs. While the latter, due to its quadratic nature, is smooth at the $r = 0$, the former is non-differentiable at the origin; the nuclear cusp. This discontinuous derivative is very hard to reproduce for GTOs. This problem is especially dramatic for small atomic system with the electrons closer to the origin. For molecular systems this problem is not as pronounced as the chemically interesting valence electrons are more likely to be found further away from the atomic sites. Therefore many chemically interesting properties such as bonds or reactivity may be captured correctly despite a poor description of the core electrons.

In view of the preceding paragraph we ought to be prepared to either sacrifice accuracy or use basis sets several times larger than what would be necessary for STOs, potentially rendering moot the computational advantages introduced by GTOs. Next we will discuss some concepts which by and large have been developed to allow for the optimization and use of relatively large sets of GTOs.

4.1.2 Tempered Bases

In leaving behind STOs, least square fitting, is no longer an available tool as there is nothing to fit to, but rather, as previously mentioned, one must find exponents minimizing the energy in accordance with the variational principle. One way to circumvent the problem of the very high dimensional optimization (with many, potentially sub-ideal minima) is to introduce so called even-tempered bases. These have the property, that the exponent are given by a simple geometric progression according to

$$\zeta_i = \zeta\beta^{i-1}, \tag{4.42}$$

thereby specifying the complete set of exponents in terms of the two parameters ζ and β, regardless of the size of the basis. As such they are particularly useful for the description of larger systems, and were first employed in the description of Amonia[113]. In addition to reducing the parameters that have to be optimized, even-tempered basis sets have the advantage that basis sets for any two "neighbouring" terms in the series 4.42, the corresponding overlap integral is the same.

4.1.3 Contractions

We recall the problem associated with the nuclear cusp problem. We observed that the main problem is the large number of GTOs needed to accurately represent regions close to atomic sites. As such, we may suspect that the description of molecules does not require large basis to accurately describe the change

in electron distribution due to bond formation, but rather to describe the core electron structure of the nuclei. Therefore one may expect improved performance by constructing a small number of contracted GTOs (CGTO), built as fixed linear combinations from a larger set primitive GTOs (PGTO), designed to capture more nuclear electronic structure for a given atom, while retaining the necessary flexibility to describe bond formation involving valence electrons.

There are a variety of different contraction schemes broadly falling into two categories: segmented and general contractions. The latter allows arbitrary linear combinations, while the former restrict the linear combinations to those in which each PGTO contributes to only one CGTO. There are a variety of contraction schemes yielding segmented CTGO of which the DZ-Basis (including two CGTOs for every occupied atomic orbital) by Dunning[114] is the most commonly encountered one which makes use of previously optimized exponents obtained in an atomic calculations. It consists a basis constructed from 9 s and 5 p type GTOs[109] contracted to 4 s and 2 p type CGTOs. These kind of contractions are categorized using the notation (in the example at hand) $(9s5p) \rightarrow [4s2p]$. In contrast to these method relying on previously optimized exponents, the split-valence basis sets n-k1G by Pople[115, 116], simultaneously optimize exponents and contraction coefficients representing core orbitals by n and valence orbitals by k CGTOs respectively. We shall not discuss general contractions here, but they will naturally emerge in what is to follow.

Before concluding the discussion of GTOs two more aspects shall have to be explored so as to provide a full theoretical account of the kind of basis functions necessary in this project. In including these two aspects we arrive at basis functions routinely in use in state of the art bound state quantum chemistry calculations. Both these aspects are particularly relevant in for the application of GTOs to molecules and as such, indispensable in most any quantum chemistry calculation. As we mentioned at the beginning of the discussion of basis functions, we shall consider basis sets for molecules as collections of "sub" basis sets centred at the atomic sites. Nothing of what we have discussed so far however, has taken into account this multi centric natures nor the additional requirements that on a basis dictated by the description of bond formation, crucially dependent on electron correlation. Rather the discussion of basis functions up to this point can effectively be seen as designing basis functions serving the purpose of atomic calculations.

4.1.4 Polarization Functions

Inherent to the study of molecular system, is as a primary objectives the accurate description of bond formation. Relying, as we have done so far, on including basis sets based on the occupied orbitals of Hartree Fock theory is therefore bound to give problems. If, to understand the bond of a diatomic molecule we consider GTOs, containing only s-orbitals we neglect the fact, that linear combination of two p-orbitals may yield a molecular orbital of symmetry σ_g which may be relevant to the description of diatomic system in question.

Therefore to model bond formation, basis sets must include GTOs of higher angular momentum than what the description of the individual atoms comprising the molecules would require. These additional basis functions are called polarization functions and greatly enhance the computational accuracy of even small basis sets, such as the ones we have mentioned so far. See [117] for the polarized DZ (DZP) and [118] for the polarized n-k1G* (added polarization d functions for atoms Lithium to Neon) and n-k1G** (further addition of p functions for Hydrogen).

4.1.5 Correlated Basis Sets

So far the discussion was heavily guided by Hartree Fock level consideration of atoms, designing GTOs to mimic as best as possible the AOs of Hartree Fock theory of chapter 2. This leaves all approaches discussed until now subject to the limitation of not describing electron correlation. Thus one should expect that for calculations including configuration interaction, this bases may not be very well suited. Without having as yet gone into the details of post Hartree Fock theories, we shall review basis functions that are equipped for this kind of calculation. It is important to distinguish between the origin of the

correction to the energy due to electron correlation. What is meant by this is, that electrons in core orbitals are found to contribute in large part only a constant contribution to the total correlation energy independent say of changing molecular geometries or external influences. In stark contrast to this is the electron correlation of valence electrons, the neglect of which (see chapter 2), leads to qualitatively faulty description for even simple systems. Therefore in order for a basis set to stand a chance of reproducing correlation we must also provide a virtual orbital space in the design of the basis functions.

Turning now to a specific example of a correlated basis set we consider the ANO (atomic natural orbital) basis sets[119, 120]. Beginning the calculation with some previously obtained PGTOs the general contractions for ANOs, are found by first carrying out a Hartree Fock Level calculation, taking the contraction coefficients from the thus found occupied canonical orbitals. The correlation part of the basis is then introduced by carrying out a CI calculation and analysing the occupation numbers of virtual natural orbital (for more details on natural orbtitals the reader is referred to chapter 3). Including progressively virtual natural orbitals as contraction in the basis yields progressively more complete sets of ANOs. ANOs have been found to give very good results but. Their main drawback is the relatively large size of theses basis sets. This issue is further amplified by the fact that often times these ANO functions are extended by PGTOs or de-contractions, to give the necessary flexibility for the outer valence region[120].

This brings us to the last type of GTOs which shall be considered in this work in some detail. These are the correlation-consistent basis sets[121, 122].

These cc-pVXZ basis functions provide sufficient flexibility for a very good description of the molecules encountered in this work, as well as any for molecules the methods presented here are likely to be applied to in the mid term. As such we shall conclude this discussion of GTOs. More recent development in the theory of GTOs include, but as these are irrelevant for the discussion of this work the reader is referred to the references provided. Before moving from this more historical discussion of GTOs to look into some of their properties we end this sections with a quote by Shavitt[112] from 1993:

> [...] Gaussian basis sets of various sizes are likely to continue to provide the bulk of the theoretical molecular structure results, at least to the end of the century.

4.2 Mathematical Properties of Gaussian Basis Functions

Clearly this was by no means overoptimistic or biased, for almost three decades later GTOs have firmly established themselves as a standard tool in Quantum Chemistry. This and the important role they will play in one of the key components of this project renders the discussion of some of their relevant mathematical properties pertinent, with an emphasize on those properties that highlight their computational advantages over functions whose exponential term is not quadratic (e.g. STOs), which as we haven gone to length to point out is the chief motivator for the deployment of GTOs.

All the different existing Gaussian Basis sets differ to larger or lesser extent in the methodology used to obtain exponents and contractions, but aside from these differences they may all be written as (up to a normalization constant)

$$G_{lm}(\mathbf{r},\zeta,\mathbf{R}) = S_{lm}(x-\hat{\mathbf{x}}\mathbf{R}, y-\hat{\mathbf{y}}\mathbf{R}, z-\hat{\mathbf{z}}\mathbf{R})e^{-\zeta(\mathbf{r}-\mathbf{R})^2} \tag{4.43}$$

being a GTO centred at $\mathbf{R}$ with angular momenta l and m as captured by the solid spherical harmonic S_{lm}. Following equations 4.12 this may be cast into a combination of Cartesian functions,

$$\begin{aligned} G_{abc} &= (x-\hat{\mathbf{x}}\mathbf{R})^a(y-\hat{\mathbf{y}}\mathbf{R})^b(z-\hat{\mathbf{z}}\mathbf{R})^c e^{-\zeta(\mathbf{r}-\mathbf{R})^2} && (4.44)\\ &= (x-R_x)^a(y-R_y)^b(z-R_z)^c e^{-\zeta(\mathbf{r}-\mathbf{R})^2} && (4.45)\\ &= x_R^a y_R^b z_R^c e^{-\zeta x_R^2} e^{-\zeta y_R^2} e^{-\zeta z_R^2} && (4.46)\\ &= G_{aR}(x)G_{bR}(y)G_{cR}(z), && (4.47) \end{aligned}$$

where the last line changed the notation for convenience and highlights one property of GTOs whose usefulness in evaluating integrals is easy to appreciate, they trivially factorize into functions of x,y and z. Clearly this is not the case for STOs and greatly aides the analytical evaluation of integrals of GTOs. Furthermore it is important that the product of any two Gaussians of this type is

$$\begin{aligned} G_{aR\zeta}(x)G_{a'R'\zeta'}(x) &= x_R^a x_{R'}^{a'} e^{-\zeta x_R^2 - \zeta' x_{R'}^2} && (4.48)\\ &= x_R^a x_{R'}^{a'} \exp\left(-px^2 + 2x(\zeta R_x + \zeta' R'_x) - \frac{(R_x^2 + R_x'^2)\bar{\zeta}}{\bar{\zeta}}\right) && (4.49)\\ &= x_R^a x_{R'}^{a'} K_x^{\bar{\zeta}\bar{R}} e^{-px_Q^2}, && (4.50) \end{aligned}$$

where in the last line we have changed to the centre of charge coordinate system, as defined by

$$\begin{aligned} \mathbf{K}^{\bar{\zeta}\bar{R}} &= \exp\left(-\frac{\zeta\zeta'}{\bar{\zeta}}\bar{\mathbf{R}}\right)\\ \mathbf{Q} &= \frac{\zeta\mathbf{R} + \zeta'\mathbf{R}'}{\bar{\zeta}} \quad \text{where}\\ \bar{\mathbf{R}} &= \mathbf{R} - \mathbf{R}' \quad \text{and}\\ \bar{\zeta} &= \zeta + \zeta'. \end{aligned}$$

Expressing now x_R and $x_{R'}$ in terms of x_Q, yields

$$\begin{aligned} x_R &= x_Q - \zeta'\bar{\zeta}^{-1}\bar{R}_x \quad \text{and} && (4.51)\\ x_{R'} &= x_Q + \zeta\bar{\zeta}^{-1}\bar{R}_x, && (4.52) \end{aligned}$$

respectively, thereby turning equation 4.50 into a linear combination of simple Gaussians

$$G_{aR\zeta}(x)G_{a'R'\zeta'}(x) = K_x^{\bar{\zeta}\bar{R}} e^{-\bar{\zeta}x_Q^2} \sum_{i=0}^{i=a+a'} B_i^{aa'\bar{\zeta}\bar{R}} x_Q^i, \tag{4.53}$$

where the B_i are simply the binomial coefficients stemming from expressions 4.51 and 4.52. Hence any product of Gaussian in the form given in equation 4.43 can be disentangled into a sum of Gaussians as function of one Cartesian coordinate. This property, as will be seem shortly, is in large part what makes possible the schemes for efficient analytic evaluation of integrals. The next step will be to actually look at the integrals encountered in quantum chemistry, listed below (this is by no means a complete list, but covers all the integrals relevant in this discussion):

$$\begin{aligned} \text{Overlap:} &\quad \langle G_{a'R'\zeta'}|G_{aR\zeta}\rangle && (4.54)\\ \text{Multipoles} &\quad \langle G_{a'R'\zeta'}|x^n|G_{aR\zeta}\rangle && (4.55)\\ \text{Kinetic Energy} &\quad \langle G_{a'R'\zeta'}|\frac{d}{dx}|G_{aR\zeta}\rangle && (4.56)\\ \text{Electron Nuclear Attraction} &\quad \langle G|r_{iA}^{-1}|G\rangle && (4.57)\\ \text{Electron Electron Repulsion} &\quad \langle GG|r_{ij}^{-1}|GG\rangle && (4.58) \end{aligned}$$

The utility of the properties of GTOs discussed so far is immediately obvious for the first three of these expression (we shall see exactly how it will be exploited shortly), as the combination of Gaussian functions and these operators is easily seen to yield only weighted sums integrals of the type

$$I = \int \mathrm{d}x x_Q^m e^{-\bar{\zeta}x_q^2}. \tag{4.59}$$

The latter two types of integral require some more thought, due to their dependence on radial distances (either between an electron and a nucleus or between electrons). For the evaluation of these integrals QCPs rely on different schemes, designed to efficiently compute these integrals. For the simpler type Hermite Gaussian Quadrature is commonly used for the more complicated r-dependent integral Rys Quadrature[123, 71] is used in MOLCAS. To get a feel for the kind of ideas involved in these methods we shall in brief explicitly address the Hermite Gaussian Quadrature necessary for the simpler kind of integral.

Hermite Gaussian Quadrature

We begin by stating the Gaussian Quadrature formula (a proof of which shall not be given here): consider an arbitrary polynomial of degree m, $g_m(x)$ and let x_i be the n distinct roots of a set of polynomials $p_n(x)$ orthogonal on some interval $[a, b]$, such as the Laguerre polynomials. Furthermore let $W(x)$ be the weight function w.r.t which the polynomials are orthogonal (as exemplified previously for Laguerre Polynomials with $W(x)$. If $m < 2n$ then

$$\int_a^b \mathrm{d}x g_m(x) W(x) = \sum_{i=n} w_i g_m(x_i) \quad \text{where} \tag{4.60}$$

$$w_i = \int_a^b \mathrm{d}x W(x) \prod_{j=1}^{n} \frac{x - x_j}{x_i - x_j}. \tag{4.61}$$

Next we introduce the Hermite Polynomials H_n to be used in place of g, which (similar to the Laguerre polynomials) constitute another orthonormal set of polynomial functions, given by the Rodrigues expression

$$H_n(x) = (-1)^n e^{x^2} \frac{\mathrm{d}}{\mathrm{d}x} e^{-x^2}. \tag{4.62}$$

Their orthogonality property is given by

$$\frac{1}{\sqrt{\pi} 2^n n!} \int_{-\infty}^{\infty} \mathrm{d}x H_n(x) H_m(x) W(x) = \delta_{mn} \quad \text{with} \tag{4.63}$$

$$W(x) = e^{-x^2}. \tag{4.64}$$

The weight function provides a first hint at how this might be useful in its application to GTOs[3]. Namely, we consider now as an example the general m^{th} order multipole-moment integral w.r.t. to some origin $x_d = x - x_0$,

$$d^m_{aR\zeta,a'R'\zeta'} = \int G_{aR\zeta}(x) x_d^m G_{a'R'\zeta'}(x) \tag{4.65}$$

$$= K^{\bar{\zeta}\bar{R}_x} \int x_R^a x_d^m x_{R'}^{a'} e^{-p x_Q^2} \tag{4.66}$$

$$= \frac{K_x^{\bar{\zeta}\bar{R}}}{\sqrt{p}} \sum_{r=1}^{o} w_r \left(\frac{x}{\sqrt{p}} - R_x \right)^a \left(\frac{x_r}{\sqrt{p}} - x_0 \right)^m \left(\frac{x_r}{\sqrt{p}} - R'_{x_r} \right)^{a'}, \tag{4.67}$$

where the second line follow from equation 4.50 and the third line follows equation 4.61 where x_r and w_r are the roots and weights (according to equation 4.61) of the Hermite polynomials of degree $o = (a + a' + m)/2 + 1$. This method allows for the efficient evaluation of all integrals of the kind of equation 4.59.

Having mentioned and in the case of the simplest integrals specifically outlines the evaluation of Gaussian integrals, we conclude this section on Gaussian basis functions. We have motivated historically the by now ubiquitous use of these functions in QC and discussed their most relevant mathematical properties. With this we conclude the part of this work dedicated to bound state electronic structure theory.

[3]We note is passing that the Hermite polynomials turn out be the (not normalized) solution to the simple harmonic oscillator Hamiltonian (which was used to motivate the construction of GTOs) expressed in Cartesian coordinates

5 Scattering Theory

In this chapter, after having developed basis sets and theories for electronic bound states, we shall switch topic by looking at the mathematical formulation of electrons that are not bound in a molecule but rather get scattered by some charge distribution. We begin by defining the basic concepts and terminology with the objective of describing an electron being scattered by a complicated charge distribution. Much like in the case for bound states, we shall see that any analytical treatment is restricted to the simplest cases, and will then see how theses cases generalize to more interesting systems. Although the mathematical tools necessary here are superficially quite different to what was encountered in the bound state case, parallels are frequently instructive to draw.

As for obtaining the solution 4.16, we start by considering the Schrödinger equation 4.1 by separating it into a radial and an angular part. The angular description of the problem carries over from the bound state discussion. For the radial part we now seek positive energy solutions, that is solutions that do not decay for large radii. We cast equation 4.2 into the form

$$\left[\frac{\mathrm{d}^2}{\mathrm{d}r^2} + \kappa^2 - U(r) - \frac{l(l+1)}{r^2}\right] u_{\kappa l}(r) = 0, \tag{5.1}$$

where $\kappa^2 = 2E$, $U(r) = 2V(r)$ and $u_{\kappa l} = rR_{\kappa l}$, where we have replace the index n by κ, which will take continuous values. We begin by assuming $U(r) = 0$ beyond some radius R_u, and consider $u(r)$ for $r > R_U$ simplifying equation 5.1 to

$$\left[\frac{\mathrm{d}^2}{\mathrm{d}r^2} + \kappa^2 - \frac{l(l+1)}{r^2}\right] u^{\mathrm{free}}_{\kappa l}(r) = 0, . \tag{5.2}$$

This equation permits as solutions linear combinations of the two functions

$$F_l(\kappa r) = \kappa r j_l(\kappa r) \tag{5.3}$$

$$G_l(\kappa r) = -\kappa r n_l(\kappa r), \tag{5.4}$$

where $j_l(\kappa r)$ and $n_l(\kappa r)$ are the spherical Bessel and Neuman functions respectively, defined via the Bessel function $J_l(\kappa r)$ as

$$j_l(\kappa r) = \sqrt{\frac{\pi\kappa r}{2}} J_{l+\frac{1}{2}}(\kappa r) \tag{5.5}$$

$$n_l(\kappa r) = (-1)^l \sqrt{\frac{\pi\kappa r}{2}} J_{-l-\frac{1}{2}}(\kappa r). \tag{5.6}$$

where the asymptotic behaviour of these functions is given by

	$\kappa r << l$	$\kappa r >> l$
$F_l(\kappa r) \to$	$\frac{(\kappa r)^{l+1}}{(2l+1)!!}$	$\sin(\kappa r - \frac{l\pi}{2})$
$G_l(\kappa r) \to$	$\frac{(2l-1)!!}{(\kappa r)^l}$	$\cos(\kappa r - \frac{l\pi}{2})$

(5.7)

F_l and G_l are referred to as the regular and irregular solutions of the the free particle problem. We may use these to understand the effect of a scattering potential on the asymptotic part of a scattered wave of angular momentum l.

In the absence of a potential $u_{\kappa l}^{\text{free}}$ is the solution to the problem, and as such the only physically admissible solution the regular solution not diverging for $r = 0$. Hence the wave function in the absence of a scattering potential is determined to within a multiplicative constant, and behaves asymptotically as $\sin(r - l\pi 2^{-1})$. In the presence of a potential, beyond the range R_u of the potential the admissible solutions are of the form

$$u_{\kappa l}(r)|_{r>R_u} = AF_l(\kappa r) + BG_l(\kappa r), \tag{5.8}$$

where A and B are complex constants. Therefore asymptotically we may write the general solution to a single, free, scattered particle as

$$\begin{aligned} \lim_{r\to\infty} u_{\kappa l}(r) &= A\sin\left(\kappa r + \frac{l\pi}{2}\right) + B\cos\left(\kappa r + \frac{l\pi}{2}\right) && (5.9)\\ &= N_l \sin(\kappa r - \frac{l\pi}{2} + \delta_l), && (5.10) \end{aligned}$$

where $\delta_l = \tan^{-1}(A/B)$ is the phase shift and $N_l = \sqrt{(A^2 + B^2)}$ the amplitude. Therefore in comparing this to the free case we see that asymptotically the effect of the potential is solely a phase shift. As in a scattering scenario any measurement is carried out far away from the interaction region, knowledge of the phase shift therefore summarises what we may know of the problem. Or to put it in other words, the solution of a scattering problem is the superposition of appropriately chosen un-scattered solutions, decomposed into its angular components each of which is shifted by its corresponding phase shift.

As a first example we'll consider a case allowing considerable simplification of the problem. Making a serious of generalizations and adapting the theory as needed, we will arrive at a formalism suitable for the description of complicated potentials.

Said case is concerned with isotropic potentials decaying faster then r^{-1} (note this specifically exclude the Coulomb case, which naturally is relevant to this work). In this case we can argue that the correct boundary condition for asymptotic wave function is given by

$$\begin{aligned} \lim_{r\to\infty} \psi(\mathbf{r}) &= \psi_{\text{in}} + \psi_{\text{sc}} && (5.11)\\ &= e^{-ikz} + f(\theta,\phi)\frac{e^{ikr}}{r}, && (5.12) \end{aligned}$$

where the scattering amplitude $f(\theta, \phi)$ is related to the differential cross section via

$$\frac{\mathrm{d}\sigma(\theta,\phi)}{\mathrm{d}\Omega} = |f(\theta,\phi)|^2. \tag{5.13}$$

This boundary condition corresponds to an spinless plane wave impinging on the system, and isotropic, scattered radial waves emanating from the scatterer. As such this is not particularly useful for the treatment of photo ionization (the ultimate goal in this work). But it allows the mathematically relatively straightforward treatment of scattering, to provide an intuitive notion of concepts that will become relevant later. We shall introduce the correct boundary condition describing photo ionization later in this chapter.

Next we expand ψ_{in} in terms of partial waves

$$e^{-ikz} = \frac{1}{\kappa r}\sum_{l=0}^{\infty} i^l \sqrt{4\pi(2l+1)} F_l(\kappa r) Y_{l0}(\theta). \tag{5.14}$$

We use this to relate equation 5.12 and δ_l and N_l of expression 5.10 by expressing ψ as a sum of the

asymptotic terms in equation 5.10:

$$\begin{aligned}
\psi_\kappa(r,\theta) &= \frac{1}{\kappa r}\sum_{l=0}^{\infty} Y_{l0}u_{\kappa l} && (5.15)\\
&= \frac{1}{\kappa r}\sum_{l=0}^{\infty} N_l Y_{l0}\sin(\kappa r - \frac{\pi l}{2} + \delta_l)\\
&= \frac{1}{\kappa r}\sum_{l=0}^{\infty} N_l Y_{l0}\Big[\cos\delta_l\sin(\kappa r - \frac{\pi l}{2}) + \sin\delta_l\cos(\kappa r - \frac{\pi l}{2}) +\\
&\quad i\sin\delta_l\sin(\kappa r - \frac{\pi l}{2}) - i\sin\delta_l\sin(\kappa r - \frac{\pi l}{2})\Big]\\
&= \frac{1}{\kappa r}\sum_{l=0}^{\infty} N_l Y_{l0}(\theta)(\cos\delta_l - i\sin\delta_l)\sin(\kappa r - \frac{\pi l}{2}) +\\
&\quad \frac{e^{i\kappa r}}{\kappa r}\sum_{l=0}^{\infty} N_l Y_{l0}(\theta) i^{-l}\sin\delta_l && (5.16)
\end{aligned}$$

Thus by inserting equation 5.14 into 5.12 and comparing the result to the last term in equation 5.16 we can identify

$$\begin{aligned}
N_l &= i^l e^{i\delta_l}\sqrt{4\pi(2l+1)}\text{and} && (5.17)\\
f(\theta) &= \frac{1}{k}\sum_{l=0} N_l\sin\delta_l i^l Y_{l0}(\theta) && (5.18)\\
&= \frac{1}{k}\sum_{l=0} e^{i\delta_l}(2l+1)\sin\delta_l P_l(\cos(\theta)), && (5.19)
\end{aligned}$$

where the last line makes use of the expression of spherical harmonics in terms of Legendre Polynomials, which we have already encountered in the discussion of basis functions, giving

$$Y_{l0}(\theta) = \sqrt{(sl+1)/4\pi}P_l(\cos(\theta)). \tag{5.20}$$

Thus we can conclude that knowledge of the phase shift directly translates to knowledge of the cross section of the scatterer.

Before moving to more general cases at this point it is convenient to introduce three quantities which are important in the study of scattering theory. Making use of equations 5.19 and 5.17 we can write u_l as

$$\begin{aligned}
u_l(r) &= e^{i\delta_l}\cos\delta_l(F_l(\kappa r) + G_l(\kappa r)\tan\delta_l) \quad \text{with} && (5.21)\\
\lim_{r\to\infty} u_l(r) &= e^{i\delta_l}\sin(\kappa r - \frac{\pi l}{2} + \delta_l) && (5.22)
\end{aligned}$$

Next we define two alternative valid expressions for u in terms of linear combinations of $F_l(\kappa r)$ and $G_l(\kappa r)$. The first is obtained by setting $\tilde{G}_l(\kappa r) = F_l(\kappa r) + iG_l(\kappa r)$ allowing us to write u_l as

$$\begin{aligned}
u_l(r) &= F_l(\kappa r) + \tilde{G}_l(\kappa r)e^{i\delta_l}\sin\delta_l \quad \text{with} && (5.23)\\
\lim_{r\to\infty} u_l(r) &= \sin(\kappa r - \frac{\pi l}{2}) + e^{i(\kappa r - \frac{\pi l}{2})}e^{i\delta l}\sin\delta_l && (5.24)
\end{aligned}$$

The second is obtained by letting $H_l^+(\kappa r) = F_l(\kappa r) + iG_l(\kappa r)$ and $H_l^-(\kappa r) = F_l(\kappa r) - iG_l(\kappa r)$ (defining the Hänkel Functions of first and second kind). Thus

$$\begin{aligned}
u_l(r) &= \frac{i}{2}\left(H_l^-(\kappa r) - H_l^+(\kappa r)e^{2i\delta_l}\right) \quad \text{with} && (5.25)\\
\lim_{r\to\infty} u_l(r) &= \frac{i}{2}\left(e^{-i(\kappa r - \frac{\pi l}{2})} + e^{i(\kappa r - \frac{\pi l}{2})}e^{2i\delta_l}\right) && (5.26)
\end{aligned}$$

Inspecting equations 5.22, 5.24 and 5.26 we let

$$K_l = \tan\delta_l \tag{5.27}$$
$$T_l = e^{i\delta_l}\sin\delta_l \tag{5.28}$$
$$S_l = e^{2i\delta_l}, \tag{5.29}$$

which will turn out to be the eigenvalues of the $\mathbb{K}$, $\mathbb{T}$ and $\mathbb{S}$ matrices, which will study in more detail, and whose matrix nature will become apparent upon considering more complicated scattering scenarios.

5.1 Close Coupling - Spin

So far we have assumed to be working with spinless particles, and the angular momentum treatment was exclusively confined to the orbital angular momentum, as captured by the spherical harmonics Y_{lm}. We will now see how the preceding formalism must be extended to allow for the electron in the continuum to have spin and for the target to have internal structure. Let now the target (t) and projectile (p) spin angular momentum operators be I_t and I_p, respectively. With $\chi_{i_\mathrm{t},m_\mathrm{t}}$ and $\chi_{i_\mathrm{p},m_\mathrm{p}}$ being the eigenfunctions these two operators. That is to say

$$\begin{aligned} \hat{\mathbf{I}}^2_\mathrm{p}\chi_{i_\mathrm{p},m_\mathrm{p}} = i_\mathrm{p}(i_\mathrm{p}+1)\chi_{i_\mathrm{p},m_\mathrm{p}} \quad ; \quad \hat{I}_{\mathrm{p},z}\chi_{i_\mathrm{p},m_\mathrm{p}} = m_\mathrm{p}\chi_{i_\mathrm{p},m_\mathrm{p}} \\ \hat{\mathbf{I}}^2_\mathrm{t}\chi_{i_\mathrm{t},m_\mathrm{t}} = i_\mathrm{t}(i_\mathrm{t}+1)\chi_{i_\mathrm{t},m_\mathrm{t}} \quad ; \quad \hat{I}_{\mathrm{t},z}\chi_{i_\mathrm{t},m_\mathrm{t}} = m_\mathrm{t}\chi_{i_\mathrm{t},m_\mathrm{t}} \end{aligned} . \tag{5.30}$$

We define now the total uncoupled spin channel function Υ to be

$$\Upsilon_{i_\mathrm{t},m_\mathrm{t},i_\mathrm{p},m_\mathrm{p}} = \chi_{i_\mathrm{t},m_\mathrm{t}}\chi_{i_\mathrm{p},m_\mathrm{p}}, \tag{5.31}$$

which contains all the structure that was not present in the previous spin less case. Expanding the solution ψ in this spin basis is possible but of limited usefulness as these do not commute with the Hamiltonian. Of more usefulness is the total spin $I = I_\mathrm{p} + I_\mathrm{t}$, as this does commute with the Hamiltonian, making the total spin a conserved quantity. Note that this fails to be true, if we work with spin dependent Hamiltonian by including for instance spin-orbit coupling. This will however, not be the case in this work. We may construct eigenstates of the total spin I^2 and its projection I_z as

$$\Upsilon_{i,m_i} = \sum_{m_\mathrm{p},m_\mathrm{t}} \langle i_\mathrm{p}, m_\mathrm{p}; i_\mathrm{t}, m_\mathrm{t}|i, m_i\rangle\, \chi_{i_\mathrm{t},m_\mathrm{t}}\chi_{i_\mathrm{p},m_\mathrm{p}}, \tag{5.32}$$

where $\langle i_\mathrm{p}, m_\mathrm{p}; i_\mathrm{t}, m_\mathrm{t}|i, m_i\rangle$ are Clebsch-Gordon Coefficient evaluated according to the spin specifications of the problem. We express now the complete solution $\psi_\kappa(\mathbf{r})$ to the problem as an expansion in the spin states each with an associated coordinate space spin-channel wave function $\psi_{im}(\mathbf{r})$

$$\psi_\kappa(\mathbf{r}) = \sum_{i,m_i} \psi_{\kappa i,m_i}(\mathbf{r})\Upsilon_{i,m_i}. \tag{5.33}$$

Next we wish to study the independently the radial part of the u of the wave functions. To this end we express the $\psi_{\kappa i,i_m}(\mathbf{r})$ in equation 5.33 via a partial wave expansion akin to that in equation 5.15. Note however, we may no longer assume, as we did before in view of the isotropy of the potential, that the solution is rotationally symmetric around the z-axis. Thus summation must now include the allowed values of m_l,

$$\psi(\mathbf{r}) = \frac{1}{\kappa r}\sum_{i,m_i}\sum_{l=0}^{\infty}\sum_{m_l=-l}^{l} u_{\kappa i,m_i,l,m_l}(r)Y_{l,m_l}\Upsilon_{i,m_i} \tag{5.34}$$
$$= \frac{1}{\kappa r}\sum_{\alpha} u_{\kappa\alpha}(r)Y_{l,m_l}\Upsilon_{i,m_i}, \tag{5.35}$$

here α is the channel index introduced for notational convenience. It is defined to specify all relevant quantum numbers; for now i, m_i, l, m_l. Furthermore let $\Upsilon_\alpha = Y_{l,m_l}\Upsilon_{i,m_i}$.

Inserting equation 5.35 into the Schrödinger equation no longer neatly factorizes into separate radial and angular equations. Rather the radial equations now couple the different $u_{\kappa\alpha}$. A set of coupled differential equations can be obtained after insertion, by multiplying the Schrödinger Equation by $\Upsilon^*_{\alpha'}$ and integrating. This yields the following equations, the solution of which are the spin-channel radial wave function u_α

$$\left[\frac{\mathrm{d}^2}{\mathrm{d}r^2} + \kappa^2 - \frac{l(l+1)}{r^2}\right] u_{\kappa\alpha}(r) - \sum_{\alpha'} U_{\alpha'\alpha} u_{\kappa\alpha'}(r) = 0, \tag{5.36}$$

where the potential term $U_{\alpha\alpha'}$ is given by

$$\begin{aligned} U_{\alpha\alpha'} &= \langle \Upsilon_\alpha | U | \Upsilon_{\alpha'} \rangle & (5.37)\\ &= \sum_{m_l m_i} \sum_{m'_l m'_i} \langle l m_l; i m_i | j m_j \rangle \langle l' m'_l; i' m'_i | j m_j \rangle & (5.38)\\ &\quad \langle Y_{l m_l} \chi_{i m_i} | U | Y_{l' m'_l} \chi_{i' m'_i s} \rangle \,. & (5.39) \end{aligned}$$

In comparing equations 5.15 and 5.39 we note that this is now a coupled set of differential equations, with solutions $u_\alpha(r)$.

Next we shall see how this coupling of the spin channels affects the asymptotic behaviour, such as we have expressed it in the spin free case given by equations 5.27, 5.28 and 5.29. To this end it is instructive to consider eigenfunctions not of the total spin angular momentum, but rather the total angular momentum $J = L + I$, where L is the orbital angular momentum operator. Proceeding as we did to obtain the total spin eigenfunctions, we couple the spin and orbital angular momentum to find construct simultaneous eigenfunctions of $\mathbf{J}^2$, J_z, $\mathbf{I}^2$ and $\mathbf{L}^2$,

$$\Upsilon_{j,m_j,l,i} = \sum_{m_i m_l} \langle l m_l; i m_i | j m_j \rangle \, Y_{l m_l} \chi_{i m_i}, \tag{5.40}$$

In the case of conserved total angular momentum the radial solutions $u_{\alpha\alpha'}$ can only couple to each other if they belong to the same block of radial solutions defined by common total common angular momentum quantum numbers j and m_j. Every solution within such a block may be constructed as a linear super position over a basis of functions u_{l_α}, corresponding to the solutions of the uncoupled problem. Such a linear superposition, coupling the regular and irregular solutions in the different channels, may be expressed as

$$u_{\kappa\alpha}(r) = \sum_{\alpha'} c_{\alpha'} u_{\alpha',\alpha\kappa}, \tag{5.41}$$

where $u_{\alpha',\alpha\kappa}$ contributes to the α' channel, so that we now write

$$\psi_\alpha(\mathbf{r}) = \sum_{\alpha'} c_{\alpha'} Y_{l',m'} \frac{u_{\alpha',\alpha\kappa}(r)}{r}. \tag{5.42}$$

Now, in analogy to how we proceeded from equations 5.8 and 5.10 to set up equation 5.27, we may obtain the expressions (valid in the region for $r > R_u$)

$$\begin{aligned} u_{\alpha',\alpha\kappa} &\propto \delta_{\alpha\alpha'} F_l(\kappa r) + K_{\alpha\alpha'} G_{l'}(\kappa r) & (5.43)\\ u_{\alpha',\alpha\kappa} &= \delta_{\alpha\alpha'} F_l(\kappa r) + T_{\alpha\alpha'} \tilde{G}_{l'}(\kappa r) & (5.44)\\ u_{\alpha',\alpha\kappa}(r) &= \frac{i}{2}\left(\delta_{\alpha\alpha'} H_l^-(\kappa r) - S_{\alpha\alpha'} H_l^+(\kappa r)\right) & (5.45) \end{aligned}$$

This defines the reactance ($\mathbb{K}$) matrix, transmission ($\mathbb{T}$) matrix and scattering matrix ($\mathbb{S}$). In the simplest case of one channel only, these reduce to the the expressions 5.27, 5.28 and 5.29 in terms of δ_l. As we did in the single channel section it is possible in the multi channel case to derive the scattering amplitude in terms of these matrices. Therefore knowledge of any one of them amounts to the solution of the problem. We will show at the end of the next section how one may derive an equation yielding the scattering amplitude in terms of the $\mathbb{S}$ matrix.

5.2 Close Coupling - Internal Structure

In the previous section we saw the kind of modifications to the single channel case necessary to account for problems including spin. Next we shall widen the scope still, by allowing the target or projectile to have additional internal degrees of freedom. The description of the photo ionization of but the simplest molecules requires this treatment so as to be able to account for internal excitations, leaving the molecule in an excited state after ionization.

Equivalent to equation 5.33 we expand the total wave functions in channel functions. Only now these channel functions will not only describe the spin of the problem, but also any other degree of freedom we may want to include in our problem. Thus we write

$$\begin{aligned} \psi(\mathbf{r}, \mathcal{X}) &= \sum_{\alpha} \psi_{\alpha}(\mathbf{r}) \Upsilon_{\tilde{\alpha}}(\mathcal{X}) && (5.46) \\ &= \frac{1}{\kappa r} \sum_{\alpha} u_{\alpha}(r) Y_{lm} \Upsilon_{\tilde{\alpha}}(\mathcal{X}), && (5.47) \end{aligned}$$

where we have separated the total channel index α into l, m and the remaining set of quantum numbers $\tilde{\alpha}$. Further more we let $\mathcal{X}$ denote the set of variables describing the internal structure of in general the target and the projectile. However as we will later focus on photo ionization, i.e. the ejection of one electron from a (complicated) molecule, we may effectively think of $\Upsilon_{\tilde{\alpha}}(\mathcal{X})$, as characterizing the molecular ionic state coupled to the spin of the ejected electron. We will formalize this in the section 5.4 on photo ionization.

We now set up the Schrödinger Equation for this problem in such way so as to allow for the internal structure to undergo excitations during the scattering process. To this end let $H_{\mathcal{X}}$ be the Hamiltonian whose eigenfunctions are the different scattering channels $\Upsilon_{\tilde{\alpha}}(\mathcal{X})$:

$$H_{\mathcal{X}} \Upsilon_{\tilde{\alpha}}(\mathcal{X}) = E_{\tilde{\alpha}} \Upsilon_{\tilde{\alpha}}(\mathcal{X}). \tag{5.48}$$

Thus the complete Hamiltonian of the system may be written as $H = H_{\mathcal{X}} + H^{\mathrm{sc}}(\mathbf{r}, \mathcal{X})$, where the former term, as just explained accounts for the internal energy of the participants of the scattering process, and the latter $H^{\mathrm{sc}}(\mathbf{r}, \mathcal{X})$, describes the interaction of the participants due to the scattering process. Hence we may write the Schrödinger equation as

$$\left[-\nabla^2 + H_{\mathcal{X}} + H^{\mathrm{sc}}(\mathbf{r}, \mathcal{X})\right] \psi_{\alpha}(\mathbf{r}, \mathcal{X}) = E \psi_{\alpha}(\mathbf{r}, \mathcal{X}) \tag{5.49}$$

Insertion of this equation 5.47 into equation 5.49 (similar to the way we obtained equation 5.36, though including only the channel functions and not the spherical harmonics in the integration for now) yields

$$\begin{aligned} -\nabla^2 \psi_{\tilde{\alpha}}(\mathbf{r}) + \sum_{\tilde{\alpha}'} V_{\tilde{\alpha}\tilde{\alpha}'} \psi_{\tilde{\alpha}'}(\mathbf{r}) &= (E - E_{\tilde{\alpha}}) \psi_{\tilde{\alpha}}(\mathbf{r}) \quad \text{where} && (5.50) \\ V_{\tilde{\alpha}\tilde{\alpha}'} &= \langle \Upsilon_{\tilde{\alpha}} | H^{\mathrm{sc}} | \Upsilon_{\tilde{\alpha}'} \rangle_{\mathcal{X}} , && (5.51) \end{aligned}$$

where $\langle\cdot|\cdot\rangle_{\mathcal{X}}$ denotes integration over all variables implied by $\mathcal{X}$. Note that in equation 5.51 the sign of the term $E - E_{\tilde{\alpha}}$ implies, whether the solution should is expected to display bound or scattering behaviour. This motivates the designation of certain channels to be either open or closed. If $E < E_{\tilde{\alpha}}$ we say the channel is closed and expect a bound channel function $\psi_{\tilde{\alpha}}$. Conversely, for $E > E_{\tilde{\alpha}}$, we consider $\tilde{\alpha}$ to be an open channel. Thus we also refer to $E_{\tilde{\alpha}}$ as the channel threshold of channels $\tilde{\alpha}$, beyond which we may expect scattering behaviour.

Next we wish to extend the idea of S and K matrix introduced in the discussion concerning spin, to cover the extension of the notion of a channel to include internal structure beyond spin. To do so we proceed analogous to the way we obtained equation 5.36 in the spin case, yielding

$$\left[-\frac{\mathrm{d}^2}{\mathrm{d}r^2} + \frac{l(l+1)}{r^2}\right] u_{\kappa\alpha}(r) - \sum_{\alpha'} U_{\alpha'\alpha} u_{\kappa\alpha'}(r) = (E - E_\alpha) u_{\kappa\alpha}(r), \tag{5.52}$$

$$= \bar{E}_\alpha u_{\kappa\alpha}(r) \tag{5.53}$$

where now

$$U_{\alpha\alpha'} = \langle Y_{lm}\Upsilon_{\tilde{\alpha}}|H^{\mathrm{sc}}|Y_{l'm'}\Upsilon_{\tilde{\alpha}'}\rangle_{\mathcal{X},\theta,\phi}\,. \tag{5.54}$$

While equations 5.36 and 5.53 are almost identical in structure there is a fundamental difference between the two. In the former the number of channels is guaranteed to be finite. In the latter on the other hand this is no longer the case (as one can easily convince oneself by considering the infinitely many ionic molecular states, that may emerge in a photo ionization process) leading to obvious difficulties in analytical or numerical treatment. Truncation to only a small, treatable number of channels, (guided by physical relevance), is referred to as the close coupling approximation and is the approximation at the core of the treatment on photo ionization we are presenting here. Furthermore we note that now the energy (or wave number) κ_α is channel dependent, changing according to the amount of energy carried off by internal excitation. With this in mind, the asymptotic behaviour of the uncoupled regular and irregular free particle solutions is now given by

$$\lim_{r\to\infty} F_l(\kappa_\alpha r) = \sin(\kappa_\alpha r - \frac{l\pi}{2}) \tag{5.55}$$

$$\lim_{r\to\infty} F_l(\kappa_\alpha r) = \cos(\kappa_\alpha r - \frac{l\pi}{2}), \tag{5.56}$$

where we define $\kappa_\alpha = \sqrt{2(E - E_\alpha)}$. As we shall see shortly, the S matrix, in allowing for inelastic scattering, turns out to depend on the normalization of the uncoupled free particle solutions. Where normalization is here meant as the usual, free particle delta function normalization given by $\langle\kappa_\alpha|\kappa'_\alpha\rangle = \delta(\kappa_\alpha - \kappa'_\alpha)$. In allowing for inelastic scattering the normalization is thus channel dependent, as is easy to see from $\delta(\kappa_\alpha - \kappa'_\alpha) \neq \delta(\kappa_{\alpha'} - \kappa'_{\alpha'})$. This gives rise to ambiguities which can be circumvented by redefining the regular and irregular solutions as

$$\bar{F}_l(\kappa_\alpha r) = \sqrt{\frac{2}{\pi\kappa_\alpha}} F_l(\kappa_\alpha r) \tag{5.57}$$

$$\bar{G}_l(\kappa_\alpha r) = \sqrt{\frac{2}{\pi\kappa_\alpha}} G_l(\kappa_\alpha r),$$

resulting in the normalization reading now $\langle\bar{F}_l(\kappa_\alpha r)|\bar{F}_l(\kappa_{\alpha'} r)\rangle = \delta(E - E')$, independent of the channels. Considering now the asymptotic behaviour of the inelastic problem, the argument is essentially equivalent to the case of including spin only. This is to say, for a given energy E we expect the solution to be a linear combination of a number of functions equivalent to the number of open channels for that given energy (akin to the way in which previously we considered channels of equal total angular momentum J

to couple). To formalize this we set up equations, in appearance identical to the corresponding equations for the elastic treatment including spin, but with the necessary modification to normalize correctly (where the definitions of $\bar{\bar{G}}$ and $\bar{H^{\pm}}$ naturally extend from those in equations 5.58), giving

$$\begin{aligned} u^{\mathbb{K}}_{\alpha',\alpha\kappa} &\propto \delta_{\alpha\alpha'}\bar{F}_l(\kappa r) + \mathbb{K}_{\alpha\alpha'}\bar{G}_{l'}(\kappa r) && (5.58)\\ u^{\mathbb{T}}_{\alpha',\alpha\kappa} &= \delta_{\alpha\alpha'}\bar{F}_l(\kappa r) + \mathbb{T}_{\alpha\alpha'}\bar{\bar{G}}_{l'}(\kappa r) && (5.59)\\ u^{\mathbb{S}}_{\alpha',\alpha\kappa}(r) &= \frac{i}{2}\left(\delta_{\alpha\alpha'}\bar{H}^{-}_l(\kappa r) - \mathbb{S}_{\alpha\alpha'}\bar{H}^{+}_l(\kappa r)\right). && (5.60)\end{aligned}$$

In terms of the $\mathbb{K}$,$\mathbb{T}$ or $\mathbb{S}$ matrix, asymptotically these $u_{\alpha',\alpha\kappa}$ behave as

$$\begin{aligned} \lim_{r\to\infty} u^{\mathbb{K}}_{\alpha',\alpha\kappa} &\propto \sqrt{\frac{2}{\pi\kappa_\alpha}}\delta_{\alpha\alpha'}\sin(\kappa_\alpha r + \frac{l\pi}{2}) + \sqrt{\frac{2}{\pi\kappa_{\alpha'}}}\mathbb{K}_{\alpha\alpha'}\cos(\kappa_\alpha r + \frac{l\pi}{2}) && (5.61)\\ \lim_{r\to\infty} u^{\mathbb{T}}_{\alpha',\alpha\kappa} &= \sqrt{\frac{2}{\pi\kappa_\alpha}}\delta_{\alpha\alpha'}\sin(\kappa_\alpha r + \frac{l\pi}{2}) + \sqrt{\frac{2}{\pi\kappa_{\alpha'}}}\mathbb{T}_{\alpha\alpha'}e^{i(\kappa_{\alpha'}-\frac{l\pi}{2})} && (5.62)\\ \lim_{r\to\infty} u^{\mathbb{S}}_{\alpha',\alpha\kappa} &= \sqrt{\frac{2}{\pi\kappa_\alpha}}\delta_{\alpha\alpha'}e^{-i(\kappa_{\alpha'}-\frac{l\pi}{2})} + \sqrt{\frac{2}{\pi\kappa_{\alpha'}}}\mathbb{S}_{\alpha\alpha'}e^{i(\kappa_{\alpha'}-\frac{l\pi}{2})}. && (5.63)\end{aligned}$$

The fact that the three matrices arise simply from different linear combinations of the irregular and regular solutions, implies that these matrices are intrinsically connected. As we shall not need it in later treatment we shall from now on disregard the $\mathbb{T}$ matrix and present only the relationship between $\mathbb{S}$ and $\mathbb{K}$ matrix. Let $\mathbf{u}_{\alpha\kappa}$ be the vector, with dimensionality equal to the number of channels, with entries $u_{\alpha',\alpha\kappa}$, for any of the three representation corresponding to $\mathbb{K}$,$\mathbb{T}$ or $\mathbb{S}$ matrix formalism. Starting from $\mathbf{u}^{\mathbf{S}_{\alpha\kappa}}$ (and using the notation $\exp(\underline{\kappa}) = (\cdots, \exp(\kappa_\alpha), \cdots)^{\mathrm{T}}$) we write

$$\begin{aligned} \lim_{r\to\infty} \mathbf{u}^{\mathbb{S}}_{\alpha\kappa} &= \mathbb{I}e^{-i\underline{\kappa}r+\frac{l\pi}{2}} + \mathbb{S}e^{i\underline{\kappa}r+\frac{l\pi}{2}} && (5.64)\\ &= -i(\mathbb{I}+\mathbb{S})\sin(\underline{\kappa}r + \frac{l\pi}{2}) + (\mathbb{I}-\mathbb{S})\cos(\underline{\kappa}r + \frac{l\pi}{2}). && (5.65)\end{aligned}$$

Comparing the coefficients of the trigonometric terms in this expression, to those arising from the equivalent K matrix expression

$$\lim_{r\to\infty} \mathbf{u}^{\mathbb{K}}_{\alpha\kappa} = N(\sin(\underline{\kappa}r + \frac{l\pi}{2}) + \mathbb{K}\cos(\underline{\kappa}r + \frac{l\pi}{2})) \tag{5.66}$$

yields, by eliminating the normalization factor N, the relation

$$\begin{aligned} -i(\mathbb{I}+\mathbb{S})\mathbb{K} &= \mathbb{I}-\mathbb{S} \quad \Leftrightarrow && (5.67)\\ \mathbb{S} &= \frac{\mathbb{I}+i\mathbb{K}}{\mathbb{I}-i\mathbb{K}}. && (5.68)\end{aligned}$$

Besides quantifying the intrinsically linked nature of the $\mathbb{S}$ and $\mathbb{K}$ matrices, this relation demonstrates the unitarity of the $\mathbb{S}$ matrix, which is a consequence of equation 5.68 and the hermiticity of $\mathbb{K}$, the latter of which is in turn a direct consequence of the hermiticity of $U_{\alpha\alpha'}$ of equation 5.54. In passing we also note that for the single channel case, equation 5.68 trivially simplifies to the trigonometric identity implied by equations 5.27 and 5.29.

Following similar steps to what was done for the single channel case by starting now from the boundary condition with the now channel dependent scattering amplitude $f_{\alpha\alpha'}$ representing an initial plane wave

in channel α,

$$\lim_{r\to\infty}\psi(\mathbf{r},\mathcal{X}) = e^{ik_\alpha}\Upsilon_{\tilde{\alpha}}(\mathcal{X}) + \sum_{\tilde{\alpha}' \text{ open}} f_{\alpha,\alpha'}(\theta,\phi)\frac{e^{i\kappa_{\alpha'}r}}{r}\Upsilon_{\tilde{\alpha}'}(\mathcal{X}) \tag{5.69}$$

we may relate the scattering amplitude to the $\mathbb{S}$ matrix as

$$f_{\alpha\alpha'}(\theta,\phi) = \sum_{l',m'} Y_{l'm'}\sum_{l}\sqrt{\frac{\pi(2l+1)}{\kappa_\alpha\kappa_{\alpha'}}}(\mathbb{S}_{\alpha\alpha'} - \delta_{\alpha\alpha'}\delta_{ll'}\delta_{mm'}). \tag{5.70}$$

We shall not prove this here[124], as the essence of this is provided in the equivalent steps for the single channel case (i.e. using the partial wave expansion of a plane wave and establishing equivalence with the expression for the boundary condition), and we present this result primarily to highlight the connection between scattering amplitude and $\mathbb{S}$ matrix for a case more complex than the single channel case.

5.3 Hydrogen

So far this discussion of scattering has not yet specified a potential but rather presented a discussion valid for any potential decaying faster than r^{-1}. We will now consider the Coulomb potential. The first thing to note is that this is in violation of exactly that condition, with the potential being given by $V(r) \propto r^{-1}$. We saw some of the eigenstates of Hydrogen already in the discussion of Hydrogenic basis functions. These however were confined to the case of bound states. We will now briefly discuss the analytical solution of continuum states, and relate them to the scattering theory of the previous section. As was the case for bound state theory, Hydrogen is the most complex case of interest to us, for which an analytical solution exists. Thus is useful not only in conceptually providing inside into scattering theory without any increasingly cluttered nomenclature, but also in providing a useful benchmark to verify the correctness (and accuracy) of the tools we develop to tackle more complex systems. Furthermore we shall see that, upon taking certain limits, problems involving more intricate systems than hydrogen, reduce to a Hydrogenic problem.

Substituting $\rho = \kappa r$, the regular radial solution to Hydrogen is give by the function

$$F(\rho,\eta)_l = 2^l\rho^{l+1}e^{i\rho-\frac{\pi\eta}{2}}\,{}_1F_1(l+1+i\eta, 2l+2; -2i\rho), \tag{5.71}$$

where $\eta = Z\kappa^{-1}$ is the Sommerfeld parameter and ${}_1F_1$ are the degenerate hypergeometric functions given for example by the expression

$${}_1F_1(a,b,z) = \sum_{n=0}^{\infty}\frac{\Gamma(a+n-1)\Gamma(b-1)}{\Gamma(b+n-1)\Gamma(a-1)n!}z^n. \tag{5.72}$$

For its limiting behaviour we may find that

$$\lim_{r\to\infty}F_l(\kappa r,\eta) = e^{i\sigma_l}\sin(kr - \frac{\pi l}{2} + \sigma_l - \eta\log(2\kappa r)), \tag{5.73}$$

where the Coulomb Phase σ_l is given by

$$\sigma_l = \arg\Gamma(l+1+i\eta). \tag{5.74}$$

As before, next to the regular solution, we must consider for general Coulombic scattering also the irregular solution and construct the full solutions to the scattering problem as a linear combination of the two. The irregular $G_l(\rho,\eta)$ solutions are given by so called Whittaker functions[125]

$$G_l(\rho,\eta) = iF_l(\rho,\eta) + e^{\frac{\pi}{2}\eta}\frac{|\Gamma(l+1+i\eta)|}{\Gamma(l+1+i\eta)}e^{-i(\rho-\frac{l\pi}{2}}(2i\rho)^{l+1}U(l+1-i\eta, 2l+2; 2i\rho) \tag{5.75}$$

where $U(a,b,z)$ are the confluent hypergeometric functions given by

$$U(a,b,z) = \frac{\Gamma(1-b)}{\Gamma(a-b+1)}\,{}_1F_1(a,b;z) + \frac{\Gamma(b-1)}{\Gamma(a)} z^{1-b}\,{}_1F_1(a-b+1,2-b;z). \tag{5.76}$$

Similar to what we found for the non-Coulombic case the asymptotic behaviour of the irregular solution is given by

$$\lim_{r\to\infty} G_l(\kappa r,\eta) = e^{i\sigma_l}\cos(kr - \frac{\pi l}{2} + \sigma_l - \eta\log(2\kappa r)),. \tag{5.77}$$

Considering now a multi channel problem in the presence of a Coulombic long range interaction between the fragments of the scattering participants we write (in analogy to equation 5.49) the radial Schrödinger Equation as

$$\left[-\nabla^2 + H_{\mathcal{X}} + \frac{Z}{r} + H^{\rm sc}(\mathbf{r},\mathcal{X})\right]\psi_\alpha(\mathbf{r},\mathcal{X}) = E\psi_\alpha(\mathbf{r},\mathcal{X}) \tag{5.78}$$

which if broken down into channels reads

$$\left[-\frac{\nabla^2}{2} + \frac{Z}{r}\right]\psi_{\tilde\alpha}(\mathrm{r}) + \sum_{\tilde\alpha'} V_{\tilde\alpha\tilde\alpha'} = (E-E_\alpha)\psi_{\tilde\alpha}(\mathrm{r}). \tag{5.79}$$

It might then seem natural to continue as was done before by considering the boundary condition 5.12 and thus derive an expression for the, say $\mathbb{S}$ matrix. But, not only would that be of no use to the problems we shall look into later, it also turns out to be impossible[126]. The reason for this is the long range nature of Coulomb potentials, which can be understood by thinking of the notion of an asymptotically free particle in the Coulomb case as invalid, i.e. the particle feels the Coulomb potential everywhere. We mention it is possible to construct a partial wave expansion for a "free" particle in a Coulombic field [127], but we shall not pursue this here.

Rather we think of the scattering phase in a multi channel case with Coulombic interaction between the fragments (as is the case between the ejected electron and the resulting ion in photoionization), as relative to that of a pure Coulombic (that is the say Hydrogenic) case, with the aforementioned regular and irregular solutions. With that in mind we continue in much the same way as before with the intention of developing equivalent radially asymptotic expressions in terms of the $\mathbb{K}$ and $\mathbb{S}$ matrices. To do so, we again modify the definition of the regular solutions to avoid ambiguities in the normalization leading (in the regular case) to:

$$\bar F_l(\rho_\alpha,\eta_\alpha) = \sqrt{\frac{2}{\pi\kappa_\alpha}} F_l(\rho_\alpha,\eta_\alpha) \quad \text{with} \tag{5.80}$$

$$\lim_{r\to\infty}\bar F_l(\rho_\alpha,\eta_\alpha) = \sqrt{\frac{2}{\pi\kappa_\alpha}}\sin(\rho_\alpha\frac{l\pi}{2} - \eta_\alpha\ln(2\rho_\alpha) + \sigma_{l\alpha}) \quad \text{where} \tag{5.81}$$

$$\sigma_{l\alpha} = \Gamma(l+1+i\eta_\alpha), \tag{5.82}$$

with equivalent definitions and asymptotic behaviours for $\bar G_l$, $\bar{\bar G}_l$ and $\bar H_l^{\pm}$. Note that this naturally leads to channel depend phase shifts. Thus for a multichannel problem in the presence of a Coulombic potential, we are lead to the definitions of the $\mathbb{K}$, $\mathbb{T}$ and $\mathbb{S}$ matrix in terms of these functions, once again in close analogy to equations 5.62 and 5.63.

5.4 Photoionization

Up until now this discussion with scattering theory has made only passing reference to photo ionization. Photo ionization being however one of the principal foci of this project, we will next turn our attention to how the formalism developed so far may be used to treat the escape of an electron into the continuum as brought about by the interaction of a molecule with a photon. The treatment of this is effectively equivalent to the standard treatment of light matter interaction between bound states, only that now one of the bound states is a continuum state. Thus we may view photo ionization as a "half scattering problem", and as such represents one of the simplest scattering processes, by virtue of involving continuum states only in its final state. In addition to setting up the relevant theory for the *ab initio* approach such as we present here, we shall also introduce an alternative, approximate treatment photo ionization cross section which was used in this project.

To capture the interaction of a molecule with time dependent electromagnetic field, the Hamiltonian is in general is given by

$$H(\mathbf{r},t) = \sum_{i=1}^{N_e}\left[\frac{1}{2}\left[\nabla_i - \mathbf{A}(\mathbf{r}_i,t)\right]^2 + \frac{\partial \mathbf{A}(\mathbf{r}_i,t)}{\partial t} + V(\mathbf{r}_i)\right] \tag{5.83}$$

$$A(\mathbf{r},t) = \hat{\boldsymbol{\varepsilon}}\int_{\Delta\omega} A_0(\omega)e^{i(\mathbf{kr}-\omega t)}, \tag{5.84}$$

were $\hat{\boldsymbol{\varepsilon}}$ is the polarization vector of the field and A_0 the amplitude of its potential. In the presence of an electron magnetic field we find the transition rate between two states a and b of the system to be proportional to the quantity M_{ab} given by

$$\begin{aligned} M_{ab} &= \sum_{i=1}^{N_e}\langle\psi_a(\mathrm{r}_1,\cdots,\mathrm{r}_{N_e})|\hat{\boldsymbol{\varepsilon}}\nabla_i e^{i\mathbf{kr}_i}|\psi_b(\mathrm{r}_1,\cdots,\mathrm{r}_{N_e})\rangle \\ &= N_e\,\langle\psi_a(\mathrm{r}_1,\cdots,r_{N_e})|\hat{\boldsymbol{\varepsilon}}\nabla_1 e^{i\mathbf{kr}_1}|\psi_b(\mathrm{r}_1,\cdots,\mathrm{r}_{N_e})\rangle \end{aligned} \tag{5.85}$$

where the second line follows from the antisymmetry of the electronic wave function and where we have neglected the term quadratic in $\mathbf{A}$, resulting from the expansion of $\left[\nabla_i - \mathbf{A}(\mathbf{r}_i,t)\right]^2$.

Assuming the variation of the laser pulse to be small across the region of space occupied by the system interacting with the pulse we may retain the first term only in the expansion $e^{i\mathbf{kr}} = 1 + i\mathbf{kr} + \cdots$. This is clear by comparing the typical size of a small molecule (such as we will investigate here) to the wave number of the kinds of pulses we shall encounter here. Retention of only the first term in the expansion of the exponent in equations 5.87 is the well known Dipole Approximation.

These transition rates may be related to the total cross section σ_{ab} of a molecule interacting with a laser field via the expression

$$\sigma_{ab} = \frac{4\pi^2\alpha}{E_{ab}}|M_{ab}|^2. \tag{5.86}$$

The result such as it is given in the above equation corresponds to working in the velocity gauge. An alternative description of the problem may be obtained via a gauge transformation, leading to the expression for the transition rate in the so called length gauge. The transition rate in length gauge (still assuming the Dipole Approximation) is given by

$$M_{ab} = N_e\,\langle\psi_a(\mathrm{r}_1,\cdots,\mathrm{r}_{N_e})|\hat{\boldsymbol{\varepsilon}}\mathbf{r}_1 e^{i\mathbf{kr}_1}|\psi_b(\mathrm{r}_1,\cdots,\mathrm{r}_{N_e})\rangle\,,, \tag{5.87}$$

which consequently leads to the following expression for the photo ionization cross sections in length gauge

$$\sigma_{ab} \quad = \quad 4\pi^2 \alpha E_{ab} |M_{ab}|^2., \tag{5.88}$$

where in equations 5.86 and 5.88 α is the fine structure constant and E_{ab} the energy difference between the two eigenstates photoinduced transition among which we consider. Despite the gauge invariance of the SE, if we work in an incomplete description of the system to carry out numerical calculations under certain circumstances one gauge may be advantageous in its description of photo ionization over the other, and further agreement between the two gauges may be taken as an indicator of an accurate description of the system.

In photoionization experiment the cross section is often the reported observable and we shall now draw from the theory developed in the previous section to see how we may evaluate the cross section for photoionization of a molecule theoretically. The presence of M_{ab} in equation 5.88 implies that the computation of scattering problems, necessarily requires the explicit computation of the scattering states, the system ionizes to. For large separations between the ionic molecule and the ejected molecule we expect the interaction between the two to be Coulombic and as such asymptotically the wavefunction is a linear combination of the regular and irregular solution to the Hydrogenic case of the previous section. To describe the region where the short range (non-Coloumbic) interaction between the molecule and the ejected electron is relevant we use the close coupling expansion of section 5.2: Given a molecular system with a set of scattering states with an electron in the continuum, we map the structure of these states to the terms introduced in the discussion of inelastic scattering theory. The fragments are now an electron and an ionic molecule. Thus the channel function $\Upsilon_\alpha(\mathcal{X})$ must now capture everything apart from the coordinate of r_{N_e} corresponding to the ion ejected into the continuum. Therefore

$$\Upsilon_{\tilde{\alpha}}(\mathcal{X}) = ^{2S+1}\left[\Phi_a(\mathbf{x}_1, \cdots, \mathbf{x}_{N_e-1}) \otimes \chi(\zeta_{N_e})\right]_\Sigma, \tag{5.89}$$

where Φ_α is the ionic state the molecule is found in after ionization, $\chi(\zeta_{N_e})$ is the spin function of the ejected electron and S and Σ are the total and projected spin of the system, respectively (which as we mentioned before are conserved quantities in the absence of say spin orbit coupling). Expanding the systems wavefunction in terms of these channel functions allows us to formally write the scattering state for arbitrarily complicated molecules as

$$\begin{aligned}
\psi_{E\alpha}(\mathbf{r}, \mathcal{X}) &= \psi(\mathbf{x_1}, \cdots, \mathbf{x}_{N_e}) = \sum_{\alpha'} \Upsilon_{\tilde{\alpha}'} Y_{l'm'}(\theta, \phi) \frac{u_{\alpha',\alpha E}(r)}{r} && (5.90)\\
&= \sum_{\alpha'} {}^{2S+1}[\Phi_a(\mathbf{x}_1, \cdots, \mathbf{x}_{N_e-1}) \otimes \chi(\zeta_{N_e})]_\Sigma Y_{l'm'}(\theta, \phi) \frac{u_{\alpha',\alpha E}(r)}{r} && (5.91)\\
&= \sum_{\alpha'} \sum_{\Sigma_a \sigma} \left[\langle S_a \Sigma_a; 2\sigma | S\Sigma \rangle \, {}^{2S_a+1}\Phi_a(\mathbf{x}_1, \cdots, \mathbf{x}_{N_e-1})_{\Sigma_a} \, {}^2\chi(\zeta_{N_e})_\sigma\right] \\
&\qquad Y_{l'm'}(\theta, \phi) \frac{u_{\alpha',\alpha E}(r)}{r}, && (5.92)
\end{aligned}$$

where in the last line $\langle S_a \Sigma_a; \frac{1}{2}\sigma | S\Sigma \rangle$ are the Clebsch-Gordon coefficient such as was outlined in the discussion of elastic scattering with spin. That is, S_a and Σ_a are the total and projected spin of the molecular ion after ejection of the electron (from now on we shall refer to this as parent ion) and σ is the (up or down) spin of the ejected electron. The channel index α specifies in this problem the angular momenta (spin or otherwise) l, m, S, Σ and the parent ion state alpha a. Equipped with this expression for the molecular scattering states with one electron in the continuum, we now turn our attention to the asymptotic behaviour of the radial function u in the case of photoionization. We follow reference [128] exploring the case of photoionization, to write the asymptotic behaviour of u in terms of the $\mathbb{S}$ matrix as

$$\lim_{r\to\infty} u_{\alpha',\alpha\kappa}(r) = \delta_{\alpha'\alpha}\sqrt{\frac{2}{\pi\kappa_\alpha}}e^{i(\rho_\alpha+\frac{l\pi}{2}+\eta_\alpha \ln(2\rho_\alpha)+\sigma_{l\alpha})} + \mathbb{S}^*_{\alpha\alpha'}\sqrt{\frac{2}{\pi\kappa_{\alpha'}}}e^{-i(\rho_{\alpha'}+\frac{l\pi}{2}+\eta_\alpha \ln(2\rho_{\alpha'})+\sigma_{l\alpha'})}, \quad (5.93)$$

Note that this equation differs from equation 5.63 via complex conjugation. This may be understood that to the discussion introducing scattering theory was based on the assumption of having incoming fragments scattering into a superposition of scattering state. For photodissociation the situation is different in that we are concerned with finding the cross section to some particular scattering channel defined by α. The argument of the exponents in equation 5.93 corresponds to the asymptotic behaviour of a true Coulomb potential, and the $\mathbb{S}$ matrix encodes the entirety of the impact the short range interaction between ejected electron and ionic molecule has on the scattering process. Thus if the $\mathbb{S}$ matrix were known, we could construct the scattering states $\psi_{\alpha\kappa}(\mathrm{r},\mathcal{X})$ and compute the cross section (within the dipole approximation) to ionize to some such scattering states from an initial neutral state ψ_n via

$$\sigma_{\mathrm{n}\alpha} = 4\pi^2\alpha E_{\mathrm{n}\alpha}\left\langle\psi_\alpha|\hat{\boldsymbol{\varepsilon}}\mathrm{r}|\psi_\mathrm{n}\right\rangle. \quad (5.94)$$

Therefore the only object we have do not yet know how to evaluate in order to find the photoionization cross section, is the $\mathbb{S}$ matrix. Before we develop the mathematical formulation of scattering theory necessary for the full *ab initio* treatment of multichannel scattering to evaluate equation 5.94 in chapter 8, we shall briefly digress here to introduce an approximate approach to obtaining information about photo ionization processes based on so called Dyson orbitals and simple assumptions about the nature of the electron ejected into the continuum. Within certain limitations this approach is quite useful and we shall later see it applied to the study of photo dissociation of Nitrogen.

5.4.1 Dyson Orbitals

A Dyson orbital D_i is defined as the overlap between the neutral ψ_n and ionic system ψ_i, before and after ionization, obtained by performing the integral over the common electronic coordinates expressed as

$$D_\alpha(\mathbf{r}) = \langle\psi_i|\psi_n\rangle = \int \mathbf{d}r_2\cdots\mathbf{d}r_{N_e}\psi_i^*(\mathbf{r}_2,\cdots,\mathbf{r}_{N_e})\psi_n(\mathbf{r},\mathbf{r}_2,\cdots,\mathbf{r}_{N_e}). \quad (5.95)$$

We now return to equation 5.94 and will investigate how we may arrive at an expression for $M_{n\alpha}$ in terms of Dyson orbitals (at this level of theory we shall not concern ourselves with the absolute value of the the cross section but rather content ourselves with relative ionization probabilities to different states α, given by the absolute value squared of the matrix elements $M_{n\alpha}$). We begin by writing (within the dipole approximation and letting $\hat{\mathbf{P}}$ be the general dipole transition moment operator without reference to a specific gauge)

$$\begin{aligned} M_{n\alpha} &= \langle\psi_\alpha(\mathbf{r}_1,\cdots,\mathbf{r}_{N_e})|\hat{\boldsymbol{\varepsilon}}\hat{\mathbf{P}}|\psi_n(\mathbf{r}_1,\cdots,\mathbf{r}_{N_e})\rangle & (5.96)\\ &= \sqrt{2}\left\langle D_i(\mathbf{r})|\hat{\boldsymbol{\varepsilon}}\hat{\mathbf{P}}|\phi(\mathbf{r})\right\rangle, & (5.97)\end{aligned}$$

where D_i now denotes the Dyson orbital obtained from the cationic states associated with the channel α and ϕ is the spatial part of the wave function of the ejected electron. For expression 5.97 to hold we assumed the following. The final state's wave function including spin may be written as (breaking with the notation of α being an up and β a down spin to avoid confusion with the channel index)

$$\psi_\alpha = \frac{\hat{\mathcal{A}}}{\sqrt{2}}\left[\psi_{i\uparrow}(\mathbf{r}_2,\cdots,\mathbf{r}_{N_e})\phi_\downarrow(\mathbf{r}_1) - \psi_{i\downarrow}(\mathbf{r}_2,\cdots,\mathbf{r}_{N_e})\phi_\uparrow(\mathbf{r}_1)\right], \quad (5.98)$$

where $\hat{\mathcal{A}} = N_e^{-1/2}(1 - \sum_i^{N_e-1} \hat{P}_{Ni})$ is the antisymmetrization operator, with $\hat{P}_{Ni}$ exchanging the N_e^{th} and i^{th} electron. This neglects the coupling between different channels (such as it is described in the close coupling expansion) and assumes the initial state ψ_n to to be a state of spin $S = 0$. Invoking then strong orthogonality we may write equation 5.97 as [129],

$$M_{n\alpha} = \sqrt{\frac{N_e}{2}} \int \mathbf{d}r_2 \cdots \mathbf{d}r_{N_e} \tag{5.99}$$

$$\langle \psi_{i\uparrow}(\mathbf{r}_2, \cdots, \mathbf{r}_{N_e})\phi_\downarrow(\mathbf{r}_1) - \psi_{i\downarrow}(\mathbf{r}_2, \cdots, \mathbf{r}_{N_e})\phi_\uparrow(\mathbf{r}_1)|\hat{\boldsymbol{\varepsilon}}\hat{\mathbf{P}}|\psi_n(\mathbf{r}_1, \cdots, \mathbf{r}_{N_e})\rangle\,, \tag{5.100}$$

which upon integrating out the spin may be identified with equation 5.97. The Dyson orbitals may be calculated using QCP, whereas in practice the ejected electron's wave function ϕ is approximated using different types of functions. Using Dyson orbitals in conjunction with different types of functions representing the ejected electron has been used in a number of works, and for sufficiently fast electrons, does provide a good approximation for relative photo ionization probabilities [130, 44]. The treatment does however neglect coupling between different channels, and for slow electrons in non atomic systems the assumption of the electron being a plane wave (the electron sees no potential) or a coulomb wave (the electron sees a Coulombic potential) become increasingly poor, and soon fail not only quantitatively as well as qualitatively.

In the course of chapter 11 some results using Dyson orbitals in combination with Coulomb waves are presented. For the more detailed treatment however, underlying the results of chapter 10, significantly more work needs to be done. Before introducing the method capable of this implemented discussed in chapter 8, we use the remainder of this chapter to introduce some more mathematical background as well as to motivate and explain some features observed in photo ionization cross sections, that a Dyson orbitals approach is incapable to account for.

5.5 Resonances

One of the most interesting and recognizable features of scattering processes, is the presence of resonance features in the at certain energies, resulting in dramatic changes in the observed cross-section in the vicinity of the energy characterizing the position of the resonance. These resonances may have their origin in different physical processes. In this work we shall focus on Feshbach resonances, arising as a consequence of for instance (singly or doubly) excited states associated with one channel embedded in the continuum above the ionization threshold associated with a different channel. As we shall see the physics in these situations is very rich, and the development of computational tools to accurately describe these features is one of the principal goals of this work. Before however going into the details of the method used here to achieve such a computational model, we shall present the theoretical considerations underpinning our understanding of resonances due to electronically excited states embedded in a continuous set of continuum states. Excited states which are in energy above the ionization threshold, are commonly referred to as autoionizing states, the reason being that due to their coupling to continuum states they are characterized by a finite lifetime, after which they decay to a states with one electron in a scattering state, leaving the system in an ionized states.

The resonance features arising in the cross section due to the presence of auto ionizing states are of a characteristic asymmetric shape. This is unlike for instance shape resonances, which in origin are attributable to the shape of potential energy landscape, leading to almost bound states decaying to ionized states. These are describe by the well known Breit-Wigner distribution[131], in the shape of a Lorentzian given by

$$\sigma(E) = \frac{\pi}{\kappa^2} \frac{\Gamma}{\frac{1}{4}\Gamma^2 + (E - E_R)^2}, \tag{5.101}$$

where Γ characterizes the lifetime of the almost bound state and E_R its energy. Γ may be related to the scattering phase via the formula

$$\Gamma = 2\left[\left.\frac{\mathrm{d}\delta}{\mathrm{d}E}\right|_{E=E_r}\right]^{-1}. \tag{5.102}$$

After publication of this formula describing shape resonance in 1946 took more than a decade until Fano [34] provided the explication of the asymmetric shape of Feshbach resonances, as having its origin in the interference between two different paths that may lead to the final ionic states. On the one hand direct ionization and on the other hand ionization with intermediate excitation of an autoionizing state, decaying in accordance with its characteristic lifetime. Subsequently, generalizations of this idea followed, accounting for the complications due to the presence of multiple electronic continua to which the auto ionizing state may decay[35] as well as the presence of multiple interfering autoionizing states close to each other in energy[132]. As we shall see, inherent to the discussion of autoionizing states is not only the behaviour of the cross section near the resonance energy, but also the change of the phase that the scattering state, which the system ionizes to, experiences[133]. We shall examine the theory underlying the variations in phase shift and photoionization cross section in some detail.

Isolated Resonance

To this end we begin by applying the results of the scattering theory such as we derived them to a model system, which while not being entirely realistic, does produce a mathematical description of the features we are interested in (see Figure 5.1). This and the next section draw in large part on the work presented in reference [132]. We consider photoionization of some system from its ground state with energy E_0, in the presence of only two channels A and B, for a range of photon energies, such that channel A is open and channel B is closed. We assume now that channel B supports a set of bound states which are well separated in energy and of which we shall focus on the state $|\phi\rangle_B$ of energy E and with radial part $u_B(r)$. Furthermore we denote the energy and radial solution of that same bound states in channel B, if coupling is neglected, by E_0 and $u_0(r)$, respectively. Similarly, we consider $|\psi\rangle_A$ to be the scattering solution of the (decoupled) channel A at the same energy above the ground state.

Focussing on the radial parts of the wave function in each channel, we may write a system of equations by following equation 5.51 coupling u_B to some scattering states u_S

$$\left[-\frac{1}{2m}\frac{\mathrm{d}^2}{\mathrm{d}r^2} + V_A(r)\right] u_A(r) + V_{AB}u_B(r) = Eu_A(r) \tag{5.103}$$

$$\left[-\frac{1}{2m}\frac{\mathrm{d}^2}{\mathrm{d}r^2} + V_B(r)\right] u_B(r) + V_{BA}u_A(r) = Eu_B(r), \tag{5.104}$$

where V_A and V_B are thought of as the the effective potentials, incorporating the angular momentum term of the radial SE. This may be cast into matrix form giving

$$\begin{bmatrix} \hat{\mathcal{H}}_A & V_{AB} \\ V_{BA} & \hat{\mathcal{H}}_B \end{bmatrix} \mathbf{u} = E\mathbf{u}, \tag{5.105}$$

where $\mathbf{u}$ is the vector $(u_A, u_B)^{\mathrm{T}}$. We assume now that $\mathbf{u}$ is restricted to the form

$$\mathbf{u} = (u_A, \alpha u_{0B})^{\mathrm{T}}. \tag{5.106}$$

Where u_{0B} is the solution of the uncoupled SE, $\hat{\mathcal{H}}_A u_{0B} = E_{0B}u_{0B}$. Note that a complete treatment following Fano's original work requires a more careful analysis of this assumptions, more specifically, considering coupling of the bound state to not only to a continuum state of the same energy but but rather of a continuous spectrum of scattering states. This somewhat complicates the analysis and as the assumption inherent in equation 5.106 captures what we are interested in we shall refer to Fano's original paper for the details of this. Use of this assumption in equation 5.105 leads to the equations

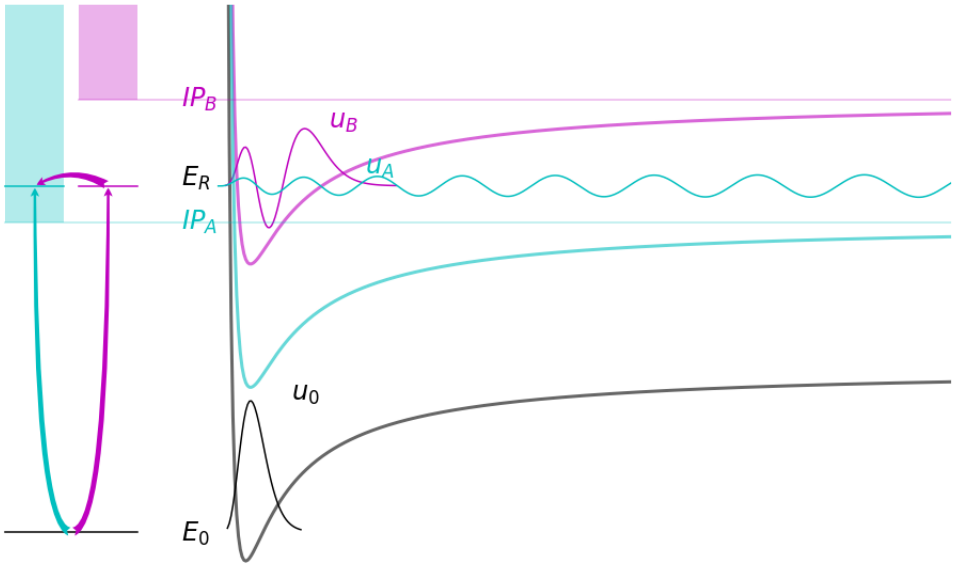

Figure 5.1: Schematic Depiction of the model used to developed the properties of isolated autionizing states decaying to a singel continuum. The right side displays in black the ground state u_0 from which the system ionizes and in cyan and magenta the states u_A and u_B. The former is a scattering state of potential A, the latter a bound state in channel B (both of them of energy $E_0 + E_R$). Furthermore the ionization thresholds associated with either channel are shown. The rectangles on the level represent the continua associated with each channels, the lines represent the states depicted on the right and the arrows mark the two possible (interefering) path leaving the system in an ionized (scattering) state.

$$V_{BA}u_A + \alpha E_{0B}u_{0B} = \alpha E u_{0B} \quad \Leftrightarrow \tag{5.107}$$
$$\langle u_{0B}|V_{BA}|u_A\rangle + \alpha u_{0B}(E_{0B} - E) = 0, \tag{5.108}$$

and

$$\hat{\mathcal{H}}_A u_a = \alpha V_{AB} u_{0B}. \tag{5.109}$$

The latter's Green functions equations reads

$$\hat{\mathcal{H}}_A \mathcal{G}(r, r') = \delta(r - r') \tag{5.110}$$

whose the solution, allows to formally recast the solution to equation 5.109 as

$$u_A(r) = u^{\text{reg}}(r) + \alpha \int_0^\infty \mathrm{d}r' \mathcal{G}(r, r') V_{AB}(r') u_{0B}(r'), \tag{5.111}$$

which, in writing the Greens function in therms of the regular and irregular solutions u^{reg} and u^{irr} of $\mathcal{H}_A u_A = 0$ as

$$\mathcal{G}(r, r') = -\pi \left[\theta(r' - r) u^{\text{reg}}(r) u^{\text{irr}}(r') + \theta(r - r') u^{\text{reg}}(r') u^{\text{irr}}(r)\right], \tag{5.112}$$

gives u_A asymptotically as

$$\lim_{r\to\infty} u_A(r) = u^{\text{reg}} - \alpha\pi \langle u^{\text{reg}}|V_{AB}|u_{0B}\rangle\, u^{\text{irr}}. \tag{5.113}$$

Making now use of the asymptotic behaviour of u^{reg} and u^{irr} given by

$$\lim_{r\to\infty} u^{\text{reg}}(r) = \sqrt{\frac{2}{\kappa\pi}}\sin(\kappa r + \delta_b) \tag{5.114}$$

$$\lim_{r\to\infty} u^{\text{reg}}(r) = \sqrt{\frac{2}{\kappa\pi}}\cos(\kappa r + \delta_b), \tag{5.115}$$

where δ_b is the phase shift in the case of decoupled channels, accounting for the influence of the potential V_A and the angular momentum term $\frac{l\pi}{2}$, gives the asymptotic solution of u_A as

$$\lim_{r\to\infty} u_A(r) = \sqrt{\frac{2}{\pi\kappa}}\left[\sin(\kappa r + \delta_b) - \alpha\pi\left\langle u^{\text{reg}}|V_{AB}|u_{0B}\right\rangle\cos(\kappa r + \delta_b)\right]. \tag{5.116}$$

At this point we introduce the resonant phase shift δ_r, identifying it with the arctangent of the coefficient of the cosine term in the previous equation, allowing to rewrite that equation to return it to its familiar scattering form, with now an additional contribution to the phase shift, characterizing the interaction between the continuum and bound states u_A and u_B via

$$\lim_{r\to\infty} u_A(r) = \frac{1}{\cos(\delta_r)}\sqrt{\frac{2}{\pi\kappa}}\sin(\kappa r + \delta_b + \delta_r). \tag{5.117}$$

Note that $\tan\delta_r$ still contains a factor of α, which is as yet unknown. To arrive at an expression for α insert the formal Greens functions solution of equation 5.111 into equation 5.108 to give

$$\alpha(E - E_0) = \langle u_{0B}|V_{AB}|u^{\text{reg}}\rangle + \alpha\left\langle u_{0B}|V_{BA}\hat{G}V_{AB}|u_{0B}\right\rangle \tag{5.118}$$

$$\tan\delta_r = -\pi\frac{|\left\langle u^{\text{reg}}|V_{AB}|u_{0B}\right\rangle|^2}{E - E_0 - \left\langle u_{0B}|V_{BA}GV_{AB}|u_A\right\rangle}. \tag{5.119}$$

From this equation we may conclude some of the key properties of auto ionizing states. Wee see that as the energy traverses the pole of equation 5.119 $\tan(\delta_r)$ jumps from $-\infty$ to ∞ translating to a rapid change in δ_b by π.

We thus associate $E_r = E_0 + \langle u_0|V_{BA}GV_{AB}|u_0\rangle$ with the energy of the auto ionizing states, and $\Gamma = \pi|\left\langle u^{\text{reg}}|V_{AB}|u_0\right\rangle|^2$ with its widths. The widths can, via the Fermi Golden Rules be related to the characteristic lifetime $\tau = \Gamma^{-1}$ after which the auto ionizing state decays to the continuum. We may thus simplify equation 5.119 to read

$$\tan\delta_r = -\frac{\Gamma}{2(E - E_r)} \tag{5.120}$$

The interpretation of E and Γ, is valid as long as we assume the terms appearing equation 5.119 to be at most weakly dependent on E in the vicinity of the auto ionizing state. This assumption holds if the auto ionizing states is well separated in energy from other auto ionizing states or ionization thresholds, the influence of which we are ignoring at present. Before investigating the effect of more complex configurations of channels complicating the situation, we shall examine the effect of the presence of an auto ionizing states on the cross section, such as it would be observed in an experiment.

We return thus to equations 5.13 and 5.13 to write the total integrated cross sections as

$$\sigma = \frac{1}{k^2}\left|\int\sum_l e^{i\delta_l}(2l+1)\sin\delta_l P_l(\cos(\theta))\mathrm{d}\Omega\right|^2 \tag{5.121}$$

$$= \frac{4\pi}{k^2}\sum_l(2l+1)\sin(\delta_{b,l} + \delta_{r,l})^2 = \sum_l\sigma_l, \tag{5.122}$$

where we have exploited the orthogonality of Legendre Polynomials given by

$$\int_{-1}^{1} P_l(\cos\theta)P_{l'}(\cos\theta)\mathrm{d}(\cos\theta) = \frac{2}{2l+1}\delta_{ll'}. \tag{5.123}$$

Focussing now on one of the terms σ_l in equation 5.122 we may rewrite this as (dropping the l-index in the background and scattering phase shift):

$$\sigma_l \propto \sin^2(\delta_b + \delta_r) = \frac{1}{1+\cot^2(\delta_b+\delta_r)} = \frac{(\cot\delta_b + \cot\delta_r)^2}{(1+\cot\delta_b)(1+\cot\delta_r)} \tag{5.124}$$

$$= \sin^2\delta_b \frac{(\varepsilon+q)^2}{(1+\varepsilon)^2} = \sin^2\delta_b F(q,\varepsilon), \tag{5.125}$$

where in the second line we have defined the reduced energy $\varepsilon = -\cot\delta_r = \Gamma(2(E-E_r))^{-1}$ and the Fano q-parameter $q = -\cot(\delta_b)$ entering in the equation as arguments to the Beutler-Fano function F. The shape of this functions is, next to the π jump in phase at E_R, one of the typical features of auto ionizing states.

Multiple Resonances

Moving now to a more complicated situation, we consider the case of how the preceding discussion changes if in addition to the bound state $|\psi_B\rangle$ there is present another bound states close in energy (what we mean when we say close in energy, is that their energetic separation is smaller than their widths). In essence this is a straightforward generalization of what we have done so fore, but the mathematical treatment is a little more involved.

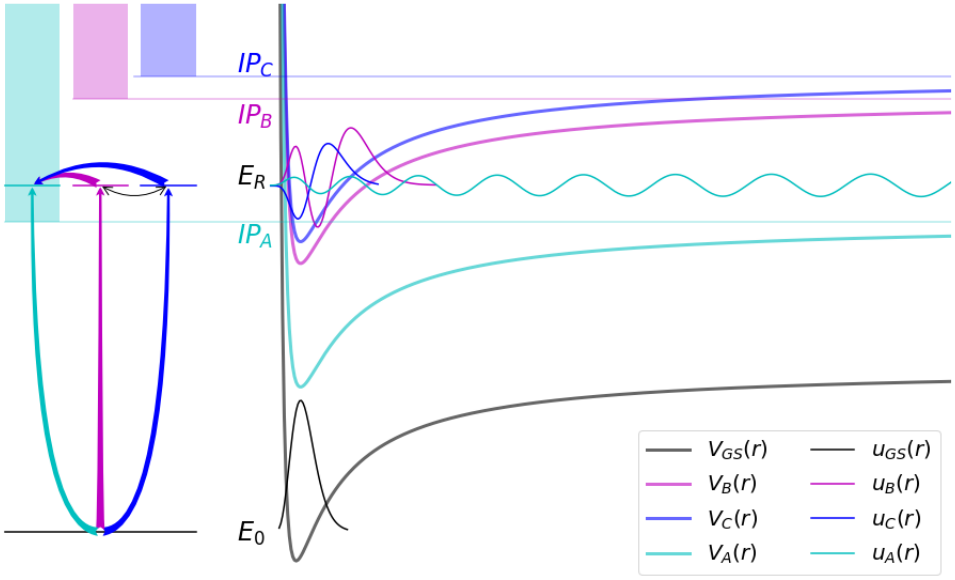

Figure 5.2: S.

The starting point is the obvious extension of equation 5.105

$$\begin{bmatrix} \hat{\mathcal{H}}_A & V_{AB} & V_{AC} \\ V_{BA} & \hat{\mathcal{H}}_B & V_{BC} \\ V_{CA} & V_{CB} & \hat{\mathcal{H}}_C \end{bmatrix} \mathbf{u} = E\mathbf{u}, \tag{5.126}$$

where now we assume $\mathbf{u} = (u_A, \alpha u_{0B}, \beta u_{0C})^{\mathrm{T}}$, with the notation being a straightforward extension of the notation used in the case of a single autoionizing state. We follow now steps essentially equivalent to what was done for the case of only one bound state embedded in the continuum of V_A. From the lower two equations resulting from equation 5.126 we obtain

$$\begin{aligned} \alpha(E_{0B} - E) + \langle u_{0B}| \left[V_{BA} |u_A\rangle + \beta V_{BC} |u_C\rangle\right] &= 0 \quad (5.127) \\ \beta(E_{0C} - E) + \langle u_{0C}| \left[V_{CA} |u_A\rangle + \alpha V_{CB} |u_B\rangle\right] &= 0, \quad (5.128) \end{aligned}$$

whereas for the first equation we once more make use of the Greens functions leading to the asymptotic behaviour

$$\begin{aligned} u_A(r) &= u^{\mathrm{reg}}(r) + \alpha \int_0^\infty \mathrm{d}r' \mathcal{G}(r,r') \left[V_{AB}(r') u_{0B}(r') + V_{AC}(r') u_{0C}(r')\right] \quad (5.129) \\ &\overset{r\to\infty}{=} u^{\mathrm{reg}} - \pi \left[\alpha \langle u^{\mathrm{reg}}|V_{AB}|u_{0B}\rangle + \beta \langle u^{\mathrm{reg}}|V_{AC}|u_{0C}\rangle\right] u^{\mathrm{irr}}. \quad (5.130) \end{aligned}$$

From this we again identify the tangent of the phase shift as the coefficient of the irregular solution

$$\tan\delta_r = -\pi \left[\alpha \langle u^{\mathrm{reg}}|V_{AB}|u_{0B}\rangle + \beta \langle u^{\mathrm{reg}}|V_{AC}|u_{0C}\rangle\right], \quad (5.131)$$

where now the two unknown coefficients α and β must be eliminated by exploiting equations 5.130. We proceed as before by first eliminating u_A by inserting its Greens Function expression giving

$$\begin{aligned} \alpha(E - E_{0B}) &= \langle u_{0B}| \left[V_{BA} |u^{\mathrm{reg}}\rangle + \alpha V_{BA}\mathcal{G}V_{AB} |u_{0B}\rangle + \beta \left(V_{BA}\mathcal{G}V_{AC} - V_{BC}\right) |u_{0C}\rangle\right] \quad (5.132) \\ \beta(E - E_{0C}) &= \langle u_{0C}| \left[V_{CA} |u^{\mathrm{reg}}\rangle + \beta V_{CA}\mathcal{G}V_{AC} |u_{0C}\rangle + \alpha \left(V_{CA}\mathcal{G}V_{AB} - V_{VB}\right) |u_{0B}\rangle\right] \quad (5.133) \end{aligned}$$

which we simplify by the following definitions (with i referring to the indeces B and C)

$$\begin{aligned} \bar{E}_i &= E_{0i} + \langle u_{0i}|V_{iA}GV_{Ai}|u_{i0}\rangle \quad (5.134) \\ W_{iA} &= \langle u_{0i}|V_{iA}|u^{\mathrm{reg}}\rangle \quad (5.135) \\ W_{BC} &= \langle u_{uB}|V_{BA}GV_{AC}|U_{0C}\rangle + \langle u_{uB}|V_{BC}|U_{0C}\rangle. \quad (5.136) \end{aligned}$$

In terms of these newly defined quantities we may solve for α ad β, which upon subsequent substitution into equation 5.131 yields the expression for the resonant phase shift

$$\tan\delta_r = -\pi \frac{(E - \bar{E}_A)|W_{CA}|^2 + (E - \bar{E}_C)|W_{BA}|^2 + 2\Im(W_{AB}W_{CA}W_{BC})}{(E - \bar{E}_A)(E - \bar{E}_B) - |W_{BC}|^2}. \quad (5.137)$$

It is easy to see how this case reduces to the simple sum of two isolated auto ionizing states if $W_{BC} = 0$, i.e. in absence of coupling the two states (either directly or indirectly via the continuum, given by the two terms in the expression for W_{BC}). In contrast to equation 5.120, equation 5.137 has two poles, the resonance energies $E_\pm$. Furthermore we may obtain the width of these resonances by means of equation 5.102. It is therefore possible to arrive simple analytical expressions for $E_\pm$ and $\Gamma_\pm$ in terms of E_B,E_C,Γ_B,Γ_C, $|W_{BC}|^2$ and $2\Im(W_{AB}W_{CA}W_{BC})$. From these expression one may deduce that, independent of the strength of the coupling parameters, the following must hold

$$\Gamma_+ + \Gamma_- = \Gamma_B + \Gamma_C, \quad (5.138)$$

a relation ship that will prove useful in the presentation of results in chapter 10.

We may also readily extend this discussion to give a basically identical expression for the cross section given

$$\sigma_l \propto \sin^2\delta_b \frac{(\varepsilon+q)^2}{(1+\varepsilon)^2} = \sin^2\delta_b F(q,\varepsilon), \tag{5.139}$$

with the only difference being, that now the reduced energy is a function of $\bar{E}_B$, $\bar{E}_C$ and the various coupling terms W as dictated by $\varepsilon = -\cot\delta_r$.

Multiple Continua

Furthermore, as a final possible complication, rather than considering two interfering auto ionizing states decaying to one continuum channel, we shall consider the case of one auto ionizing state decaying in the presence of several continua. We shall forgo a diagrammatic depiction of this situation as, given the previous discussion, the different channels and states this implies should be clear. We note that in the presence of only one open channels, as was the case so far, the $\mathbb{S}$ matrix simplifies to the scalar phase shift $e^{\delta} = e^{\delta_b}e^{\delta_r}$. For the multichannel case this is no longer the case, and we must treat the matrix nature of $\mathbb{S}$ to account for the coupling between different channels. We shall not present a derivation to the same level of detail for the equations governing this situation. Rather we note that in the single channel case

$$\mathbb{S} = e^{2i(\delta_b\delta_e)} = e^{2i\delta_b}\exp\left[2i\tan^{-1}\frac{-\Gamma}{2(E-E_r)}\right] \tag{5.140}$$

$$= e^{2i\delta_b}\frac{E-E_r-i\frac{\Gamma}{2}}{E-E_r+i\frac{\Gamma}{2}} = e^{2i\delta_b}\left[1-\frac{i\Gamma}{E-E_r+\frac{i\Gamma}{2}}\right]. \tag{5.141}$$

For one this shows, that a resonance manifests itself as a pole of the S-Matrix. Furthermore we can now easily extend this equation now to account for the multi channel nature of the problem, writing the resonant part of the S-Matrix as

$$\mathbb{S}_r = 1 - \frac{i\mathbb{A}}{E-E_r+\frac{i\Gamma}{2}}. \tag{5.142}$$

Unitarity of $\mathbb{S}$ implies that $\Gamma^{-1}\mathbb{A}$ must be idempotent and unitary, if we assume that $\mathbb{A}$ varies only weakly with energy in the vicinity of the auto ionizing state, suggesting the notation

$$\mathbb{A}_{\alpha\alpha'} = \gamma_\alpha\gamma^*_{\alpha'} \quad \text{such that} \sum_\alpha |\gamma_\alpha|^2 = \Gamma. \tag{5.143}$$

The properties of $\mathbb{A}$ identify $\mathbb{S}_r - 1$ as a projection operator. In the single channels case we related the width Γ to the decay of the bound state to the scattering state via the Fermi Golden Rule as,

$$\Gamma = \pi|\left\langle u^{\text{reg}}|V_{AB}|u_0\right\rangle|^2 = \pi|\left\langle \Psi_{\text{inital}}|H\text{sc}|\Psi_{\text{final}}\right\rangle| \tag{5.144}$$

where in the second term we have returned to the notation of section 5.2. In analogy we extend to the multi channel case by writing

$$\gamma_\alpha = \sqrt{\pi}\left\langle \Psi_{\text{in}}||\frac{u_\alpha}{r}\Upsilon_\alpha\right\rangle \tag{5.145}$$

and introduce $\Gamma_\alpha = |\gamma_\alpha|^2$ as the partial width and Γ_α/Γ as the branching ratios, quantifying the probability to end up in given channel α. Similar to partial widths it is natural to enquire how analogous definitions of partial parameters may be obtained in the multichannel case. Hazi[133] showed that the partial phase shifts experienced by the individual channels upon traversing an auto ionizing states, obey

$$\delta = \sum_\alpha \delta_\alpha = \delta_b + \tan^{-1}\frac{\Gamma}{2(E-E_r)}, \tag{5.146}$$

where the total resonant phase shift, experiences the usual π phase shift. Further, Fano[35] showed that the profile of the total cross section is effected by the presence of coupled channel requiring for its parametrization, in addition to the shape parameter q, the correlation parameter $\rho^2 \leq 1.0$,

$$\sigma(E) = \frac{\sigma_b(E)}{\varepsilon^2 + 1}(\varepsilon^2 + 2\rho^2 q\varepsilon + 1 - \rho^2). \tag{5.147}$$

An analysis of the partial cross sections σ_α combining to yield σ of equation 5.147 was done by Starace[134] requiring a complex extension of the correlation parameter ρ^2, denoted for each channel by ρ_α and referred to as Starace parameter,

$$\sigma(E)_\alpha = \frac{\sigma_{b\alpha}(E)}{\varepsilon^2 + 1}(\varepsilon^2 + 2\varepsilon\left[q\Re(\rho_\alpha) - \Im(\rho_\alpha)\right] + 1 - 2\left[q\Re(\rho_\alpha) + \Im(\rho_\alpha)\right] + |\rho_\alpha|^2(q^2 + 1)). \tag{5.148}$$

The Starace parameters are not independent from each other but rather satisfy

$$\frac{\sum_\alpha \sigma_{b\alpha}|\rho_\alpha|^2}{\sigma_b} = \rho^2. \tag{5.149}$$

6 Basis Sets 2 - Scattering States

The chapters 2 and 3 dealt with the theory of electronic bounds states and chapter 4 introduced the kind of basis function successful in reproducing them. In a similar spirit we shall now, after having explored in details some important aspects of the mathematical description of scattering states, turn to the kind of basis functions that are useful in a scattering scenario.

The key feature of continuum electrons which is easy to understand, even without the more extensive analysis of the properties of scattering states of the previous section, is that they have a continuous spectrum and are not elements of the space of square integrable functions $\mathcal{L}^2(\mathbb{R}^3)$, or in other words they are not normalizable in the traditional sense (as opposed to say Dirac-δ normalization). This is exemplified by simple inspection of the oscillatory asymptotic behaviour of the scattering functions of the previous chapter.

We shall be guided by these properties in motivating the necessity of non-Gaussian basis functions. The basis functions we shall ultimately end up working with in this project are commonly referred to as B-Splines (that is Basis Splines). Following the same philosophy as that of chapter 4 introducing GTOs, this section serves as a mixture of an introduction to the theory behind B-Splines, as well as a review of works leading to, pioneering and applying this type of basis function.

We begin by addressing the non-normalizability of the wave function for a continuum electron. As we have demonstrated in great detail in the theoretical discussion of scattering theory, an electron located beyond the range of the short range potential of the parent ion, may be expressed in terms of analytical solutions of the Coulombic case, considering the molecule as a point charge distribution located at the centre of charge of parent ion. Therefore, a set of basis functions which we wish to capture the short range interaction, may be confined to a finite box, if sufficiently large, will still capture accurately the short range interaction, will at the same time restoring normalizability of the basis functions (that is placing them in $\mathcal{L}^2(\mathbb{R}^3_U)$). Within this box the basis set must be capable of reproducing the oscillatory behaviour of the scattering states, and care must be taken to correctly match the wavefunction at the boundary of the box to physical scattering states (this is a point we will return to in chapter8).

In the case of the description of an atomic continuum states, effectively all types of basis functions which we have encountered in the bound in chapters 4 and 4.1 have been put to use to describe scattering states, before BSplines were established as a useful tool. This includes STOs as applied to Hydrogen and Helium[135, 136, 137, 138, 139], Laguerre Functions[140, 141] and GTOs[142, 143]. For atomic systems the use of these exponentially decaying functions has been quite successful in reproducing the oscillatory nature of scattering states. The same is not true for molecular system even of moderate size. Following the same approach as in QC, that is to say placing sets of Gaussian basis functions at different atomic sites large enough to reproduce the individual atomic continua does exactly that: reproduce the different *atomic* continua without accurately not reflectin the molecular nature of the problem [42]. A way to work around this issue using an expansion in GTOs centred at one centres only. This does work for small (primarily diatomic) systems, with results being reported for even the relatively complicated case of N_2 [144, 145]. But with increasing complexity of the molecule and the desire to study wide ranges of photonenergies the basis set required become infeasible large leading to problems with linear dependencies in the basis set. Also after the length we have gone through in chapter 4 to use the ease with which integrals centred at different site can be computed to motivate the use of GTOs in QC, it would surely seem like a step back to now return to a single center expansion.

As an alternative to the zoo of functions characterized by an exponentially decaying basis functions, the use of B-Spline basis functions has enjoyed increasing popularity over the last thee decades. As the next section will lay out in more detail they have a properties which make them very well suited for the description of scattering states, among which the absence of problems with linear dependencies is of chief importance. Their first application to an atomic system (Hydrogen) was seen in 1973[146], but it was not until more than ten years later that interest in these function's applicability as basis functions for continuum states peaked, seeing a number of publications over the space of a few years [147, 148, 149, 150, 151] all of which concerned with the investigation of their capability to atomic systems with one or two electron. The exploration of B-Spline continued with a series of publications [152, 153, 154, 155] considering photoionization of the same small atomic systems considering also the presence of static electric fields[156, 157], and for the detailed analysis of resonances due to autoionizing states. If the success of B-Splines were confined to the atomic case their use would not have presented much progress compared to the use of GTOs. So the next important step was the transition to apply them also to molecular system with the natural choice of system once again being molecular Hydrogen. Here they have proven to be greatly successful leading to the succesful description of [41, 42, 43, 55]. More recently they have also been applied larger system to study photoionization of Argon and Water [158].

From this brief historical overview it is clear that by the end of the last century BSplines had been established as a crucially important tool in the study of increasingly complex (though from a chemists point of view still tiny) molecules. We will now introduce the BSplines mathematically. This discussion will be limited to the definition of Bsplines and discussion of their properties focussing on results rather than proofs (we refer to [159] as a classic work on the mathematical intricacies of BSplines, which arguably has helped furthering the use of BSplines in quantum chemistry in no small part, furthermore references [42, 160] contain comprehensive reviews of B-Splines used in quantum chemistry).

6.1 B-Splines

Splines are piecewise polynomial functions that may be seen as a generalization of polynomial functions, for the purposes of approximating arbitrary functions. Specifically a set of B-Spline (short for basis spline) functions consists of piecewise polynomial functions and can be concisely and uniquely defined by two objects:

1. The order $k \in \mathbb{N}$, $k > 0$
2. The knot vector $\mathbf{t} = (t_1, \cdots, t_{\mu_1}, t_{\mu_1+1}, \cdots, t_{\mu_{l+1}})$ whose elements satisfy $t_i \in \mathbb{R}$, $t_i <= t_{i+1}$, which by disregarding repetitions gives the so called vector of breakpoints $\mathbf{v} = (t_1, t_{\mu_1+1}, \cdots, t_{\mu_l+1})$ (that is $t_i = t_j$ iff $\mu_\beta + 1 < i, j \leq \mu_{\beta+1}$, for some β ($\mu_0 = 0$ always)), whose size we denote by $l+1$, dividing the interval $[t_1, t_{\mu_l+1}]$ into l subintervals $I_j = [t_{\mu_{j-1}+1}, t_{\mu_j+1}]$, and where we associate with every break point the multiplicity μ_i.[1]

The set of B-Splines is then generated by the recurrence relations

$$B_i^k(x) = \frac{x - t_i}{t_{i+k-1}} B_i^{k-1}(x) + \frac{x - t_i}{t_{i+k-1}} B_{i+1}^{k-1}(x) \tag{6.1}$$

$$B_i^1 = \begin{cases} 1 & t_i \leq x \leq t_{i+1} \\ 0 & \text{otherwise} \end{cases} \tag{6.2}$$

From this definition we may view the i^{th} B-Splines, $B_i^k(x)$ as consisting of a concatenation of a set of polynomial functions of degree k, $p(x) = \sum_{i=1}^{k-1} a_i x^i$. These are produced by defining each polynomial's domain to be an element of the set of intervals $\{I_j\}$. The B-Splines may be shown to

1. be non-zero only for $x \in]t_i, t_{i+k}[$
2. be positive

[1] The knot vector is set up so that is completely defines the B-Splines (for some k). The nomenclature we derived from it only serves the easy of discussion.

3. have a continuous $(k-\mu_i)^{\text{th}}$ derivative at the break point μ_i

A multitude of intriguing properties of sets of B-Splines, depending on different sizes (which may in principal be infinite) and structure of knot vectors, may be derived. However, we shall not concern ourselves with these, as in B-Splines' application to the description of Bound states, a fairly simple choice of knot vector is usually made, given by unit multiplicity of all but the first and last breakpoint, and maximum multiplicity for the first and last breakpoint, where maximum multiplicity is k, allowing for a discontinuity in the B-Splines themselves at that breakpoint). That is

$$\mathbf{t} = (t_1, \cdots, t_1, t_2, t_3, \cdots, t_{l+1}, \cdots, t_{l+1}) \tag{6.3}$$

A set of B-Splines generated from such a knot vector fulfils the following properties

1. it contains $l + k - 1$ B-Splines
2. for any given interval there are k B-Splines are non-zero
3. any B-Spline overlaps with k B-Splines to its "left" and "right" right, respectively. Thus the overlap matrix $\mathbf{S}$ satisfies $S_{ij} \neq 0$ iff $|i-j| < k$.
4. arbitrary functions $f(x)$ expanded in B-Splines, are represented by k B-Splines at every x.

where we may note that the last three properties are all more or less obviously equivalent, but are mentioned explicitly as they highlight different expects underlining why B-Splines have become widely applied in the study of scattering states. See figure 6.1 for an example, explicitly displaying these properties. Furthermore it is immediately obvious that none of these properties hold for GTOs, as these are non-zero everywhere.

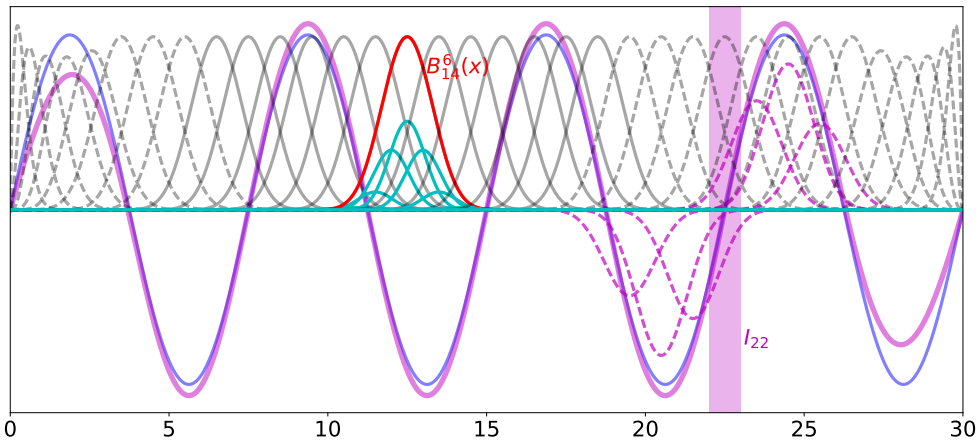

Figure 6.1: A sample set of B-Splines. This set was generated with the parameters $k = 6$ and $\mathbf{t} = (0, \cdots, 0, 1, 2, \cdots, 30, \cdots, 30)$, subject to the standard knot vector structure mentioned. The dashed grey lines constitute the set of B-Splines. The red line is the (arbitrarily) chosen 14^{th} B-Spline $B^6_{14}(x)$, with the full grey lines corresponding to those B-Spline, it has non-zero overlap with and the cyan lines being the respective products $B_i(x)B_{14}(x)$. Furthermore a (blue) sinosoidal function as well as its expansion (full magenenta) in this set of B-Splines is depicted. The dashed magenta lines are the B-Splines contributing to the expansion in the indicated (shaded magenta box) interval scaled by the correct expansion coefficient. This exemplifies all of the most relevant properties of B-Splines that were elaborated on in the text.

From a computational point of view these properties, make clear why B-Splines (in particular when viewing them as compared to GTOs) turn out to be successful in representing continuum states,

1. They are complete in the limit of letting the spacing between breakpoints go to 0[160].

2. due to the disjoint nature of most B-Splines, the matrices we have to deal with, have a sparse, banded ($k-1$ non zero values on either side of the diagonal) structure. Not only does this reduce the computational exertions needed, but also lowers the memory requirements from n^2 to $(n*(2k-1))$[160].

3. Linear Dependencies are unproblematic, even for comparatively large basis sets[161].

In chapter 8 we present the GABS basis mentioned in the introduction that makes uses of these properties on the one hand, to represent the part of molecular scattering states characterized by extensive oscillatory behaviour.

7 The Nuclear Wavefunction

So far we have been almost exclusively concerned with the electronic wavefunction either in a bound or in a scattering state scenario, with the nuclei so far considered fixed at a certain geometry contributing to the one electron Hamiltonian (and fixing the structure of the basis functions we consider by defining their origins). But as was mentioned in the introduction this work also includes results relating to photo dissociation, meaning the fragmentation of a molecule after having been excited to an highly excited, repulsive electronic state. Therefore this chapter is dedicated to the nuclear part of the wave function. The discussion begins by introducing the Born Oppenheimer Approximation and then explores computational methods for the evaluation of nuclear eigenfunctions given electronic structure calculations for some set of nuclear geometries.

Furthermore, apart from the very fleeting mention to time dependence in motivating cross sections in the case of photo ionization, the discussion of theory has been entirely confined to the time independent study of the electronic part of the wave function of a molecular system. In contrast to this we shall dedicate large parts of this chapter on nuclear wavefunction explicitly including time dependence. This includes methods for solving the time dependent SE as well as a section on non-adiabatic effects, going beyond the Born Oppenheimer approximation.

7.1 Nuclear Wavefunction - Time Independent

We return to the full SE such as it is given in equation 2.2, recalling the Hamiltonian as being given by

$$\hat{\mathcal{H}} = -\sum_{i=1}^{N_e}\frac{1}{2}\nabla_i^2 - \sum_{A=1}^{N_n}\frac{1}{2M_A}\nabla_A^2 - \sum_{i=1}^{N_e}\sum_{A=1}^{N_n}\frac{Z_A}{r_{iA}} \tag{7.1}$$

$$+\sum_{i=1}^{N_e}\sum_{j>i}^{N_e}\frac{1}{r_{ij}} + \sum_{A=1}^{N_n}\sum_{B>A}^{N_n}\frac{Z_A Z_B}{R_{AB}}, \tag{7.2}$$

and assuming the wave function to be separable in electronic and nuclear coordinates

$$\Psi(\mathbf{r},\mathbf{R}) = \sum_i \psi_i(\mathbf{r};\mathbf{R})\chi_i(\mathbf{R}), \tag{7.3}$$

where now $\chi_i(\mathbf{R})$ explicitly denotes the the nuclear wave function associate with the electronic state i. In chapters 2 and 3 the effect of the nuclear wave function was entirely accounted for via the Coulombic repulsion and the assumption of zero nuclear kinetic energy. We shall now relax the latter assumption. We begin by substituting the complete $\Psi(\mathbf{r},\mathbf{R})$ into the SE considering for now all the terms thus arising due to the nuclear kinetic energy operator ∇_A. Everything we have dealt with in the discussion of HF theory and CI is contained in the familiar electronic Hamiltonian $\mathcal{H}_e$

$$\mathcal{H}(\mathbf{r},\mathbf{R})\Psi(\mathbf{r},\mathbf{R}) = \mathcal{H}_e\Psi(\mathbf{r},\mathbf{R}) \tag{7.4}$$

$$+\sum_j\sum_A^{N_n} -\frac{1}{2M_A}\left[\psi_j(\mathbf{r},\mathbf{R})\nabla_A^2\chi_j(\mathbf{R})\right. \tag{7.5}$$

$$\left.+2\nabla_A\psi_j(\mathbf{r},\mathbf{R})\nabla_A\chi_j(\mathbf{R}) + \nabla_A^2\psi_j(\mathbf{r};\mathbf{R})\chi_j(\mathbf{R})\right]. \tag{7.6}$$

Of the terms appearing in the second line of this equation we note that the last two terms depend on the derivative with respect to nuclear coordinates of the electronic part of the wave function. A complete treatment would have to include these terms, however a commonly made assumptions is the disappearance of these, notoriously difficult to compute terms. This is the so called Born-Oppenheimer approximation (BOA). Qualitatively, at the core of the BOA is the idea, that in general electronic and nuclear motion take place at very different time scales, so that in considering the motion of one, does not require simultaneous consideration of the other. We will later go on to investigate in some detail the conditions under which the BOA breaks down and how we may remedy this by considering more explicitly the effects of coupling electronic and nuclear motion, but for now we shall assume the BOA to hold, yielding the simplified SE

$$\hat{\mathcal{H}}\sum_j \psi_j(\mathbf{r},\mathbf{R})\chi_j(\mathbf{R}) = \sum_j\left[\mathcal{H}_e\psi_j(\mathbf{r},\mathbf{R})\chi_j(\mathbf{R}) - \sum_A^{N_n}\frac{1}{2M_A}\psi_j(\mathbf{r},\mathbf{R})\nabla_A^2.\chi_j(\mathbf{R})\right] \tag{7.7}$$

$$E_i\chi_i(\mathbf{R}) = \sum_j H_{ij}^{\mathrm{a}}(\mathbf{R})\chi(\mathbf{R}) - \sum_A\frac{1}{2M_A}\nabla_A^2\chi_i(\mathbf{R}) \tag{7.8}$$

$$= \left[E_i^{\mathrm{a}}(\mathbf{R}) - \sum_A\frac{1}{2M_A}\nabla_A^2\right]\chi_i(\mathbf{R}), \tag{7.9}$$

where in the second line we multiplied by ψ_i^* and integrate out the electronic coordinates and where $H_{ij}^{\mathrm{a}} = \langle\psi_i|\mathcal{H}_e|\psi_j\rangle$ is the diagonal, adiabatic Hamiltonian matrix and E_i^{a} are its diagonal entries. We shall without loss of generality simplify this by anticipating the case of diatomic molecules, whose geometry is specified by the internuclear separation R, so that the nuclear kinetic energy terms (neglecting rotational motion of the molecule) of the previous equation simplifies to $T_N = -\frac{1}{2\mu}\frac{d^2}{dR^2}$, where μ is the reduced mass of the system, giving

$$E_i\chi_i(R) = [E^{\mathrm{a}}(R)_i + T_N]\chi_i(R). \tag{7.10}$$

This implies that in the absence of external field (which we shall get to shortly) and under the BOA the nuclear wave functions of the associated with the different electronically excited states are completely independent of each other. Therefore we may find the nuclear eigenfunctions by performing electronic structure calculations for a set of geometries yielding the potential energy surface (PES) $E_i^{\mathrm{a}}(R)$ and applying for instance the Fourier Grid Hamiltonian Method (FGHM)[162].

Again, we shall restrict our discussion of this to the one dimensional case, in anticipation of our dealing with diatomic molecules only whose geometry is fixed by the separation of their nuclei, but generalizatio to higher dimensional cases is not difficult. The FGHM relies on expressing the nuclear wave function in a discrete Fourier Basis[163, 164], using as basis functions, orthogonal functions of the kind $\phi_k(x) \propto \exp(ikr)$. Enforcing orthonormality in a finite truncated space for $x < L$ (as is we will naturally have to do), via

$$\int \phi_k(x)\phi_{k'}\mathrm{d}x = \frac{1}{L}\int_0^L e^{-ikx}e^{ik'x} = \delta_{kk'}, \tag{7.11}$$

requires a separation $\Delta k = k - k' = 2\pi L^{-1}$. This together with a discretization of the x-coordinates to a set of N grid points at which the PES is evaluated (turning the integral $\int\cdots\mathrm{d}x$ in the previous equation into a sum $\sum\cdots\Delta x$), dictates the basis functions as given by

$$\phi_{k_i}(x_j) = L^{-\frac{1}{2}} e^{\sqrt{-1}2\pi ij/N}. \tag{7.12}$$

The FGHM make use of this discretization in evaluating the matrix elements $\langle x|H|x'\rangle = \langle x|V+T|x'\rangle =$ as a finite matrix of size $N \times N$, the diagonalization of which then yields the discretized eigenfunctions. In our case $V(x)$ is then the $E_i^a(x)$ for some PES i, and $T = \hat{p}^2/2m$

$$\begin{aligned} \langle x|V+T|x'\rangle &= \frac{1}{4\pi m}\int \mathrm{d}k\mathrm{d}k' e^{ikx} \langle k|\hat{p}^2|k'\rangle e^{-ik'x'} + V(x)\delta(x-x') && (7.13)\\ &= \frac{1}{4\pi m}\int \mathrm{d}k e^{ikx} k^2 e^{-ikx'} + V(x)\delta(x-x') && (7.14) \end{aligned}$$

where we inserted complete sets of states $|k\rangle\langle k|$ and made use of the fact, that in momentum representation $\hat{p}|k\rangle = k|k\rangle$. Turning this expression into a sum yields

$$\langle x_i|T+V|x_j\rangle \approx \frac{1}{2m}\left(\frac{2K}{N}\right)^2 \sum_{n=-(N-1)/2}^{(N-1)/2} \frac{e^{\sqrt{-1}2\pi ni/N}}{\sqrt{N}} n^2 \frac{e^{-\sqrt{-1}2\pi nj/N}}{\sqrt{N}} + V(x_i)\delta_{ij}, \tag{7.15}$$

where we have truncated and discretized the momentum space to represent such that $-K = -(N-1)/2\Delta k < k < K$. Therefore if we can evaluate this sum and have knowledge of the PES at the grid points we may evaluate and diagonalize the discretized Hamiltonian. The analytical evaluation of this sum is possible[162] yielding (for an even number of gridpoints, chosen to facilitate the use of fast fourier transforms later)

$$\langle x_i|\hat{p}^2|x_j\rangle = \begin{cases} \frac{K^2}{3}\left(1+\frac{1}{N^2}\right) & \text{if } i=j \\ \frac{2K^2}{N^2}\frac{(-1)^{j-i}\cos(\pi\frac{j-i}{N})}{\sin^2(\pi\frac{j-i}{N})} & \text{if } i\neq j \end{cases} \tag{7.16}$$

This may be simplified if rather than carrying out a discrete sum over k we consider continuous k[165], which unsurprisingly is equivalent in the discrete case in the limit of infinitely many grid points N. The FGHM provides an easy to implement and efficient method to find the nuclear eigenfunctions corresponding to some electronic PES, and serves as a useful starting point for time dependent calculations that at time $t = 0$ are known to be in the eigenstate of some PES.

7.2 Nuclear Wavefunction - Time Dependent

Having elaborated on a method of how a molecules nuclear eigenfunction may be obtained we shall now investigate systems that are not in an eigenstate. In other words we shall now introduce time dependence. The ideas are largely applicable to any time dependent system, and not confined to nuclear dynamics, however as nuclear motion is the only case we shall consider, we shall use nomenclature and notation confined to the nuclear case. That is, given a nuclear wave function at some time t_0 that is not in an eigenstates, such as we may find it by the FGHM, we aim to investigate its time dependence subject to the influence of some (time dependent) Hamiltonian. The time dependent SE (TISE) for χ_i reads

$$-i\frac{\partial}{\partial t}\chi_i(\mathrm{R},t) = [H_{ii}^{\mathrm{a}}(R) + \mathcal{T}_n]\,\chi_i(\mathrm{R},t) = H\chi_i(\mathrm{R},t), \tag{7.17}$$

where the (for now diagonal) matrix H_{ij}^{a} contains the electronic contribution as well as the nucleus-nucleus repulsion and whose solution is the well known equation (written now in matrix form)

$$\boldsymbol{\chi}(R,t) = \boldsymbol{\chi}(R,t_0)e^{-i\mathbf{H}(R)(t-t_0)} = \mathbf{U}(t,t_0,R)\boldsymbol{\chi}(R,t_0), \tag{7.18}$$

defining the the time evolution operator $U(t,t_0)$ evolving the system at $\mathbf{R}$ from time t_0 to t. In this work we carried out numerical time propagation via use of the split operator method. This method

is motivated by approximating the time evolution operator so as to give products of exponentials of the kinetic and the potential part of the Hamiltonian, the usefulness of which we shall make apparent shortly. Comparing the expansions for a small time step (assuming $t_0 = 0$) of the actual operator $U = \exp(-i(V+T)\Delta t)$ with the approximate expression $\tilde{U} = \exp(-iV\Delta t/2)\exp(-iT\Delta t)\exp(-iV\Delta t/2)$ gives

$$
\begin{aligned}
U &= \mathbf{I} - i(\mathbf{V}+\mathbf{T})\Delta t - \frac{1}{2}(\mathbf{V}+\mathbf{T})^2\Delta t^2 + i\frac{1}{6}(\mathbf{T}+\mathbf{V})^3\Delta t^3 + O(\delta t^4) && (7.19)\\
\tilde{U} &= \left[e\mathbf{I} - i\frac{1}{2}\mathbf{V}\Delta t - \frac{1}{8}\mathbf{V}^2\Delta t^2 + O(\Delta t^3)\right] \times \left[e\mathbf{I} - i\mathbf{T}\Delta t - \frac{1}{2}\mathbf{T}^2\Delta t^2 + O(\Delta t^3)\right] \times && (7.20)\\
&\quad \left[e\mathbf{I} - i\frac{1}{2}\mathbf{V}\Delta t - \frac{1}{8}\mathbf{V}^2\Delta t^2 + O(\Delta t^3)\right] && (7.21)
\end{aligned}
$$

collecting terms in either expression to first, second and third order we can find the error to be of order

$$\tilde{U} - U = O(\Delta t^3). \tag{7.22}$$

Therefore in order to propagate $\boldsymbol{\chi}$ from $t_0 = 0$ to time t, we may dived t into N intervals of length Δt, which if sufficiently small will yield accurate results using $\tilde{U}$ instead of U.

In view of the structure of $\tilde{U}$, we need to concern ourselves with successive applications of operators of the types $e^{-i\mathbf{V}\Delta}$ and $e^{-i\hat{T}\Delta}$, where the former is a scalar matrix and the latter a matrix of differential operators. We shall address the former first. So far all the potential matrix $\mathbf{V}$ appearing in the evolution operator has been diagonal, making the evaluation of the exponential term trivial:

$$\left[e^{-\mathbf{H}\Delta t}\right]_{ij} = e^{-H_{ij}\Delta t} \tag{7.23}$$

The diagonal nature of the potential matrix however is lost if we include the effects of a laser field. The laser field's effect manifests itself in allowing population transfer between different PES, i.e. coupling the different electronic states via addition to the Hamiltonian of the matrix $V^E_{ij}(t) = \mathbf{E}(t)\langle\psi_i|\boldsymbol{\varepsilon}\hat{P}|\psi_j\rangle$. In this case the potential part of the Hamiltonian is no longer diagonal. The problems associated with evaluating the exponential of an off diagonal matrix is dealt with, by means of a unitary transformation $\boldsymbol{\chi}' = \mathbf{U}_W\boldsymbol{\chi}$ (we shall write the time evolution explicitly as an exponential from now so as to avoid confusion with the unitary transform), with $\mathbf{U}_W$ being the matrix that diagonalizes the total potential part $\mathbf{W} = \mathbf{V} + \mathbf{V}^E(t)$ of the Hamiltonian, i.e. $\mathbf{W} = \mathbf{U}^\dagger_W\boldsymbol{\Lambda}_{\boldsymbol{W}}\mathbf{U}_W$ with $\boldsymbol{\Lambda}_W$ being the diagonal matrix of eigenvalues of $\mathbf{W}$. Thus

$$
\begin{aligned}
e^{-i\mathbf{W}(t)\Delta t}\boldsymbol{\chi}(\mathbf{R}) &= \mathbf{U}\mathbf{U}^\dagger e^{-i\mathbf{W}(t)\Delta t}\mathbf{U}\mathbf{U}^\dagger\boldsymbol{\chi} && (7.24)\\
&= \mathbf{U}e^{-i\boldsymbol{\Lambda}_W(t)\Delta t}\boldsymbol{\chi}', && (7.25)
\end{aligned}
$$

where one may convince oneself of the second line by Taylor expansion of the exponential. This treatment to deal with a non diagonal Hamiltonian was motivated by the coupling induced by the presence of a time dependent electromagnetic field and therefore requires diagonalization of the Hamiltonian $W(t)$ at every time step. But it should be noted that this treatment is (obviously) equally applicable for couplings of different origins, such as for instance those that arise if we move beyond the BOA which will be addressed in the section on non-adiabatic effects. Unlike in the time dependent case, where the off diagonal terms change for the duration of the laser pulse, these couplings are time independent, so that only a single diagonalization has to be carried out.

We now turn to the kinetic part of the time evolution. We may avoid the explicit calculation of any derivative, by transformation of χ to momentum representation, such as was already pointed out in the

discussion of the FGHM. The momentum space representation of χ is simply given by the the Fourier transform $\tilde{\chi}(k) = \mathcal{F}[\chi(R)]$. Therefore the kinetic part of the Hamiltonian appearing in the propagator is dealt with using

$$e^{i\mathcal{T}\Delta t}\chi(R) = \mathcal{F}^{-1}\left[e^{-i\frac{k^2}{2m}}\mathcal{F}\left[\chi(R)\right]\right]. \tag{7.26}$$

Combining the Split Operator method with the methods provided to propagate the different terms of the Hamiltonian amounts to the propagation by one time step Δt.

Computational Aspects of Time Propagation

The potentially expensive nature of time propagation calculations with many potential energy surface, long laser pulses and large ranges of R and k may be controlled by various careful considerations on how to implement the different aspects Split Operator Method. At every time step the time consuming operations are the Fourier transform and the (if necessary) diagonalization of W. Especially the diagonalization becomes prohibitively expensive if calculations are carried out involving large numbers of PES. The time taken for this step may be drastically reduced by noting that a complete diagonalization of W, while of course solving the problem in allowing us to then compute $\boldsymbol{\chi}' = \mathbf{U_W}\boldsymbol{\chi}$, provides far more information than we need. We are only interested in the effect of the operator $e^{-i\mathbf{W(t)}\Delta t}$ on the wave function $\boldsymbol{\chi}(t)$ to propagate from t to $t + \Delta t$. Therefore rather than carrying out full and costly diagonalization we may apply an algorithm based on a Lanczos propagator generating Krylov Spaces at every iteration.

We generate an n dimensional Krylov space spanned by the vectors ξ obtained following a Gram-Schmidt type procedure,

$$\begin{aligned}
\boldsymbol{\xi}_1 &= \boldsymbol{\chi}/|\boldsymbol{\chi}| && (7.27)\\
&\vdots && (7.28)\\
\boldsymbol{\xi}_n &= \tilde{\boldsymbol{\xi}}_n/|\tilde{\boldsymbol{\xi}}_n|, \text{ where} && (7.29)\\
\tilde{\boldsymbol{\xi}}_n &= \mathbf{W}\boldsymbol{\xi}_{n-1} - \sum_{j=1}^{n-1}\boldsymbol{\xi}_j\left\langle\boldsymbol{\xi}_j|\mathbf{W}\boldsymbol{\xi}_{n-1}\right\rangle. && (7.30)
\end{aligned}$$

We define $\mathcal{P}_\xi^n = \sum_{i=1}^n |\boldsymbol{\xi}_i\rangle\langle\boldsymbol{\xi}_i|$ as the operator projecting onto that Krylov space and write the approximate $\chi(t+\Delta t)$ as

$$\begin{aligned}
\chi(t+\Delta t) &= \mathcal{P}_\xi^n e^{-i\mathbf{W(t)}\Delta t}\mathcal{P}_\xi^n\,|\boldsymbol{\chi}(t)\rangle && (7.31)\\
&= \sum_{i,j}^{n}\boldsymbol{\xi}_i e^{-i\tilde{\mathbf{W}}\Delta t}\left\langle\boldsymbol{\xi}_j|\boldsymbol{\chi}(t)\right\rangle, && (7.32)
\end{aligned}$$

where now $\tilde{\mathbf{W}}_{ij} = \langle\boldsymbol{\xi}_i|\mathbf{W}|\boldsymbol{\xi}_j\rangle$ is the matrix of reduced dimensionality n, the explicit diagonalization of which has to be carried out. Therefore the propagation of $\boldsymbol{\chi}(t)$ may be carried out by computing $\boldsymbol{\chi}(t+\Delta t)$ using increasingly larger Krylov Spaces until convergence has been achieved to within satisfactory precision. It is not always guaranteed that this algorithm converges quickly, and care has to be take to sidestep such issues, relating in particular to the size of the time step Δt. For more details on this algorithm we refer to reference [166] and references therein.

In addition to using efficient methods to carry out the potential part of the propagation, we note that it is by no means obligatory to write the propagation operator in split operator formalism as

$$\tilde{U} = \exp(-iV\Delta t/2)\exp(-iT\Delta t)\exp(-iV\Delta t/2). \tag{7.33}$$

Equally well we may write it as

$$\tilde{U} = \exp(-iT\Delta t/2)\exp(-iV\Delta t)\exp(-iT\Delta t/2). \tag{7.34}$$

In the absences of a laser field (leaving us with a Hamiltonian whose time independent off diagonal terms may dealt with, by a single transformation at the beginning of the calculation) it is natural to use the former requiring only a single Fourier Transform. In the presence of a time dependent couplings however it may be notably cheaper to Fourier transform twice (especially using Fast Fourier Transform) so as to only require a single Lanczos Propagation.

Floquet Picture

In motivating the time dependent theory we referred to time dependent electric field, such as are present when studying the effects of laser pulses on a system. In the special case of a laser pulse periodic in time, this temporal periodicity may be exploited to provide another way of looking at the interaction with a laser pulse, known as the Floquet Picture [167]. The periodicity is expressed by $H(\mathbf{r},t;R) = H(\mathbf{r},t+T;R)$. Consider now as a trial function the modified wave function $\psi_\lambda(\mathbf{r},t;R) = e^{-i\varepsilon_\lambda t}\zeta_\lambda(\mathbf{r},t;R)$ which we shall endeavour to expand the solution $\psi(\mathbf{r},t;R)$ in. Substitution of this into the TISE yields, neglecting for now the nuclear coordinate R,

$$H_F(\mathbf{r},t)\zeta_\lambda(\mathbf{r},t) = \varepsilon_\lambda\zeta_\lambda(\mathbf{r},t) \text{ where} \tag{7.35}$$

$$H_F(\mathbf{r},t) = H(\mathbf{r},t) - i\frac{\partial}{\partial t}, \tag{7.36}$$

where $H_F(R,t)$ and $\zeta_\lambda(R,t)$ are known as the Floquet Hamiltonian and Floquet Eigenstates, respectively. Next we note that the definition of the Floquet states may be rewritten as

$$\psi(\mathbf{r},t) = e^{-i\varepsilon_\lambda t}\zeta_\lambda(\mathbf{r},t) = e^{-i(\varepsilon_\lambda+n\omega)t}e^{n\omega t}\zeta_\lambda(\mathbf{r},t) = e^{-i(\varepsilon_\lambda+n\omega)t}\zeta_{\lambda n}(\mathbf{r},t), \tag{7.37}$$

where $\omega = 2\pi/T$. This provides a set of Floquet states for every integer value of n with the same periodicity as ζ_λ. Any one of these sets provides an identical description if used to express $\chi(\mathbf{r},t)$. Therefore the Floquet States of a system are defined up to modulo $m\omega$. Given these set of Floquet states we extent our Hilbert Space to include both space and time, with the new inner product defined as

$$\langle\zeta_{\lambda n}|\zeta_{\nu m}\rangle_F = \frac{1}{T}\int_0^T\int \zeta^*_{\lambda n}(t,\mathbf{r}),\zeta_{\nu m}(t,\mathbf{r})\mathrm{d}\mathbf{r}\mathrm{d}t, \tag{7.38}$$

forming a complete set of states in the extended Hilbert space. We may now proceed by exploiting to time periodicity of the Floquet Hamiltonian as well as the Floquet states, to expand their time dependent part as a Fourier series, yielding for the different PES:

$$\int \mathrm{d}\mathbf{r}\psi_i^{0*}(\mathbf{r})\zeta_\lambda(\mathbf{r},t) = \sum_{n=\infty}^{\infty} c(R)_{in\lambda}e^{in\omega t} \tag{7.39}$$

$$\int \mathrm{d}\mathbf{r}\psi_i^{0*}(\mathbf{r})H(\mathbf{r},t)\psi_j^0(\mathbf{r}) = \sum_{n=\infty}^{\infty} H_{ijn}(R)e^{in\omega t} \tag{7.40}$$

where ψ_i^0 are the eigenfunctions of the time independent Hamiltonian in the absence of a perturbing field and on the right hand side we have made explicit the dependence on nuclear geometry. Substitution of this in the SE yields the now time independent Floquet Hamiltonian governing the the behaviour of the Floquet states, whose matrix expression is

$$\langle in|H_F|jm\rangle_F = H_{ij(n-m)} + n\omega\delta_{ij}\delta_{nm}, \tag{7.41}$$

which for $n = m$ takes the form

$$\langle in|H_F|jn\rangle_F = \langle i0|H|j0\rangle_F + n\omega\delta_{ij} = \frac{1}{T}\int_0^T \langle i|H(x,t)|j\rangle + n\omega\delta_{ij}, \tag{7.42}$$

which for a Hamiltonian given by $H = H_0 + E_0\cos(\omega t)$, is simply the unperturbed Hamiltonian whose diagonal is shifted by $n\omega$. For $n \neq m$ we find

$$\langle in|H_F|jm\rangle_F = \frac{E_0}{T}\boldsymbol{\epsilon}\langle i|\boldsymbol{\mu}|j\rangle\int_0^T \cos(\omega T)e^{i\omega t}, \tag{7.43}$$

where $\langle i|\mu|j\rangle$ are the dipole transition moments and $\boldsymbol{\epsilon}$ is the polarization vector of the field. The integral may by trivially evaluated, most importantly yielding zero if $|n-m|>1$. Therefore in shifting to the Floquet picture we are able to carry out a time dependent calculation in the presence of a sinusoidally varying field in a completely time independent way by including additional PES surface corresponding to the absorption of different numbers of photons. In theory this would require infinitely many PES but in practice we can often restrict ourselves to the absorption of a small number of photons.

The preceding discussion hinges on the time dependence of the field being of a sinusoidal nature, somewhat limiting its scope of applicability. However, theories exist extending this to the study of fields with a more complex temporal structure including for instance envelopes[168, 169, 170, 171]. These theories are largely based on considering the time dependence of the envelope as a function of an additional temporal, independent variable t', thereby further extending the Hilbert space and re-establishing physical meaningfulness by enforcing $t=t'$ at a later point.

7.3 Beyond Born Oppenheimer

Having discussed how, once they haven been computed, PES and can be used to study nuclear dynamics following equation 7.8, which as it core has the BOA assuming the negligibility of the last two terms of equation 7.6, both of which involve derivatives of the electronic part $\psi(\mathrm{r},R)$ with respect to the nuclear coordinates. We shall now discuss under which circumstances these assumption may turn out to be valid and what can be done to remedy the break down of the BOA is such a circumstance.

Overview

The diagonal Hamiltonian such as it appears in equation 7.6 is the so called adiabatic Hamiltonian. We now turn our attention to the terms neglected in this equation, specifically $2\nabla_A\psi(\mathbf{r},R)\nabla_A\chi(R)$ and $\nabla_A^2\psi(\mathbf{r};R)\chi(R)$, which lead to the discussion of nuclear dynamics on decoupled (in absence of an external filed) PES of equation 7.8. We shall now investigate the effect of these neglected terms, both of which can, as we shall see, lead to vibronic coupling allowing for population transfer between adiabatic PES. Following the steps leading to equation 7.10 but retaining now the previously neglected terms yields

$$E\chi_i=\sum_j\left[H_{ij}^{\mathrm{a}}+\frac{1}{2\mu}T''_{ij}+\frac{1}{\mu}T'_{ij}\frac{\partial}{\partial R}+\delta_{ij}T_N\right]\chi_j, \tag{7.44}$$

where

$$T'_{ij} = \langle\psi_i|\frac{\partial}{\partial R}|\psi_j\rangle \tag{7.45}$$

$$T''_{ij} = \langle\psi_i|\frac{\partial^2}{\partial R^2}|\psi_j\rangle\,. \tag{7.46}$$

The presence oh these indicates that now the different nuclear wave function χ_j are now coupled as a consequence of the derivative terms of the electronic part of the wave function with respect to the nuclear geometry. Thus if either of these terms is non-negligible the dynamical coupling between the two types of motion (electronic and nuclear) cannot be ignored. We shall confine our discussion of the former of the two term, as its effect is more pronounced and knowledge of the form implies knowledge of the latter[172, 173] via $\mathbf{T}''=-(\nabla\mathbf{T}')-\mathbf{T}'^2$. We may gauge the importance of these non-adiabatic couplings, by noting that the Hellmann-Feynman Theorem allows to state

$$T'_{ij}=\frac{\langle\psi_j|\nabla\mathcal{H}_e|\psi_j\rangle}{E_i^{\mathrm{a}}-E_j^{\mathrm{a}}}. \tag{7.47}$$

Therefore the derivative couplings between two states i and j are inversely proportional to the energy separation of the two states (and also inversely proportional to the reduced mass μ). Therefore the non-adiabatic effects are most pronounced in light systems with PES approaching each other in the vicinity of avoided crossings. In such a case the BOA no longer poses a valid approximation to make. Non-adiabatic physical effects manifest themselves in a variety of phenomena, such as radiationless electronic decay or effect related to conical intersections (for an extensive exposition on conical intersections see references [174, 175]). Note that we mention conical intersections for completeness sake only. To us they are of no concern, as conical intersection are not present in diatomic systems, characterized by one dimensional PES.

Many different approaches have been proposed to deal with the Breakdown of the BOA, requiring the wave function to be written as a liner combination of BO states of the type $\chi_i\psi_i$. Possible the most immediately obvious approach to handle this would be to explicitly evaluate the derivative couplings and carry out subsequent propagations on multiple PES. There are however problems associated with this; for one the split operator formalism we introduced as a propagator is not applicable if the Hamiltonian contains operator that mix coordinate and momentum operators, which notably is the case for the third term in equation 7.44 proportional to $\mathbf{T}'(R)\frac{\partial}{\partial R}$. Other propagator (we mention for instance Crank-Nicholson[176]) are equipped to handle this, but would still suffer problems for very closely approaching adiabatic PES; a circumstance leading in the most extreme case to divergence of $T_{ij}(R)$ if the states i and j undergo a sudden change in electronic structure. Therefore most methods aiming to account for non-adiabatic couplings follow a different approach based on transforming the adiabatic electronic states $\psi_i(R)$ to so called diabatic states; being a representation in which the derivative couplings vanish (diabatic states) or at least are as close to vanishing as possible (quasidiabatic states). The (quasi)diabatic states correspond to a unitary transformations of the adiabatic sets of states. They are characterized by a diabatic Hamiltonian $H^{\mathrm{d}_{ij}}$ with off diagonal elements, whose diagonal entries are the smooth diabatic PES, which may intersect each other.

There is no one unique definition for diabaitc PES, and it has been shown[177] that for systems with more than one nuclear degree of freedom it not generally possible to obtain diabatic states. A multitude of methods have been proposed for the determination of diabatic states, many of which content themselves with quasi diabatic states, which although not capturing not all of the non-adiabatic effects, often provide a sufficiently good description. The approaches taken to find diabatic states can be divided into two categories depending on whether or not they require the explicit calculation of $\mathbf{T}'$. The methods that do rely on the computation of the derivative couplings and subsequently use these to carry out a transformation that in as far as possible minimizes the derivative couplings between the thus obtained diabatic states[178, 179, 180, 181, 182, 183, 184, 185, 186].

Alternatively one may attempt the construction of diabatic states while sidestepping the explicit, costly evaluation of $\mathbf{T}'$. Within this class of approaches to diabatization we may differentiate between methods that look for diabatic states as those that yield smooth molecular properties and those that look for diabatic states as those that yield a smooth wave function. The former approach, considering molecular properties is commonly referred to as the Mulliken-Hush[187, 188] method which is discussed in[189, 190]. It is based on the observation that molecular properties such as the dipole transition moments or quadrupole moments can be expected to vary smoothly for diabatic states, and thus for say, two states an angle may be obtained mixing them in such a way so as to achieve smoothness.

The approach we will present falls into the second category mentioned in the precious paragraph based on looking for diabatic states as those whose wavefunction (given by a combination of CI vectors and molecular orbitals) is smoothly varying with respect to the nuclear coordinates. It is easy to appreciate that for smoothly varying set of states ψ^d we can expect the derivatives T'_{ij} to be small. One existing methods of this kind is the block diagonalization method pioneered by Pacher[191, 192] and further developed by Domcke[193, 194] base on seperating the states ψ into distinct subsets which do not couple via non-adiabatic interaction, and bringing the Hamiltonian into a block diagonal (quasidiabatic) from. Another method is base on the "enforcement of configurational uniformity"[195, 196], based on the observation that in a region with well separated PES (i.e. equivalent diabatic and adiabatic states), the states are dominated by a small number of configurations. The diabatic states are then considered to be those that retain this CI-structure for all nuclear geometries in as far as is possible. We mention also the more recent work by Troisi[197] achieving diabaticity by enforcing certain structures on the CI-vector

and MO-coefficients. This last method bears some resemblance to what shall be presented here.

Method

The goal is to identify a unitary transformation U_{ij} such that the transformed adiabatic states $\psi_i^d = \sum U_{ij}\psi_j$ are diabatic in the sense of yielding negligible or at least small derivative couplings $\mathbf{T}'$. Using the MCSCF methodology to gives the N_a adiabatic states in the form

$$\psi_i = \sum c_{i\alpha} \left|\mathrm{CSF}_\alpha\right\rangle, \tag{7.48}$$

where c_i an $|\mathrm{CSF}_i\rangle$ are the CI-coefficients and CSFs respectively. We include now explicitly the dependence of such a state on the nuclear coordinate and consider the derivative with respect to it

$$\frac{\partial}{\partial R}\psi_\alpha(R) = \sum \left[c_{i\alpha}\frac{\partial}{\partial R}\left|\mathrm{CSF}_\alpha\right\rangle + \frac{\partial}{\partial R}(c_{i\alpha})\left|\mathrm{CSF}_\alpha\right\rangle \right]. \tag{7.49}$$

We shall address the two terms independently, which may be viewed as two independent diabatization procedures addressing the R-dependence of $c_{i\alpha}$ and $|CSF_\alpha\rangle$. We begin with the CI-vector. We achieve a zero derivative for this term by enforcing a trivial structure onto the CI-vector which nevertheless does not reduce the quality of the description of the relevant states. Letting N_{CSF} be the number of CSFs in the given active space we define a set of $N_{CSF} \geq N_a$ states ψ_i^d each of which has a constant CI vector given by $c_{i\alpha}(R) = \delta_{i\alpha}$. Naturally then the first term in equation 7.49 disappears. This somewhat blunt approach works so long as we include all N_{CSF} such states, from which we may recover the original N_a adiabatic states by diagonalization of the $N_{CSF} \times N_{CSF}$ diabatic Hamiltonian $H_{ij}^d = \langle\psi_i^d|\mathcal{H}_e|\psi_i^d\rangle$ and retaining the lowest N_a eigenvalues. The matrix U_{CSF} diagonalizing H_{ij}^d is the sought after diabatic transformation for the CI-part, which, following this prescription, did not have to be computed explicitly. Not having to compute U_{CSF} explicitly has another major advantage over method which do have to do so. Computing $\mathbf{U}(R)$ independently at each grid point from a set of adiabatic states, while leading to potentially viable diabatic states, does not guarantee smoothness of molecular properties such as the transition dipole moments. For systems with many PES theses discontinuities may be extremely difficult to remove after the fact, and plague many existing methods whose starting point are adiabtic states[195, 196].

An obvious limitation of this approach, is that we can only guarantee recovery of the adiabatic states by working with N_{CSF} diabatic states. Depending on the molecule and active space under consideration this number may be too large to compute H_{ij}^d, much less allowing for propagations of nuclear wavepackets on the resulting PES. We present an extension to the blunt method yielding an R-independent set of CI vectors of size $N_a \leq N_d \leq N_{CSF}$ allowing recovery of ψ to within high accuracy. Assuming the second term of equation 7.49 to be at least reasonably small to begin with (more on this shortly), we consider the "CI overlap" of two adiabatic states at different geometries R_p and R_q to be $O_{ijR_pR_q}^{CI} = \sum c_{i\alpha}(R_p)c_{j\alpha}(R_q)$. For N_R grid points resulting CI overlap matrix is of size $N_RN_a \times N_RN_a$. Removal of linear dependencies from the set of CI vectors $\mathbf{c}_i(R_p)$ by diagonalization of $\mathbf{O}^{CI}$ and retention of eigenvectors with eigenvalues above a certain threshold, then yields a set of N_d diabatic CI-vectors the quality of which may be ascertained by diagonalizing H_{ij}^d comparing its N_a lowest eigenvalues to those of H_{ij}^a. Once a threshold is found containing the adiabatic PES to within reasonable accuracy we have identified a set of R-independent CI vectors tailored to describe the adiabatic states at all nuclear geometries.

Moving on now to the second term of equation 7.49. It will be easier to consider a description of ψ in terms of $|\mathrm{det}_i\rangle$ determinants rather than CSFs, the transformation between the two may easily be carried out using GUGA-tables (see chapter 3). To account for the derivative couplings due to the change in the Slater determinants we largely follow the work of[197]. Noting that

$$\langle\mathrm{det}_i|\frac{\partial}{\partial R}|\mathrm{det}_j\rangle \tag{7.50}$$

may with the help of the Slater Condon Rules for one electron operators be related to derivatives of molecular orbitals $B_{ij} = \langle \phi_i | \partial / \partial R | \phi_j \rangle$. This matrix may be written as

$$\mathbf{B} = \mathbf{C}^T \mathbf{S} \mathbf{C}' + \mathbf{C}^T \mathbf{S}' \mathbf{C} \tag{7.51}$$

where $\mathbf{C}(R)$ and $\mathbf{C}'$ are the matrix of MO coefficients and its derivative, $\mathbf{S}$ is the basis overlap and $\mathbf{S}' = \langle i | \partial / \partial R | j \rangle$ with i and j denoting basis functions here. Evaluating the this matrix may proof to show (as is the case of the results of chapter 11) that the non-adiabaticity primarily stems from the nuclear derivative term of the CI vector. In that situation disregarding the non-adiabaticity due the second term in equation 7.49 can be expected to already yield a fairly good set of quasi-diabatic states already. For completeness sake we mention as strategy one may follow if that is not the case, even though we will encounter no such case in this work. To this end we consider now a transformation $\mathbf{U}_{MO}$ that renders $\mathbf{B}$ zero, establishing the MO with the desired property of zero derivative coupling:

$$\sum_{pq} \langle \phi_p | \, U_{pi}^{MO*} \frac{\partial}{\partial R} \left(U_{jq}^{MO} \, | \phi_q \rangle \right) = 0 \tag{7.52}$$

From this we may obtain the differential equation $\partial / \partial R \mathbf{U} + \mathbf{U}\mathbf{B} = 0$ with solution

$$\mathbf{U}(R) = \exp \left(- \int_{R_0}^{R} \mathbf{B}(R') \mathrm{d}R' \right). \tag{7.53}$$

It is important to note that the antihermiticity of $\mathbf{B}$ guarantees the unitary of the transformation $\mathbf{U}$. In practice we proceed for the evaluation of $\mathbf{U}$ similar as we did in dealing with non-diagonal Hamiltonians in the split operator method. That is to say we find the matrix diagonalizing $\int \mathbf{B}(R') \mathrm{d}R'$, and apply $\mathbf{U}$ in the basis characterized by a diagonal matrix in the exponential. In this case we note that upon obtaining the rotated (diabatic) orbitals, we must repeat the SA-CASSCF calculations (disabling of course orbital rotation) and use the new CI-vectors to obtain the matrix $\mathbf{O}$, whose diagonalization yields the diabatic CI vectors. In the brute force approach (characterized by CI vectors of the form $c_{i\alpha}(R) = \delta_{i\alpha}$), this is evidently not necessary, but nevertheless all molecular properties must be calculated using the rotated, diabatic orbitals.

We thus conclude the section on non-adiabatic couplings having established methods to force both terms of equation 7.49 to vanish yielding a diabatic representation. Having dealt with the relevant aspects of the nuclear part of the molecular wave function in this chapter, as well as the electronic bound and scattering states in the previous chapters, we have established all the theoretical tools relevant to the description of photo ionization and photo dissociation of diatomic molecules. Before going on to present results obtained from with these theoretical tools, the next chapter is dedicated to a more technical review of how the part of the photo ionization related to the description of bound states was implemented.

Part II

XCHEM Approach

8 The XCHEM Approach

In chapters 2, 3 and 4 we outlined the theory for electronic bound states and the Gaussian basis functions commonly used in bound state calculations. Chapters 5 and 6 on the other hand dealt with scattering states with an electronic in the continuum, as well as presenting the radically different basis functions necessary to describe them successfully, if we wish to go beyond the simplest systems. In brief the the XCHEM approach may be described as combing the ideas from both of these "worlds" to give a description of ionization process in complex molecular systems. With QC and Gaussian Basis functions taking over the descriptions of the intricate electronic structure typical for molecular bound states, and scattering theory and B Splines handling the description of an electron in the continuum. The novelty of the XCHEM lies in the way the "boundary" of these two aspects of the calculation is handled. This chapter is divided into two parts, the former outlining how we combine Gaussian and B-Spline Bases two achieve the description of an electronic passing from a bound to a continuum states, the latter outlining how (using the new basis) the theoretical aspects relating to either bound or continuum states are combined.

8.1 The GABS Basis

In chapter 6 we have already mentioned the drawback and limitation of attempts relying on either Gaussians to describe the continuum, or B-Spline to describe molecular bound states. It is suggestive therefore to employ a hybrid basis containing both types of functions each describing the part of the problem suited to it. The most straightforward approach of simply "adding" B-Splines centred at the CoM of the molecule to a standard Gaussian QC basis (say cc-pVQZ [121, 122]) with Gaussian basis functions at every atomic site (PC Gaussians), leads to extremely costly bielectronic integrals including Gaussian and B-Splines centred at different origins. A way to remedy this is by introducing an auxiliary Gaussian Basis centred at the CoM of the molecule (MC Gaussians), completely enveloping the PC Gaussians and extending up to a radius of R_1. The MC Gaussians are of the familiar form

$$G^{\alpha}_{klm}(\mathbf{r}) = \sqrt{\frac{1}{2}}\left(\frac{\pi}{\alpha}\right)^{0.25}\sqrt{\frac{(4k+2l+1)!!}{(4\alpha)^{2k+l+1}}}r^{2k+l}e^{-\alpha r^2}Y_{lm}(\hat{\mathbf{r}}), \tag{8.1}$$

with $\hat{\mathbf{r}}$ denoting the angular coordinates and where the maximum values included for the quantum numbers are chose to provide sufficient angular flexibility (larger l) as well as sufficient radial extension (larger k, though also aided by larger l). The MC Gaussian basis set is set up to be even tempered (recall this means the exponent α following a geometric progression), which, in addition to some nice analytical properties, have been proven to give comparatively fewer problems as a consequence of linear dependencies in the basis[198].

The B-Splines are constructed to begin at a radius $R_0 < R_1$, with R_0 chosen to guarantee overlap with the MC-Gaussians while being far enough away from the molecule to permit the assumption that the overlap between MC Gaussians and PC Gaussians is zero. We shall refer to the combined basis of MC Gaussians and B-Splines introduced to account for the continuum as a hybrid Gaussian B-Spline (GABS) basis. Figure 8.1 depicts schematically the structure of such a configuration of basis functions.

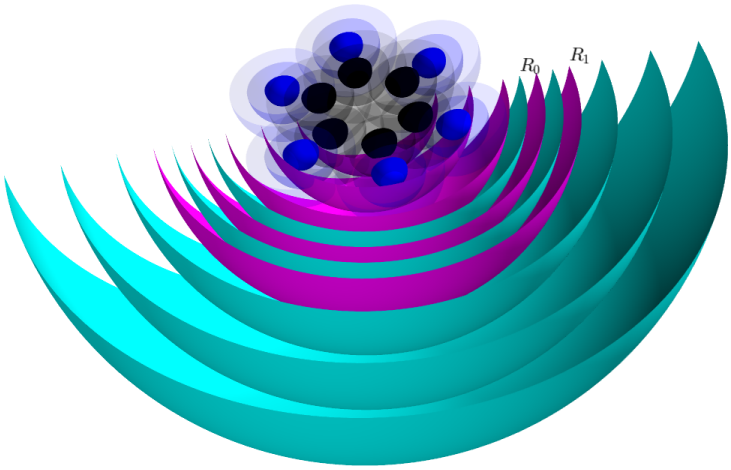

Figure 8.1: Schematic depiction a GABS Basis configuration, here in the sample case for Benzene. The black and blue spheres represent the QC PC Gaussians, for the Carbon and Hydrogen atoms respectively. The magenta spheres correspond to MC Gaussians at the CoM of the molecule extending to R_1 and the cyan spheres to the B-Splines starting at R_0. Note that the PC Gaussians and the B-Splines do not overlap.

This basis was introduced by Marante[51]. In this work the feasibility of such as basis was ascertained, by expressing in a GABS basis the Hydrogen bound (including highly excited states) as well as continuum states. Comparison with the results obtained carrying out analytical computations is shown to yield excellent agreement for the radial wavefunction of bound and continuum states as well as bound-bound, continuum-bound and continuum-continuum dipole matrix elements (in both length and velocity gauge) in time independent calculations and furthermore ATI photoelectron spectra and photoelectron angular distributions in time dependent calculations.

This clearly identifies the GABS basis as a useful candidate for the description of photoionization, having proven beyond doubt its capability to accurately reproduce scattering variables at least in the single particle case. A similar basis to the GABS basis was recently proposed and applied to the study of water by Zdenek[199], dividing the regions of space to be represented using B-Splines or Gaussians in a similar fashion. This method however is restricted to MC Gaussians with $k = 0$ reducing radial flexibility of the diffuse basis, and furthermore is, unlike the XCHEM approach, based on the R-matrix method [200].

8.2 Close Coupling Revisited

Having established a basis to work in, the question is now how to use it to describe scattering states in complicated molecular systems. To this end we return to equations 5.92 and 5.93 summarizing the problem in the close coupling approach, if one (and only one) of the electrons is sufficiently far from the ionic molecule r_{N_e} so as to not feel the short range structure of the molecule, feeling what may be considere a Coulomb potential. If the N^{th} electron is within a radius R_0 from the molecule we consider it to be in a short range state, describing the whole system purely in terms of Gaussian Basis functions (MC and PC). We therefore expand the wavefunction of the system (following reference [52]) in terms of the short range states $\aleph$ and the extended channel functions $\bar{\Upsilon}$ given in the usual notation, with α being the channel index)

$$\Psi_{\alpha E} = \sum_i \aleph_i c_{i\alpha E} + \sum_{\beta,i} \bar{\Upsilon}_{\beta i} c_{\beta i \alpha E}, \tag{8.2}$$

where the extended channel functions are defined as antisymmetrized product of the normal channel

functions and a radial function designed to describe the continuum, explicitly reading

$$\bar{\Upsilon}_{\alpha i} = N_{\alpha i}\mathcal{A}\Upsilon_\alpha(\mathbf{x}_1, \cdots, \mathbf{x}_{N_e-1}, \hat{\mathbf{r}}_{N_e}, \zeta_{N_e})\phi_i(r_{N_e}), \tag{8.3}$$

which noting the asymmetry implicit in the design of the channel function Υ_α (the cationic states obtained from QC calculations will always be anti symmetric) we may simplify to

$$\bar{\Upsilon}_{\alpha i} = \frac{N_{\alpha i}}{N_e}\sum_i (1 - \mathcal{P}_{iN_e})\Upsilon_\alpha(\mathbf{x}_1, \cdots, \mathbf{x}_{N_e-1}, \hat{\mathbf{r}}_{N_e}, \zeta_{N_e})\phi_i(r_{N_e}), \tag{8.4}$$

where here $\mathcal{P}_{ij}$ is the operator permuting electrons i and j. In practice these extended channel functions are obtained by an augmentation procedure acting on some cationic state with the creation operator and subsequently projecting out the part of the resulting state that has the correct total and projected spin, demanded of the system including all N_e electrons. This gives the augmented channel functions Υ'

$$\Upsilon'_{\alpha i} = \mathcal{P}^{S\Sigma} a^\dagger_{il_\alpha, m_\alpha, \sigma}\Phi_{\alpha,\Sigma_\alpha}, \tag{8.5}$$

augmenting the cation $\Phi_{\alpha\Sigma_\alpha}$ (a linear combination of Slater determinant) with an electron in an orbital of angular momenta l_α,m_α and of spin σ and removing, by application of $\mathcal{P}^{S\Sigma}$, whatever undesirable spin contamination brought about by the creation operator. The details of how to create valid sets of orbitals to represent the cationic wavefunction Φ in, as well as to augment in, are discussed in the next chapter. By comparison of equations 5.92 and 8.5 we may relate the augmented to the extended channel functions via

$$\bar{\Upsilon}' = (-1)^p \frac{\sqrt{N_e}}{N_{\alpha i}} C^{S\Sigma}_{S_\alpha\Sigma_\alpha}\bar{\Upsilon}_{\alpha i} \tag{8.6}$$

where the sign change p is due to the sign change inherent to the definition of the creation operator and depends on the orbital that the augmenting electron is created in. This relates the close coupling formalism to what is accessible to us coming from quantum chemistry, with the augmentation being in either occupied, localized orbitals of the cation (giving short range states $\aleph$), diffuse orbitals Gaussian orbitals (giving states of the kind $\Upsilon\phi^{\mathrm{d}}$) or B-Splines (giving ΥB). The next step is to evaluate the matrix elements of the thus resulting states. Matrix elements relating short range states $\aleph$ and diffuse Gaussian states $\Upsilon\phi^{\mathrm{d}}$ fall in the realm of quantum chemistry and are explored in the next chapter. Evaluation of elements involving states of the kinds $\Upsilon\phi^{\mathrm{d}}$ and ΥB is carefully outlined in reference[51] and shall not be discussed here. Matrix elements of short range states $\aleph$ and states ΥB are zero by virtue of the assumption of depreciable PC Gaussian contributions beyond R_0 (the resulting matrix structure of the XCHEM Hamiltonian H_X is outlined in figure 8.2; the overlap matrix S_X has an identical structure).

Upon interaction with a photon of energy ω, electrons my be found in scattering states with momenta, depending on the cationic states of the different channels open at ω. Asymptotically these scattering states behave according to equation 5.93. We must therefore extract eigenstates of H_X whose behaviour in the asymptotic region agrees with the expected asymptotic behaviour as predicted by scattering theory. The fixed so called boundary condition approach achieves this implicitly by considering the generalized eigenvector problem

$$(\mathbf{H}_X - \mathbf{S}_X E)\mathbf{c} = 0, \tag{8.7}$$

enforcing the basis coefficients corresponding to basis functions that do not disappear at the box boundary to be zero (i.e. disregarding the last B-Spline). Whence it is possible to proceed by straightforward diagonalization, yielding a discrete spectrum. The obvious problem posed by the discreteness of the resulting spectrum can be addressed by changing the size of the box so as to include the scattering state with the desired energy, with special attention being paid to the way in which to account for the differences in normalization of the true scattering states compared to normalization in a finite domain[160, 198].

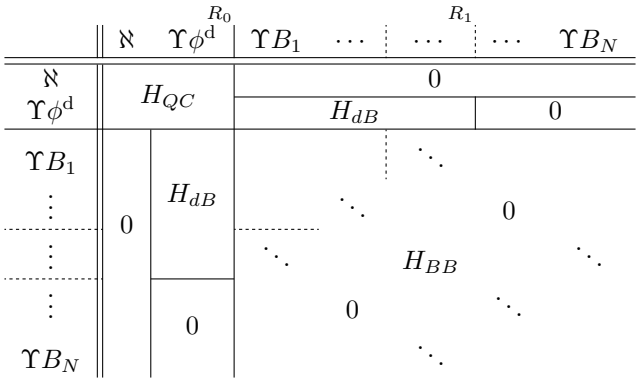

Figure 8.2: Structure of XCHEM Hamiltonian. States involving only Gaussians are labelled as the QC Hamiltonian H_{QC}. The short range states $\aleph$ do not couple to the cations augmented with B-Spline (starting at R_0) and beyond R_1 neither do the states augmented with diffuse orbital. The B-Spline-B-Spline elements H_{BB} are characterized by a sparse matrix structure.

An alternative approach[151, 201, 202, 203] (pursued in this work) deals with the continuous spectrum of the scattering states in a different manner; by not enforcing a boundary condition at the end of the box. This allows to produce scattering states of a desired energy directly, by not selecting a priori a set of scattering states subject to the (arbitrary) boundary condition of vanishing at the box boundary. The resulting systems of equation for some channel is then under defined, having one more variable than equations, as expressed by

$$\begin{pmatrix} \beth^{\alpha} & \cdots & & & & \\ \vdots & A^{\alpha}_{11} & A^{\alpha}_{12} & \cdots & & \\ & A^{\alpha}_{21} & \ddots & & & \\ & \vdots & & A^{\alpha}_{N_b-1N_b-1} & & \\ & & & & x^{\alpha} - ES^{\alpha}_{N_bN_b} \end{pmatrix} = \mathbf{c}^{\alpha}, \tag{8.8}$$

where $\beth^{\alpha}$ now denotes the matrix $H_{QC} - ES_{QC}$ for all states in channel α obtained by augmenting in orbitals not involving B-splines. Conversely $\mathbf{A}^{\alpha} = H_{ij} - ES_{ij}$, for B Spline augmentations vanishing at the end of the box. All values for x lead to a valid solution for equation 8.7 if no boundary condition is enforced. We have not made explicit the coupling terms, the structure of which has been exhibited in 8.2.

Extending this to the full system with all N_c channels and the couplings between them leads to (the Hamiltonian part of which is essentially a rearranged version of what is depicted in 8.2),

$$\begin{pmatrix} \beth^{1} & \cdots & & & & & \\ \vdots & \ddots & & & & & \\ & & \beth^{N_c} & & & & \\ & & & \mathbf{A}^{1} & \cdots & & \\ & & & \vdots & \ddots & & \\ & & & & & \mathbf{A}^{N_c} & \\ & & & & & & \mathbf{x} - E\mathbf{S}_{N_bN_b} \end{pmatrix} = \mathbf{c}, \tag{8.9}$$

where $\mathbf{x}$ now contains N_c unknown terms. The resulting set of N_c (obtainable by letting all $x^{\alpha} = 1$, leading to arbitrary normalization) linearly independent solutions may then be related to the physically relevant solution by fitting to the asymptotically correct linear combination of regular and irregular solutions to the Coulombic system, the radially oscillatory part of the β^{th} channel contribution to the α^{th} solutions

$$u_{\alpha\beta}(r) = a_{\beta\alpha}F_\beta(r) + b_{\beta\alpha}G_\beta(r), \tag{8.10}$$

hence yielding values for $\mathbf{a}$ and $\mathbf{b}$, which may be directly related to the $\mathbb{S}$ matrix via (where $\tilde{a}_{\beta\alpha} = \sqrt{\frac{\pi k_\beta}{2}}$ and $\tilde{\mathbf{b}}$ analogously),

$$\mathbb{S} = \frac{\tilde{\mathbf{a}} + i\tilde{\mathbf{b}}}{\tilde{\mathbf{a}} - i\tilde{\mathbf{b}}}. \tag{8.11}$$

As was previously discussed the eigenvalues of are closely related to the phase shift of the scattering state. Furthermore having found the $\mathbb{S}$ matrix (or equivalently the scattering states) we may proceed to evaluate further properties of the system such as the dipole transition matrix element related between different states, most importantly for us between bound and continuum states in different gauges (currently implemented are length and velocity), which closely related to the to the photo ionization cross section. This conclude the theoretical discussion of the XCHEM approach. For more details we refer to (especially on matrix element evaluation)[51, 52].

8.3 Benchmark Calculations

The XCHEM approach has several appealing qualities, making it a good candidate for a multitude of future investigations. First and foremost the computational effort, while being outrageous if compared to other methods in its application to simple bench mark systems, can be expected to grow very slowly once a certain complexity of molecule has been reached. This is a consequence of the core assumption that the PC Gaussians and B-Spline do not overlap. Therefore, as long as the MC Gaussians are sufficiently extensive to allow choosing $R_0 < R_1$ (the starting point of the B-Splines) so that no PC Gaussians protrude beyond R_0, the scattering calculations are effectively immune to the complexity of the molecular structure contained within radii smaller than R_0. A further advantage of the XCHEM method is the fact that all calculations concerning Gaussians are, in essence, standard quantum chemistry calculations building on the matrix elements of the PC and MC Gaussians. We may therefore construct the short range states exploiting QC packages. While some tweaking and modifying is necessary (extensively discussed in the next chapter) to adapt the QC package to the requirements of the XCHEM methods, it nevertheless represents an ample architecture for the construction of short range states at a high level of theory.

In chapter 9 we will show the details of how merging the QC packages with the scattering aspects is achieved, while keeping computational costs to a minimum. The entirety of the XCHEM codes prowess will then be demonstrated in chapter 10 by applying it to a relatively complex systems. Before we begin these considerations related to larger systems, we stop to apply the XCHEM method to the smallest benchmark systems, to ensure its viability and get and idea of its accuracy.

The XCHEM code was put to the test in the smallest non-Hydrogen systems (with ample theoretical and experimental reference data available), to gauge the accuracy, reliability and cost of the code. The first natural candidates are Helium and molecular Hydrogen[52], introducing multiple atomic site as well as the presence of multiple electrons, of which the latter is particularly interesting as with more than one electron we may study auto ionizing states (present in He and H_2 in the form of doubly excited states). As the focus of this work is on diatomic systems, leading up to a discussion of molecular Nitrogen, the next section will review the results that were obtained for molecular Hydrogen, this being a natural precursor to N_2. The discussion of these results serves multiple purposes; it serves as a benchmark allowing comparison with readily obtainable reference data and should also serve to further elucidate the central ideas of the XCHEM approach. Finally, at the end of this chapter we shall briefly comment on atomic benchmark systems.

8.3.1 Molecular Hydrogen

H_2 presents the first molecular target, for which accurate benchmark calculations are readily available[204, 205].

	MRCIS	XCHEM-1	XCHEM-2	XCHEM
		Energy (a.u.)		
$^1\Sigma_g^+$	-1.1674	-1.1380	-1.650	-1.1650
	-0.6908	-0.5682	-0.6905	-0.6905
	-0.5717	-0.0185	-0.6263	-0.6263
$^1\Sigma_u^+$	-0.7047	-0.5156	-0.7040	-0.7040
	-0.6159	0.0163	-0.6280	-0.6279
		Dipole (a.u.)		
$1(^1\Sigma_g^+) - 1(^1\Sigma_u^+)$	0.4546	0.3643	0.4537	0.4539
$1(^1\Sigma_g^+) - 2(^1\Sigma_u^+)$	0.3105	0.0296	0.2145	0.2201
$2(^1\Sigma_g^+) - 1(^1\Sigma_u^+)$	0.0370	-0.1722	0.0382	0.0382
$2(^1\Sigma_g^+) - 2(^1\Sigma_u^+)$	0.1956	0.0140	0.1465	0.1468
$3(^1\Sigma_g^+) - 1(^1\Sigma_u^+)$	-0.1088	-0.0452	-0.1713	-0.1724
$3(^1\Sigma_g^+) - 2(^1\Sigma_u^+)$	-0.1595	0.0037	-0.00873	-0.0129

Table 8.1: Comparison of bound state results obtained using the MRCIS module of Molpro and the XCHEM code. The three columns labelled XCHEM show the results obtained by gradually including the different ingredient making up the full XCHEM approach. XCHEM −1: Augmentation only in polycentric Guassians; XCHEM −2 Augmentation in all Gaussians (polycentric and monocentric); XCHEM : full XCHEM calculation including polycentric Gaussians and the GABS basis. The listed dipoles are caclulated along the z-direction in velocity gauge.

For molecular Hydrogen a truncated version of the aug-cc-pV6Z PC Gaussian basis set was used, describing the cationic states carrying out SA-CASSCF calculation including in the active space the orbitals $1s\sigma_g$,$2s\sigma_g$,$2p\sigma_u$,$2p\pi_u$ and $3d\pi_g$, (leading to CAS(7,1) when taking into account the doubly degenerate nature of the π states - which is to say one electron is allowed to occupy seven orbitals). As will be explained in more detail in chapter 9, the orbitals were optimized using the QCP Molpro and then converted to be compatible with Molcas, better suited for the augmentations procedure. The resulting orbitals are shown in figure 8.3.

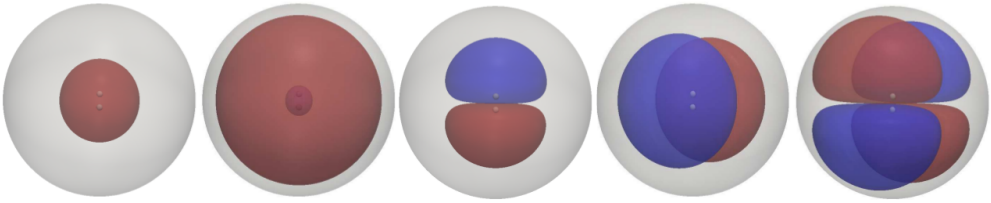

Figure 8.3: The orbitals included in the actice space of the H_2^+ parent ion, from left to right: $1s\sigma_g$, $2p\sigma_u$, $2p\pi_u$ and $3d\pi_g$. The sphere defining the region in which B-splines are not present is also show in grey.

The subsequent augmentation to yield the neutral system was done over (in addition to the orbitals obtained from Molpro) a set of diffuse orbitals created using a GABS basis with B-Splines of order 7 and extending to 400 a.u. and the Gaussian part being created from a set of 22 exponents. The first test was to check the capability of the XCHEM code to accurately reproduce bound state properties, in this simplest molecular system, by comparing the results to what is easily obtainable from QCPs. Specifically the lowest few bound states of symmetries $^1\Sigma_g$ and $^1\Sigma_u$ of the augmented system were computed as well as their dipole transition moments between them. Table 8.1 shows these values. The agreement with MRCIS (explained in chapter 3) calculation is very good, with the XCHEM code surpassing the QC calculations for some excited states due to its better representation of diffuse states. Also it should be noted that the (in bound state QC) non-standard B-Spline basis functions never leads to deterioration of the results, allowing us to conclude the GABS basis set is as accurate as standard basis sets for the descriptions of low-energy bound states.

Having established the minimum requirement of not decreasing the quality of the bound states, the next

step is to consider continuum states. To this end we used the CC expansion given in table 8.2 (the angular momenta of the GABS basis were chose accordingly) to build channels leaving the system in a ${}^1\Sigma_u^+$ state after ionization.

cation	CC			
Φ_α	(l,m)			
$1s\sigma_g$	$(3,0)$,	$(2,0)$,	$(1,0)$,	$(0,0)$
$2p\sigma_u$	$(3,0)$,	$(2,0)$,	$(1,0)$,	$(0,0)$
$(2p\pi_u)_{x,y}$	$(3,\pm1)$,	$(2,\pm1)$,	$(1,\pm1)$	
$2s\sigma_g$	$(3,0)$,	$(2,0)$,	$(1,0)$,	$(0,0)$
$(3d\pi_g)_{x,y}$	$(3,\pm1)$,	$(2,\pm1)$,	$(1,\pm1)$	

Table 8.2: Close Coupling Expansion used in the study of the photo ionization of H_2 in the ${}^1\Sigma_u^+$ channel, using the XCHEM code.

The XCHEM code was then used to perform fixed nuclei calculations for the first three ($n = 1, 2, 3$) resonances appearing in the ${}^1\Sigma_u^+$ continuum. The results were compared with those obtained from a independent calculation utilising a different method [204]. Table 8.3 summarizes these results quoting values for the position and widths of the autoionizing states at different internuclear separations.

R	n	E_{ref}	Γ_{ref}	E	Γ
1.0	1	0.2853	$8.74 \cdot 10^{-3}$	0.2847	$8.94 \cdot 10^{-3}$
1.0	2	0.3708	$1.89 \cdot 10^{-3}$	0.3703	$1.97 \cdot 10^{-3}$
1.0	3	0.3808	$2.71 \cdot 10^{-4}$	0.3809	$2.86 \cdot 10^{-4}$
1.4	1	$-3.592 \cdot 10^{-2}$	$1.54 \cdot 10^{-2}$	$-0.3602 \cdot 10^{-2}$	$1.45 \cdot 10^{-2}$
1.4	2	$4.237 \cdot 10^{-2}$	$3.58 \cdot 10^{-3}$	$4.206 \cdot 10^{-2}$	$3.89 \cdot 10^{-3}$
1.4	3	$4.794 \cdot 10^{-2}$	$6.21 \cdot 10^{-4}$	$4.792 \cdot 10^{-2}$	$5.88 \cdot 10^{-4}$
2.0	1	-0.2926	$2.55 \cdot 10^{-2}$	-0.2899	$2.33 \cdot 10^{-2}$
2.0	2	-0.2236	$3.52 \cdot 10^{-3}$	-0.2225	$1.39 \cdot 10^{-3}$
2.0	3	-0.2212	$3.94 \cdot 10^{-3}$	-0.2223	$6.45 \cdot 10^{-3}$
3.0	1	-0.4783	$4.10 \cdot 10^{-2}$	-0.4673	$3.67 \cdot 10^{-2}$
3.0	2	-0.4238	$2.80 \cdot 10^{-3}$	-0.4230	$2.21 \cdot 10^{-3}$
3.0	3	-0.4177	$1.15 \cdot 10^{-2}$	-0.4170	$9.73 \cdot 10^{-3}$

Table 8.3: First three ${}^1\Sigma_u^+$ resonance energies and widths (in a.u.) for a selection of internuclear distances R. The results obtained unsing the XCHEM approach with the CC expansion of table 8.2 and the basis specification named in the text is compared to reference values taken from reference [204]

The results reported in table 8.3 show overall good agreement with the reference data, except for a slightly larger error (40%) in the resonances width for an internuclear separation of 2.0 a.u. where the second and third auto ionizing state are in the vicinity of a sharp avoided crossing, leading to the system's high sensitivity with respect to small errors in the relative energies of these states[204].

Lastly the photo ionization cross section was computed (see figure 8.4) (at $R_{H-H} = 1.13$ a.u.) from the neutral ground state to the ${}^1\Sigma_u 1$ continuum of photon energies including the first of the auto ionizing states reported in table 8.3 ($n = 1$), once again giving very satisfactory agreement compared to existing results (carried out also in the fixed nuclei approximation)[42, 206]. Furthermore a comparison with data obtained from the approach of reference[207] is presented having excluded inter channel coupling; the resulting background (naturally void of resonance features) is in excellent agreement.

The presented data proves beyond reasonable doubt, that the XCHEM method is certainly capable of competing with existing methods for the simple benchmark case of molecular Hydrogen. Therefore we have at least established the XCHEM method as a candidate for more complex systems, in chapter 10 we show that the XCHEM method can not only handle benchmark systems, but is able to also deal with polyelectronic diatomic systems.

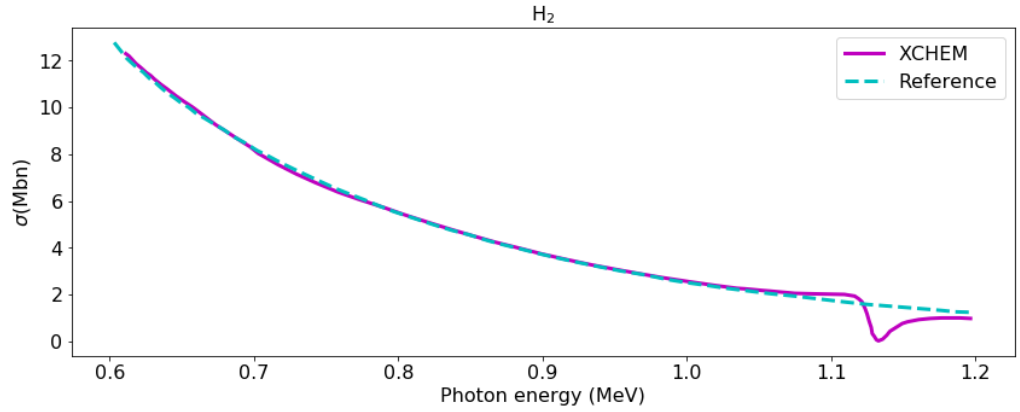

Figure 8.4: Continuus magenta line: Photoionization cross section from the H_2 ground state at equilibrium distance to the ${}^1\Sigma_u^+$ continuum. Cyan dashed line: Reference caluclation. Note the reference calculation only shows the backgroun contribution to the cross section, whereas the XCHEM calculation is indeed capable or reprducing the resonance.

8.3.2 Atomic Benchmark Systems

Without going into details, we mention here that reference calculations were also carried in the atomic system Helium and Neon, with the latter representing a very significant advance in the sense that the system is no polyelectronic, containing ten electrons that need to be accounted for.

For Helium the same bases as for H_2 was used and a CC expansion including the parent ions $1s$, $2s$ and $2p$, coupled to electrons escaping the system with angular momenta $l \leq 2$ (and all allowed values for m). In the case of Neon the CC expansion includes as parent ions the ${}^2P$ ($1s^2 2s^2 2p^5$) and ${}^2S$ ($1s^2 2s^1 2p^6$) states using the cc-pVQZ basis and an actives space including $2s$,$2p_{x,y,z}$,$3p_{x,y,z}$,$3d_{-2,-1,0,2,1}$ and 4_s orbitals (i.e. CAS(13,4)). Based on these these specification the photo ionization cross sections from the neutral ground states to the ${}^1P$ continuum in the case of He, and the continua ${}^1P$ and ${}^1S$ in the case if Ne, were computed. The result are shown in 8.5 and a more thorough analysis [52] shows them to be in excellent agreement with reference calculations.

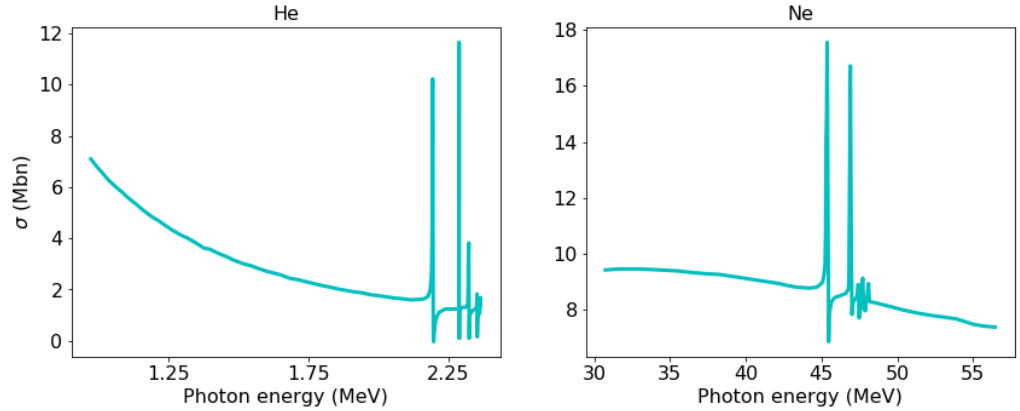

Figure 8.5: Photoionization cross sections for two atomic benchmark systems. The lefthand panel shows the results obtained for Helium. The righthand panel show the results obtained for Neon. Clearly visible in both cases are resonance features due to the presence of auto ionizing states.

We have outlined the theoretical details of the XCHEM approach and exhibited benchmark results for molecular Hydrogen as well as making reference to benchmark calculation in atomic systems. The next chapter is dedicated to an in-depth description of the details of the implementation of the part of the

XCHEM code the addresses everything accessible to QCPs.

9 XCHEM-QC - Current Implementation

The discussion of the XCHEM approach showed that the creation of the neutral system including bound as well as scattering states is done by augmenting the ionic system with an electron in either the localized orbitals obtained from the calculation of the parent ion states included in the close coupling expansion or in the orbitals added by the inclusion of the GABS basis. Where, as we already mentioned, the B-Spline part of the GABS basis is necessary for the description of the continuum states, and the monocentric Gaussian part provides a bridge between localized Gaussian and B-Splines which allows the assumption of zero overlap between the two. This augmentation procedure therefore naturally divides into two parts. The scattering part by considering states with non zero contribution from B-Spline basis functions and the bound state part comprised of everything related to bound states expressed only in terms of either monocentric or localized Gaussian basis functions.

The main contribution of this work to the XCHEM code is the following. Given a set of parent ion states produced by a calculation carried out using a QCP, expressed in terms of CSFs over the active orbitals some active space, the code we designed proceeds by i) creating a set of monocentric orbitals and ii) using our implementation of an augmentation procedure, that takes as a starting point the parent ions and generates neutral states with a user defined spin, by adding electron in localized and monocentric orbitals. The details of the implementation of this code are the subject of this chapter and the developed code will be referred to as XCHEM-QC .

The main requirements on the code prior to its implementation were usability, scalability, flexibility and portability understood as follows. Usability: the code should be executable requiring input of the user at level of complexity similar to what is encountered in QCP. Flexibility: the user should be at liberty to tackle a wide range of problems without having to engage in modifications. Scalability: the computational time should have as little dependence as possible on the size of the parent ion molecules. Portability: the code should exploit well established and widely available commercial QCPs wherever possible. What we found in practice is that given the idiosyncrasies of different QCPs and the complexity of the resulting code, to some degree a trade-off between these requirements is unavoidable.

What would be required from a QCP to facilitate this kind of calculation is the following. Given the specifications of the molecular geometry of the system, the localized and monocentric Gaussian basis functions and the details of the active space, the QCP would first have to carry out a standard quantum chemistry calculation at say CASSCF level using only the localized basis functions. Given then the mono centric basis functions, the operator matrix elements among them and between them and the localized basis have to be calculated and furthermore a set of orbitals orthogonal to the parent ion orbitals should be constructed from them. Next for each parent ion a set of neutral states should be generated by augmenting with an electron in each active space orbital and each mono centric orbital. Finally given this (potentially quite large) set of states the matrix operator elements between them necessary for scattering calculations need to be evaluated. These are the one and two electron Hamiltonian, the transition dipole moments for calculations in length and velocity gauge, and, should one wish to verify the Virial Theorem, the kinetic energies.

Even superficial familiarity with QCPs should suffice to lead one to the conclusion that exclusively using QCPs such a calculation can not be realized without modification. But not only is it necessary to bridge certain gabs in QCPs by modifying them or writing programs for tasks that QCPs are wholly unsuited for. Also, for reasons that will be pointed out throughout this chapter, it proved difficult to work with a single QCP only. Therefore before going into the details of how the various parts the calculation were

realized a comment is in order on our choice of QCPs. Ultimately we employed a mixture of calculations carried out in Molcas and Molpro, as either program had certain advantage and disadvantages for different sections of the project. Broadly speaking the advantage of Molcas is that its source code is significantly more accessible making it possible to modify it to suit our needs. The reason we didn't exclusively use Molcas is of a more technical nature and will become apparent in the discussion of the implementations below.

Before we outline the XCHEM-QC code an overview is provided over the modules of Molcas and Molpro relevant to this work. That includes modules explicitly used in the XCHEM-QC code as well as modules that were used for testing of the XCHEM-QC code by comparing the results of the smallest possible systems (primarily H,H_2, HHe and Ne with a reduced monocentric basis and minimal or small active spaces, thus covering the majority of complications that may arise due to different symmetry properties, heteroatomic structure polyelectronic structure and different active spaces). The limited (minimal) size of these test systems is useful in two ways. On the one hand it allows for the computation of the results in more than one way, which may be prohibitively expensive in larger systems, and on the other hand it allows direct inspection of say individual integrals or CI coefficient which would be cumbersome to the point of being impossible in larger systems.

Molpro

SEWARD Given sets of basis functions g_i centred at different sites, the SEWARD module (common to Molcas and Molpro) analytically calculates the integrals necessary at various stages of the subsequent calculation. The relevant integrals are (where G_i denotes some Gaussian with the $G^{\alpha_i \mathbf{r}_i}_{k_i l_i m_i}(r) = N(\mathbf{r}-\mathbf{r}_i)^{2k+l} e^{-\alpha_i(\mathbf{r}-\mathbf{r}_i)^2} Y_{l_i m_i}(\theta,\phi)$)

$$\text{Overlap} \quad S_{ij} = \langle G_i | G_j \rangle \tag{9.1}$$

$$\text{Dipoles} \quad d^x_{ij} = \langle G_i | x | G_j \rangle \tag{9.2}$$

$$d^y_{ij} = \langle G_i | y | G_j \rangle \tag{9.3}$$

$$d^z_{ij} = \langle G_i | z | G_j \rangle \tag{9.4}$$

$$\text{Velocities} \quad v^x_{ij} = \langle G_i | \frac{d}{dx} | G_j \rangle \tag{9.5}$$

$$v^y_{ij} = \langle G_i | \frac{d}{dy} | G_j \rangle \tag{9.6}$$

$$v^z_{ij} = \langle G_i | \frac{d}{dz} | G_j \rangle \tag{9.7}$$

$$\text{One electron Hamiltonian} \quad h_{ij} = \langle G_i | -\frac{1}{2}\nabla^2 + \sum_A \frac{Z_A}{|\mathbf{r}-\mathbf{r}_a|} | G_j \rangle \tag{9.8}$$

$$\text{Two electron Hamiltonian} \quad g_{ijkl} = \langle G_i G_j || G_k G_l \rangle \tag{9.9}$$

HF The HF module carries out restricted (closed shell) and unrestricted (open shell) SCF calculations, yielding Hartree Fock Orbitals as linear combinations of basis functions.

MULTI Defining sets of occupied, active and virtual orbitals the MULTI module carries out a State Averaged MCSCF calculation yielding optimized orbitals as linear combinations of basis functions and CI vectors as linear combinations of CSFs over the MCSCF orbitals.

Molcas

GATEWAY The GATEWAY module allows the user to specify the molecular geometry and symmetry as well as the basis functions to be used. It allows for the inclusion of sets of basis functions

associated with a ghost atom. This we shall use to include the mono centric basis in the calculation if integrals, by placing a ghost atom at the centre of mass of the molecule.

SEWARD Identical to the SEWARD module of Molpro. Note that if working with symmetry only the integrals between orbitals belonging to the same irreducible representation of the point group of the molecule need to be calculated. The largest point group allowed Molcas and Molpro is D_{2h}.

RASSCF The RASSCF module is similar to the MULTI module of Molpro carrying out MCSCF calculations, allowing for the division of orbitals into the sets RAS1, RAS2 and RAS3 as was explained in chapter 3, resulting in optimized orbitals $\chi_i = \sum_j b_{ij} G_j$ and CI vectors $\mathbf{C}$ over CSFs. The resulting information is saved in a binary, so called JOBIPH file.

MOTRA The MOTRA module allows for the conversion of integrals of basis function to integrals of orbitals. By carrying out in the case of overlaps for example $S_{ij}^{\text{orb}} = \langle \chi_i | \chi_j \rangle = \sum_{kl} b_{ik} b_{jl} S_{kl}$.

RASSI The RASSI calculate operator matrix elements between different states provided for example by a MCSCF calculation, by calculating the corresponding reduced one or two electron density matrices.

CASPT2 The principal purpose of the CASPT2 module is to perform perturbation theory calculations. However, we exploit primarily the fact that the CASPT2 module in requesting verbose output provides the GUGA (graphical unitary group approach, see chapter 3) table.

EXPBAS The EXPBAS module allows for the manipulation of orbital files. We exclusively used it for its DESY keyword. A set of molecular orbitals obtained by working in symmetry group with more than one irreducible representation is then converted to the symmetry free case by padding it with zeros where necessary.

The code that was developed can be loosely divided into three parts. As we will see this division followed computational rather than contextual consideration so as to allow the parts of the XCHEM-QC code to run in parallel in as far as possible: the first part is concerned with evaluating the basis integrals including the localized and monocentric Gaussian basis and the second handles the augmentation of the parent ion states' CI vectors with an additional electron, and subsequent evaluation of the one and two electron reduced density matrices. Finally the third part computes the monocentric orbital transforming all basis integrals two orbital integrals and finally using the basis and orbital integrals to compute the operator matrix elements for the augmented states. Of these three part the first two may be run concurrently whereas the third part depends on the results of the first two. Before going into more detailed explanations of the workings of these parts a section will be devoted to an explanation of how a user must specify a problem for the XCHEM-QC code to understand it.

9.1 Input Specifications

All three part read a common input file defined by the user specifying the (parent ion) problem with the following keywords:

project specifies a project name

gatewayFile specifies the file in which the user defines the local basis Gaussian basis set, the symmetry properties and molecular geometry of the problem. The format in which this must be done is that which is required for the input of the GATEWAY module of Molcas.

inactive specify the number of inactive (doubly occupied) orbitals in each symmetry.

RAS1 specify the number of orbitals of each irreducible representations to be associated with the RAS1 space.

RAS2 specify the number of orbitals of each irreducible representations to be associated with the RAS2 space.

RAS3 specify the number of orbitals of each irreducible representations to be associated with the RAS3 space.

nElecRAS1 specifies the maximum number of holes (with respect to the fully occupied case) in the RAS1 orbitals.

nElecRAS2 specifies the number of electrons in the RAS2 space within which a full CI calculation is carried out.

nElecRAS3 specifies the maximum number of electrons allowed to occupy orbitals of the RAS3 space.

symStatesParent specifies the symmetries of the parent ion states

numStatesParent specifies the number of parent ion states of each symmetry specified in symStates-Parent

multiplicityParent specifies the spin multiplicity of the parent ions.

multiplicityAugmented specifies the spin multiplicity after augmentation with an additional electron.

spinAugmentedElectron species the spin of the electron with which the parent ion states are to be augmented to be either α or β.

symSourceStates one may wish to include in the problem specific states (referred to as source states) from which to ionize. Note that to within reasonable accuracy these may be generated in the augmentation procedure, this however is by no means guaranteed. The symSourceStates keyword follow the same logic as symStatesParent

numSourceStates analogous to numStatesParent

createSourceFromParent for each symmetry specified in symSourceStates a boolean must be provided specifying whether the corresponding source states are to be calculated or are provided by the user.

sourceFiles depending on createSourceFromParent, these are the names of the files to which the source states are written or from which they are read.

orbFile name of a binary Molpro file containing the orbitals to be used for parent ion state and source state calculation. If none is provided, the code will created one based on a HF and subsequent State Averaged RASSCF calculation subject to the active space restrictions. Whether or not one should be provided depends on the complexity of the system. That is to say if many or exotic source states are included it is likely that the default parent ion orbital will not turn out to be satisfactory.

kMonocentric the monocentric Gaussian basis set will include functions G_{klm} the values for $0 \leq k \leq$ kMonocentric.

lMonocentric the monocentric Gaussian basis set will include functions G_{klm} the values for $0 \leq l \leq$ lMonocentric.

linearDependenceThr specifies the threshold for the removal of linear dependencies in the set of monocentric orbitals.

Below is given a sample input file. This corresponds in fact to the Nitrogen photoionization problem the result of which we shall study in extensive detail in chapter 10.

```
&INPUT
        project="N2"
        gatewayFile="gateway.in"
        inactive=1-0-0-0-1-0-0-0
        ras2=2-1-1-0-2-1-1-0
        ras3=4-2-2-1-4-2-2-1
        nElecRas2=9
        nElecRas3=2
        symStatesParent=au-b1u-b2u-b3u
        numStatesParent=1-1-1-1
```

```
multiplicityParent=2
multiplicityAugmented=1
spinAugmentedElectron=beta
sourceFiles=GS-PiU1-PiU2-SiU
createSourceFromParent=T-T-T-T
symStatesSource=1-2-3-5
numStatesSource=1-1-1-2
orbFile=n2.wf
lMonocentric=2
kMonocentric=3
linearDependenceThr=1e-5
&END
```

Having explained and exemplified the structure of the input the following three sections are dedicated to explaining the different parts of the code, where we shall frequently refer to the values given in the above input so as to provide examples.

9.2 Part I (INT) - Integrals

As was pointed out before, the SEWARD module allows for the specification of basis sets centred at ghost atoms, that do not interact. The most straightforward way to include the monocentric basis is therefore, given the (well tempered) set of basis exponents, to include it for every desired combination of l and k, making also use of SEWARD's capability to work with spherical rather than Cartesian Gaussian. However care must be taken in how this is achieved. Recall that the polynomial part of a Gaussian basis function G_{klm} is r^{l+2k}. In SEWARD basis sets are specified for each $L = 2l + k$ assuming by default $k = 0$, with the necessary radial flexibility controlled by the number of exponents in a given basis set. This yields for, say, the case of $L = 3$ basis basis functions of the type $1s$, $2p_{-1}$, $2p_0$, $2p_{+1}$, $3d_{-2}$, $3d_{-1}$, $3d_0$, $3d_{+1}$, $3d_{+2}$. For our purposes however it is necessary to control k independently. This may be achieved by SEWARD's keyword `contaminant all` which for a given L enforces consideration of all Gaussian functions fulfilling $L = l + 2k$. Returning to the example of $L = 3$, in addition to the aforementioned list of functions SEWARD would calculate also the integrals for $3s_0$ functions. Naturally this procedure has the side affect of potentially shooting over the mark, as for some combination of desired maximum $l_{\max}$ and $k_{\max}$ we must work with $L_{\max} = l_{\max} + k_{\max}$. For some $L \leq L_{\max}$ we will then be forced to include in SEWARD values for l or k beyond their desired maximum. In the sample input file provided in the previous section for instance $L_{\max} = 8$ which would include also the combination $l = 8$, $k = 0$. Care must be taken to disregard these basis functions.

Considering the way SEWARD generates basis functions for some given L we may quickly arrive at the total number of monocentric basis functions N_{MG} to be

$$N_{MG} = \frac{N_\alpha (L+1)(L+2)(L+3)}{6}, \tag{9.10}$$

where N_α is the number of exponents, such that the total number of basis functions is $N_G = N_{MG} + N_{LG}$. The expensive part of the SEWARD calculations will evidently be the calculation of the two electron integrals of which there are of the order of $O(\frac{N_G^4}{8})$. Specifically we find that an even tempered basis set of 22 exponents has proven to give good results. Furthermore a typical set of values for $l_{\max}$ and $k_{\max}$ giving sufficient radial and angular freedom so as to avoid overlap between the localized Gaussians and the B-Splines in diatomic molecules are $l_{\max} = 2$ and $k_{\max} = 3$. Therefore (neglecting the localized Gaussian basis set, which for those values of l and k tends to be significantly smaller than the monocentric set) we would obtain of the order of

$$\frac{1}{8}\left[22\frac{9 \cdot 10 \cdot 11}{6}\right]^4 \approx 2.2 \cdot 10^{13} \tag{9.11}$$

two electron integrals. Clearly this number of integrals is far beyond anything that can be stored and much less worked with. We may however substantially reduce this number, by realizing, that as we are

interest in single ionization only and the parent ion states are expressed purely in terms of localized Gaussian functions. Therefore any neutral state obtained by augmenting a parent ion, contains at most one electron whose orbital has a non-zero B-Spline component. Therefore of the two electron integrals g_{ijkl}, we may neglect all those with at least three indeces referring to monocentric Gaussian basis functions. It should be clear, that this eliminates the need to calculate the vast majority of integrals. Specifically, rather than having a quartic dependence on the basis size the number of two electron integrals N_g now grows as

$$N_g = O\left(\frac{N_L^4}{8} + \frac{N_L^2 N_M^2}{8}\right), \tag{9.12}$$

which, with the number of monocentric function easily exceeding the number of localized basis functions by a factor of 10 marks a significant reduction of two electron integrals required to be computed. This already allows for the calculations of interesting systems, but, while possible, still becomes quite expensive in the case we have been using as an example so far.

Further progress in cutting the integrals down to size, may be made by the following observation. Consider the two mono centric Gaussians G_{klm} and $G_{k'l'm'}$. The orthogonality of spherical harmonics implies that

$$\langle G^{\alpha}_{klm} | G^{\alpha'}_{k'l'm'} \rangle = C^{\alpha\alpha'}_{kk'} \delta_{ll'} \delta_{mm'}. \tag{9.13}$$

Therefore subsets of basis functions corresponding to different k, unlike subsets corresponding to different l or m, do not necessarily have zero overlap. Therefore in including now different values for k, we may reduce the size of the bases by, rather than using the same basis for any combination of l and k, designing separate, smaller monocentric basis sets for each pair of l and k, labelled $\mathcal{B}_{lk}$. This is done by removing from the original set of basis functions $\mathcal{B}$ those basis functions which may be expressed as linear combinations of basis functions contained in the sets $\mathcal{B}_{lk'<k}$. We shall postpone the mathematical procedure of how this is accomplished to the discussion of the design of the monocentric orbitals, of which the design of $\mathcal{B}_{lk}$ is essentially a simplified version. To quantify what we gain by this consider the size of the union of basis sets $\mathcal{B}_l = \mathcal{B}_{l0} \cup \mathcal{B}_{l1} \cup \mathcal{B}_{l2}$. Using all the exponents of $\mathcal{B}$ would leave each $\mathcal{B}_l$ to contain 66 functions. In removing linear dependencies this number is reduced to 26,29 and 29, for $l = 0$,$l = 1$ and $l = 2$, respectively, with similar results for larger l. The relative improvement can be expected to increase with the addition of each further value for k. Due to the scaling behaviour of the number of two electron integral with respect to the size of the basis, this translates to a speed up by approximately an order of magnitude. Clearly this dramatic improvement is only true for adding bases $\mathcal{B}_{lk}$ with increasing k, the same is not the case for adding basis sets for further values of l due their orthogonality. To incorporate these optimized basis sets $\mathcal{B}_{lk}$, the structure of the way the monocentric bases are specified in the SEWARD input has to be modified, to allow this division of basis functions, without resulting in excessive calculation of superfluous integrals. Namely, rather than working with a single ghost atom for the entirety of monocentric basis functions, we now add a ghost atom X_l for every allowed value for $0 \leq l \leq l_{\max}$ padded with empty basis sets $\mathcal{B}_0$, thereby constructing the monocentric basis such as is outlined in table 9.1.

Lastly we shall make use of the symmetry inherent in the two electron integrals g_{ijkl}, which was given already in equation 2.48. Note that it may not be immediately obvious that exploitation of theses symmetry properties used in conjunction with the neglect of all g_{ijkl} with three or more of the indeces referring to monocentric basis functions, does not result in the neglect of relevant integrals. Inspection of the indicial permutations however confirms that this is not the case.

Having addressed in some detail the various ways we used to reduce the number of basis functions, we shall next look at some limitations of the SEWARD module of Molcas, which despite the ideas developed so far in this section, present obstacles to a straightforward use of SEWARD given an appropriate basis set. SEWARD calculates the integrals in two steps. The first comprises a the "raw" analytical evaluation of the necessary integrals. In the second step the integrals are prepared for their being used in subsequent HF or MCSCF calculations. It is the second of theses steps that turns out to be problematic. SEWARD will either order the analytically evaluated integrals in their exact form, or use a Cholesky decomposition. Even for relatively modest values of L, certainly smaller than $L = 8$, such as in the sample case, the

ghost atom X_l	L	basis	(l,k)
X_0	0	$\mathcal{B}_{0,0}$	$\underline{(0,0)}$
	1	$\mathcal{B}_0$	$\underline{(1,0)}$
	2	$\mathcal{B}_{0,1}$	$\underline{(0,1)}$, $(2,0)$
	3	$\mathcal{B}_0$	$\underline{(3,0)}$, $(1,1)$
	4	$\mathcal{B}_{0,2}$	$\underline{(0,2)}$, $(2,1)$, $(4,0)$
	$\vdots$	$\vdots$	$\vdots$
X_1	0	$\mathcal{B}_0$	$(0,0)$
	1	$\mathcal{B}_{1,0}$	$\underline{(1,0)}$
	2	$\mathcal{B}_0$	$(0,1)$, $(2,0)$
	3	$\mathcal{B}_{1,1}$	$\underline{(1,1)}$,$(3,0)$
	4	$\mathcal{B}_0$	$(0,2)$, $(2,1)$, $(4,0)$
	5	$\mathcal{B}_{1,2}$	$\underline{(1,2)}$, $(3,1)$, $(5,0)$
	$\vdots$	$\vdots$	$\vdots$
$\vdots$	$\vdots$	$\vdots$	$\vdots$

Table 9.1: Structure of basis function sets for different l and k distributed among different ghost atoms. The rightmost column gives all the pairs (l,k) which SEWARD generates for the given L. The underlined pair marks that of interest to us, disregarding the rest. Note for values of L, with no underlined pair, we use the empty dummy basis $\mathcal{B}_0$

former yields infeasibly large memory requirements, while the latter fails to give result in reasonable computational time. Therefore we are in effect, forced to modify SEWARD to output the raw integrals after the intermediate step and process these ourselves, exploiting several properties, unique to the requirements of the XCHEM treatment. What was found in practice that MOLCAS most naturally can be coaxed into outputting the raw integrals, is in a set of arrays each associated with four shells (where a shell, identified by $s = (L, X_l)$, is a subset of basis functions defined by a common value of L for a common ghost atom X_l) $\mathbf{q}_{s_i s_j s_k s_l}$. Each such array contains the integrals g_{ijkl}, such that $L(b_i)$ and $X_l(b_i)$ correspond to s_i (correspondingly for s_j, s_k and s_l) , are stored with their position in the array encoding the corresponding k,l and m. In this form the integrals are still quite useless to us for three reasons: **a)** Molcas does not fully exploit all symmetries of g_{ijkl}, writing superfluous values for g_{ijkl} **b)** rather than the cumbersome identification of a basis function via shells and position in an array, we need a unique index, such as it will be used to expand the orbitals in basis functions **c)** our orbitals will frequently posses a symmetry higher than what Molcas is aware of, which leads to large numbers of zeros integrals being stored.

To remedy these deficiencies we implemented a code compressing the integrals (by full exploitation of the symmetry of g_{ijkl} and removal of integrals smaller than a threshold value equivalent to the accuracy with which Molcas evaluates the integrals), and associating a unique key with each encoding the values of i, j, k and l such that they correspond to the order in which the basis functions coefficients arise in the expansion of molecular orbitals $\chi_i = \sum_j c_{ij} b_j$ in basis functions.

A final limitation of exploiting SEWARD for the integral evaluation, that we must comment on, is that it has an inbuilt maximum of $L_{\max} \leq 10$. While this would be a hard problem to deal with, we have found that this maximum was quite sufficient for our purposes. That being said, future implementations for much larger molecules with less symmetry, requiring larger values of l to describe the more complicated structure of the wave functions of the escaping electron, may have to face this limitation of SEWARD.

9.3 Part II (CAS) - Localized Orbitals, Augmentation and Reduced Density Matrices

While the first part was concerned with the evaluations of monocentric and local basis integrals, the second part part addresses the localized orbitals (working completely independently of the monocentric basis we may wish to employ), and the CI vectors of the parent and sources states. Due to the way in which we will go on to compute the reduced density matrices, an important restriction to which our code is currently subjected is, that all states, of different symmetry or corresponding to either (ionic) parent states or (neutral) source states, must be expressed in terms of a common set of molecular orbitals. Regarding the symmetry part of this restriction, is the reason (alluded to before) for our having to use Molpro as well as Molcas. In Molpro the possibility of carrying out State Average RASSCF calculations, optimizing the sets of orbitals simultaneously for states of different symmetries is implemented. In Molcas this is not the case. Therefore whenever one wishes to carry out calculations involving orbitals of more than one symmetry (which was the case in virtually all systems we considered), we must begin by creating the orbitals in Molpro. In principal this is not a problem, but leads to the surprisingly awkward complication of having to develop code, that translates orbitals from Molpro format to Molcas' RasOrb format.

Having obtained the molecular orbitals, we generate the CI vectors of all parent and source states we are interested in, using Molcas' RASSCF module (having one more modified Molcas to allow for the convenient input and output of CI vectors), which allows one to deactivate the orbital optimization, thereby ensuring their maintained validity of all relevant symmetries. With knowledge of the CI vectors of the source states Ψ_P^-, the next step is to augment them with an additional electron, to create the neutral states Ψ_{Pi}, corresponding to Ψ_P^- with an extra electron in orbital χ_i:

$$\Psi_{Pi} = \hat{a_{i\sigma}}^\dagger \left|\Psi_p^-\right\rangle \tag{9.14}$$

$$= \sum_r^{N_{\mathrm{CSF}}} C_r \hat{a_{i\sigma}}^\dagger \left|\mathrm{CSF}_r\right\rangle . \tag{9.15}$$

Now, it is this augmentation with an electron, that is at the heart of the quantum chemistry part of the XCHEM code. We may distinguish between augmenting either in a localized molecular orbital (obtained from the aforementioned state average MCSCF Molpro calculation) or augmenting in a diffuse orbital (expressed using the monocentric Gaussian basis functions) the details of the creation of which we have yet to develop, and whose existence we shall assume for the moment. For now, we simply account for the monocentric orbitals in the augmentation procedure, by increasing the active space in size to included two more (virtual, not optimized) dummy orbitals. The structure of these dummy orbitals is irrelevant as they merely serve as place holders, occupation of which shall amount to occupation of a diffuse orbital (which shall substituted in for the dummy orbitals once they have been calculated).

As shown in equation 9.15, the parent states Ψ_P^- such as we obtain them for RASSCF are give as expansions in CSFs. In view of the discussion in the chapter 3, the CSF are convenient to to ensure the sates are eigenfunctions of the spin operator, with the correct eigenvalue requested by the user. However, they are much less convenient if the result of the creation operator being applied to them is desired, as is the case in the augmentation procedure. The reasons for that is, that CSFs are not an eigenfunction of the occupation number operator $N_{i\sigma}$. And, as the result of creating an electron in some orbital χ_i depends on the eigenvalue of the occupation number operator of said orbital being either 1 or 0, it is more convenient to work with a determinantal description of the parent ion states during augmentation. Therefore the augmentation procedure of the states Ψ_P^- must be carried out by considering them as a linear combination of not CSFs but determinants.

Thus the creation of an augmented state based on some parent ion state Ψ_P^-, happens in three steps. The first step is the conversion of Ψ_P^- from CSF to determinantal description. The second step is creating a set of augmented states by applying the creation operators $\hat{a_{i\sigma}}^\dagger$, including augmentation in the two

dummy orbitals not present in the original active space. The last step is transforming the augmented states back to a CSF description.

The conversion between CSF and determinantal description is achieved using GUGA tables, detailing the linear combination of determinants the yields each CSF included in the active space,

$$|\mathrm{CSF}_r\rangle = \sum_{s}^{N_\alpha^{\mathrm{det}}} G_{rs} \, |\mathbf{k}_s\rangle \, . \tag{9.16}$$

We may obtain theses GUGA table as a non standard output of the CASPT2 module of Molcas (while preventing it from actually carrying out any perturbation theory). The necessary GUGA tables (using the notation ${}^{S}\mathfrak{G}^{\mathrm{sym}}_{\mathrm{irrep}}$ to label the GUGA table for the conversion of states belong to the irreducible representation of some symmetry of spin multiplicity S) involved in the three steps of the augmentation procedure are:

parent ion, with symmetry ${}^{S_P}\mathfrak{G}^{\mathrm{sym}}_{\mathrm{irrep}}$ for instance $\mathfrak{G}^{D_{2h}}_{B_{2u}}$, GUGA table for a given irreducible representation for the active space such as it is defined in the gatewayInputFile, required for every symmetry of the parent and source states

parent ion, without symmetry ${}^{S_P}\mathfrak{G}^{C1}_{A}$, GUGA table for the active space equivalent to that defined in the gatewayInputFile, but with all electrons occupying orbitals belonging to the C_1 point group

extended ${}^{S_S}\bar{\mathfrak{G}}^{C_1}_{A}$ equivalent to $\mathfrak{G}$ with the RAS3 space extended by two (dummy) orbitals, and the number of active electrons in the system increased by one, with the "new" electron being allowed to occupy the RAS3 space. The calculation of this GUGA table might be quite costly, the reason being that working in C_1 symmetry, adding two orbitals to the RAS3 space as well as an electron allowed to occupy said space, may results in an active space with millions of CSFs quite easily.

The tables ${}^{S_P}\mathfrak{G}^{\mathrm{sym}}_{\mathrm{irrep}}$, are used to obtain the Ψ^-_P in determinants, the space of available determinants to augment in is extended by two (to account for the dummy orbitals, taking the place of the diffuse orbitals) and the augmentations are carried out. Afterwards ${}^{S_S}\bar{\mathfrak{G}}^{C1}_{A}$ is used to convert back to CSFs. Given that we will carry on working with determinants in construction of reduced density matrices, it may seem superfluous to convert the augmented states back into a CSF description. However, this is not the case as the creation operator does not commute with the total spin operator. Therefore in augmenting an initially (for example) singlet state parent ion, we cannot be sure of its spin properties after augmentation. Thus in transforming back to CSFs with the appropriate $\mathfrak{G}$, we ensure that the augmented state is of the correct spin multiplicity, specified by the user.

A further aspect of augmentation is that in adding en electron we may change the symmetry of the resulting determinant. Therefore we convert back after augmentation using the ${}^{S_S}\bar{\mathfrak{G}}^{C1}_{A}$ with no symmetry restrictions. An alternative approach (potentially useful in a future implementation) would keep track of how the symmetry changes under addition of an electron to give the symmetry of the augmented determinant to be $I(CSF)\otimes I(\chi_i)$, and convert back to CSFs using a ${}^{S_S}\bar{\mathfrak{G}}$, with the appropriate symmetry specifications.

In having found the augmented states, we completed the description of the CI vectors of the (neutral) source states in as far as they can be dealt with using quantum chemistry. As ultimately the purpose of the XCHEM-QC part of the XCHEM is the computation of the operator matrix elements of the augmented states, we can make one further step without explicit knowledge of the monocentric orbitals (comprised of the $\mathcal{B}_{lk}$ basis sets). Returning to equation 3.25, for any one electron operator, in conjunction with the definition of the one electron reduced density matrix if equation 3.29, we see that progress can be made toward computing any one electron operator matrix, by computing D_{IJ} for all combinations of augmented states. The efficient calculation of these only depends on the orthogonality of the orbitals and the CI vectors of the augmented states, but no their explicit expansion in terms of basis functions (note that this will also allow us to substitute any monocentric orbitals in place of the dummy orbitals, introduced in anticipation of said orbitals). The analogous argument for the two electron operator case using the two electron reduced density matrix of equation 3.37 is obvious.

Our evaluation of both, the one and two electron reduced density matrix, proceeds using equation 3.27

$$\bar{D}^{IJ}_{pq} = \langle \Psi_I | \hat{a}^\dagger_p \hat{a}_q | \Psi_J \rangle \tag{9.17}$$

$$= \sum_{rs} c_r c_s \langle \mathbf{k}_r | \hat{a}^\dagger_p \hat{a}_q | \mathbf{k}_s \rangle , \tag{9.18}$$

which is to say a contribution to D^{IJ}_{pq} from all pairs of determinants whose occupation vectors $\mathbf{k}_r$ and $\mathbf{k}_s$ are equalized by destroying and creating an electron in $\mathbf{k}_s$, in orbitals q and p, respectively . An alternative way to identify these contributions (corresponding to our implementation), can be realized by applying the Slater Condon rules for one electron operators, identifying for every pair of determinants $\mathbf{k}_r$, $\mathbf{k}_s$, those pairs of orbitals p and q yielding a contribution to an arbitrary one electron operator and updating d^{IJ}_{pq} accordingly by addition of contribution of $\pm C_r C_s$, where the sign arises from antisymmetric nature of electronic wavefunction, characterized the presence of (-1) in the definition of the creation and annihilation operators (see equations 3.2 and 3.2). We may proceed in a closely analogous way for the two electron operator starting now from

$$\bar{d}^{IJ}_{pqrs} = \langle \Psi_I | \hat{a}^\dagger_p \hat{a}_q | \Psi_J \rangle \tag{9.19}$$

$$= \sum_{\mu\eta} C_\mu C_\eta \langle \mathbf{k}_\mu | \hat{a}^\dagger_p \hat{a}^\dagger_q \hat{a}_r \hat{a}_s | \mathbf{k}_\eta \rangle , \tag{9.20}$$

with once again the possibility two use the Slater Condon Rules, now for two electron operators, to evaluate all $\bar{d}^{IJ}_{pqrs}$, with a single loop over all pairs of determinants appearing in Ψ_I and Ψ_J. Of the two reduced density matrices, the two electron density is evidently more expensive to compute, as a much larger set of determinants can be made to agree with the freedom to change the orbital, which two (rather than one) electrons occupy (or returning to Slate Condon Rules, we cannot categorically dismiss all pairs of determinants whose occupation vector differ by more than one occupation number). Therefore in our implementation, some effort went into organizing the determinants, dividing them into groups, with determinants in differing block guaranteed to differ in more than two occupation numbers. Nevertheless, evaluation of the two electron reduced density may become costly for active spaces containing several million determinants. However, once we obtain them and the orbital integrals, the evaluation of the matrix elements, can be realized rather efficiently. Furthermore, as was mentioned before, this potentially rather impressive size of the active space, is in effect the reason which gives rise to the restriction of having to use one orthogonal set of orbitals, describing all parent and source states, of all symmetries, allowing for the straightforward application of Slater Condon rules.

9.4 Part III (ORB) - Diffuse Orbitals and Operator Matrix Elements

The previous two parts, are able to run completely independently, as the first only deals with the evaluation and manipulation of integrals of basis function. The second, on the other hand, is entirely concerned with the structure of the CI vectors, which requires no knowledge of the basis functions. To put these two parts together, to yield the necessary operator matrix elements, corresponding to the augmented states, we endeavour to make use of equations 3.25 and 3.33. The reduced density matrices appearing in these equations, were the subject of the previous part. This leaves creating the diffuse monocentric orbitals, and subsequently using the expansions of those and the original localized orbitals in terms of basis function, to evaluate the orbital integrals, before the operator matrix elements can be evaluated.

9.4.1 The Diffuse Orbitals

The diffuse, monocentric orbitals are of central importance to the successful application of the XCHEM method. They play the role, of bridging an intermediate radial region by being constructed from the

diffuse Gaussians, overlapping with both localized Gaussians as well as B-Splines, which among each other are not permitted to overlap. Therefore the diffuse orbital are instrumental in describing short range effects in the photo ionization of complex molecules. The set of diffuse orbitals must satisfy two properties; **a)** orthonormality with respect to the localized orbitals as well as among themselves, as the creation of the reduced density matrices is done under the assumption of one orthonormal set of orbitals and **b)** their radial extension, must be such that it totally envelops the localized orbital. That is to say no localized orbitals may protrude to radii beyond which the diffuse orbitals are zero. This is key to the assumption of zero overlap between localized Gaussians and B-Spline not leading to an inherently faulty description of the system, by ignoring relevant integral.

As a starting point to finding such a set of orbitals, labelled from now on by χ_p^d, will be the matrix of basis overlap integrals $\mathbf{S}$ containing N_b^d diffuse and N_b^l localized Gaussians (one of the results of the calculation of integrals of section 9.2). From this overlap matrix the χ_p^d shall be identified as linear combinations of the diffuse Gaussians in accordance with the two properties that were just elaborated on. To this end let b_i^d and b_i^l denote the diffuse and localized Gaussian respectively. With a similar notation of χ_p^d and χ_p^l for the orbitals. Furthermore let $\mathbf{b}_p^d$ and $\mathbf{b}_p^l$ be the vector of coefficients yielding orbital χ_p^d and χ_p^l, respectively.

We may thus express the condition **a** as,

$$\langle \boldsymbol{\chi}^l | \boldsymbol{\chi}^l \rangle = \mathbb{I} \tag{9.21}$$
$$\langle \boldsymbol{\chi}^l | \boldsymbol{\chi}^d \rangle = 0 \tag{9.22}$$
$$\langle \boldsymbol{\chi}^d | \boldsymbol{\chi}^d \rangle = \mathbb{I}, \tag{9.23}$$

the first equation, is not strictly necessary, but merely reiterates the orthonormality of the localized orbitals such as they are obtained from the State Averaged RASSCF calculation. The latter two equations enforce orthormality of all orbitals to be maintained upon addition of the diffuse orbitals, whose basis coefficients we are yet to find. The matrix $\mathbf{S}$ is now broken up into sub matrices denoted by $\mathbf{S}^{ll}$, $\mathbf{S}^{dd}$ and $\mathbf{S}^{ld}$ of dimensions $N_b^l \times N_b^l$, $N_b^d \times N_b^d$ and $N_b^l \times N_b^d$, respectively, corresponding to local-local, diffuse-diffuse and local-diffuse basis overlaps:

$$\mathbf{S} = \begin{bmatrix} \mathbf{S}^{ll} & \mathbf{S}^{ld} \\ \mathbf{S}^{dl} & \mathbf{S}^{dd} \end{bmatrix} = \begin{bmatrix} \langle b_1^l | b_1^l \rangle & \cdots & \langle b_1^1 | b_{N_B^l}^l \rangle & \langle b_1^l | b_1^d \rangle & \cdots & \langle b_1^l | b_{N_B^d}^d \rangle \\ \vdots & \ddots & \vdots & \vdots & \ddots & \vdots \\ \langle b_{N_B^l}^l | b_1^l \rangle & \cdots & \langle b_{N_B^l}^l | b_{N_B^l}^l \rangle & \langle b_{N_B^l}^l | b_1^d \rangle & \cdots & \langle b_{N_B^l}^l | b_{N_B^d}^d \rangle \\ \langle b_1^d | b_1^l \rangle & \cdots & \langle b_1^d | b_{N_B^l}^l \rangle & \langle b_1^d | b_1^d \rangle & \cdots & \langle b_1^d | b_{N_B^d}^d \rangle \\ \vdots & \ddots & \vdots & \vdots & \ddots & \vdots \\ \langle b_{N_B^d}^d | b_1^l \rangle & \cdots & \langle b_{N_B^d}^d | b_{N_B^l}^l \rangle & \langle b_{N_B^d}^d | b_1^d \rangle & \cdots & \langle b_{N_B^d}^d | b_{N_B^d}^d \rangle \end{bmatrix} \tag{9.24}$$

We saw in chapter 2 how diagonalization of an overlap matrix $\mathbf{S}$ may be used to find orthogonal orbitals. Following the same procedure neglects however, the need to maintain the localized orbitals to remain unchanged and the fact, that due to the large size of the diffuse basis, there may be linear dependencies, which have to be removed. The former is addressed first, by noting that in requiring 9.22 to hold it will be necessary to allow the diffuse orbitals to have a contribution from the localized orbitals, as the space spanned by $\boldsymbol{\chi}^l$ is not a subspace of the space spanned by the diffuse Gaussians, nor orthogonal to it. Therefore we write a general set of diffuse orbitals as,

$$|\boldsymbol{\chi}^d\rangle = |\boldsymbol{\chi}^l\rangle \, \mathbb{U}^{ld} + |\boldsymbol{b}^d\rangle \, \mathbb{U}^{dd} \tag{9.25}$$

where $\mathbb{U}^{ld}$ and $\mathbb{U}^{dd}$ are the matrices specifying the correct linear combinations of local and diffuse orbitals to the set of diffuse orbitals. Substituting equation 9.25 into equation 9.22 yields

$$\mathbb{U}^{ld} = -\langle \boldsymbol{\chi}^l | \boldsymbol{b}^d \rangle \, \mathbb{U}^{dd}. \tag{9.26}$$

Substituting equation 9.25 into equation 9.23 and using equation 9.26 then gives

$$\mathbb{U}^{dd\,\mathrm{T}} \left[\mathbf{S}^{dd} - \langle \mathbf{b}^d | \boldsymbol{\chi}^l \rangle \langle \boldsymbol{\chi}^l | \mathbf{b}^d \rangle \right] \mathbb{U}^{dd} = \mathbb{I} \tag{9.27}$$

Thus we can identify

$$\mathbb{U}^{dd} = \mathbb{D}^{\mathrm{T}} \mathbf{\Lambda}^{-\frac{1}{2}}, \tag{9.28}$$

where $\mathbb{D}$ is the matrix diagonalizing the matrix $\mathbb{A}$ given by

$$\mathbb{A} = \mathbf{S}^{dd} - \langle \mathbf{b}^d | \boldsymbol{\chi}^l \rangle \langle \boldsymbol{\chi}^l | \mathbf{b}^d \rangle , \tag{9.29}$$

so that in

$$\mathbb{A} = \mathbb{D}^T \mathbf{\Lambda} \mathbb{D} \tag{9.30}$$

the matrix $\mathbf{\Lambda}$ is the diagonal matrix of eigenvalues of $\mathbb{A}$. Thus with knowledge of $\mathbb{U}^{dd}$ and using equation 9.26 we can construct the diffuse orbitals from equation 9.25. In this derivation we have passed over the problem of linear dependencies either present within the diffuse basis, or due to the possibility, that some diffuse Guassians may be expressed as linear combinations of local orbitals. These linear dependencies would manifest themselves as eigenvalue of $\mathbb{A}$ close to zero to within some user defined threshold. Therefore in constructing the matrices $\mathbb{D}$ and $\mathbf{\Lambda}$ so that the eigenvalues appear in decreasing order down the diagonal of $\mathbf{\Lambda}$, we may construct the conditioned matrices $\tilde{\mathbb{D}}$ and $\tilde{\mathbf{\Lambda}}$, by setting the eigenvalues below the threshold, as well as their corresponding eigenvectors in $\mathbb{D}$ to zero. In terms of these matrices we can write the $\mathbb{A}$ accurate to within the threshold used as a cut-off to disregard small eigenvalues, as

$$\mathbb{A} = \left[\begin{array}{c} \tilde{\mathbb{D}}^{\mathrm{T}} \\ \hline \cdots \quad 0 \quad \cdots \\ \vdots \end{array}\right] \left[\begin{array}{c|ccc} \tilde{\mathbf{\Lambda}} & \vdots & & \\ \hline \cdots & 0 & \cdots & \\ & \vdots & & \end{array}\right] \left[\begin{array}{c|ccc} & \vdots & & \\ \tilde{\mathbb{D}} & 0 & \cdots & \\ & \vdots & & \end{array}\right] . \tag{9.31}$$

Constructing then $|\boldsymbol{\chi}^d\rangle$ from the accordingly obtained $\tilde{\mathbb{U}}^{dd}$ and $\tilde{\mathbb{U}}^{ld}$, we obtain a set of diffuse orbitals in accordance with the desired properties.

In carrying out this construction of $|\boldsymbol{\chi}^d\rangle$ we make sure that the diffuse orbitals reflect the symmetry structure of the localized orbitals, by constructing the set of diffuses orbitals as a union of sets, each obtained using the method just presented, but taking into account only localized orbitals and diffuse Gaussian basis functions corresponding to some irreducible representation of the symmetry group used in the creation of the local orbitals.

Referring back to the construction of the sets of basis functions $\mathcal{B}_{l,k}$, it is easy to appreciate, how we may use the same approach to deal with linear dependencies present in some $\mathcal{B}_{l,k} = \mathcal{B}$, by considering simply the basis set $\mathcal{B}_{l,0} \cup \cdots \cup \mathcal{B}_{l,k-1}$ to take the place of the localized orbitals $|\chi_p^d\rangle$. We thus obtain $\mathcal{B}_{l,k}$ with all "internal" dependencies remove as well as those functions that are already contained as linear combinations of functions in $\mathcal{B}_{l,0} \cup \cdots \cup \mathcal{B}_{l,k-1}$.

9.4.2 The Orbital Integrals

The construction of the diffuse orbitals done, the next step is, to calculate the orbital integrals from the expansion coefficients of the diffuse and localized orbitals in terms of basis functions, and the already computed basis function integrals. Conceptually this is very straightforward, summarized by the expression for the orbital one and two electron integrals

$$\langle \chi_p | \hat{o} | \chi_q \rangle = \sum_{ij} b_{ip} b_{jq} \langle b_i | \hat{o} | b_j \rangle \tag{9.32}$$

$$\langle \chi_p \chi_q || \chi_r \chi_r \rangle = \sum_{ijkl} b_{ip} b_{jq} b_{kr} b_{ls} \langle b_i b_j || b_k b_l \rangle . \tag{9.33}$$

The problem that we may encounter in using the latter equation for the two electron case, is that for even comparatively modest values for $l_{\max}$ and $k_{\max}$, the number of basis function and diffuse orbitals may be of the order of thousands and hundreds respectively. The sum over the four indeces specifying the basis

functions, may then become extremely costly to evaluate. Some progress may be made by once again exploiting for the orbitals (just as was done for the basis integrals), the symmetry in the orbital indeces inherent to the structure of the two electron Hamiltonian (see equation 2.48) and (more importantly) by noting that the integral

$$g_{pqrs} = \langle \chi_p \chi_q || \chi_r \chi_r \rangle \tag{9.34}$$

can only be non zero if no more than two orbitals are diffuse orbital. The reason for the latter is, as was mentioned for the basis integral case already, that only electrons being ejected from the system can be found in diffuse orbitals, which in the case of single photo ionization is at most one. It is in effect this restriction to only one electron in the continuum, which makes this calculations possible, as the computational effort at this point (other complications associated with double ionization aside) would be too large. Careful optimization and parallelization of the code evaluating the orbital integrals, has made it possible to carry out calculations up to values of $l_{\max}$ and $k_{\max}$ allowing for the description of fairly interesting systems (more on this in chapter 10). That being said the calculation of the orbital integrals is, in the current implementation of the code, the bottleneck; consuming the majority of computational resources, and any future implementation aiming to reduce the computational time needed, will require a way to drastically reduce the scale of this part of the calculation.

9.4.3 The Operator Matrix Integrals

Once, despite the computational cost, the orbital integrals and the reduced density matrices haven been calculated, the last step towards creating the augmented system in the presence of a diffuse basis, may be carried out. Once again there is no conceptual difficulty in doing so, requiring essentially only a computational implementation of equations 3.28 and 3.36. At this point however we must recall that in the reduced density matrix we extended the RAS3 by only two dummy orbitals. Therefore the calculation of the operator matrix elements must proceed in the following fashion. We use the reduced density matrix in the form such as we obtained them with only two dummy orbitals, in charge of the entirety of the diffuse structure, and repeatedly use equations 3.28 and 3.36 by considering in each calculation different pairs of diffuse orbitals to be taking the place of the dummy orbitals. Therefore one such calculation is necessary to account for the operator matrix elements between states obtained by augmentation in a local orbital, N_o^d calculations are necessary for the matrix elements between locally and diffusely augmented states (one for each local orbital occupying one of the dummy slots) and $N_o^d(N_o^d+1)/2$ calculations are necessary for the computation matrix elements between states resulting from augmentation in a diffuse orbital. Care is taken so that no matrix elements are computed repeatedly.

This slightly convoluted approach begs the question why the active space was not designed taking into account the correct number of diffuse orbitals, saving the seemingly unnecessary trouble of swapping around the orbitals. The reasons for this is twofold, first the approach using two place holder orbitals, means that all calculations related to determinants and CI vectors is independent of the number of orbitals, allowing us to carry out the first two parts of the calculation in parallel, at which point the number diffuse orbitals is unknown. The second and more important reason is that an active space of hundreds of orbitals, such as we might easily find in introducing the diffuse orbitals is far beyond anything Molcas and Molpro are designed to handle, and even if it were possible would yield gargantuan GUGA tables and lead to very expensive (and highly redundant) reduced density matrix calculations.

9.4.4 Tests

With the evaluation of the operator matrix elements the XCHEM-QC part of the XCHEM code, is concluded. Before proceeding however a few remarks shall be made on how, in (very) small reference systems, the vast majority of the steps just explained may be carried out using almost exclusively the architecture provided by Molcas. This was tremendously useful in the development of the XCHEM-QC code, as otherwise the very large size of the objects and the large number of interlocking parts of the code we have to deal with, may make errors in the code, manifesting themselves only once all steps

of calculation are concluded (eigenvalues of the augmented Hamiltonian below the groundstate of the neutral system, to name but one of the oddities we have come across), extremely time consuming and frustrating to trace.

Assuming a sufficiently small diffuse basis SEWARD may be run without problem to the end, not requiring the premature dumping of the integrals. Consequently we may use (upon having obtained the augmented CI vectors in terms of CSFs (which to our knowledge cannot be done in Molcas) and having modified Molcas to allow for the input of user defined CI vectors), the RASSI module of Molcas can be used to directly compute the operator matrix elements. Assuming for there to be more than a trivial number of diffuse orbitals, we still have to shift the diffuse orbitals (the creation of which, cannot be done in Molcas) into the correct position pairwise, but this is easily achieved by manipulating the Molcas File containing the orbitals. Furthermore the RASSI module can be used (using the trd1 and trd2 key words not appearing anywhere in the documentation of the code) to print the reduced density matrices, and the MOTRA module can be used calculate and print (the printing requiring modification of the Molcas source code) of the orbital integrals. In this way the correctness of effectively every step of the calculation in the final implementation could be verified using Molcas modules.

This leaves open the question, why we do not use said modules and modifications directly, circumventing the need for much of the developed code. In the case of MOTRA the integral transformation requires the aforegoing SEWARD calculation to terminate successfully, which as was explained before becomes impossible for diffuse basis sets of the size necessary for the treatment of interesting systems. In the case of using RASSI to compute the reduced density matrix we found that we were able to significantly improve on the efficiency of the calculations of reduced density matrices, as well as RASSI having an inbuilt limit on the number of states that can be treated, which we readily surpass augmenting several parent ions in the large number of mono centric orbitals we find ourselves working with (the latter can theoretically be overcome but separately treating subsets of augmented states and carrying out repeated RASSI calculations with different pairs of subsets of states (all the while exchanging orbitals). But at this point using RASSI for the sake of structural simplicity of the code, starts becoming self defeating from the get go).

In conclusion what we found is, that while large sections of the necessary calculation or in principal possible with Molcas (with the notable exception of the augmentation and the creation of the diffuse orbitals), the limitations that impede us from doing so at various stages of the calculation are primarily limitations resulting from the large number of basis functions, orbitals, CSFs and CI vectors (i.e. augmented states). To circumvent these a number of codes had to be written, the complete structure in which they work together and interface with QCPs is summarized in Figure 9.1.

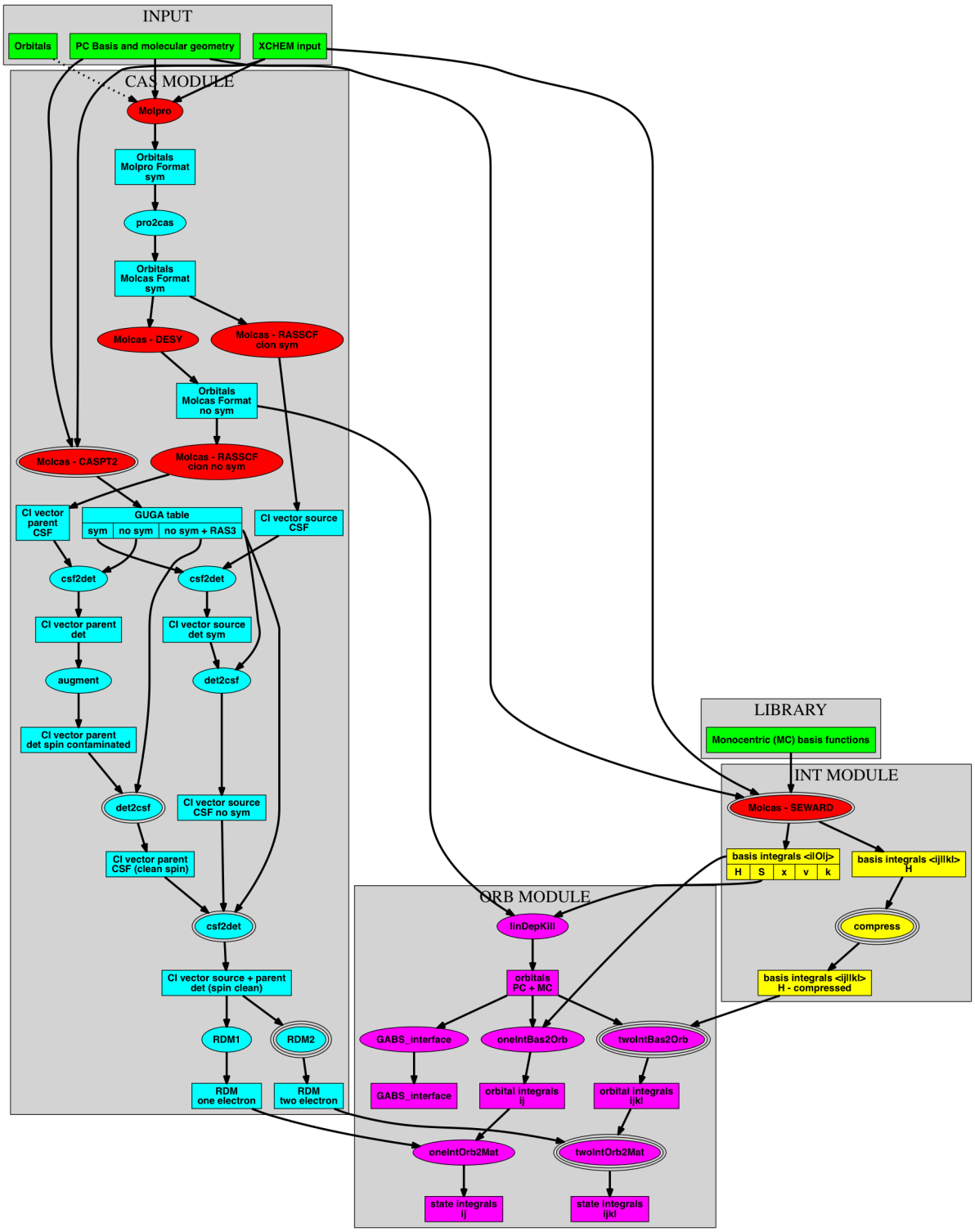

Figure 9.1: Complete overview of the different steps carried out by the XCHEM-QC code. Ellipses refer to the execution of code and rectangle to objects such as for exmaple integrals or obitals. The red ellipses indicate the use of QCPs (Molcas or Molpro), the cyan steps are those carried out in part I, the yellow steps those of part II and the magenta steps those of part III. Steps with no peripheries require negiligble computational time, steps with one peripherie require long (several hours) serial computation and steps with two peripheries long (several hours to days) parallel computation running on multiple nodes.

Part III

Results

10 Photoionization of Molecular Nitrogen

In the development of the XCHEM code (explained in chapters 8 and 9) we were largely guided throughout the development stage, by the code's application to the study of photo ionization in small benchmark systems. The first natural candidate for a calculation that is beyond what is more or less routinely available by existing codes is molecular Nitrogen. We shall investigate the photo ionization of N_2 for photon energies between the first and third ionization thresholds (photon energies between 15.1eV and 18.7eV). This combines the challenges of quantum chemistry as well as scattering theory by virtue of being a diatomic system with more than two electrons with a rich continuum structure due to the presence of a large number auto ionizing states, decaying to the continuum via interchannel coupling.

Experimentally the photo ionization spectrum of N_2 for this energy range has been under investigation for almost a century, dating back to two articles by Hopfield from 1930[208, 209]. In them two Rydberg series of autoionizing states between the second $^2\Pi_u$ and third ionization $^2\Sigma_u$ threshold are identified and are now referred to as the Hopfield absorption and emission series. In 1962 Ogawa and Tanaka carried out a more detailed experimental investigation[65], identifying in addition to the two Hopfield series another series in the same energy range; the Ogawa-Tanaka series. Subsequently a host of experimental works have explored these series in more detail. In 1977 Gürtler[66] measured the absorbption cross section with heretofore unattainable resolution. Parr[210] obtained electronically resolved cress sections and in Dehmer[68] and Woodruff [67] vibrationally resolved cross sections. In 1993 Huber[69] carried out a study with very high resolution investigating the rotationally induced effects at room temperature. Figure 10.1 displays a summary with the experimental results for the total photo ionization cross section, clearly depicting sets of resonance structures.

The interpretation of these features observed by Hopfield, Ogawa and Tanaka dates back to Mulliken[211] assigning the Hopfield series to the two series of Rydberg states $nd\sigma_g$ (absorption sereies) and $ns\sigma_g$ (emission series) approaching the $^2\Sigma_u$ ionization threshold. The assignment of the Ogawa-Tanaka series has undergone repeated reinterpretation since its experimental discovery. Ogawa and Tanaka themselves assigned their series to the auto ionizing $ns\sigma_g$ series of Rydberg states. This was called into doubt by a theoretical work Tuckwell[212] investigating the photoionization using Quantum Defect Theory. In it he assigned it to the Rydberg series $nd\pi_g$ of auto ionizing states, which restores consistency with Hopfield's original assignment. This was however called into question again by Woodruff[67] who inverted the assignment of the the Hopfield emission series with that of the Ogawa-Tanaka series. Raoult[213], using multi channel Quantum defect theory, provided the first theoretical results giving at least semi quantitative results for the total and partial ionization cross sections, and supported assigning the $nd\pi_g$ states to the Ogawa-Tanaka series. Furthermore, following the work of Jungen[214] on NO, Raoult suggested that the Hopfield absorption and emssion peaks for some n such as it is marked in figure 10.1, correspond to the $nd\sigma_g$ and $(n+1)\sigma_g$ states(in spite of this we shall collectively refer to a set of resonances $nd\sigma_g$, $nd\pi_g$ and $(n+1)s\sigma_g$ as the n^{th} resonances). Data for a wider range of photon energies (though compared to Raoult in slighly worse agreement with experimental data) was produced by Lucchese [215] using a multi-channel frozen core Hartree-Fock approach, whose assignment of the Ogawa Tanaka series agrees with Raoult. Since then a variety of theoretical models have been applied to the study of photo ionization of N_2 in the energy region close to the first few ionization thresholds. To name but a few: Stratman[63] performed calculations using a multi channel CI CASSCF and produced encouraging results, limited though to photo ionization beyond the $^2\Sigma_u$ ionization threshold. Tashiro[64] carried out R-Matrix calculations suffering from the presence of spurious resonances. Plesiat[46] used density functional theory and time dependent density functional theory, yielding good results, though

once again, primarily for energies beyond the Hopfield and Ogawa-Tanaka series. Other works studying this problem have used the random phase approximation[216], many body perturbation theory[62] and scattered wave $X\alpha$ method[61], some of which give good results in terms of absolute value but all which ignore or struggle with the presence of autoionizing states. For more comprehensive review of existing theoretical works we refer to[46] and reference therein.

Despite the wealth of theoretical methods available, no convincing results have as yet been obtained to study the Hopfield and Ogawa-Tananka series, with existing theoretical methods typically facing less problems for higher photon energies. Therefore an accurate description of the autoionizing states in Nitrogen, responsible for the Hopfield and Ogawa-Tananka series, is an excellent system in evaluating the viability of the XCHEM code. It represents the first case with accurate experimental data available, which not accessible by other computational models and is theoretically appealing given the presence of multiple series of auto ionizing states, which have sparked ongoing experimental and theoretical investigation for close to 100 years.

Motivating N_2 as our molecule of choice even more is a very recent resurgence in the interest of photoionization in N_2 brought about by the availability of atto second XUV light sources, leading to a study in 2016 by Reduzzi[70] using ultra short XUV ionizing pulse and subsequent probing via an IR pulse to study the time dependent behaviour of auto ionizing states in the series of states we are interest in. The results of this experiment have inspired works suggesting effects such as interference stabilization[217] and rotational couplings [218], play a role in understanding these low lying auto ionizing of Nitrogen.

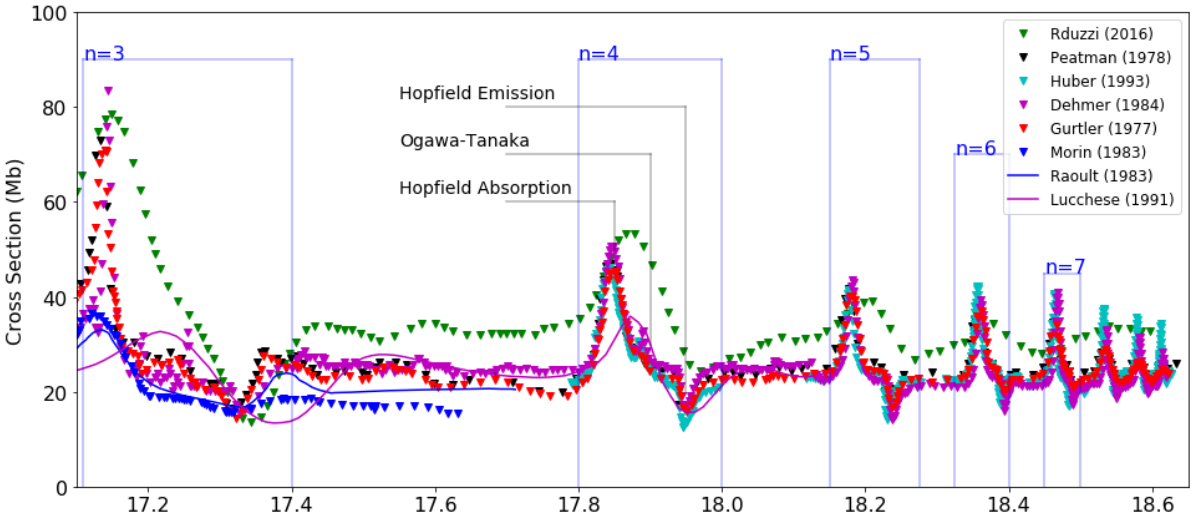

Figure 10.1: Collected experimental and theoretical results for the total photoionization cross section of N_2. The resonoances features are grouped together according to the principal quantum number of the Hopfield absorption series. For $n = 4$ the features are associated to the series they are identified with. The exerimental (dotted lines) data are taken from the following references: Reduzzi[70], Peatman[219], Huber[69], Dehmer[68], Gürtler[66], Morin[220]. The theoretical data (continuous lines) are taken from Raoult[213] and Lucchese[215]. We note that for $n = 3$ Raoult provides better agreement with the experiment, while the agreement improves for $n = 4$ for Lucchese with no data being available for these energies in Raoult's work.

10.1 Details of XCHEM calculation

The XCHEM shall be applied to study the process

$$N_2 + \gamma \rightarrow N_2^+ + e^-_{k\sigma}, \tag{10.1}$$

${}^1\Sigma_g$	${}^1\Pi_u$
$X^2\Sigma_g \otimes p\sigma_u$	$X^2\Sigma_g \otimes d\pi_u$
$X^2\Sigma_g \otimes f\sigma_u$	$X^2\Sigma_g \otimes f\pi_u$
$A^2\Pi_u \otimes d\pi_g$	$A^2\Pi_u \otimes s\sigma_g$
$B^2\Sigma_u \otimes s\sigma_g$	$A^2\Pi_u \otimes d\sigma_g$
$B^2\Sigma_u \otimes d\sigma_g$	$A^2\Pi_u \otimes d\delta_g$
	$B^2\Sigma_u \otimes d\pi_g$

removing an electron from the ground states of molecular Nitrogen via interaction with a single photon. The expelled electron leaves the system with some angular momentum and energy, which together with the cationic system left behind defines the channels we have to consider.

Following either of the suggested ways of assigning the series of autoionizing states, the fact remains that we wish to include in our calculation the three series $ns\sigma_g$, $nd\sigma_g$ and $nd\pi_g$. This requires inclusion of the first three ionization thresholds, leaving the molecule in one of the states $X^2\Sigma_g$,$A^2\Pi_u$ or $B^2\Sigma_u$, which depending on the angular moment of the electron ejected leaves the total system in a final state of either ${}^1\Sigma_u$ or ${}^1\Pi_u$ symmetry. Following this, the close coupling expansion will include the channels given in table 10.1, with the left and right side each displaying how the cation and ejected electron combine to give systems of symmetry ${}^1\Sigma_u$ and Π_u, respectively.

The same information is diagrammatically displayed in figure 10.2, furthermore showing how removal from different orbitals (HOMO, HOMO-1, HOMO-2) gives rise to different cations, as well as indicating the positions of the auto ionizing states of the three Rydberg series of figure 10.1. It is noteworthy that we are thus in a position of having to describe auto ionizing states potentially decaying to as many as five continua.

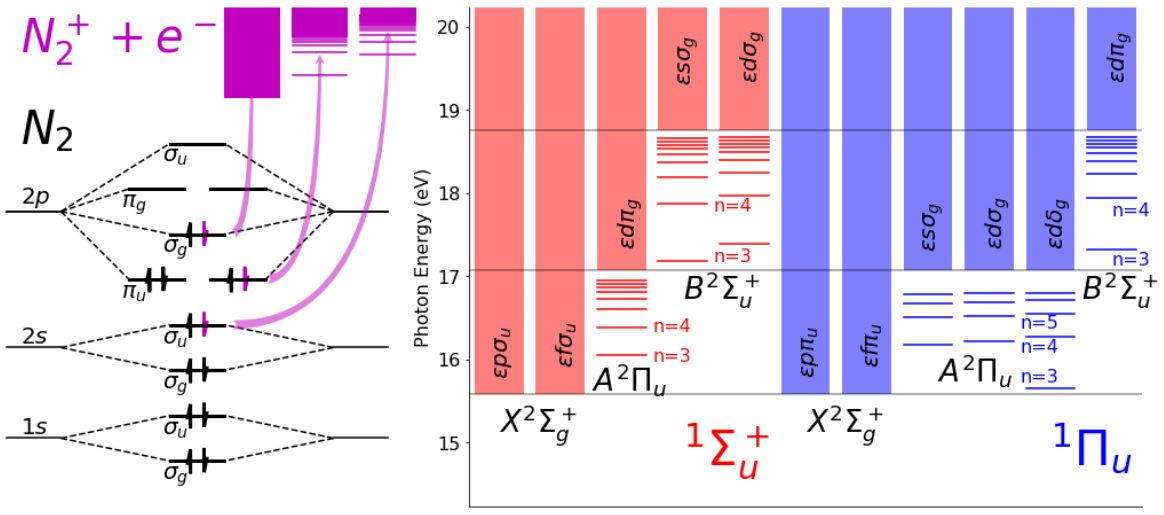

Figure 10.2: Diagramatic depiction of the channels included in the close coupling expansion. An electon is removed from either the HOMO, HOMO-1 or HOMO-2 orbital leaving the system in one of three cationic states, each of which is coupled with several electrons, leading to a total of eleven channels.

The selection of channels (as shown in figure 10.2) specifies what has to be computed with the XCHEM-QC code to fully describe the multichannel scattering problem such as it is presented. The task is to create the cationic states and, following the discussion of chapter 8, augment them with an additional electron to describe the short range states of the neutrals systems. The cationic states are calculated using the SA-CASSCF methodology. As we wish to describe ionization from the ground states, we shall furthermore explicitly include the ground state CI vector. This will lead to strong linear dependencies in the Hamiltonian, as the ground states will already be reasonably well approximated by say, augmenting the $X^2\Sigma_g$ states with in the σ_g orbital (and equivalently for the remaining cations). However it is not

hard to remove these and an accurate description of the wave function of the system being ionized is crucial to the accurate calculation of photo ionization cross sections.

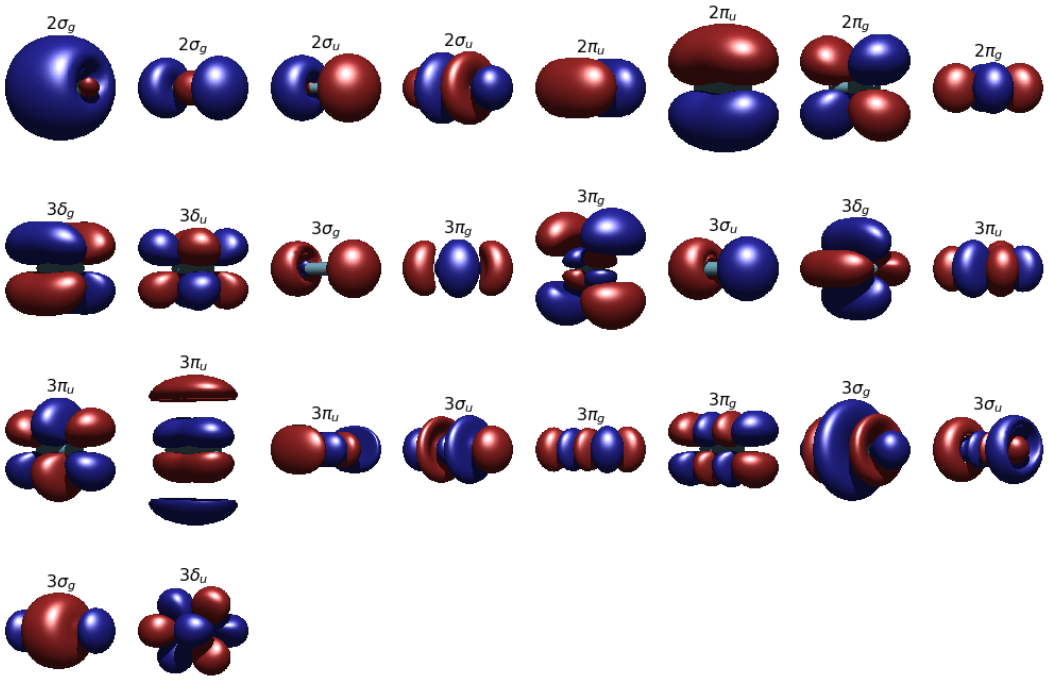

Figure 10.3: Active orbitals used in obtaining source and parent ions. The first row are the RAS2 orbitals and the rest the RAS3 orbitals occupied by at most two electrons in every configuration.

With that in mind and recalling from chapter 9 we must choose our active space and basis with care so as to ensure that the same set of orbitals can provide accurate descriptions of the cationic parent ions as well as the neutral ground state. Table 10.1 displays a set of results obtained from SA-CASSCF calculations to optimize the orbitals, with different active spaces and different states over which to average, compared to an MRCI calculation. All CASSCF calculations include the $2s2p$ atomic orbitals in their active space. The active space is then further augmented to include single or single and double excitations to the RAS3 space comprised of the $3s3p3d$ orbitals. It may seem odd that while a state average over ionic as well as neutral states is included for the CAS, the same is not the case for calculations including a RAS3 space. The reason for this is mundane: MOLPRO allows SA-RASSCF calculations only over states of equal charge, whereas the same restriction is absent for SA-CASSCF calculations. Nevertheless, we found the best results to be given by inclusion of the RAS3 space, optimizing with respect to the neutral states $X^1\Sigma_g$, $A^1\Pi_u$, $B^1\Sigma_u$ and $C^1\Sigma_u$, only. The resulting orbitals turn out to provide sufficient flexibility to reproduce the relative energies of the ionic as well as the neutral states to within 0.08eV compared to the corresponding MRCI results. Figure 10.3 shows the final orbitals that were used throughout the rest of the calculations. All the calculations of table 10.1 were obtained using the standard cc-pVQZ basis set. Calculations with larger basis sets provided almost no improvement, and run the risk of proving problematic when assuming zero overlap between PC Gaussians and B-Splines.

We also note that not all of the neutral states are required to be well described for the simple direct ionization from the neutral ground states. However inclusion of additional neutral states forces the orbitals to be more flexible on the one hand, and on the other hand equips the resulting data for future calculations, studying more complicated processes requiring intermediate excitation to neutral excited states. This concludes preliminary quantum chemistry calculations necessary for N_2 photo ionization. Using these orbitals as a starting point for the XCHEM-QC code and including the MC Gaussians basis functions for maximum values of $l = 3$ and $k = 2$, the monocentric (diffuse) orbitals, augmented states as well as the operator matrix elements between them are computed. During the augmentation procedure only active space PC orbitals and MC orbitals are augmented, as augmentation in PC virtual orbitals

	State	D_{2h} irrep	CASSCF+MRCISD		CASSCF	
RAS2			$2s2p$			
State Avg.			$X^1\Sigma_g$, $A^1\Pi_u$, $B^1\Sigma_u$, $X^2\Sigma_g$, $A^2\Pi_u$, $B^2\Sigma_u$			
Molecule			E_{MRCI} (au)	ΔE_{MRCI} (eV)	E (au)	$\Delta E - \Delta E_{\mathrm{MRCI}}$ (eV)
N_2	$X^1\Sigma_g$	A_g	−109.3814	0.0000	−109.3277	0.0000
	$A^1\Pi_u$	B_{1u}	−108.8827	13.5703	−108.8320	0.6958
		B_{2u}	−108.8827	13.5703	−108.9425	0.6958
	$B^1\Sigma_u$	B_{3u}	−108.9970	10.4596	−108.7470	0.5257
N_2^+	$X^2\Sigma_g$	A_g	−108.8179	15.3336	−108.7651	−1.0476
	$A^2\Pi_u$	B_{1u}	−108.7649	16.7767	−108.7106	−0.9197
		B_{2u}	−108.7649	16.7767	−108.7106	−0.9197
	$B^2\Sigma_u$	B_{3u}	−108.7001	18.5378	−108.6487	−1.0872

	State	D_{2h} irrep	RASSCF			
RAS2			$2s2p$			
RAS3			$3s3p3d$ ($N_e = 1$)			
State Avg.			$X^1\Sigma_g$, $A^1\Pi_u$, $B^1\Sigma_u$		$X^2\Sigma_g$, $A^2\Pi_u$, $B^2\Sigma_u$	
Molecule			E (au)	$\Delta E - \Delta E_{\mathrm{MRCI}}$ (eV)	E (au)	$\Delta E - \Delta E_{\mathrm{MRCI}}$ (eV)
N_2	$X^1\Sigma_g$	A_g	−109.2371	0.0000	−109.2189	0.0000
	$A^1\Pi_u$	B_{1u}	−108.7368	0.1240	−108.6605	1.7032
		B_{2u}	−108.7368	0.1240	−108.6605	1.7032
	$B^1\Sigma_u$	B_{3u}	−108.8454	0.1784	−108.7849	2.3886
N_2^+	$X^2\Sigma_g$	A_g	−108.6962	−0.5905	−108.7116	−1.5061
	$A^2\Pi_u$	B_{1u}	−108.6398	−0.5395	−108.6566	−1.4942
		B_{2u}	−108.6398	−0.5395	−108.6566	−1.4942
	$B^2\Sigma_u$	B_{3u}	−108.5746	−0.4488	−108.5900	−1.3647

	State	D_{2h} irrep	RASSCF			
RAS2			$2s2p$			
RAS3			$3s3p3d$ ($N_e = 2$)			
State Avg.			$X^1\Sigma_g$, $A^1\Pi_u$, $B^1\Sigma_u$		$X^2\Sigma_g$, $A^2\Pi_u$, $B^2\Sigma_u$	
Molecule			E (au)	$\Delta E - \Delta E_{\mathrm{MRCI}}$ (eV)	E (au)	$\Delta E - \Delta E_{\mathrm{MRCI}}$ (eV)
N_2	$X^1\Sigma_g$	A_g	−109.3277	0.0000	−109.3277	0.0000
	$A^1\Pi_u$	B_{1u}	−108.8320	−0.0795	−108.8320	1.4767
		B_{2u}	−108.8320	−0.0795	−108.9425	1.4767
	$B^1\Sigma_u$	B_{3u}	−108.9425	0.0230	−108.7470	1.8137
N_2^+	$X^2\Sigma_g$	A_g	−108.7651	−0.0231	−108.7651	−0.7097
	$A^2\Pi_u$	B_{1u}	−108.7106	0.0175	−108.7106	−0.6911
		B_{2u}	−108.7106	0.0175	−108.7106	−0.6911
	$B^2\Sigma_u$	B_{3u}	−108.6487	−0.0608	−108.6487	−0.7082

Table 10.1: Results of QC calculations ascertaining the viability of various active spaces for the creation of the polycentric orbitals. Calculations at CAS level for different RAS3 spaces are compared to an MRCI calculation. We see that the best results by far are obtained including double excitations to $3s$,$3p$ and $3d$ orbitals, optimizing the orbitals with respect to a state average over the neutral states indicated in the table (highlighted in red).

would lead to highly diffuse, polycentric orbitals which may protrude into the B-Spline region, rendering moot the assumption of zero overlap between B-Splines and PC Gaussians.

A potential complication that we must take care to avoid may arise from a poor choice of the R_0 beyond which we consider the PC-Gaussian part to negligible. We must ensure that the source and cationic states, represented using the PC Gaussians, concentrate all but a negligible part of their electron density inside the radius R_0. Figure 10.4 shows the integrated electron density for the parent ions. We see that the cut off at 7.0 atomic units is sufficient to also avoid problems with the spatial extension of the cationic and source states.

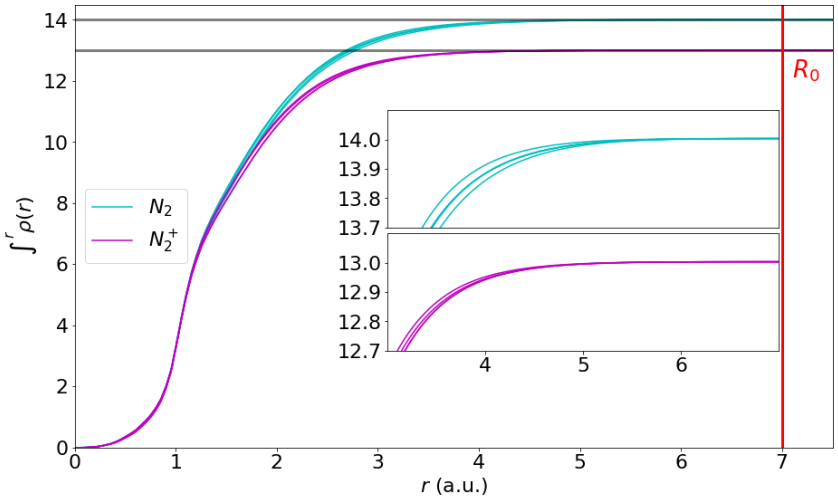

Figure 10.4: Integrated electron density of the N_2^+ parent ions and N_2 source states. The inlets display zooms into the regions for large radii, approaching 13 and 14 for ionic and neutral states, respectively. The red line indicates the chosen R_0 at which point the remaining electrons density, not accounted for, is considered negligible.

Having motivated all aspects drawing from quantum chemistry, we address the details of representing the scattering states using B-Splines. Fixing R_0 leaves us to fix R_∞ at which we consider the electron to be in the asymptotic region, and hence being well described by a Coulomb Wave. For the asymptotic fitting to be physical it must furthermore be ensured that for the electron energies under study, the B-Splines must be capable to reproduce at least a full oscillation of the electronic wave function in the box. For an electron with momentum $|k|$ this is ensured if $kR_\infty >> 1$. As we are concerned with the photo ionization very close to the $X^2\Sigma_g$ and $A^2\Pi_u$ thresholds, special attention must be paid to this point. Returning to figure 10.1 we note that the first resonance structures subjected to our scrutiny appear at around 17.0 eV. Decaying to the $A^2\Pi_u$ state ejects an electron with $E_{e^-} > 0.2$ eV. Choosing $R_\infty = 200$ a.u. gives $kR_\infty = 17.14$. This is expected to be sufficiently large to allow for a physically meaningful representation of the slowest escaping electrons. Nevertheless we did carry out sample calculations for values of $R_\infty = 400$ a.u. and $R_\infty = 600$ a.u. leaving the data virtually unchanged, thereby justifying a box size of 200 atomic units to be perfectly adequate.

10.2 Results for Photoionization of Nitrogen

We present now the results obtained using the XCHEM code with the aforementioned specifications regarding basis sets, active spaces and channels to include. Figure10.5 shows the theoretical results obtained from our calculation, in three different contexts. The uppermost panel shows the total photo ionization cross section as well as partial ionization cross sections either leaving the system in $^1\Sigma_u$ or $^1\Pi_u$ symmetry. The middle panel compares the total cross section to the comparatively low resolution result from[70]. Finally the lower panel compares the total cross section to the more highly resolved experimental results obtained at synchrotron facilities. The theoretical results in the lower two panels

are presented convoluted with a Gaussian to account for the finite spectral resolution of the experimental data.

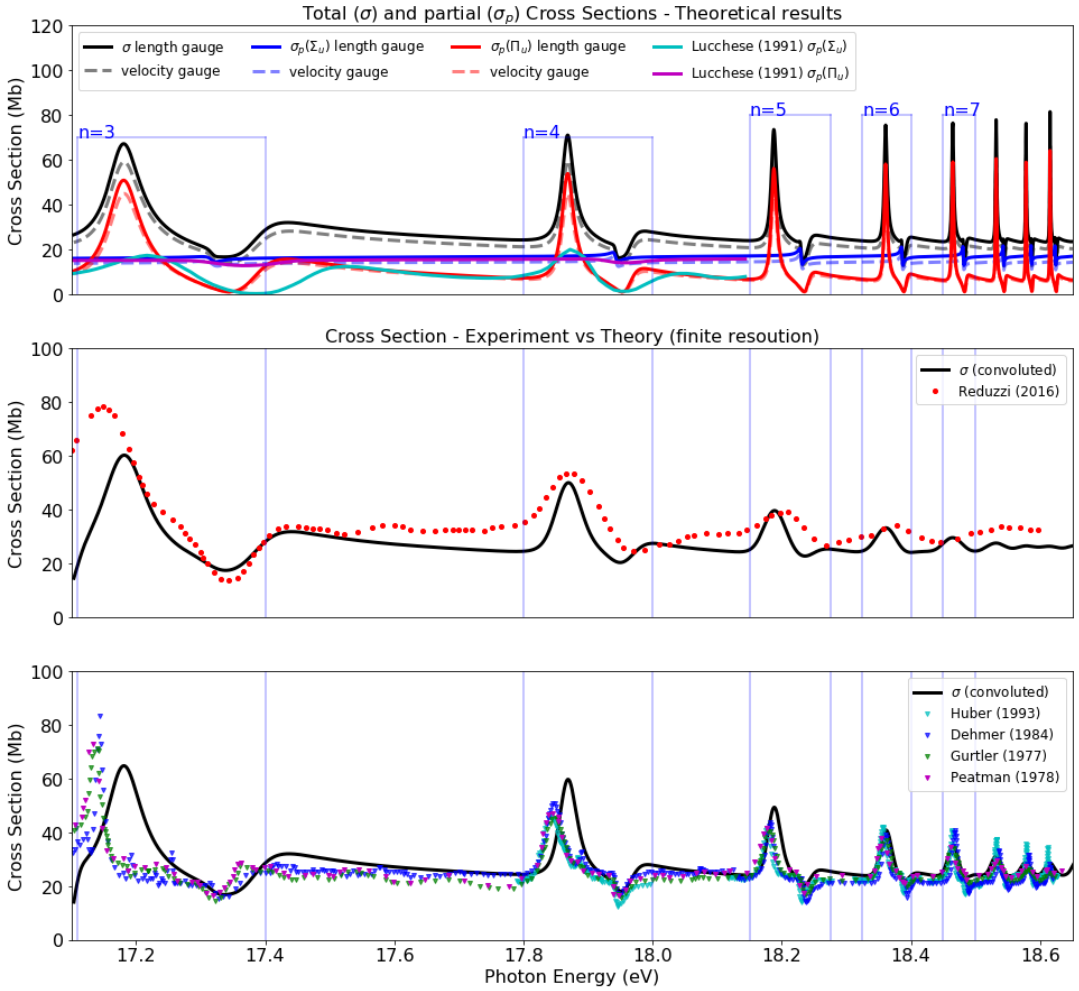

Figure 10.5: Results obtained using the XCHEM method compared to different sets of data. The first panel shows (in velocity and length gauge) the total cross section as well as the partial cross sections corresponding to leaving the system in a Σ_u state (red curves corresponding to red channels in figure 10.2) or a Π_u sate (blue curves corresponding to blue channels in figure 10.2). The cyan and magenta curve are the relevant partial cross section from reference [215]. The middle panel compares the total cross section to the results of reference [70]. The bottom panel presents an equivalent comparison for the indicated sets of experimental data (see figure 10.1 for the references).

From the lower two panel we infer that qualitatively our the theoretical results compare very well to the experimental ones. For the $n = 3$ resonance structures, quantitative agreement in the lower panel is observed only for the Hopfield emission and Ogawa-Tanaka peaks, while the Hopfield absorption peak appears shifted as well as broadened. For resonances at higher energies the agreement becomes progressively better, being essentially perfect for $n > 4$. Compared to the therotical efforts of references [213, 215] we observe that the former provides better agreement for the position of the Hopfield absorption series, but appears to underestimate its height. Compared to the latter reference we see that the XCHEM results constitute and improvement for effectively all features at all available energies. It is particularly noteworthy that the disagreement seen in the XCHEM results for resonance $n = 3$ appears to be amplified in the results of reference [215], with the absorption feature being even more shifted and even broader. The upper panel allows for the unequivocal assignment of the Ogawa-Tanaka to the $nd\pi_g$ series yielding $^1\Pi_u$ symmetry, leaving the broader, more pronounced features to the Hopfield series with the system in $^1\Sigma_u$ symmetry. Given the overall convincing nature of these results, efforts are made to

extract information about the auto ionizing states underlying the resonance features, as well as studying partial resonances.

It should be noted that for this photo electron energy range at hand, and most strikingly so for the resonance $n = 3$, the system is highly sensitive to the choice of parameters. This is due to the low energy of the escaping electron. Thus great care has to be taken in obtaining the results, for a significant change in R_0 in either direction causes problems. For lower values, the assumption that the PC Gaussian and the B-Splines do not overlap ceases to be valid leading to absurd results, whereas for larger R_0 electron correlation is lost providing poorer description of the resonant behaviour (using larger R_0 without deterioration of the results, should be possible if more extensive MC Gaussian Basis sets are used, coming however at a significant increase in computational times). This dependence is awkward to deal with computationally, requiring careful zeroing in on the appropriate parameters. This may cause problems for systems without experimental reference data comparable to what is presented in figure 10.1 for N_2. But it should be recalled that the present study very much represents an extreme case of what is theoretically possible to begin with (We recall the benchmark studies on Ne or H_2 for example, focused on more cleanly isolated resonances at higher photo electron energies); it is unduly optimistic to hope for an entirely unproblematic description of electrons ejected with very low energies in relatively complex systems, or in fact any system. Rather the very capability of describing this notoriously difficult case conclusively proves the XCHEM method to be a powerful tool in the study of photo ionization, which if applied with care to less problematic photo electron energies and or with greater computational resources can be expected to yield good results consistently and reliably. We shall now turn our attention to extract from the computational data information about the auto ionizing states responsible for the rich structure in the cross section.

Ogawa-Tanaka series

We begin by focussing on the Ogawa Tanaka series, which is somewhat easier to dealt with given the well separated, apparently clean nature of the resonance features, clearly displaying the characteristic Fano line shape. Besides the Fano profile in the cross section we may also glean information about the position and the width (that is life time) of the $nd\pi_g$ states by studying the dependence of the phase shift of the scattering state on the photon energy. Figure 10.6 shows said phase shift, clearly displaying a jump of π at the position of every resonance.

Following the results of chapter 5 we may obtain the the positions of the resonances by locating the poles of $\tan(\phi) = -\Gamma(2(E - E_r))^{-1}$, as well as their widths from

$$\Gamma = 2 \left[\frac{\mathrm{d}\phi}{\mathrm{dE}} \right]^{-1} \Bigg|_{E=E_r} \tag{10.2}$$

We may additionally confirm these values as, well as extract values for the Fano parameters q and ρ^2, by fitting the cross section corresponding to ionization to $^1\Pi_u$ states (green curve in Figure 10.5) to the theoretical prediction for the cross section in the presence of isolated auto ionizing states decaying to several channels recalling equation 5.147:

$$\sigma(E) = \frac{\sigma_b(E)}{\varepsilon^2 + 1}(\varepsilon^2 + 2\rho^2 q\varepsilon + 1 - \rho^2). \tag{10.3}$$

The resulting values are presented for the resonances $3 \leq n \leq 8$ in table 10.2. To go beyond these values for n requires higher energetic resolution (as can be seen in figure 10.6 by the unexpected decrease in the peaks of $\mathrm{d}\phi/\mathrm{d}E$ for $n > 9$) while leading to little additional insight. The different methods, via which we obtained the parameters, show very convincing agreement with the only the shape parameter q, being the most sensitive of the parameters characterizing Fano resonances, showing some notable discrepancy for $n = 3$ and $n = 4$.

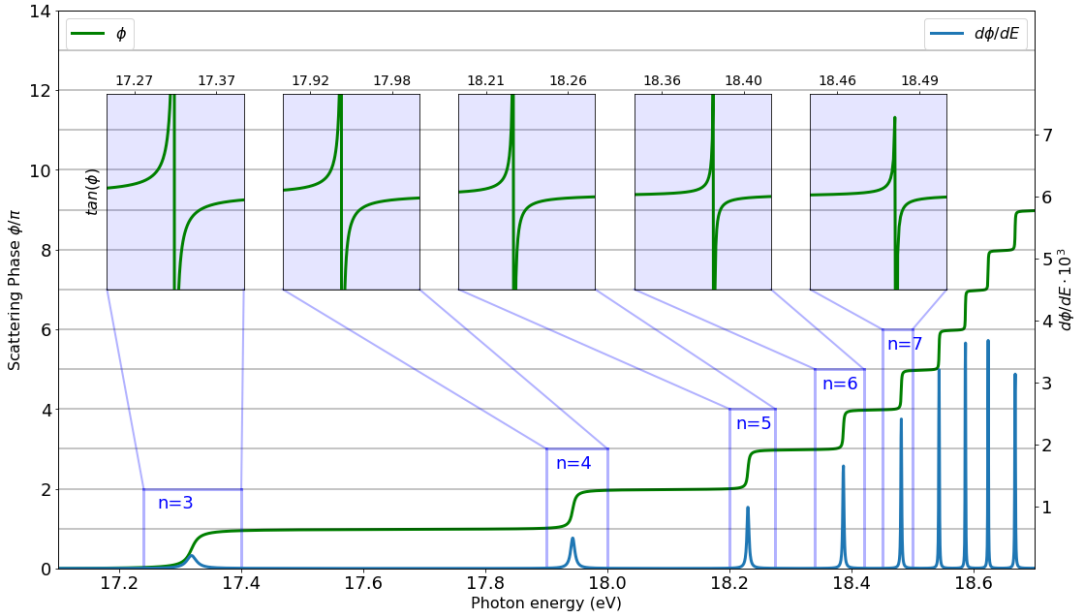

Figure 10.6: Dependence of phase shift ϕ of scattering states in $^1\Pi_u$ channels. The clean isolated nature of the $nd\pi_g$ resonances is apparent in the gree line displaying the phase shif. The inlets show $\tan(\phi)$ zoomed into the indivdual resonances, diaplaying a pole at the position of the auto ionizing states. Furthermore the derivative of the phase shift with respect to the photon energy is shown (blue line), the inverse of which at the resonance postion is proportional to the lifetime

Partial Cross Section

The division of the cross section by the symmetry the system is in after ionization (i.e. division into Ogawa Tanaka and Hopfield series), is straightforward, as the corresponding channels do not couple to each other. More care has to be taken in analysing the breakdown of the cross section by individual channels which may couple. In this case we must obtain the relevant parameters by fitting to the equation 5.148. The resulting number of parameters to fit is therefore quite large, and there is a plethora of non-optimal local minima the fitting procedure may converge to, especially when taking into account that the Starace Parameters must also fulfil equation 5.149. Following references [134, 221, 52] we may develop an alternative parametrization, describing cross sections as a function of two new real parameters C_1 and C_2,

$$\sigma_\alpha = \frac{\sigma_0(E)}{\varepsilon^2+1}(\varepsilon^2 + C_1\varepsilon + C_2), \tag{10.4}$$

related to the complex Starace Parameters ρ_α via

$$\Re(\rho_\alpha) = \frac{qC_1 + 2 \pm \sqrt{4C_2 - C_1^2}}{2(1+q^2)} \tag{10.5}$$

$$\Im(\rho_\alpha) = \frac{q\left((2 \pm \sqrt{4C_2 - C_1^2}\right) - C_1}{2(1+q^2)}. \tag{10.6}$$

While it is easier to carry out the fitting procedure in this parametrization, care has to be taken in choosing the correct of the two possible solution, by comparing to a fit obtained from equation 5.148. Furthermore one must ensure that the C_1 and C_2 yield real values for $\Re(\rho_\alpha)$ and $\Im(\rho_\alpha)$. Table 10.3 summarizes the thus obtained values characterizing the partial cross sections for different n, while figure 10.8 displays the partial cross sections themselves for both the data obtained from the XCHEM code, and the parameters obtained in the fitting procedure. The agreement between length and velocity gauge is seen

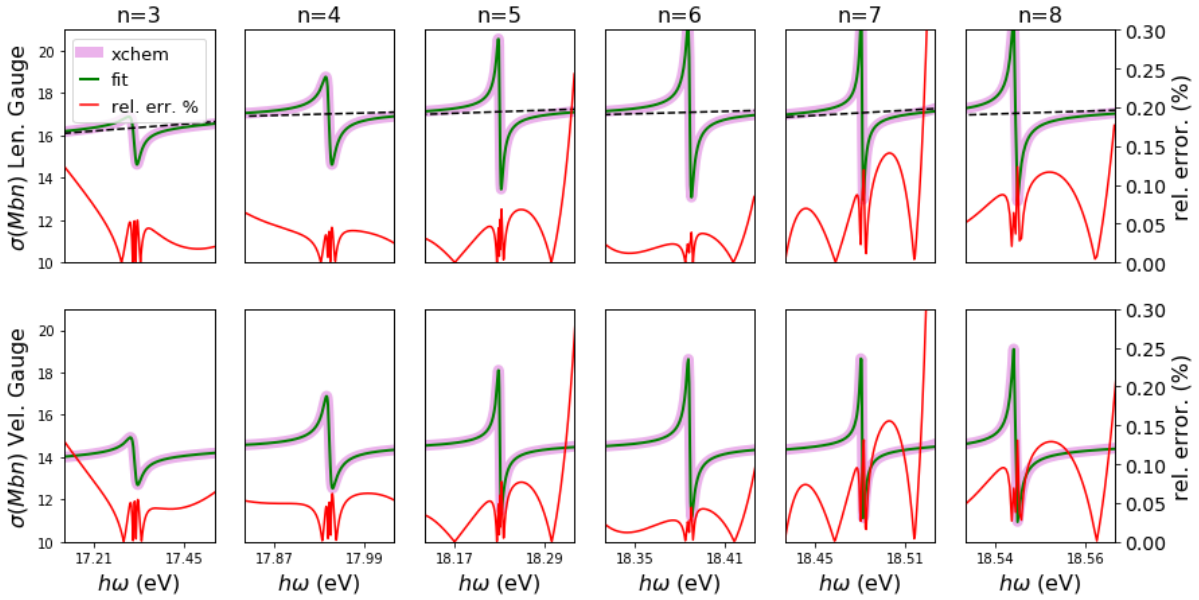

Figure 10.7: Phtoionization cross sections, comparing the XCHEM results, with fits obtained by optimizing E, Γ, q and ρ^2 in equation 5.147. Convincing fits are obtainable for all auto ionizing states $nd\pi_g$ with the relative error not exceeding 0.3%.

to excellent and thus for the sake of clarity we have forgone including also the velocity gauge results in this figure.

Hopfield series

The Hopfield series is more problematic to analyse for two reasons. First, as was already hinted at, the agreement with the experimental results, especially for the resonance $n = 3$ but also for $n = 4$, shows a noticeable discrepancy compared to the experimental data, in the lower panel of figure 10.5. It is intriguing that in comparison with the results of the most recent experiment (middle panel of the same figure) we appear to have good agreements even for $n = 3$, however in view of the overwhelmingly consistent data obtained at different synchrotron facilities we must conclude that this is coincidental. It is not surprising that these problems arise for resonances corresponding to low electron energies, as the short range interaction of an electron with a long wavelength is more complex.

In light of these discrepancies, we focus our attention on the resonances that do agree with the experiment. Unlike the Ogawa-Tanaka series (a single series of Rydberg states, separated from each other by an energetic region of many times their own width), the Hopfield series, are the consequence of two series of autoionizing states, appearing in pairs quite close to each other in energy (each structure, according to[213], arising from an auto ionizing state of the $nd\sigma_g$ series and a energetically higher but close $(n+1)s\sigma_g$ auto ionizing state). Unlike the relatively straightforward analysis of the Ogawa-Tanaka series, we must now take into account for the possibility of the two decaying states interacting with each other. The underlying theory was described in chapter 5. The resonance energies $E_{rs,d}$ and widths $\Gamma_{s,d}$ are unaffected by this complication as we may still find them as the poles of equations 5.137 governing the phase shift. The resulting values are presented in table 10.4 with the corresponding behaviour of the scattering phase shown in figure 10.9.

We turn now to the parameters pertaining to the coupling of the two weakly separated auto ionizing states. Obtaining values for the coupling parameters $2\Im(W_{AB}W_{CA}W_{BC})$ and $|W_{BC}|^2$ via a fit to equation 5.137 is cumbersome due to the large number of parameters. In fact a straightforward fitting (even given the knowledge of $E_{rs,d}$ and $\Gamma_{s,d}$) to obtain the coupling parameters is impossible in the absence of further information fixing some of the parameters. This may be inferred from equation 5.137.

n	ϕ fit		ϕ pole		σ Len.		σ Vel.		
3	$E_r =$	17.3190	$E_r =$	17.3196	$E_r =$	17.3187	$E_r =$	17.3187	eV
	$\Gamma =$	19.3816	$\Gamma =$	19.3997	$\Gamma =$	19.2340	$\Gamma =$	19.2316	meV
					$q =$	-0.5236	$q =$	-0.7093	a.u.
					$\rho^2 =$	0.3851	$\rho^2 =$	0.3766	a.u.
4	$E_r =$	17.9432	$E_r =$	17.9434	$E_r =$	17.9432	$E_r =$	17.9432	eV
	$\Gamma =$	8.1926	$\Gamma =$	7.9994	$\Gamma =$	8.0976	$\Gamma =$	8.0991	meV
					$q =$	-0.8201	$q =$	-1.0439	a.u.
					$\rho^2 =$	0.4292	$\rho^2 =$	0.4237	a.u.
5	$E_r =$	18.2304	$E_r =$	18.2304	$E_r =$	18.2304	$E_r =$	18.2304	eV
	$\Gamma =$	4.0678	$\Gamma =$	3.8454	$\Gamma =$	3.9194	$\Gamma =$	3.9175	meV
					$q =$	-0.9608	$q =$	-1.0735	a.u.
					$\rho^2 =$	0.5075	$\rho^2 =$	0.5022	a.u.
6	$E_r =$	18.3865	$E_r =$	18.3867	$E_r =$	18.3867	$E_r =$	18.3867	eV
	$\Gamma =$	2.4208	$\Gamma =$	2.2104	$\Gamma =$	2.2440	$\Gamma =$	2.2436	meV
					$q =$	-1.0119	$q =$	-1.1144	a.u.
					$\rho^2 =$	0.5264	$\rho^2 =$	0.5213	a.u.
7	$E_r =$	18.4814	$E_r =$	18.4815	$E_r =$	18.4815	$E_r =$	18.4815	eV
	$\Gamma =$	1.6602	$\Gamma =$	1.3756	$\Gamma =$	1.4182	$\Gamma =$	1.4171	meV
					$q =$	-1.0342	$q =$	-1.1401	a.u.
					$\rho^2 =$	0.5338	$\rho^2 =$	0.5290	a.u.
8	$E_r =$	18.5432	$E_r =$	18.5435	$E_r =$	18.5435	$E_r =$	18.5435	eV
	$\Gamma =$	1.2489	$\Gamma =$	0.9458	$\Gamma =$	0.9489	$\Gamma =$	0.9488	meV
					$q =$	-1.0507	$q =$	-1.1632	a.u.
					$\rho^2 =$	0.5364	$\rho^2 =$	0.5314	a.u.

Table 10.2: Results extracted from the XCHEM calculations. We report values for resonance positions E_r, width Γ, Fano parameter q, correlation coefficient ρ^2. The former three we obtained from: fitting the phase jump to equation 5.120, locating the poles of equation 5.120 and evaluating its derivative and fitting of the total cross section to equation 5.125 in length and velocity gauge. q and ρ^2 cannot be inferred from the phase shift and equation 5.125 for the cross sections must be used.

We may convince ourselves (as is graphically suggested in figure 10.10) that for any two E_B and E_C (which may be interpreted as the resonance energies such as they would be observed in the absence of any interference between the two auto ionizing states) such that $E_{rd} \leq E_A \leq E_B \leq E_{rs}$ and any two $\Gamma_B = 2\pi|W_{BA}|^2$ and $\Gamma_C = 2\pi|W_{CA}|^2$, such that $\Gamma_B + \Gamma_C = \Gamma_s + \Gamma_d$, a valid solution for the coupling parameters $2\mathfrak{I}(W_{AB}W_{CA}W_{BC})$ and $|W_{BC}|^2$ exists.

To make progress it is therefore necessary to fix some of these parameters by different means, for a fit like those shown in figure 10.10 to yield a unique, physically meaningful value for the remaining parameters. An obvious method to do obtain values for E_B, E_C, Γ_B and Γ_C is to consider the two Hopfield series independently, thereby not allowing them to interfere. Due to the considerable computational effort that would be necessary to completely disentangle the two Rydberg series of autoionizing states, we excluded only the B-Spline component yielding either the $B^2\Sigma_u^+ \otimes ns\sigma_g$ or $B^2\Sigma_u^+ \otimes nd\sigma_g$ channel. We therefore expect this procedure only to work for Rydberg states, that are sufficiently diffuse to be represented almost entirely in term of B-Splines. We focus therefore on the $n = 8$ resonance for this discussion, as for $n < 6$ excluding either set of B-Splines still yields two resonances for every n. This indicates that the Gaussian part, which we failed to exclude, is non-negligible for these autoionizing states. In light of this the following discussion should be regarded as somewhat preliminary, showing rather how it is conceptually possible to extract all relevant parameters, until fully decoupled calculations have been carried out.

We obtain the following values for the decoupled $n = 8$ resonance: $E_B = 18.5386$, $E_B = 18.5391$, $\Gamma_B = 5.70158$ and $\Gamma_C = 5.70158$. By using these values in a fit of equation 5.137 we obtain for the

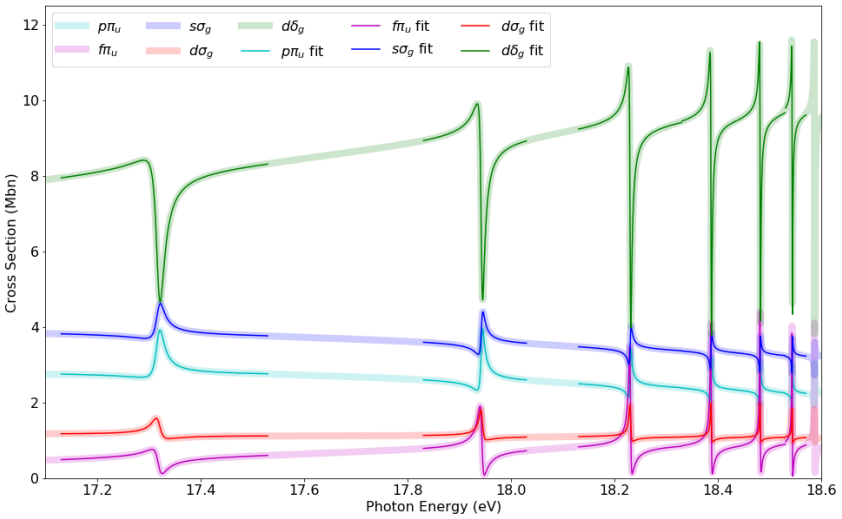

Figure 10.8: Photoionization cross sections for the different channels leaving the complete system in a $^1\Pi_u$ state after ionization. The transparent broad lines are the results obtained from XCHEM , whereas the superimposed thin lines correspond to the fitted data using the parameters of table 10.3

coupling parameters the following values $|W_{BC}|^2 = 4.9608 \cdot 10^{-5}$ and $\Im(W_{AB}W_{CA}W_{BC}) = 1.8936 \cdot 10^{-6}$. The quality of this result may be checked by analytically evaluating the roots of the denominator of equation 5.137 given the value for $|W_{BC}|^2$. The roots are given by

$$E_{rs,d} = \frac{E_A + E_B}{2} \pm \sqrt{\frac{E_A - E_B}{2}^2 + |W_{BC}^2|}, \tag{10.7}$$

which upon substitution of the values from the fit yields $E_{rd} = 18.5318$ and $E_{rs} = 18.5459$. Which upon comparison with the values for resonance $n = 8$ in table 10.4 proves to be in agreement to within 0.002 eV, which while not perfect does indicate that the approach we used to decouple the resonance has succeeded to a reasonably good degree. Using equation 5.102 we similarly, after some algebra, may express $\Gamma_{s,d}$ as

$$\Gamma_{s,d} = \pi(|W_{BA}|^2 + |W_{CA}|^2) \pm \pi \frac{\frac{1}{2}(E_A + E_B)(|W_{BA}|^2 - W_|CA|^2) + 2\Im(W_{AB}W_{CA}W_{BC})}{\sqrt{\frac{1}{4}(E_A - E_B)^2 + |W_{BC}|^2}} \tag{10.8}$$

giving $\Gamma_s = 4.8575$ meV and $\Gamma_d = 6.5464$ meV , once again not in perfect agreement, but reasonably close given the way we obtained Γ_B and Γ_C.

Inaccuracy of n=3 Resonance

Having present the results of the calculation and extracted in as far as possible information about the auto ionizing states from them, we address what we believe to be the reasons for a quantitatively less than perfect description of the photo ionization cross section. We alluded to this earlier when pointing out that in comparison to the experimental data the resonances $n = 4$ and $n = 3$ prove to more problematic than the resonances ejecting the electron into the continuum at higher energies. We recall that we constructed the diffuse MC orbitals by enforcing orthonormality not only among them but also with respect to the localized QC PC orbitals. During the orthonormalization procedure it is unavoidable that the diffuse orbitals acquire a PC Gaussian component. This is not problematic if the PC Gaussian component of the diffuse orbital is entirely contained within the cut off radius R_0. But during the orthonormalization diffuse orbitals may be create with comparatively huge basis coefficients on the order of 10^5. In this situation, even though we ensured the almost vanishing nature of the PC Gaussians beyond R_0, a PC

n	α	$p\pi_u$	$f\pi_u$	$s\sigma_g$	$d\sigma_g$	$\mathrm{d}\delta_g$
3	$\Re(\rho_\alpha)$	−0.1841	0.5822	−0.1010	−0.0225	0.2326
	$\Im(\rho_\alpha)$	−0.0227	0.2658	−0.0239	0.1942	0.0117
	C_1	0.2381	−1.1414	0.1537	−0.3648	−0.2670
	C_2	1.3883	0.6359	1.1908	1.2970	0.6162
n	α	$p\pi_g$	$f\pi_g$	$s\sigma_g$	$d\sigma_g$	$\mathrm{d}\delta_g$
4	$\Re(\rho_\alpha)$	−0.2167	0.8612	−0.1062	−0.0163	0.2520
	$\Im(\rho_\alpha)$	−0.0550	0.4441	−0.0529	0.2477	0.0167
	C_1	0.4654	−2.3008	0.2801	−0.4687	−0.4468
	C_2	1.4268	1.5763	1.1493	1.5418	0.6301
n	α	$p\pi_g$	$f\pi_g$	$s\sigma_g$	$d\sigma_g$	$\mathrm{d}\delta_g$
5	$\Re(\rho_\alpha)$	−0.1650	0.9575	−0.0819	0.0086	0.3103
	$\Im(\rho_\alpha)$	−0.0630	0.7391	−0.0666	0.2782	0.0126
	C_1	0.4430	−3.3181	0.2905	−0.5729	−0.6214
	C_2	1.2688	3.3190	1.0572	1.6666	0.5891
n	α	$p\pi_g$	$f\pi_g$	$s\sigma_g$	$d\sigma_g$	$\mathrm{d}\delta_g$
6	$\Re(\rho_\alpha)$	−0.1518	1.0162	−0.0726	0.0163	0.3233
	$\Im(\rho_\alpha)$	−0.0667	0.7959	−0.0711	0.2846	0.0109
	C_1	0.4406	−3.6483	0.2890	−0.6023	−0.6760
	C_2	1.2243	3.9503	1.0222	1.7079	0.5871
n	α	$p\pi_g$	$f\pi_g$	$s\sigma_g$	$d\sigma_g$	$\mathrm{d}\delta_g$
7	$\Re(\rho_\alpha)$	−0.1502	0.9282	−0.0676	0.0072	0.3250
	$\Im(\rho_\alpha)$	−0.0751	0.8747	−0.0759	0.2868	0.0210
	C_1	0.4609	−3.6692	0.2916	−0.5885	−0.7142
	C_2	1.2033	4.3192	0.9996	1.7491	0.6129
n	α	$p\pi_g$	$f\pi_g$	$s\sigma_g$	$d\sigma_g$	$\mathrm{d}\delta_g$
8	$\Re(\rho_\alpha)$	−0.1578	1.1980	−0.0720	0.0314	0.3347
	$\Im(\rho_\alpha)$	−0.0644	0.7036	−0.0712	0.2871	−0.0017
	C_1	0.4602	−3.9245	0.2939	−0.6400	−0.6999
	C_2	1.2413	4.1434	1.0160	1.7160	0.5627

Table 10.3: Real and imaginary part of Starace parameters for the auto ionizing states of the Ogawa Tanaka series as well as the corresponding values for the alternative parameters C_1 and C_2. The values correspond to data calculated in length gauge. Similar values may be obtained for velocity gauge.

Gaussian pollution beyond R_0 of the diffuse orbital may be the consequence. The XCHEM approach would neglect the contribution of these polluting Gaussian during the evaluation of the integrals.

A method to determine if such a pollution is present, is possible in a relatively straightforward and is based on evaluating the PC-Gaussian component of the diffuse orbitals beyond R_0. In a diatomic molecule this may still be done in a relatively painless way. Let

$$\xi_{ip} = c_{ip} \int_{R_0}^{\infty} \mathrm{d}^3 r G_{\mathrm{PC}}(\mathbf{r}) \chi_i^d(\mathbf{r}) \tag{10.9}$$

be the contribution of the p^{th} PC Gaussian to the i^{th} diffuse orbital. As a consequence of not integrating over all space, these integrals are no longer analytically solvable and must be approached numerically. Figure 10.11 shows the Nitrogen molecule, the PC Gaussian basis functions as well as a sphere of radius R_0, the space beyond which we aim to integrate over.

Numerically integrating equation 10.9 requires evaluation of Gaussians which are most naturally expressed in spherical polar coordinates centred at their respective origins. Transforming the polar coordinates r and ϕ of a PC Gaussian to the monocentric coordinate systems, while exploiting the invariance

		3	4	5	6	7	8	
$nd\sigma_g$	E_e	17.1711	17.8716	18.1896	18.3623	18.4659	18.5324	eV
	Γ	62.2539	24.7099	11.1275	7.4299	5.1756	2.6634	meV
$(n+1)s\sigma_g$	E_r	17.3881	17.9767	18.2463	18.3958	18.4871	18.5474	eV
	Γ	98.1303	53.2992	28.4602	17.4039	10.7512	8.3967	meV

Table 10.4: Energies and widths of the Hopfield absorption and emission series for the resonances $3 \leq n \leq 8$ obtained by finding the poles equation 5.137.

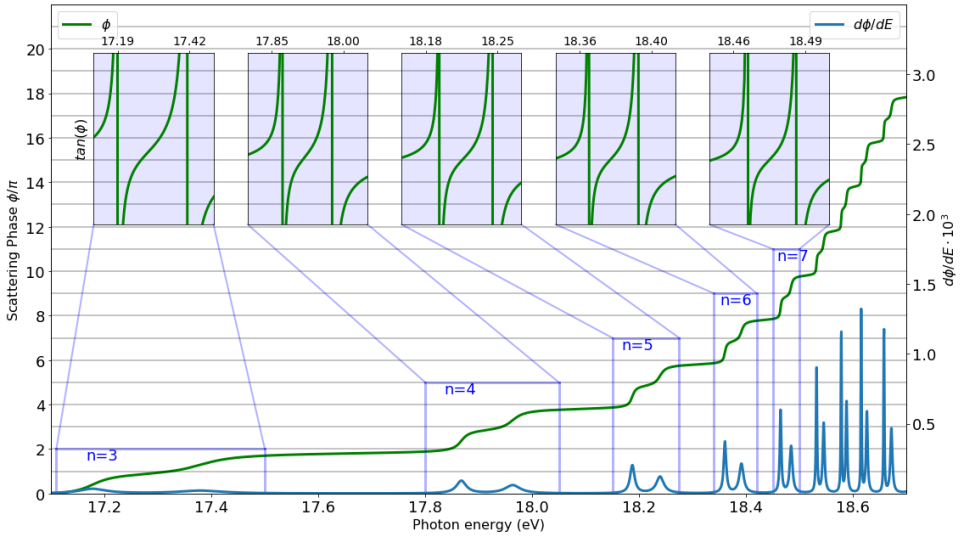

Figure 10.9: Dependence of phase shift ϕ of scattering states in ${}^1\Sigma_u$ channels. We can easily identfy auto ionizing states appearing in pairs, evidenced by the double step features occuring repeatedly. The blue line show the derivative of the phase shift, related to the width of the auto ionizing states. The inlets show $\tan(\phi)$ zoomed into the indivdual resonances, diaplaying two poles at the position of the auto ionizing states of the Hopfield emission and absroption series.

of the system under rotation around the z-axis by setting $\theta = 0$, gives

$$r_{1/2} = \sqrt{r^2 + \frac{d^2}{4} \pm r d\cos(\phi)} \tag{10.10}$$

$$\phi_1 = \cos^{-1}\left(\frac{d + r\cos(\phi)}{\sqrt{r^2 + \frac{d^2}{4} + r d\cos(\phi)}}\right) \tag{10.11}$$

$$\phi_2 = \pi - \cos^{-1}\left(\frac{d + r\cos(\phi)}{\sqrt{r^2 + \frac{d^2}{4} - r d\cos(\phi)}}\right), \tag{10.12}$$

where $r_{1/2}$ and $\phi_{1/2}$ are to understood as in figure10.11. Therefore equation 10.9 may be written as

$$\xi_{ip} = c_{ip} \int_{R_0}^{\infty} \int_0^{2\pi} \int_0^{\pi} \mathrm{d}r\mathrm{d}\phi\mathrm{d}\theta G_{\mathrm{PC}}(r_{1/2}, \phi_{1/2}, \theta)\chi_i^d(r, \phi, \theta) \tag{10.13}$$

This numerical evaluation, while expensive, is possible by exploiting the $D_{\infty h}$ symmetry of N_2. The first step is then to check if non negligible values are present. If this is not the case no pollution is present. If however we do find a part of the PC-Gaussian protruding into regions where there ought to be no PC Gaussian we may try to address this problem by attempting represent the polluting part in terms of MC Gaussian. Currently this is under investigation.

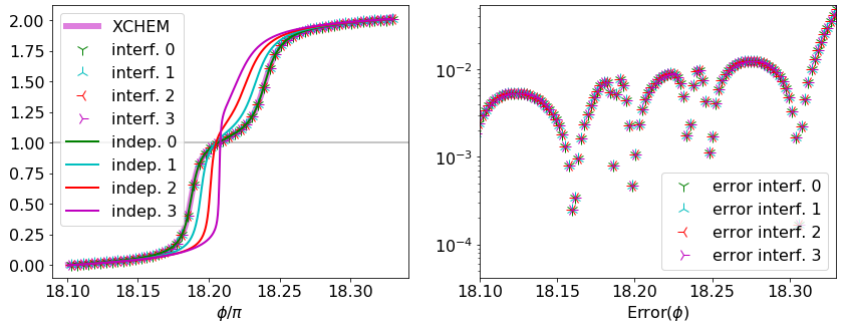

Figure 10.10: The left panel shows plots for the phase shift using different "uncoupled" parameters E_B, E_C, Γ_B and Γ_C (subject to the restrictions pointed out in the text). The thin lines show the phase shift in the absence of interference of the auto ionizing states, and the thick magenta line shows the XCHEM data. For each of these, the corresponding set of markers shows the fits to the XCHEM data obtained by varying $2\Im(W_{AB}W_{CA}W_{BC})$ and $|W_{BC}|^2$. The right panel shows the error of each fit compared to the XCHEM data. The different fits can be seen to be virtually identical in quality.

Below the $A^2\Pi_u$ threshold

Having obtained very convincing results between the $A^2\Pi_u$ and $B^2\Sigma_u$ ionization thresholds, it is natural to see if the same can be done below the $A^2\Pi_u$. The computational effort is aided by the fact that rather than seven, we now only have to consider 4 open channels. In spite of this region of photon energies is found to be significantly more challenging. Figure 10.12 shows the XCHEM results compared to experimental results.

It is immediately obvious that there is no agreement worth speaking of. In part this may be due to the insufficient spectral resolution of the experiment, failing to resolve the extremely sharp features suggested by the experimental results. Nevertheless, in light of these results, it is likely that effects play role that require the inclusion of nuclear motion to lead to a successful description of this region of photon energies. This may include simple vibrational motion, which may now no longer be negligible (the extremely sharp peaks indicate very long lifetimes of the auto ionizing states, making the explanation a likely candidate). Furthermore it cannot be ruled out for non-adiabatic effects to play a role. A description of all of these possible origins for the disagreement of theory and experiment make for formidable problem, of extremely high computational complexity, which would provide a very complete picture of auto ionizing states, including electronic motion, nuclear motion as well as the coupling between the two. At present no code capable of such a treatment is implemented, but this would make for an enticing problem to address in the future.

Conclusion

We have used the XCHEM code to present a first study photo ionization in a molecular multielectronic system. We were able to obtain results which qualitatively are in agreement with a variety of experimental results between the $B^2\Sigma_u^+$ and $A^2\Pi_u$ thresholds. Specifically, we reproduce the Hopfield absorption and emission series, as well as the Ogawa Tanaka series of auto ionizing states. In the Ogawa Tanaka series we presented an extensive analysis of widths, positions, Fano parameters q and correlation ρ^2. Furthermore we provided a breakdown into partial cross sections extracting also the imaginary and real part of the Starace parameters ρ_α. In the Hopfield series we focused on the $n = 8$ resonance to investigate the parameters related to the coupling of two auto ionizing states to each other either directly or via the continuum. Furthermore we provided a likely explanation for the less accurate results for the $n = 3$ resonance, compared to the other resonances.

We also note that in all likelihood we may disregard the proposition of[218] that the inclusion of rotational couplings is necessary (which in part appears to be due to an erroneous assignment of the auto

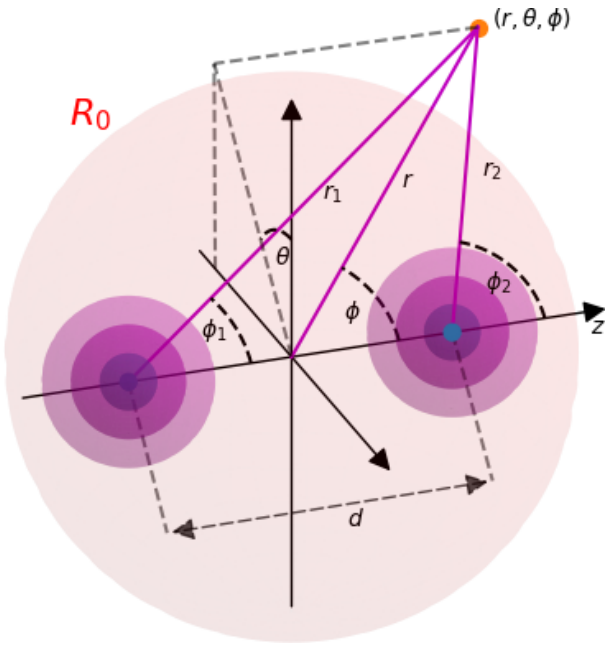

Figure 10.11: Nitrogen moleclue with PC Gaussian basis functions centered at the molecular sites. Furthermore for some point $\mathbf{r} = (r, \theta, \phi)$, the coordinates specfying that point using PC Gaussians as well as MC Gaussians are indicated. The red sphere representes the location of the cut off radius R_0 beyond which PC Gaussians are assumed to be zero. To account for possible pollution of diffuse orbitals with PC Guassians the overlap integrals have to be evaluated outside this region.

ionizing states), given that we are able to provide superior agreement without inclusion of said couplings. Furthermore, in view or prelimiary results but awaiting final confirmation from results improving the agreement of $n = 3$ resonances, we expect to also be able to disregard the presence of interference stabilization proposed in [217]. This can be motivated, by comparing the experimental results in the lower two panels of figure 10.5, of which the results in the lower panel appear to show the $s\sigma_g$ and $d\sigma_g$ resonances as clearly separated.

Finally we also presented XCHEM results below $A^2\Pi_u$ threshold the agreement of which with experimental data is severely flawed. We have proposed a likely explanation for this disagreement, the investigation of which would provide an interesting if highly complex problem for the future.

In conclusion, we believe the results presented here to convincingly display the utility of the XCHEM method, having for the first time provided accurate results on the photo ionization cross section of N_2 in the mentioned energy range, including a multitude of auto ionizing states.

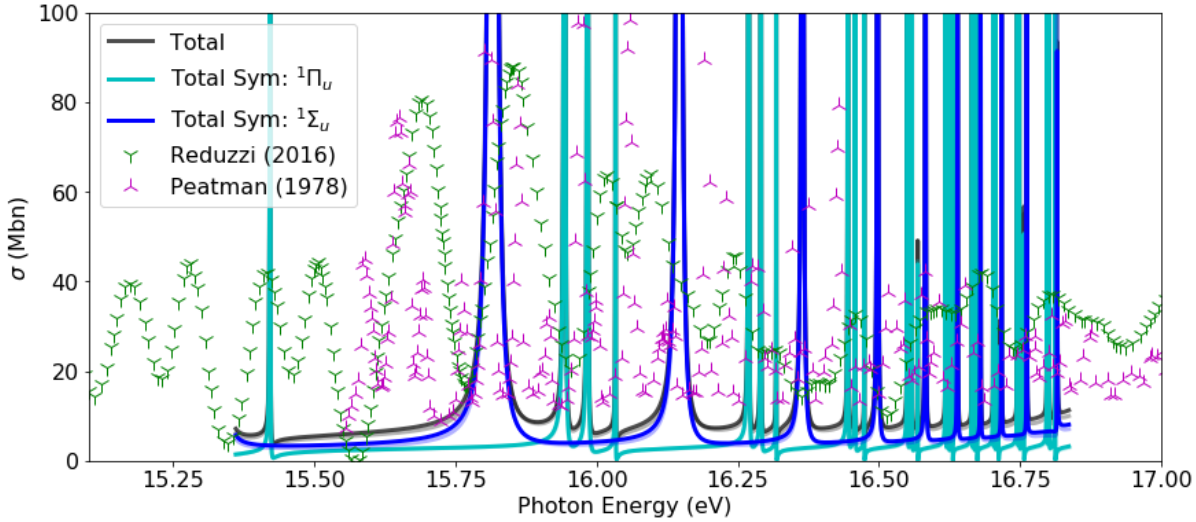

Figure 10.12: Photo ionization cross section between the $X^2\Sigma_u$ and $A^2\Pi_u$ thresholds. The black continuous line shows the total cross section obtained from the XCHEM code, whereas the cyan and magenta line correspond to the partial cross sections decaying to either a final $^1\Sigma_u$ or $^1\Pi_u$ state. The crosses mark two experimental sets of values. It is clear that there is no agreement between theory and experiment. However it should also be pointed out theres is an equal absence of agreement between the different experimental results. Finally, it is noteworthy that while the theory does not agree with the experiment the XCHEM results are nevertheless suggestive in their structure. For the $^1\Sigma_u$ symmetry we see isolated resonances probably corrsponsing $nd\pi_g \otimes A^2\Pi_u$ auto ionizing states. For the $^1\Pi_u$ the resonance appear in closely lying triples which may likely be identified with the Rydberg states corresponding to the series $ns\sigma_g \otimes A^2\Pi_u$, $nd\sigma_g \otimes A^2\Pi_u$, $nd\delta_g \otimes A^2\Pi_u$. Therefore it is likely the case, that the calculations are correct within the fixed nuclei approximation, but that vibtrational effects play a role that may not be negelected.

11 Photodissociation of Molecular Nitrogen

The previous chapter's discussion of photoionization of molecular Nitrogen, was concerned with the very accurate description of said process, yielding almost exact photoionization cross sections for ionization events leaving the charged molecule in either the ground or the lowest electronically excited state of the cation. The PES of either of these states are characterized by a pronounced potential minimum close to that of the neutral molecule. Therefore the cationic molecule in this scenario is stable and does not break apart into fragments of atomic (ionized) Nitrogen. We shall now look at a situation where this is radically different by considering ionization by a significantly more energetic photons, allowing for ionization to electronic states of the ionic molecule that are highly repulsive, and thus begin a process of dissociation after the ionization event has taken place; this dissociation process following ionization is the primary focus of this chapter.

Moreover, unlike the previous chapter, which was concerned with the accurate reproduction of well known and well understood phenomena, with vast experimental data available to gauge the success of the XCHEM method, this chapter's investigation was carried out with a different objective. Namely, in collaborating with the group of Nisoli et. al. who carried out experimental work in dissociative photoionization using state of the art light sources, this dynamics was studied in the Nitrogen molecule [59]. In addition to the attractive features of molecular Nitrogen mentioned in the introduction, which focussed primarily on its complexity compared to other systems, it is worth commenting also on the important role photodissociation of N_2 in particular, plays in a variety of (exotic) environments.

Nitrogen is of particular relevance as it is the most abundant species in the Earth's atmosphere and is one of the major constituents if the upper atmospheres of Jupiter, Saturn and its moon Titan [222]. Ionized Nitrogen molecules as well as ionic and neutral Nitrogen atoms have been shown to be crucial ingredients in the formation of prebiotic molecules (such as HCN, CH_3CN or C_2N_2) found in Titan's atmosphere [223, 224, 225]. Furhter, in Earth's upper atmosphere the extreme ultraviolet radiation (XUV) spectral region of the solar radiation is mostly attenuated by the presence of N_2[226], which absorbs the XUV radiation and inevitably leads to ionization and dissociation of the molecule via adiabatic and non-adiabatic relaxation (see chapter 7) of highly excited electronic states. Thus the investigation of the ultrafast dissociative mechanism leading to the production of N and N^+ is of prime importance for understanding the radiative transfer processes. That being said, the experimental study of the N_2^+ ultra relaxation dynamics from excited states is not trivial and its theoretical study challenging due to the important role of electronic correlations in excited multi electronic states.

The experimental results whose reproduction and explanation we endeavour in this chapter, were obtained using an attosecond XUV-pump/femtosecond IR-probe type setup. This means that the neutral molecular system is stripped of an electron by interaction with a single attosecond XUV pulse. The dissociation process is probed by the second pulses which impinges on the system after a variable time delay. Finally the kinetic energy of the ionic fragments is recorded as a function of the time delay between the two pulses. The theoretical description of the ionization step was done using different approach to the one used in chapter 10. The principal reason for using single attosecond pulses (compared to a train of attosecond pulses, achieved experimentally more easily) is the reduced temporal resolution associated with recurring excitation events. Recently, isolated attosecond pulses have been used to trigger the electron dynamics in the biologically relevant molecule phenylalanine; an amino acid. The charge dynamics after ionization has been probed on a few femto second time scale with sub-4-fs IR pulses[30]. However, due to the complexity of the system the dynamics induced by the IR probe could not be fully understood.

This is unlike the dissociation process in Nitrogen after the ionization event. The relative simplicity of Nitrogen (compared to say phenylalanine) allows a precise description of the PES and couplings that includes all the electrons of the system and its single degree of freedom in molecular geometry allows the use of quantum dynamics to understand the nuclear motion. While this is generally difficult, the simulation of the molecular dynamics initiated by attosecond pulses is furthermore challenging because the large bandwidth of the attosecond pulse leads to the possibility of exciting to many electronically excited states, all of which have to be included in the time dependent treatment. Therefore as we shall see, despite its simplicity N_2, it is nevertheless a challenging molecule the photodissociation of which to study.

11.1 Details of Method

Experimental Setup

NIR/VIS with a 4 fs duration, 2.5-Mj energy and a residual single-shot carrier envelope phase fluctuation of $\approx$ 200 mrad (rms) are obtained by hollow core fibre compression of 25 fs duration, 6 mJ energy and 1 kHz repetition rate pulses [227]. The ultrabroad spectrum of the NIR/VIS pulse is reported in figure 11.1b: the spectrum displays a strong blueshift due to the ionization in the hollow core fibre.

The NIR/VIS beams is divided into two parts using a beam splitter with 50% reflection. A scheme of the interferometric setup is shown in figure 11.1a. The transmitted beam is focused by a spherical mirror with 1 m radius of curvature into a pulsed Argon-gas jet operating at 1 kHz repetition rate to produce XUV radiation by high harmonic generation. Isolated attosecond pulse, with energy of several hundred pico-joules, and a continuous extending up to 50 eV are produced by the polarization gating technique [228]. A 100 nm thick aluminium filter is used to filter out the fundamental radiation nad the energy region of the spectrum below 16 eV. The frequency resolved optical gating tachinque for complete reconstruction of atto second bursts [229] is implemented to measure an XUV pulse duration of 300 as. The spectrum of the XUV radiation is characterized by using a highly resolving flat-field soft-x-ray spectrometer consisting of a grating, followed by microchannel plates (MCP), a phosphor screen and a CCF camera [230]; a typical XUV spectrum is show in figure 11.1c. The remaining part of the NIR/VIS beam is properly delayed with attosecond resolution by using a piezoelectric translation stage and then collinearly recombined with the XUV beam by using a drilled mirror. Both beams are collinearly focused by a gold-coated toroidal mirror into a pulsed N_2 gas jet operating at 1kHz and interated in the repeller electrode of a velocity map imaging spectrometer [231]. N^+ fragments are selected by applying a 150 ns wide gate to the MCP assembly. The NIR/VIS intensity is adjusted in order to avoid production of N^+ in the presence of the NIR/VIS pulse only.

Theory

In order to simulate the dynamics of the N_2^+ molecular ion in the presence of the IR laser pulse, the time dependent SE is solved using the split operator technique [232, 233, 234] outlined in chapter 7 in combination with Fast Fourier techniques [235]. As was further explained in chapter 7 the nuclear wave packet is discretized on a a grid of internuclear distances and the propagation of the wave packets is performed on the same grid (though with denser spacing of grid points obtained by interpolating PES as well as the molecular properties, namely the diabatic electronic Hamiltonian and the transition dipole moments). These electronic states of N_2^+, whose PES the propagation is performed on, are modelled at *ab initio* level using the SA-CASSCF methodology (explained in chapter 3) with the cc-pVQZ basis. In the present case nine electrons are considered in an active space comprising the $2p$ and $2s$ atomic orbital (i.e. giving a CAS(9,8) space). Since the calculations are performed with symmetry constraints, two separate sets of orbitals are optimized. Both sets of orbitals are calculated using a states average of 13 states, covering the four lowest dissociation limits. The first set includes Σ_g and Δ_g states. Figure 11.2 shows the resulting adiabatic PES.

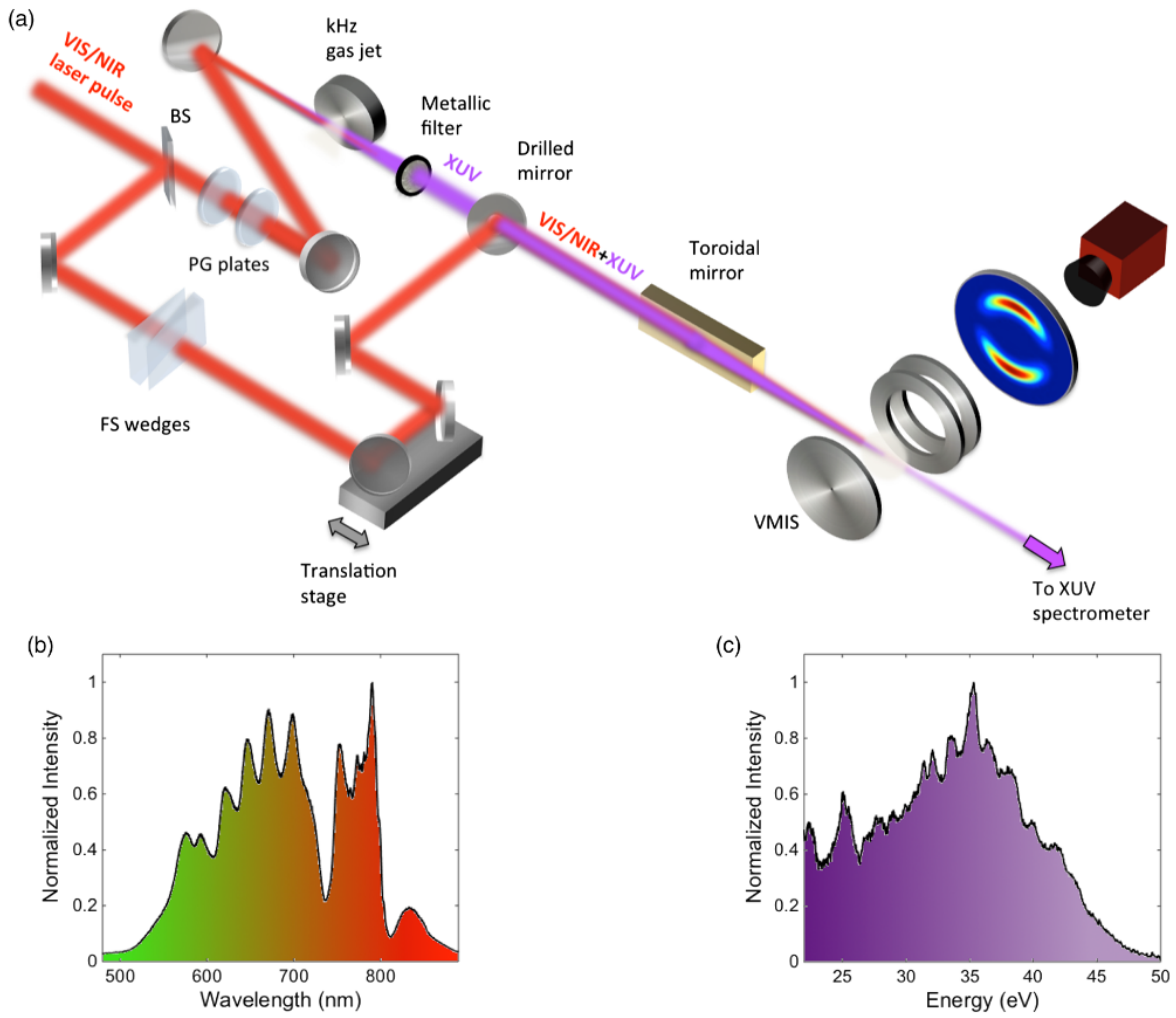

Figure 11.1: (a) Scheme of the experimental setup. In the figure, BS stands for Beam Splitter, FS wedges stands for Fused Silica wedges, PG plates stands for Polarization Gating plates and VMIS stands for Velocity Map Imaging Spectrometer. Panels (b) and (c) show the acquired spectrum of the NIR/VIS and XUV pulses, respectively.

In order to simulate the dynamics, it is crucial to include an accurate description of non-adiabatic effects between all relevant electronic states. For the description of these couplings we use the approach for obtaining diabatic PES outlines in chapter 7. In the propagations carried out to yield the results presented here, we use quasi diabatic PES obtained, neglecting the change of the orbitals in the non-adiabatic coupling, forcing the fist term of equation 7.49 to vanish. This is motivated by the observation, that the molecular orbitals, unlike the CI vectors, do not radically change with changing molecular geometry. A subsequent numerical analysis of the effect of the first term in equation 7.49 has largely validated this assumption, suggesting that while not entirely negligible, the change in the CI vector is responsible for the bulk of non-adiabatic effects. Furthermore in the active space used here, we may resort to a the crude version of the diabatization scheme, propagating on a set of PES equal in size to the number of CSFs in the active space. For CAS(9,8) this translates to a total of 616 PES divided into two sets of 308 corresponding to the different symmetries of electronic states.

The initial nuclear wave packet is created assuming an instantaneous ionization by the XUV laser pulse. To calculate the relative population of the different electronic ionic states we used, rather than the XCHEM approach, the approach based on Dyson Orbitals presented in chapter 5. Recall that the Dyson orbital obtained from the ground state of N_2, Ψ_{N_2} and some excited ionic state α denoted by $\Psi\alpha_{N_+}$ is

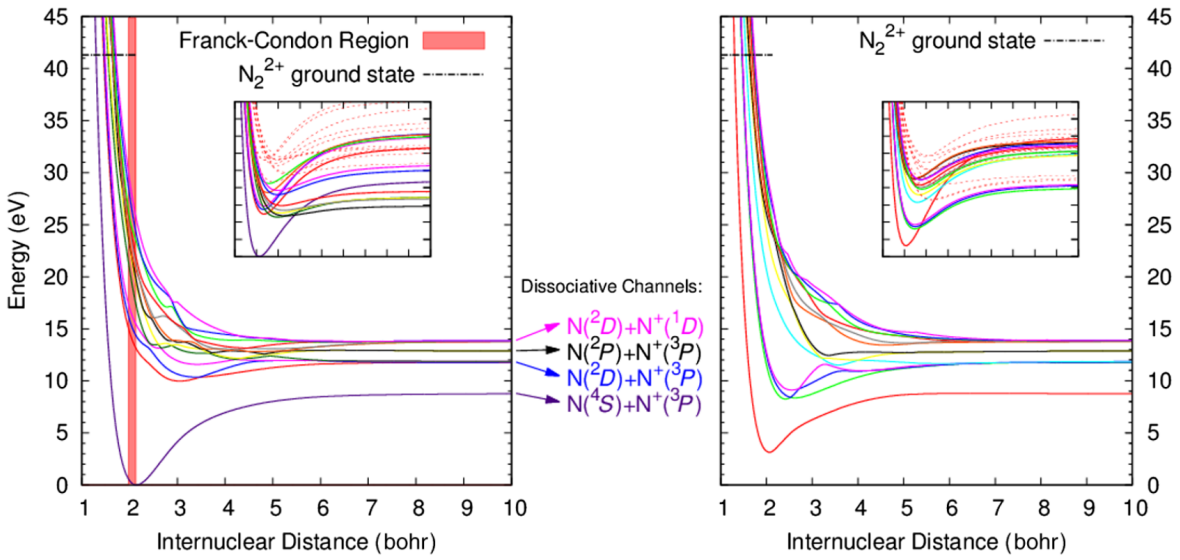

Figure 11.2: PES of symmetries including $^2\Sigma_g$ (left) and $^2\Sigma_u$ (right) electronic states. The main panels show the adiabatic states whose orbitals are optimzed and the inlets show the quasi diabatic states used for propagation, including also some higher lying states (faint lines) obtained with the method outlined in section 11.1 and chapter 7

given by

$$D^{\alpha}(\mathbf{r}) = \int \Psi^*_{N_2}(\mathbf{r}, \mathbf{r}_2, \cdots \mathbf{r}_{N_e}) \Psi \alpha_{N_+}(\mathbf{r}_2 \cdots \mathbf{r}_{N_e}) \mathrm{d}\mathbf{r}_2 \cdots \mathrm{d}\mathbf{r}_{N_e} \tag{11.1}$$

giving to first-order perturbation theory the ionization amplitude for en electron ejected with momentum k

$$c_{\alpha,k} = -i \int D^{\alpha}(\mathbf{r}) \hat{\mu}(\mathbf{r}) \psi^{\mathrm{el}}(\mathbf{r}) \mathrm{d}r \tag{11.2}$$

The Dyson orbitals are evaluated using the aforementioned adiabatic electronic states previously calculated, at the equilibrium geometry and considering a single state wavefunction CAS(10,8) for the ground state the system in initially in. To account for the fact, that in the experiment the ionized fragments are recorded along the internuclear axis (z axis), the dipole moment in equation 11.2 was considered in that direction only. Finally, the wave function of the ejected electron Ψ^{el} is modelled by a Coulomb function with k chosen so that only electrons with energy compatible with the bandwidth of the XUV pulse are considered. For each k Coulomb functions with angular momenta $l = 1, 3, 5$ and $m_l = 0$ are included. Note that these choices of angular momenta, together with the different ionic states we allow the system to ionize to, corresponds to the choice of channels in the CC expansions, if this step were carried out using the XCHEM code. Of course in not using the XCHEM code all interchannel couplings are neglected and the effect of auto ionizing states disregarded. Work is currently in progress to apply the XCHEM code to this problem, with preliminary results confirming the relative ionization probabilities obtained using Dyson Orbitals.

The PES used in the propagations are computed with symmetries given by the point group D_{2h} (the largest subgroup of $D_{\infty h}$, describing the symmetry properties of $N_2^{(+)}$). The states considered as being ionized to are of symmetry A_g of D_{2h} (corresponding to Σ_u and Δ_u of $D_{\infty h}$). Specifically after ionization by the XUV pulse, the sates $X^2\Sigma_g$, $F^2\Sigma_g$, and $3^2\Sigma_g$ are found to carry real relative initial amplitude 0.973, -0.173 and 0.106, respectively. A laser pulse polarized along the internuclear axis couples A_g states to B_{1u} (corresponding to Σ_u and Δ_u of $D_{\infty h}$). Figure 11.2 shows the PES of these symmetries.

The sates are shown in their adiabatic as well as quasi diabatic representations. Propagating the initial states on the quasi diabatic PES in the absence of the probe pulse yields the kinetic energy spectrum displayed in figure 11.3. This propagation serves as an example as well as a reference to investigate how a probe pulse a different time delays affect the kinetic energy spectrum. Given the absence of a probe pulse, there can be no population transfer between states of different symmetries. Figure 11.3 thus shows the kinetic energy spectra of the dissociative channels in the Σ_g symmetry (coloured lines) as well as their sum (black line). Two band are clearly visible at approximately 1 and 3 eV, respectively. The inlet explicitly shows the nuclear wave packet evolving in position space during the propagation. The dissociating part of the wave packet can easily be identified and assigned to the peaks in the kinetic energy spectrum. All the propagations in this work are run a grid of 1024 points with grid spacings of $1.66 \cdot 10^{-2}$ a.u. The wave function is evolved forward in time by increments of 1 a.u. for a total of 8192 a.u. ($\approx$ 200 fs). For nuclear separations greater than 14 a.u. the molecule is considered dissociated and thus the kinetic energy spectra are calculated at this point. Any part of the wave function beyond this point is removed by a complex absorber[236] to avoid spurious reflections. In order to allow for efficient propagations in view of the large number (616) of potential, a Lanczos algorithm (see chapter 7) is implemented to circumvent the explicit diagonalization of large matrices where possible.

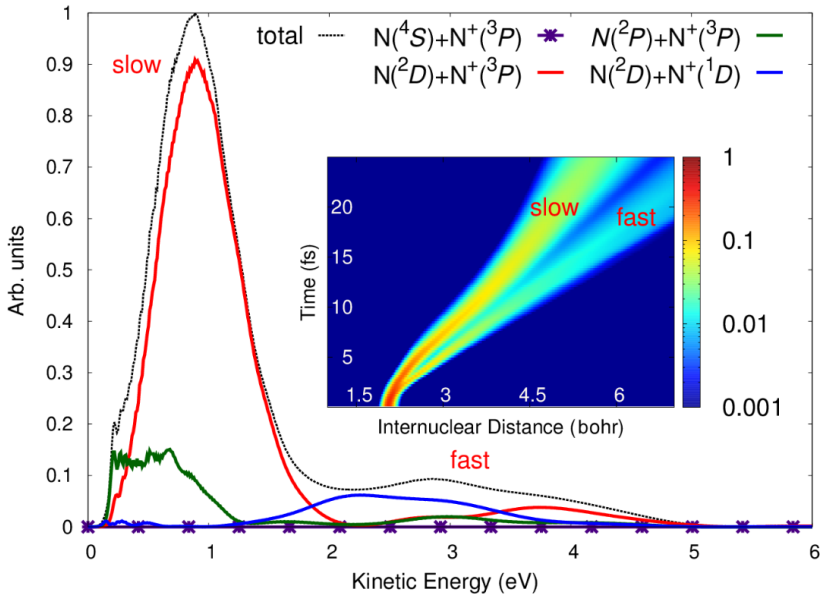

Figure 11.3: Theoretical N^+ kinetic energy spectrum (black dashed line) and the partial contributions of groups of states leading to the different dissociation channels (in increasing order of energy of the dissociative limit: magenta, red, green, blue). The inlet shows the time evolution of the initial wace packet ultimately resulting in the given kinetic energy spectrum.

11.2 Results

Isolated attosecond pulses with a photon energy in the range 16-50 eV and a pulse duration of 300 as are used to ionize, through single-photon transitions, N_2 molecules. Figure 11.4 shows the PES of the ground state of N_2 and the relevant electronic states of N_2^+. Among these excited states, the most relevant ionization channels with Σ_g symmetry are the $X^2\Sigma_g$, $F^2\Sigma_g$ and $3^2\Sigma_g$ states, which are reported in the same figure in purples, red and green respectively, the details of the calculation yielding these PES are summarize in section 11.1.

The experiment measures the angularly resolved momentum distribution of the N^+ fragments, resulting from the dissociative ionization by the dissociative ionization by the XUV pulses, by using a velocity

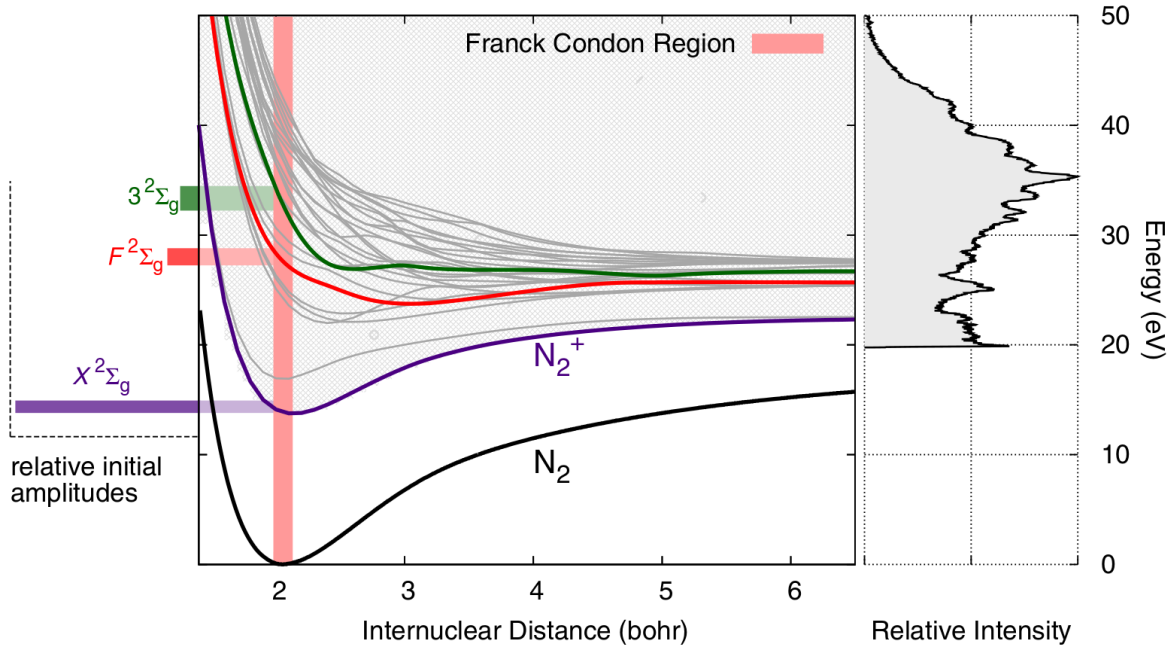

Figure 11.4: Potential energy surfaces of the ground state of N_2 (blck curve) and the relevant electronic states of N_2^+ (grey curves). The most relevant electronic states in the inoization process, with Σ_g symmetry, namely the $X^2\Sigma_g$, $F^2\Sigma_g$ and $3^2\Sigma_g$ states, are shown in purple, red and green lines, respectively. Left Relative initial populations of the $X^2\Sigma_g$, the $F^2\Sigma_g$ and the $3^2\Sigma_g$ states. Right; Measured XUV spectrum.

map imaging spectrometer[230]. The charged fragments are projected by a strong electric field onto a microchannel plate followed by a phosphor screen, and the N^+ fragments isolated by using a time-of-flight gate acquisition. A two-dimensional projection of the momentum distribution of the ions is measured, and the three-dimensional momentum distribution is retrieves by using a Legendre polynomial based inverse Abel transformation. Figure 11.5a shows the kinetic energy spectrum of the N^+ ions, obtained by integration of the momentum over narrow angular range around the laser polarization axis. A strong peak aruond 1 eV and aband peaked around 2.5 eV can be observed in the kinetic energy spectrum. The former (hereafter call F-band) can be associated with direct dissociation from the $F^2\Sigma_g$ state[58, 237], while the latter can be assigned to dissociation from the manifold if excited states of N_2^+ including the $3^2\Sigma_g$ state.

In order to probe the XUV induced ionization dynamics, properly delayed 4 fs NIR/VIS probe pulses with a peak intensity of $8 \cdot 10^{12}$ W/cm^2 (for more details we refer to section 11.1) were used. The presence of the NIR/VIS pulse significantly alters the kinetic energy spectrum, as can be seen in the time dependent measurement reported in figure 11.5b. At zero time delay between the pump and the probe pules (identified by monitoring the ponderomotive streaking in the photo electron spectrum[238]), a sudden increase of the kinetic energy is visible (with respect to the XUV-only case or negative time delays in figure 11.5b) due to two color ionization. Moreover a clear depletion of the F band accompanied by the appearance of a band extending up to 2.5 eV can be observed around 8 fs after the zero time delay.

Figure 11.6a shows a zoom of the pump probe dynamics in a temporal window between 5 and 16 fs. A clear sub cycle modulation of the ion yield is visible, with a periodicity of 1.22 ± 0.5 fs. Two important observations may be obtained from the experimental data: **a)** the periodic modulation of the ion yield is present in a temporal window, where pump and probe pulse do not overlap and **b)** the phase of the oscillation display a kinetic energy dependence, as clearly shown in figure 11.6b, which results in a tilt of the fringes (negative slope compared with the vertical fringes) as a function of the time delay. The subcycle modulation of the N^+ yield is a clear signature of the quantum interference between different dissociative paths. To understand the role of the manifold of electronic excited states in the features

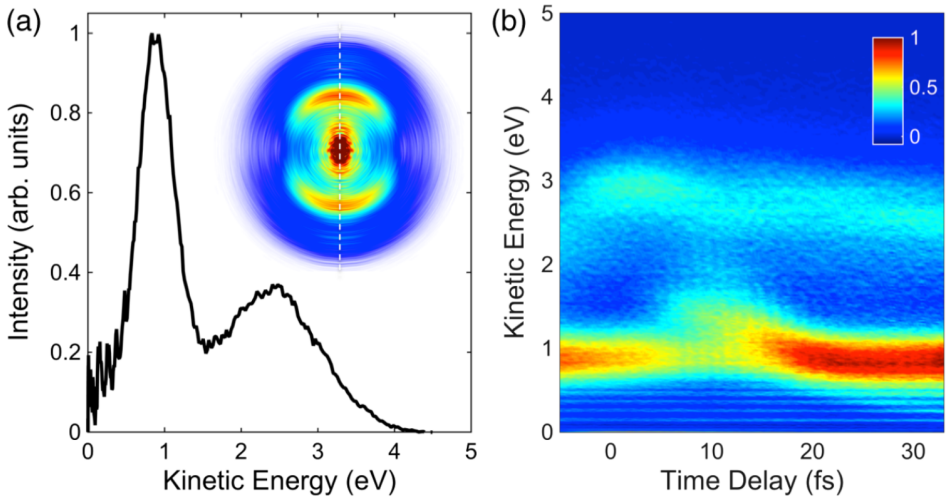

Figure 11.5: (a) N^+ kinetic energy spectrum obtained by integrating the retrieved 3D momentum distribution (inlet) within 20 around the laser polarization axis (white dashed line). (b) N^+ kinetic energy spectrum as a function of the delay between the XUV pump pulse and the NIR/VIS probe pule.

observed in the pump-probe delay scan, a detailed theoretical analysis is required. To this end carried out model calculations based on the methods explained in chapters 7 and 3 (for more details on how exactly there methods were put to use we once again refer to section 11.1).

In summary, the TDSE is solved using a basis set of 616 electronic states of N_2^+ taking into account the coupling induced by the NIR/VIS probing laser pulse. The initial wave function amplitudes in the cation are calculated using the ionization model based Dyson orbital (see chapter 5 as well as equation 11.2). Figure 11.3 shows the theoretical kinetic energy spectrum (black dashed line) obtained by considering only the interaction with the XUV pulse. As in the experimental case (figre 11.5a), the theoretical kinetic energy spectrum exhibits a very intense band between 0 and 15 eV and a much weaker band between 2 and 4 eV. The intensity of the latter band is significantly underestimated by the theoretical model, since this band results mainly from population of highly excited states of N_2^+ [239] and of dissociative channels of N_2^{2+} not included in the present calculations. As can be observed in figure 11.3, there are only two groups of states that significantly contribute to the lower band, namely those leading to dissociation in channels given by the following electronic states of the fragments: $N(^2D) + N(^3P)$ and $N(^2P) + N(^3P)$. Conversely all four dissociative channels included in our calculation contribute to the upper band. The relative dissociation ionization yields, integrated over kinetic energy are given in equation 11.3. We can infer that neutral atomic Nitrogen is mainly produce in the ^2D state, but there is also a significantly in the ^2P state (14%). Similarly, N^+ is mainly produced in the ground states ^3P state, but there is also a non-negligible probability to find it in the excited ^1D state (8.5%):

$$N_2^+ \longrightarrow \begin{cases} N(^4S) + N(^3P) & 0\% \\ N(^2D) + N(^3P) & 77.1\% \\ N(^2P) + N(^3P) & 14.0\% \\ N(^2D) + N(^1D) & 8.5\% \end{cases} \tag{11.3}$$

The results of the calculations in the presences of the NIR/VIS pulse are shown in figure 11.7a: the main features observed in the experiment are clearly present. In particular we observe a depletion of the F band around 0.9 eV for time delays between approximately 6 and 16 fs. This is accompanied by a quick modulation of the signal with the same tilt present in the experimental data (figure 11.7b). As previously mentioned, our theoretical approach is not equipped to fully describe the dynamics of the energy band at 2-4 eV.

For better visualization of the subcycle dynamics, figures 11.8a and 11.8b report the experimental and theoretical oscillatory pattern left after a fifth order polynomial fit of the slowly varying background

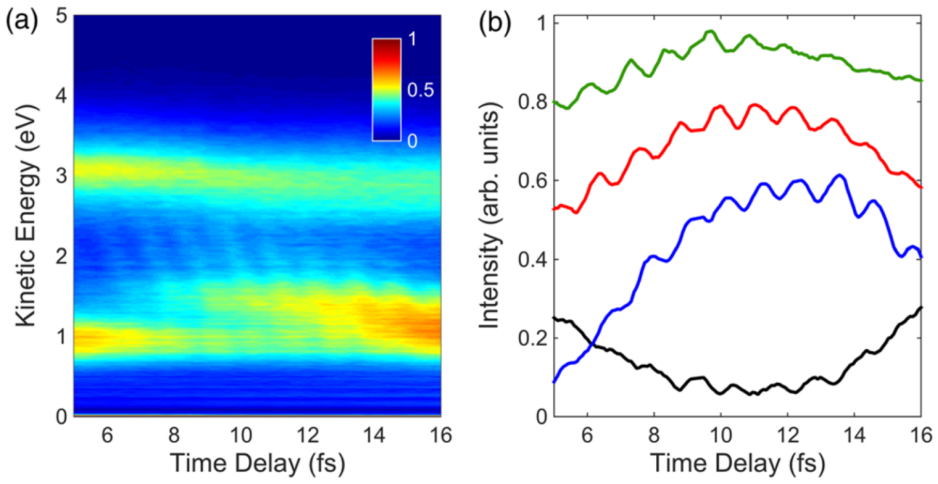

Figure 11.6: (a) Time-dependent N^+ kinetic energy spectra acquired within a pump-probe delay interval between 5 and 16 fs. (b) N^+ yield integrated in a 0.3 eV wide energy band around 0.8 eV (black curve), 1.6 eV (blue curve), and 2.2 eV (green curve). An arbitrary offset has been added to the curves to aid visualization.

is subtracted. As is observed in these figures, there is a very good agreement between theory and experiment, which is also confirmed by the presence if a clear peak at 0.8 PHz in the Fourier transform of the calculated oscillatory pattern around 2.2 eV, very close to the measured one of 0.82 ± 0.1 PHz. Moreover, the simulated oscillations carry the same phase as the experimentally observed oscillations, indicating that the tilt of the fringes is perfectly reproduced by the numerical calculations.

11.3 Discussion

Having obtained a theoretical results of satisfactory accuracy, we identify a smaller subset of PES capable of reproducing the main structures found in the full simulation. This subset is shown in figure 11.9a and is composed of two dissociative sates $F^2\Sigma_g$ and $3^2\Sigma_g$ described above, which carry relatively high initial population, and of the $C^2\Sigma_u$ and $5^2\Sigma_u$ state.

Figure 11.10a shows the time dependent N^+ kinetic energy spectra calculated within the four-state model: from the comparison between this figure and figure 11.7a, we can see that there is qualitatively good agreement between the full calculation and the model. This smaller subset of states has allowed us to identify a simple physical mechanism that explains the main features observed in experiment. The proposed mechanism is summarized in figure 11.9 and suggests the following interpretation: the strong depletion of the F band observed around 8 fs after zero time delay is due to two resonant single photon transitions that transfer population to two different states, namely laser induced population transfer from the $^2F\Sigma_g$ state to the $^25\Sigma_u$ state and from the $^2F\Sigma_g$ state to the $C^2\Sigma_g$ state (these transition are indicated in figure 11.9 by double-headed black arrows). The measured delay of 8 fs represents the time required by the nuclear wave packet to reach the internuclear distance at which the single photon transition from the Σ_g state to the $^25\Sigma_u$ state can occur. The fringes, on the other hand, are the results of two photon-transitions from the $^2F\Sigma_g$ state to the $3^2\Sigma_g$ state using the $5^2\Sigma_u$ state as a virtual intermediate state (indicated in figure 11.9 by single-headed magenta arrows), which interferes with the initial population in the $3^2\Sigma_g$ state. This interpretation was further corroborated by carrying out propagations in a Floquet approach allowing for interaction with either one or one and two photons (see chapter 7), identifying beyond doubt the aforementioned process as the origin of the interference pattern (clearly the approximation of a periodicity is quite crude given the profile of the probe pulse, meaning this approach cannot be expected to give quantitatively correct results). Furthermore it is noteworthy, that the $C^2\Sigma_u$ state appears to be the natural candidate for the intermediate state in the two photon

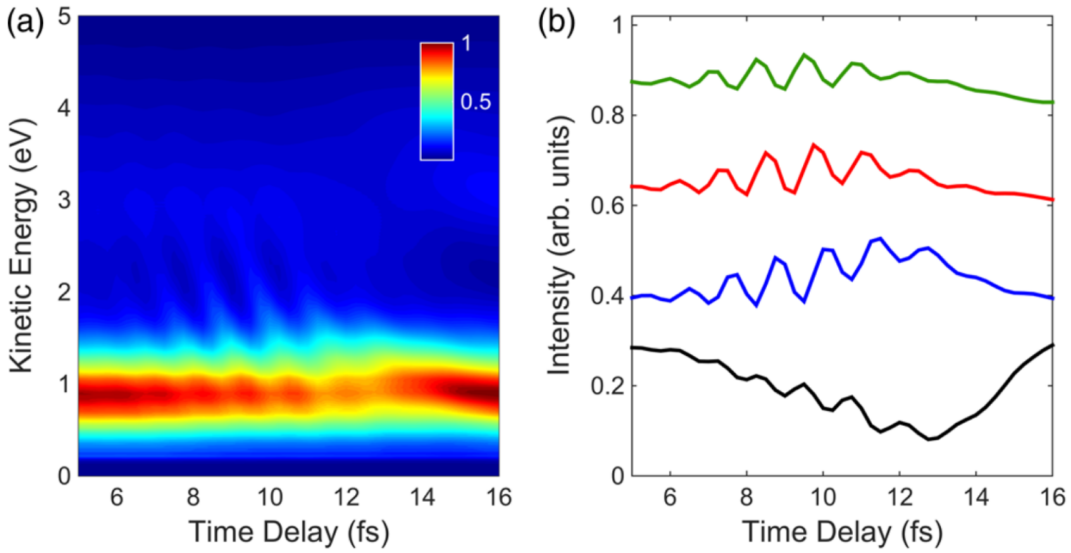

Figure 11.7: (a) Time dependent N^+ kinetic energy specta calculated by including all states within the pump-probe delay interval bewteen 5 and 16 fs. (b) N^+ yield integrated in a 0.3 eV wide energy band around 0.8 eV (black curve), 1.6 eV (blue curve), and 2.2 eV (green curve). An arbitrary offset has been added to the curves to aid visualization.

process, being a more energetically favourable transition, however the relevant dipole transition moments involving $C^2\Sigma_u$ are several order of magnitude smaller than those involving the $5^2\Sigma_u$.

In order to better visualize these physical processes, figure 11.10 shows the time dependent kinetic energy spectra for each individuals state of this model after subtraction of the kinetic energy spectrum obtained in the absence of a probing pulse. An increase and a reduction of time dependent population of each state are represented in red and blue, respectively. The bottom panel evidences the presence of a strong depletion of the $F^2\Sigma_g$ state. Corresponding emerging populations can be observed in the $^2 5\Sigma_u$ channel (top right hand panel) and in the $C^2\Sigma_u$ channel (bottom right hand panel) at ca. 11 and 8 fs, respectively. Interference, on the other hand occurs exclusively in the $3^2\Sigma_g$ channel, which can be clearly observed as red and blue fringes int the top left hand panel.

In our approach the XUV pulse leads to a coherent superposition of different N_2^+ electronic states in which the corresponding nuclear wave packets are identical (in other words, the initial nuclear velocity distribution is the same in all electronic states). As the nuclear wave packets evolve in different electronic states (in this case the $3^2\Sigma_g$ and $F^2\Sigma_g$ states), they follow different paths and the accumulated phases are different. Thus when the two nuclear wave packets reach an internuclear distance at which absorption of two NIR/VIS photons from the $^2F\Sigma_g$ state to the $^3\Sigma_g$ state is favourable (striped area in figure 11.9), the difference in the accumulated phase leads to interferences, which appear in the form of fringes in the kinetic energy distribution. The tilt of the fringes is due to the fact, that the nuclear wave packet components with higher kinetic energies arrive earlier in the region of internuclear distances in which two photon transition may take place, thus leading to an interference pattern shifted at earlier times. This interpretation can be verified by artificially modifying the gradient of, for example the $3^2\Sigma_g$ PES, since this will change the kinetic energy components of the corresponding nuclear wave packet. Figure 11.11 shows a set of artificially constructed potentials for the $3^2\Sigma_2$ state together with the corresponding interference patterns: steeper gradients lead to an increase in the tilt due to the larger contribution of the of high energy components in the nuclear wave packet, while flatter gradients lead to the opposite trend. In both cases, extreme gradients results in destruction of the fringe's pattern. Therefore, the slope if the fringes is directly linked to the slope of the PES of the molecular cation that are activated by the XUV pulse.

Finally in view of the accuracy of the theoretical model to reproduce the observed sub-femto second IR-induced dynamics, one can safely assume that the values of the dissociated ionization yields presented

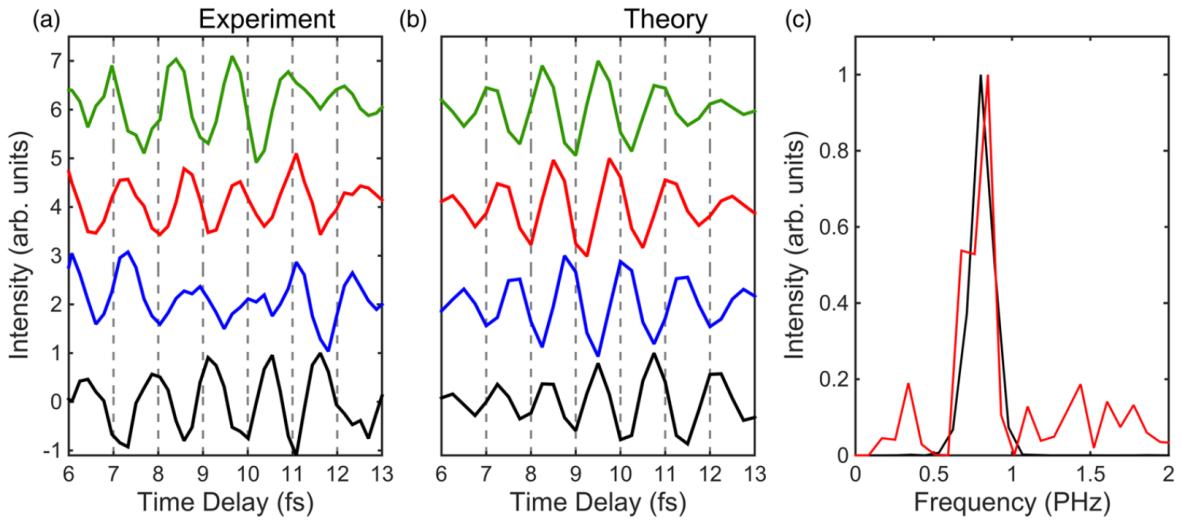

Figure 11.8: Oscialltory pattern obtained after subtraction of a fifth-order polynomial fitting curve to filter out the slow dynamics in both the experimental (a) and the theoretical (b) data around 0.8 eV (blck curve), 1.9 eV (red curve), and 2.2 eV (green curve). (c) Fourier transformed power spectrum of the experimental curve (red line) and the theoretical curve (black line) around 2.2 eV.

in equation 11.3 are also accurate. In existing literature, e.g. on the modelling of Nitrogen reactivity in Titan's atmosphere[224] or on the attenuation of the XUV light in Earth's upper atmosphere[226], it is generally that dissociation of N_2^+ excited states below 35 eV leads to N and N^+ products through the reaction $N_2^+ \rightarrow N(^2D) + N^+(^3P)$. However as equation 11.3 shows, almost 23% of dissociation events lead to states not accessible through this channel. This implies that a realistic modelling of Nitrogen chemistry in planetary atmospheres should also incorporate the presence of Nitrogen atoms or ions in various excited states, which are likely to have a different reactivity.

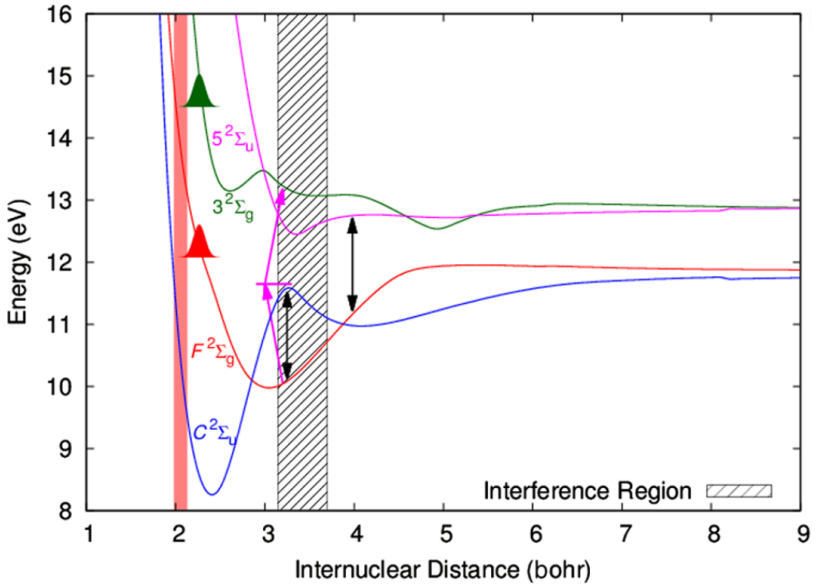

Figure 11.9: PES with schematic depiction of initial populations shortly after ionization. Red transparent areas: Franck-Condon region. Black striped area: region with significant population transfere between the $3^2\Sigma_g$ and $F^2\Sigma_g$ state for time delays where the interference is observed. The magenta single headed arrows depict the two photon process population populating the $3^2\Sigma_g$ state using the $5^2\Sigma_u$ state as a virtual intermediate state. The black double-headed arrow shows points of resonant single photon transitions.

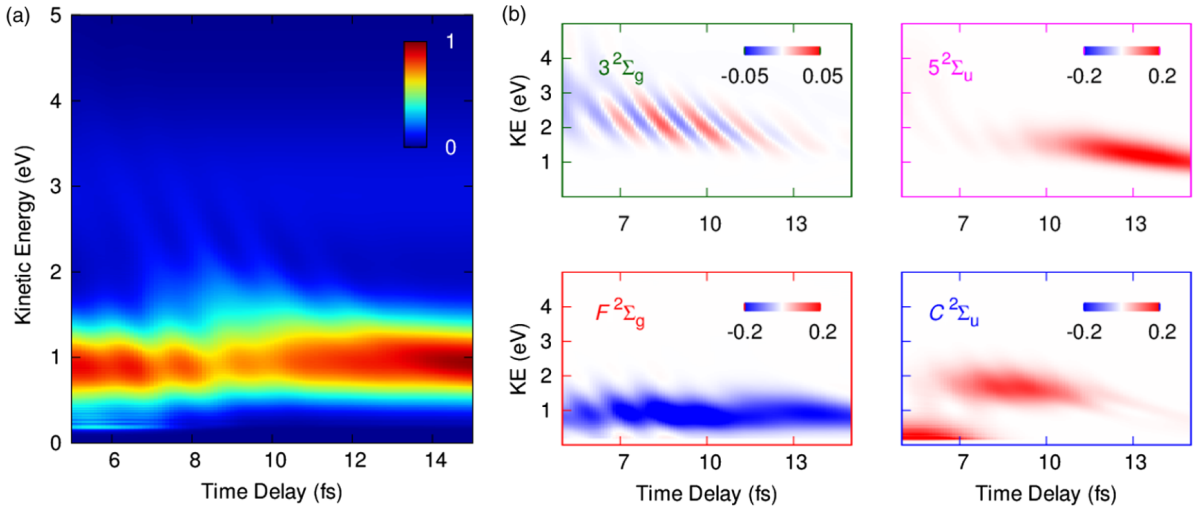

Figure 11.10: Time-dependent N^+ kinetic energy (KE) spectra calculated (a) within the four state model and (b) for each individual state of this model. To clearly show the effect of the probe pulse, the KE spectrum corresponding to a calculation without probe pulse is subtracted from each of the panels reported in (b)

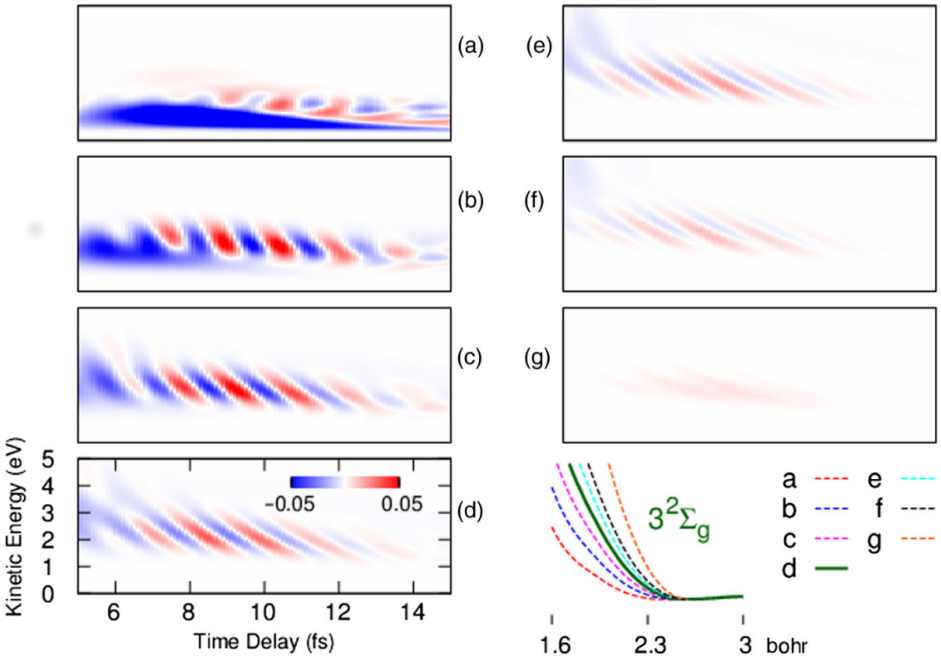

Figure 11.11: (a)-(g) Time dependent N^+ kinetic energy spectra coresponding to the set of gradients of the $3^2\Sigma_g$ state displayed in the bottom right-hand panel (with (d) corresponding to the unaltered $3^2\Sigma_g$ state). As in figure 11.6b, the results of a reference calculation without the probe pulse are subtracted.

12 Conclusions

In this project we have presented the underlying theory, the implementation and application of various computational tools applicable to the study of photoionization of small molecular system. We focussed in particular on the description of diatomic system, and presented results for the Hydrogen molecule as a benchmark system before moving on to provide a more extensive set of results for the study of molecular Nitrogen.

The photoionization calculations were carried out using the newly developed XCHEM code based on a close coupling expansion of the wavefunction and the use of a three tier set of basis functions, comprised of localized Gaussian basis functions centred at the atomic sites of the atoms in the molecule, Gaussian basis functions centred at the centre of mass of the molecule (completely enveloping the localized Gaussian basis functions), and a set of B-Splines starting a radius so that they overlap with the monocentric Gaussian while the opposite is true for the polycentric Gaussians. The monocentric Gaussian basis functions combined with B-Splines have been dubbed GABS basis.

The benchmark calculation carried out in the Hydrogen molecule provided us with the certainty that the XCHEM code works and gives reliable results. The subsequent calculation working with N_2 showed that the XCHEM method does not fail to work for larger systems, but does in fact provide very good agreement with experimental results, and in the given range of photon energies is unequalled in quality compared to existing computational models applied to the same system. That being said the agreement is not perfect for electrons leaving the system at very low kinetic energies leading to some quantitative differences regarding autoionizing states close to an ionization threshold. We have presented a likely sources of this discrepancy and methods are being implemented to remedy this issue.

It is true that other methods can be expected to be capable to yielding similarly convincing results [240, 158, 199] for the case of N_2, but a major advantage of the XCHEM method is that its computational cost can be expected to scale very nicely with increasing complexity of the system. As we mentioned, this is due to the fact, that as long as the XCHEM-QC calculation is carried out ensuring that the neutral and cationic states necessary are fully enveloped by the set of monocentric basis functions, the subsequent scattering calculations including B-Splines is essentially unaware of the complexity contained in the part of the wavefunction that is expressed in terms of polycentric Gaussian functions. For the cases of Nitrogen and particularly Hydrogen this advantage could not yet be put to its full use, where especially for the latter it must be said that the XCHEM method is far too elaborate too yield competitive results in term of computational cost, but also leading to costly calculations for Nitrogen. But as we have gone to length to point out the comfort zone of the XCHEM code is not to provide new tools for the study of the smallest system, but its future application to larger systems.

In addition to the previous results of molecular Nitrogen we have also presented a study on dissociative photoionization which was carried out with the intention of understanding the results obtained in a pump-probe experiment recording the dependence of the kinetic energy spectrum of the fragments as a function of the time delay between the two pulses with sub-femtosecond resolution. Despite the very large number of PES involved we extracted a concise four stated model, allowing for a pleasingly simple interpretation of the results. The ionization step in this case was modelled following a less comprehensive approach than what the XCHEM method is capable of providing, based on Dyson orbitals combined with Coulomb functions. An obvious extension of this work (which is currently being investigated) is therefore to ascertain the accuracy of the results obtained using Dyson orbitals by repeating the calculation of the ionization step using the XCHEM approach.

Future Developments

Having summarized in broad strokes the results of the work presented here we now turn to how this work may be carried on in the future, making use of the XCHEM as the versatile tool that it has proved to be. One direction to take future calculation in, would be, as was repeatedly hinted at, the study of larger systems. Going beyond the diatomic polyelectronic case of Nitrogen, brings into view some very interesting molecules to study, with natural first candidates being water and Benzene, which while still being moderate in size are molecules of tremendous importance. These molecules are expected to further increase the computational cost as the more anisotropic nature of them means larger angular momenta have to be included in the monocentric basis to accurately describe the electron ejected into the continuum; an expectation which preliminary calculations on water seem to confirm. Beyond this however, the computational effort can be expected to plateau for even more complex system, which means that biologically relevant molecules such as the amino acid Glycine can be expected to shift into the focus of XCHEM calculations. We should however mention, that the preliminary work on water indicates that to make these calculations what one might consider routine calculations, it will be inevitable to investigate methods to further speed up the current bottleneck of the calculation, which as was pointed out in chapter 9, is the conversion of two electron basis integrals to orbital integrals.

The other promising avenue that future work is likely to investigate is the extension to the study of time dependent problems. This would allow for instance the fully correlated theoretical investigation of ATAS in much larger systems, than what is currently possible. Once again, preliminary investigations are being done in this direction considering Neon. Neon is a good candidate for a first ATAS investigation in a none trivial system due to its atomic nature. Once we abandon the requirement of systems in time dependent studies being atomic, the set of processes that may be investigate once more grows considerably. Carrying out multiple XCHEM calculations (like the one that was presented in chapter 10), for different nuclear geometries, would allow to go beyond the fixed nuclei approximation. We have speculated in chapter 10, that the break down of the agreement between theory and experiment below the second ionization threshold in Nitrogen, may be due to the extremely long life time of the autoionizing states in this region, giving the nuclei time to move and thus render inaccurate the fixed nuclei approximation. The inclusion of nuclear motion would resolve this problem. A natural step after the inclusion of nuclear motion would be to also include non-adiabatic effects, coupling the electronic and nuclear motion.

Also it is worth noting that the entirety of this work's investigation of the XCHEM code restricted itself to the study of photoionization including the effect of autoionizing states from valence orbitals. However a variety of other ionization processes exist, the study of which future work may wish to endeavour. Of particular interest would be the investigation of Auger decay. That is to say investigating the electron dynamics between the removal of a core electron and the subsequent ejection of an electron. Specifically this would allow the theoretical investigation of hole dynamics, which has attracted the curiosity of experimental works [50]. A first step in this direction was the study of using quantum chemistry to generate the PES of electronic states with a core electron removed [241], which is beyond what QCPs normally offer. Using these results in conjunction with the XCHEM codes to study core hole dynamics, will however still require substantial amounts of work and computer time.

Another process, related to Auger decay, that the XCHEM code may serve to elucidate in the future is inter-coulmbic decay [242, 243]. Inter-coulombic decay is observed in loosely bound systems where upon core ionization, relaxation via ejection of an Auger electron of the individual components is energetically forbidden. The system may then nevertheless relax by ejection of an electron from a neighbouring component. One system, which may be investigated, which exhibits this behaviour are Neon dimers [244]. However due to the large size of systems in which inter-coulombic decay occurs (Neon dimer being one of the smallest systems that exhibits inter-coulombic decay has a bond length of close to 6 a.u.), these calculations can be expected to be very expensive at the current stage, by virtue of requiring huge monocentric basis set to contain the whole system.

With this discussion of possible future applications of the XCHEM code we conclude this work on the development and implementation of theoretical methods for the study of photoionization of molecular Nitrogen. It is our believe that the presented methods provide highly promising tools for the investigation of a wide range of molecules and processes. Taking furthermore into account the rapid advances that

have been made in the field of attochemistry it seems very likely that these methods will not just result in an theoretical exercise treating increasingly complex systems for the sake of it, but will form a valuable tool as the refinement of attosecond technology opens up the possibility to probe even deeper into the electronic processes driving chemical reactions.

Conclusión

En este proyecto hemos presentado la teoría, la implementación y el uso de varias herramientas computacionales aplicables al estudio de foto ionización en sistemas moleculares pequeños. Nos hemos centrado en la descripción de sistemas diatómicos, presentando primero la molécula de Hidrógeno como sistema de referencia, y continuando con la molécula de Nitrógeno, donde se ha conseguido explotar el potencial de la herramienta desarrollado.

Los cálculos de foto ionización se han realizado usando el nuevo método XCHEM basado en una expansión "close coupling" de la función de onda y el uso de un conjunto de funciones de bases de tres tipos: funciones gausianas localizadas en las posiciones de los átomos que constituyen la molécula, funciones gausianas centradas centradas en el centro de masas de la molécula (cubriendo completamente las primeras) y un conjunto de B-splines empezando a partir de una distancia elegida de forma que no exista solapamiento con las gausianas localizadas, solapándose sólo con las gausianas monocéntricas.

El primero cálculo se realizó en la molécula de Hidrógeno, donde es posible comparar con otro tipo de metodologías, para cerciorarnos de la habilidad del código XCHEM para reproducir resultados fiables. Los cálculos posteriores se han realizado en la molécula de Nitrógeno, mostrando la fiabilidad del código XCHEM en sistemas más grandes. Al comparar con otros cálculos teóricos, la implementación mostrada en esta tesis es capaz de dar un mejor acuerdo con los experimentos realizados (en el rango de energías del fotón consideradas en este trabajo). Sin embargo, el acuerdo no es perfecto para energías de fotón cercanas del umbral de ionización, dado que es necesario representar electrones con energía cinética muy baja. Las posibles causas de esta discrepancia se han identificado y se están implementando métodos para corregirla.

Si bien otros métodos probablemente podrían ser capaces de producir resultados similares para el caso de N_2 [240, 158, 199], la ventaja principal del método XCHEM es que su coste computacional crece lentamente con el tamaño de la molécula que se estudia. Esto es debido al hecho de que en el cálculo XCHEM-QC siempre nos aseguramos que los estados catiónicos y neutros no sobresalen a regiones en las que las gausianas localizadas se solaparían con los B-Splines. En tal caso los B-Splines están desacoplados de la parte de la función de onda expresada en gausianas localizadas (mucho más compleja). En los casos de las moléculas de Nitrógeno e Hidrógeno esta ventaja aún no ha sido totalmente explotada. Para empezar, en el caso de Hidrógeno el método XCHEM es demasiado elaborado para que pueda competir computacionalmente con otros métodos creados específicamente para esta molécula. Por supuesto, en el caso de la molécula de Nitrógeno, el método XCHEM es mucho más adecuado, pero aún así los cálculos son demasiado costosos computacionalmente. Finalemnte, como hemos mencionado ya varias veces, el método XCHEM no fue diseñado para este tipo de sistemas, sino para su aplicación pendiente en sistema moleculares de mayor tamaño.

En la parte final, se ha presentado la foto ionización disociativa de la molécula de Nitrógeno, lo que nos ha permitido entender los resultados obtenidos en un experimento bombeo-sonda. En este experimento se midió con resolución temporal por debajo de los femtosegundos la distribución de energía cinética de los fragmentos de la disociación como función del retraso entre los dos pulsos. A pesar del elevado número de potenciales involucrados, se ha conseguidp extraer un modelo de cuatro potenciales que nos permite llegar a una interpretación satisfactoria de lo que se observa experimentalmente. En este estudio,

el paso de ionización se calculó usando un modelo basado en orbitales de Dyson acoplados con ondas culombianas (con un descripción de ionización menos completa que el método XCHEM). Por lo tanto un extensión obvia de este proyecto (que se están llevando al cabo actualmente) es volver a calcular la ionización usando el método XCHEM para determinar la calidad de los resultados obtenidos con orbitales de Dyson.

Desarollos Futuros

Después del resumen sobre los resultados presentados en este trabajo revisaremos como se puede continuar este proyecto, usando el método XCHEM implementado durante esta tesis. Una posibilidad, sería, como mencionamos varias veces, el estudio de sistemas de mayor tamaño. Ir mas allá de las moléculas diátomicas como el Nitrógeno, nos permitiría describir la fotoionización de moléculas como agua o benceno. Estas moléculas, que aún son comparativamente pequeñas, tienen una importancia tremenda en química y biología. Se espera que estas moléculas necesiten más tiempo computacional debido a su estructura más anisotrópica, que implica la necesidad de incluir bases monocéntricas mas grandes para poder tener un descripción adecuada del electrón en el continuo (este aumento computacional se esta manifestando en cálculos preliminares). Para sistemas aún mayores, se espera que el coste computacional escale más lentamente con el tamaño, debido a que la mayoría de las necesidades computacionales residen en las gausianas monocéntricas, prácticamente invariantes. Eso significa que podría ser posible llevar a cabo cálculos para moléculas biológicamente relevantes, como por ejemplo glicina. Sin embagro los cálculos de agua parecen indicar que será imprescindible implementar métodos que aceleren la conversión de integrales de dos electrones de funciones de bases a orbitales, ya que este paso es de momento el que requiere la mayoría de los recursos computacionales.

Además de sistemas de mayor tamaño, es posible extender lo que hemos visto ahora para incluir de manera explicita la dependencia temporal, lo que permitiría estudiar la ionización de manera dínamica. De esta forma, sería posible por ejemplo investigar teóricamente ATAS en sistemas mucho mayores de lo que es actualmente. En este momento, se está investigando la posibilidad de incluír la dependencia temporal en el átomo de Neón. Finalmente, yendo más allá de sistemas atómicos, el abánico de procesos que es posible estudiar crece considerablemente. Sin embargo esto requiere cálcular con XCHEM (como el que presentamos en capítulo 10) las distintas geometrías moleculares, pudiendo ir más allá de la aproximación de núcleos fijos. En el capítulo 10 especulamos que la ausencia de acuerdo entre teoría y experimento para las secciones eficaces entre el primer y segundo umbral de ionización puede ser debida a que el tiempo de vida es muy largo en los estado autoionizantes presentes en ese rango de energía, lo que permite que se muevan los núcleos de manera considerable. La inclusión del movimiento nuclear solucionaría este problema. Además del movimiento nuclear sería también interesante incluir efectos no adiabáticos, acoplando el movimiento nuclear y el movimiento electrónico.

En este proyecto, tal como lo presentamos, XCHEM parece restringido al proceso de auto ionización directamente desde orbitales de valencia. Sin embargo, el código XCHEM podría ser utilizado para investigar otro tipo de procesos de ionización. Por ejemplo, un proceso muy interesante que podría investigar sería la producción de electrones Auger. Eso significaría investigar la dinámica electrónica al ionizar un electrón de un orbital de baja energía dando lugar a un proceso de cascada que termina con la emisión de un electrón Auger. Esto permitiría estudiar la dinámica del agujero que se encuentra después de ionización. Existen varios trabajos experimentales sobre este tema [50], por lo que un estudio teórico complementario podría ser de gran ayuda. El primer paso vendría dado por la descripción de los PES de estados excitados en los que se eliminan electrones de orbitales internos [241]. Usar estos PES junto con el código XCHEM para estudiar la dinámica, a pesar del tiempo computacional y de desarrollo que requiere, podría resultar en una descripción muy completa del proceso de foto ionización, posiblemente incluyendo canales disociativos.

Otro proceso relacionado con electrones Auger, que se podría elucidar con el método XCHEM es intercoulombic decay (ICD) [242, 243]. ICD se observa en sistemas débilmente ligados, en los que la emisión de un electrón Auger en el componente ionizado no es favorable desde un punto de vista energético. Sin embargo, es posible la emisión de un electrón desde el otro fragmento, lo que permite transferir la ionización en el sistema incluso a largas distancias. Un sistema que exhibe este comportamiento son dímeros de Neon [244]. El problema es que la distancia necesaria para que se produzca ICD suele ser

grande (Neon requiere una separación de sus componentes de casi 6 unidades atómicas), con lo cual los cálculos con el código XCHEM serían muy costosos, como consecuencia de la necesidad de usar una base monocéntrica muy grande.

Con esta presentación de las posibles aplicaciones futuras del código XCHEM concluimos este trabajo sobre el desarrollo y la implementación de métodos teóricos para la investigación de foto ionización, fundamentalmente en la molécula de Nitrógeno. Creemos que los métodos presentados han dado lugar a herramientas altamente prometedoras para la investigación de un rango amplio de moléculas y procesos. Además, teniendo en cuenta los últimos avances que hemos visto en el campo de attoquímica es muy probable que estos métodos se puedan utilizar para tratar moléculas cada vez de mayor tamaño, dando lugar a un método valioso dado que la tecnología de attosegundos permite acceder a procesos electrónicos cada vez más fundamentales.

Bibliography

[1] U. Keller, "Recent developments in compact ultrafast lasers," *Nature*, vol. 424, no. 6950, pp. 831–838, 2003.

[2] F. Krausz and M. Ivanov, "Attosecond physics," *Reviews of Modern Physics*, vol. 81, no. March, pp. 163–234, 2009.

[3] M. Nisoli, P. Decleva, F. Calegari, A. Palacios, and F. Martín, "Attosecond Electron Dynamics in Molecules," *Chemical Reviews*, p. A, 2017.

[4] D. J. Tannor, *Introduction to Quantum Mechanics - A Time Dependent Perspective*. University Science Books, 2007.

[5] J. A. Valdmanis and R. L. Fork, "Design Considerations for a Femtosecond Pulse Laser Balancing Self Phase Modulation, Group Velocity Dispersion, Saturable Absorption, and Saturable Gain," *IEEE Journal of Quantum Electronics*, vol. 22, no. 1, pp. 112–118, 1986.

[6] R. L. Fork, C. H. Brito Cruz, P. C. Becker, and C. V. Shank, "Compression of optical pulses to six femtoseconds by using cubic phase compensation," *Optics Letters*, vol. 12, no. 7, p. 483, 1987.

[7] M. Nisoli, S. Stagira, S. De Silvestri, O. Svelto, S. Sartania, Z. Cheng, M. Lenzner, C. Spielmann, and F. Krausz, "A novel-high energy pulse compression system: generation of multigigawatt sub-5-fs pulses," *Applied Physics B: Lasers and Optics*, vol. 65, no. 2, pp. 189–196, 1997.

[8] M. Schnürer, Z. Cheng, S. Sartania, M. Hentschel, G. Tempea, T. Brabec, and F. Krausz, "Rapid communication Guiding and high-harmonic generation of sub-10-fs pulses in," *Applied Physics B*, vol. 67, pp. 263–266, 1998.

[9] M. Nisoli, G. Sansone, S. Stagira, C. Vozzi, S. De Silvestri, O. Svelto, B. Schenkel, J. Biegert, and U. Keller, "3.7 Fs Pulses From Adaptive Pulse Compression of a Cascaded Hollow Fiber Supercontinuum," *Conference on Lasers and Electro-Optics Europe - Technical Digest*, vol. 28, no. 20, p. 437, 2003.

[10] A. H. Zewail, "Femtochemistry: Recent Progress in Studies of Dynamics and Control of Reactions and Their Transition States," *The Journal of Physical Chemistry*, vol. 100, no. 31, pp. 12701–12724, 1996.

[11] A. H. Zewail, "Femtochemistry: Atomic-Scale Dynamics of the Chemical Bond ," *The Journal of Physical Chemistry A*, vol. 104, no. 24, pp. 5660–5694, 2000.

[12] T. Südmeyer, F. Brunner, E. Innerhofer, R. Paschotta, K. Furusawa, J. C. Baggett, T. M. Monro, D. J. Richardson, and U. Keller, "Nonlinear femtosecond pulse compression at high average power levels by use of a large-mode-area holey fiber," *Optics Letters*, vol. 28, no. 20, p. 1951, 2003.

[13] T. Tanaka, "Proposal for a pulse-compression scheme in x-ray free-electron lasers to generate a multiterawatt, attosecond x-ray pulse," *Phys. Rev. Lett.*, vol. 110, p. 084801, Feb 2013.

[14] P. B. Corkum, "Plasma Perspective on Strong-Field Multiphoton Ionization," *Physical Review Letters*, vol. 71, no. 13, pp. 1994–1997, 1993.

[15] M. Lewenstein, P. Balcou, M. Y. Ivanov, A. L'Huillier, and P. B. Corkum, "Theory of high-harmonic generation by low-frequency laser fields," *Physical Review A*, vol. 49, no. 3, pp. 2117–2132, 1994.

[16] K. S. Budil, P. Salieres, A. L'Huillier, T. Dimitri, and M. D. Perry, "Influence of ellipticity on harmoic generation," *Phys Rev A*, vol. 48, no. 5, pp. 3437–3440, 1993.

[17] P. Dietrich, N. H. Burnett, M. Ivanov, and P. B. Corkum, "High-harmonic generation and correlated two-electron multiphoton ionization with elliptically polarized light," *Physical Review A*, vol. 50, no. 5, pp. 3585–3588, 1994.

[18] M. Drescher, "X-ray Pulses Approaching the Attosecond Frontier," *Science*, vol. 291, no. 5510, pp. 1923–1927, 2001.

[19] A. Baltuska and T. Udem, "Attosecond control of electronic," *Nature*, vol. 421, no. February, 2003.

[20] K. Zhao, Q. Zhang, M. Chini, Y. Wu, X. Wang, and Z. Chang, "Tailoring a 67 attosecond pulse through advantageous phase-mismatch," *Optics Letters*, vol. 37, no. 18, p. 3891, 2012.

[21] P. M. Paul, "Observation of a Train of Attosecond Pulses from High Harmonic Generation," *Science*, vol. 292, no. 5522, pp. 1689–1692, 2001.

[22] Y. Mairesse and F. Quéré, "Frequency-resolved optical gating for complete reconstruction of attosecond bursts," *Physical Review A - Atomic, Molecular, and Optical Physics*, vol. 71, no. 1, pp. 1–4, 2005.

[23] R. López-Martens, K. Varjú, P. Johnsson, J. Mauritsson, Y. Mairesse, P. Salières, M. B. Gaarde, K. J. Schafer, A. Persson, S. Svanberg, C. G. Wahlström, and A. L'Huillier, "Amplitude and phase control of attosecond light pulses," *Physical Review Letters*, vol. 94, no. 3, pp. 1–4, 2005.

[24] M. Hentschel, R. Kienberger, C. Spielmann, G. A. Reider, N. Milosevic, T. Brabec, P. Corkum, U. Heinzmann, M. Drescher, and F. Krausz, "Attosecond metrology," *Nature*, vol. 414, no. 6863, pp. 509–513, 2001.

[25] R. Kienberger, E. Goulielmakis, M. Uibracker, A. Baltuska, V. Yakovlev, F. Bammer, A. Scrinzi, T. Westerwalbesloh, U. Kleineberg, U. Heinzmann, M. Drescher, and F. Krausz, "Atomic transient recorder," *Nature*, vol. 427, p. 817, 2004.

[26] F. Krausz and M. Ivanov, "Attosecond physics," *Reviews of Modern Physics*, vol. 81, no. March, pp. 163–234, 2009.

[27] M. Nisoli and G. Sansone, "New frontiers in attosecond science," *Progress in Quantum Electronics*, vol. 33, pp. 17–59, 2009.

[28] G. Sansone, F. Kelkensberg, J. F. Pérez-Torres, F. Morales, M. F. Kling, W. Siu, O. Ghafur, P. Johnsson, M. Swoboda, E. Benedetti, F. Ferrari, F. Lépine, J. L. Sanz-Vicario, S. Zherebtsov, I. Znakovskaya, A. L'Huillier, M. Y. Ivanov, M. Nisoli, F. Martín, and M. J. J. Vrakking, "Electron localization following attosecond molecular photoionization," *Nature*, vol. 465, no. 7299, pp. 763–766, 2010.

[29] F. Lépine, M. Y. Ivanov, and M. J. Vrakking, "Attosecond molecular dynamics: fact or fiction?," *Nature Photonics*, vol. 8, no. 3, pp. 195–204, 2014.

[30] F. Calegari, D. Ayuso, A. Trabattoni, L. Belshaw, S. De Camillis, S. Anumula, F. Frassetto, L. Poletto, A. Palacios, P. Decleva, *et al.*, "Ultrafast electron dynamics in phenylalanine initiated by attosecond pulses," *Science*, vol. 346, no. 6207, pp. 336–339, 2014.

[31] L. Cederbaum and J. Zobeley, "Ultrafast charge migration by electron correlation," *Chemical Physics Letters*, vol. 307, no. July, pp. 205–210, 1999.

[32] J. Breidbach and L. Cederbaum, "Universal attosecond response to the removal of an electron," *Physical review letters*, vol. 94, no. 3, p. 033901, 2005.

[33] S. Chelkowski, G. L. Yudin, and A. D. Bandrauk, "Observing electron motion in molecules," *Journal of Physics B: Atomic, Molecular and Optical Physics*, vol. 39, no. 13, p. S409, 2006.

[34] U. Fano, "Effects of configuration interaction on intensities and phase shifts," *Physical Review*, vol. 124, no. 6, pp. 1866–1878, 1961.

[35] U. Fano and J. W. Cooper, "Line Profiles in the Far-uv Absorption Spectra of the Rare Gases," *Physical Review*, vol. 137, pp. A1364–A1379, mar 1965.

[36] S. Salomonson, S. L. Carter, and H. P. Kelly, "Calculation of helium photoionization with excitation including angular distribution and resonance structure," *Phys Rev A*, vol. 39, no. 10, p. 5111, 1989.

[37] R. Moccia and P. Spizzo, "Helium photoionization between the N=2 and N=3 thresholds including angular distribution and resonance properties: A K-matrix L2 basis-set calculation," *Physical Review A*, vol. 43, no. 5, pp. 2199–2214, 1991.

[38] L. Argenti, C. Ott, T. Pfeifer, and F. Martín, "Attosecond Transient Absorption Spectroscopy of doubly-excited states in helium," *Journal of Physics: Conference Series*, vol. 488, p. 032030, 2014.

[39] K. Schulz, M. Domke, R. Püttner, A. Gutiérrez, G. Kaindl, G. Miecznik, and C. Greene, "High-resolution experimental and theoretical study of singly and doubly excited resonances in ground-state photoionization of neon," *Physical Review A*, vol. 54, no. 4, pp. 3095–3112, 1996.

[40] T. Carette, J. M. Dahlström, L. Argenti, and E. Lindroth, "Multiconfigurational Hartree-Fock close-coupling ansatz: Application to the argon photoionization cross section and delays," *Physical Review A - Atomic, Molecular, and Optical Physics*, vol. 87, no. 2, pp. 1–13, 2013.

[41] I. Sánchez and F. Martn, "Resonant effects in photoionization of H2 and D2," *The Journal of Chemical Physics*, vol. 107, no. 20, pp. 8391–8396, 1997.

[42] F. Martín, "Ionization and dissociation using B-splines: photoionization of the hydrogen molecule," *Journal of Physics B: Atomic, Molecular and Optical Physics*, vol. 32, pp. R197–R231, 1999.

[43] J. D. Bozek, J. E. Furst, T. J. Gay, H. Gould, A. L. D. Kilcoyne, J. R. Machacek, F. Martín, K. W. McLaughlin, and J. L. Sanz-Vicario, "Production of excited atomic hydrogen and deuterium from H2 and D2 photodissociation," *Journal of Physics B: Atomic, Molecular and Optical Physics*, vol. 39, no. 23, pp. 4871–4882, 2006.

[44] S. Gozem, A. O. Gunina, T. Ichino, D. L. Osborn, J. F. Stanton, and A. I. Krylov, "Photoelectron Wave Function in Photoionization: Plane Wave or Coulomb Wave?," *Journal of Physical Chemistry Letters*, vol. 6, no. 22, pp. 4532–4540, 2015.

[45] M. Spanner and S. Patchkovskii, "One-electron ionization of multielectron systems in strong non-resonant laser fields," *Physical Review A - Atomic, Molecular, and Optical Physics*, vol. 80, no. December, pp. 1–11, 2009.

[46] E. Plésiat, P. Decleva, and F. Martín, "Vibrational branching ratios in the photoelectron spectra of N_2 and CO: interference and diffraction effects," *Physical Chemistry Chemical Physics*, vol. 14, p. 10853, 2012.

[47] V. Gruson, L. Barreau, Á. Jiménez-Galan, F. Risoud, J. Caillat, A. Maquet, B. Carré, F. Lepetit, J.-F. Hergott, T. Ruchon, L. Argenti, R. Taïeb, F. Martín, and P. Salières, "Attosecond dynamics through a Fano resonance: Monitoring the birth of a photoelectron," *Science*, vol. 354, no. 6313, pp. 734–738, 2016.

[48] A. Kaldun, S. Donsa, H. Wei, R. Pazourek, S. Nagele, C. Ott, C. D. Lin, and T. Pfeifer, "Observing the ultrafast buildup of a Fano resonance in the time domain," *Science*, vol. 166, no. 2014, pp. 162–166, 2016.

[49] E. Goulielmakis, Z.-H. Loh, A. Wirth, R. Santra, N. Rohringer, V. S. Yakovlev, S. Zherebtsov, T. Pfeifer, A. M. Azzeer, M. F. Kling, S. R. Leone, and F. Krausz, "Real-time observation of valence electron motion," *Nature*, vol. 466, no. 7307, pp. 739–743, 2010.

[50] M. S. Schoffler, J. Titze, N. Petridis, T. Jahnke, K. Cole, L. P. H. Schmidt, A. Czasch, D. Akoury, O. Jagutzki, J. B. Williams, N. A. Cherepkov, S. K. Semenov, C. W. McCurdy, T. N. Rescigno, C. L. Cocke, T. Osipov, S. Lee, M. H. Prior, A. Belkacem, A. L. Landers, H. Schmidt-Bocking, T. Weber, and R. Dorner, "Ultrafast Probing of Core Hole Localization in N_2," *Science*, vol. 320, no. 5878, pp. 920–923, 2008.

[51] C. Marante, L. Argenti, and F. Martín, "Hybrid Gaussian B -spline basis for the electronic continuum: Photoionization of atomic hydrogen," *Physical Review A*, vol. 90, p. 012506, jul 2014.

[52] C. Marante, M. Klinker, I. Corral, J. González-Vázquez, L. Argenti, and F. Martín, "Hybrid-Basis Close-Coupling Interface to Quantum Chemistry Packages for the Treatment of Ionization Problems," *Journal of Chemical Theory and Computation*, vol. 13, no. 2, pp. 499–514, 2017.

[53] C. Marante, M. Klinker, T. Kjellsson, and E. Lindroth, "Photoionization of Ne using the XCHEM approach : total and partial cross sections and resonance parameters above the $2s^2\ 2p^5$ threshold," *submitted*, pp. 1–13, 2017.

[54] F. Kelkensberg, C. Lefebvre, W. Siu, O. Ghafur, T. T. Nguyen-Dang, O. Atabek, A. Keller, V. Serov, P. Johnsson, M. Swoboda, T. Remetter, A. L'Huillier, S. Zherebtsov, G. Sansone, E. Benedetti, F. Ferrari, M. Nisoli, F. Lépine, M. F. Kling, and M. J. J. Vrakking, "Molecular dissociative ionization and wave-packet dynamics studied using two-color XUV and IR pump-probe spectroscopy," *Physical Review Letters*, vol. 103, no. 12, pp. 16–19, 2009.

[55] F. Martín, J. Fernández, T. Havermeier, L. Foucar, T. Weber, K. Kreidi, M. S. Schöffler, L. Schmidt, T. Jahnke, O. Jagutzki, a. Czasch, E. P. Benis, T. Osipov, a. L. Landers, a. Belkacem, M. H. Prior, H. Schmidt-Böcking, C. L. Cocke, and R. Dörner, "Single photon-induced symmetry breaking of H_2 dissociation," *Science*, vol. 315, no. 5812, pp. 629–33, 2007.

[56] A. S. Sandhu, E. Gagnon, R. Santra, V. Sharma, W. Li, P. Ho, P. Ranitovic, C. L. Cocke, M. M. Murnane, and H. C. Kapteyn, "Observing the creation of electronic feshbach resonances in soft x-ray-induced o_2 dissociation," *Science*, vol. 322, no. 5904, pp. 1081–1085, 2008.

[57] I. Znakovskaya, P. von den Hoff, S. Zherebtsov, A. Wirth, O. Herrwerth, M. J. J. Vrakking, R. de Vivie-Riedle, and M. F. Kling, "Attosecond control of electron dynamics in carbon monoxide," *Phys. Rev. Lett.*, vol. 103, p. 103002, Sep 2009.

[58] M. Lucchini, K. Kim, F. Calegari, F. Kelkensberg, W. Siu, G. Sansone, M. J. J. Vrakking, M. Hochlaf, and M. Nisoli, "Autoionization and ultrafast relaxation dynamics of highly excited states in N_2," *Physical Review A*, vol. 86, p. 043404, oct 2012.

[59] A. Trabattoni, M. Klinker, J. González-Vázquez, C. Liu, G. Sansone, R. Linguerri, M. Hochlaf, J. Klei, M. Vrakking, F. Martín, M. Nisoli, and F. Calegari, "Mapping the Dissociative Ionization Dynamics of Molecular Nitrogen with Attosecond Time Resolution," *Physical Review X*, vol. 5, p. 041053, dec 2015.

[60] S. Horvath, R. M. Pitzer, and A. B. McCoy, "Theoretical investigations of the time-resolved photodissociation dynamics of IBr-," *Journal of Physical Chemistry A*, vol. 114, pp. 11337–11346, 2010.

[61] J. Davenport, "Ultraviolet Photoionization Cross Sections for N_2 and CO," *Physical Review Letters*, vol. 36, no. 16, pp. 945–949, 1976.

[62] L. Veseth, "Many-body calculation of total and partial photoabsorption cross sections in N_2," *J. Phys. B: At. Mol. Opt. Phys.*, vol. 27, pp. 481–496, 1994.

[63] R. E. Stratmann, G. Bandarage, and R. R. Lucchese, "Electron-correlation effects in the photoionization of N_2," *Physical Review A*, vol. 51, no. 5, pp. 3756–3765, 1995.

[64] M. Tashiro, "Application of the R-matrix method to photoionization of molecules," *Journal of Chemical Physics*, vol. 132, no. 13, pp. 0–10, 2010.

[65] M. Ogawa and Y. Tankaka, "Rydberg Absorption Series of N_2," *Canadian Journal of Chemistry*, vol. 40, p. 1593, 1962.

[66] P. Gurtler, V. Saile, and E. E. Koch, "High Resolution Absorption Spectrum of Nitrogen," *Chemical Physics Letters*, vol. 48, no. 2, p. 245, 1977.

[67] P. R. Woodruff and G. V. Marr, "The Photoelectron Spectrum of N_2, and Partial Cross Sections as a Function of Photon Energy from 16 to 40 eV," *Proceedings of the Royal Society A*, vol. 358, no. 1692, pp. 87–103, 1977.

[68] M. P. Dehmer, P. J. Miller, and W. A. Chupka, "Photoionization of N_2 X 1Σ+g, v"=0 and 1 near threshold. Preionization of the Worley-Jenkins series," *The Journal of Chemical Physics*, vol. 80, p. 1030, 1984.

[69] K. P. Huber, G. Stark, and K. Ito, "Rotational structure in the Hopfield series of N_2," *J. Chem. Phys.*, vol. 98, no. 6, pp. 4471–4477, 1993.

[70] M. Reduzzi, W. C. Chu, C. Feng, A. Dubrouil, J. Hummert, and F. Calegari, "Observation of autoionization dynamics and sub-cycle quantum beating in electronic molecular wave packets," *Journal of Physics B: Atomic, Molecular and Optical Physics*, vol. 49, no. 6, p. 0, 2016.

[71] T. Helgaker, P. Jorgensen, and J. Olsen, *Molecular Electronic-Structure Theory*. John Wiley and Sons Ltd, 2002.

[72] A. Szabo and N. Ostlund, *Modern Quantum Chemistry*. Dover Publications, Incorporated, 1989.

[73] W. H. Press, *Numerical Recepies*. Cambridge University Press, 1986.

[74] J. Olsen, P. Jørgensen, and J. Simons, "Passing the one-billion limit in full configuration-interaction (FCI) calculations," *Chemical Physics Letters*, vol. 169, no. 6, pp. 463–472, 1990.

[75] E. R. Davidson, "The iterative calculation of a few of the lowest eigenvalues and corresponding eigenvectors of large real-symmetric matrices," *Journal of Computational Physics*, vol. 17, no. 1, pp. 87–94, 1975.

[76] C. F. Bender and E. R. Davidson, "A Natural Orbital Based Energy Calculation for Helium Hydride and Lithium Hydride," *Journal of Physical Chemistry A*, vol. 70, no. 8, pp. 2675–2685, 1966.

[77] K. H. Thunemann, J. Romelt, S. D. Peyerimhoff, and R. J. Buenker, "A study of the convergence in iterative natural orbital procedures," *International Journal of Quantum Chemistry*, vol. 11, no. 5, pp. 743–752, 1977.

[78] P. A. Malmqvist, "Calculation of transition density matrices by nonunitary orbital transformations," *International Journal of Quantum Chemistry*, vol. 30, no. 4, pp. 479–494, 1986.

[79] K. Ruedenberg, L. M. Cheung, and S. T. Elbert, "MCSCF optimization through combined use of natural orbitals and the Brillouin-Levy-Berthier theorem," *International Journal of Quantum Chemistry*, vol. 16, no. 5, pp. 1069–1101, 1979.

[80] B. O. Roos, "The complete active space SCF method in a fock matrix based super CI formulation," *International Journal of Quantum Chemistry*, vol. 18, no. 14 S, pp. 175–189, 1980.

[81] J. Olsen, B. O. Roos, P. Jorgensen, and H. J. A. Jensen, "Determinant based configuration interaction algorithms for complete and restricted configuration interaction spaces," *The Journal of Chemical Physics*, vol. 89, no. 4, p. 2185, 1988.

[82] H. Jogen, A. Jensen, P. Jorgensen, and T. Helgaker, "a Multiconfigurational Linear Response Study," *Chemical Physics Letters*, vol. 162, no. 43, pp. 355–360, 1989.

[83] P. A. Malmqvist, A. Rendell, and B. O. Roos, "The restricted active space self-consistent-field method, implemented with a split graph unitary group approach," *The Journal of Physical Chemistry*, vol. 94, no. 14, pp. 5477–5482, 1990.

[84] D. Ma, G. Li Manni, and L. Gagliardi, "The generalized active space concept in multiconfigurational self-consistent field methods," *Journal of Chemical Physics*, vol. 135, no. 4, 2011.

[85] U. Schollwock, "The density-matrix renormalization group," *Reviews of Modern Physics*, vol. 77, no. 1, pp. 259–315, 2005.

[86] J. Hachmann, J. J. Dorando, M. Avilés, and G. K.-L. Chan, "The radical character of the acenes: a density matrix renormalization group study.," *J. Chem. Phys.*, vol. 127, no. 13, p. 134309, 2007.

[87] D. A. Mazziotti, "Quantum Chemistry without Wave Functions: Two-Electron Reduced Density Matrices," *Acc. Chem. Res.*, vol. 39, no. 3, pp. 207–215, 2006.

[88] R. Shepard, M. Minkoff, and S. R. Brozell, "Nonlinear Wave Function Expansions: A Progress Report," *Int. J. Quant. Chem.*, vol. 107, p. 3203, 2007.

[89] R. Fletcher, *Practical Methods of Optimization*. Wiley, 1987.

[90] C. W. Bauschlicher and D. R. Yarkony, "On the electronic structure of the 2 1A1 state of methylene," *The Journal of Chemical Physics*, vol. 69, no. 8, pp. 3875–3877, 1978.

[91] Y. Yamaguchi, C. D. Sherrill, and H. F. Schaefer, "The $\tilde{X}^3B_1$, $\tilde{a}^1A_1$, $\tilde{b}^1B_1$ and $\tilde{c}^1A_1$ Electronic States of CH_2," *The Journal of Physical Chemistry*, vol. 100, no. 19, pp. 7911–7918, 1996.

[92] K. P. Lawley, *Advances in Chemical Physics*. John Wiley and Sons, 1987.

[93] H.-J. Werner, "A quadratically convergent MCSCF method for the simultaneous optimization of several states," *The Journal of Chemical Physics*, vol. 74, no. 10, p. 5794, 1981.

[94] R. Pauncz, *Spin Eigenfunctions - Constructions and Use*. Springer, 1979.

[95] I. Shavitt, "Graph theoretical concepts for the unitary group approach to the many-electron correlation problem," *International Journal of Quantum Chemistry*, vol. 12, no. S11, pp. 131–148, 1977.

[96] I. Shavitt, "Matrix element evaluation in the unitary group approach to the electron correlation problem," *International Journal of Quantum Chemistry*, vol. 14, no. S12, pp. 5–32, 1978.

[97] L. Laaksonen, P. Pyykko, and D. Sundholm, "Fully numerical hartree-fock methods for molecules," *Computer Physics Reports*, vol. 4, no. 5, pp. 313–344, 1986.

[98] T. Shiozaki and S. Hirata, "Grid-based numerical Hartree-Fock solutions of polyatomic molecules," *Physical Review A - Atomic, Molecular, and Optical Physics*, vol. 76, no. 4, pp. 1–4, 2007.

[99] J. R. Higgins, *Completeness and Basis Properties of Sets of Special Functions*. Cambridge Tracts in Mathematics, Cambridge University Press, 1977.

[100] J. C. Slater, "Atomic shielding constants," *Physical Review*, vol. 36, no. 1, pp. 57–64, 1930.

[101] E. Clementi, C. C. J. Roothaan, and M. Yoshimine, "Accurate analytical self-consistent field functions for atoms. II. Lowest configurations of the neutral first row atoms," *Physical Review*, vol. 127, no. 5, pp. 1618–1620, 1962.

[102] B. Klahn and W. A. Bingel, "The convergence of the Rayleigh-Ritz Method in quantum chemistry - II. Investigation of the convergence for special systems of Slater, Gauss and two-electron functions," *Theoretica Chimica Acta*, vol. 44, no. 1, pp. 27–43, 1977.

[103] D. Feller, "The role of databases in support of computational chemistry calculations," *Journal of Computational Chemistry*, vol. 17, no. 13, pp. 1571–1586, 1996.

[104] K. L. Schuchardt, B. T. Didier, T. Elsethagen, L. Sun, V. Gurumoorthi, J. Chase, J. Li, and T. L. Windus, "Basis set exchange: A community database for computational sciences," *Journal of Chemical Information and Modeling*, vol. 47, no. 3, pp. 1045–1052, 2007.

[105] W. J. Hehre, R. F. Stewart, and J. A. Pople, "Self Consistent Molecular Orbital Methods . I. Use of Gaussian Expansions of Slater Type Atomic Orbitals," *Journal of Chemical Physics*, vol. 51, p. 2657, 1969.

[106] W. J. Hehre, R. Ditchfield, R. F. Stewart, and J. A. Pople, "Self Consistent Molecular Orbital Methods. IV. Use of Gaussian Expansions of Slater Type Orbitals. Extension to Second Row Molecules," *The Journal of Chemical Physics*, vol. 52, no. 5, pp. 2769–2773, 1970.

[107] W. J. Pietro and W. J. Hehre, "Molecular orbital theory of the properties of inorganic and organometallic compounds 5. Extended basis sets for firstrow transition metals," *Journal of Computational Chemistry*, vol. 8, no. 6, pp. 861–879, 1987.

[108] R. McWeeny, "X-ray scattering by aggregates of bonded atoms. III. The bond scattering factor: simple methods of approximation in the general case," *Acta Crystallographica*, vol. 6, no. 7, pp. 631–637, 1953.

[109] S. Huzinaga, "Gaussian-Type Functions for Polyatomic Systems. I," *The Journal of Chemical Physics*, vol. 42, no. 4, p. 1293, 1965.

[110] A. Meckler, "Electronic Energy Levels of Molecular Oxygen," *The Journal of Chemical Physics*, vol. 21, no. 10, p. 1750, 1953.

[111] M. Tinkham and M. Strandberg, "Theory of the Fine Structure of the Molecular Oxygen Ground State," *Physical Review*, vol. 97, no. 4, pp. 937–951, 1955.

[112] I. Shavitt, "The History and Evolution of Gaussian Basis Sets," *Israel Journal of Chemistry*, vol. 33, no. 4, pp. 357–367, 1993.

[113] C. M. Reeves, "Use of Gaussian Functions in the Calculation of Wavefunctions for Small Molecules. I. Preliminary Investigations," *The Journal of Chemical Physics*, vol. 39, no. 1, pp. 1–10, 1963.

[114] T. H. Dunning, "Gaussian basis functions for use in molecular calculations. Contraction of (12s9p) atomic basis sets for the second row atoms," *Chemical Physics Letters*, vol. 7, no. 4, pp. 423–427, 1970.

[115] R. Ditchfield, "Self-Consistent Molecular-Orbital Methods. IX. An Extended Gaussian-Type Basis for Molecular-Orbital Studies of Organic Molecules," *The Journal of Chemical Physics*, vol. 54, no. 2, p. 724, 1971.

[116] W. J. Hehre, R. Ditchfield, and J. A. Pople, "Self Consistent Molecular Orbital Methods. XII. Further Extensions of Gaussian Type Basis Sets for Use in Molecular Orbital Studies of Organic Molecules," *The Journal of Chemical Physics*, vol. 56, no. 5, pp. 2257–2261, 1972.

[117] A. Canal Neto, E. P. Muniz, R. Centoducatte, and F. E. Jorge, "Gaussian basis sets for correlated wave functions. Hydrogen, helium, first- and second-row atoms," *Journal of Molecular Structure: THEOCHEM*, vol. 718, no. 1-3, pp. 219–224, 2005.

[118] P. C. Hariharan and J. A. Pople, "The influence of polarization functions on molecular orbital hydrogenation energies," *Theoretica Chimica Acta*, vol. 28, no. 3, pp. 213–222, 1973.

[119] J. Almlof and P. R. Taylor, "General contraction of Gaussian basis sets. I. Atomic natural orbitals for first- and second-row atoms," *The Journal of Chemical Physics*, vol. 86, no. 7, p. 4070, 1987.

[120] J. Almlöf and P. R. Taylor, "Atomic Natural Orbital (ANO) Basis Sets for Quantum Chemical Calculations," *Advances in Quantum Chemistry*, vol. 22, no. C, pp. 301–373, 1991.

[121] T. H. Dunning Jr, "Gaussian basis sets for use in correlated molecular calculations. I. The atoms boron through neon and hydrogen," *J. Chem. Phys.*, vol. 90, no. 1989, p. 1007, 1989.

[122] J. Dunning, K. A. Peterson, and A. K. Wilson, "Gaussian basis sets for use in correlated molecular calculations. X. The atoms aluminum through argon revisited," *Journal of Chemical Physics*, vol. 114, no. 21, pp. 9244–9253, 2001.

[123] M. Dupuis, J. Rys, H. F. King, M. Dupuis, J. Rys, and H. F. King, "Evaluation of molecular integrals over Gaussian basis functions Evaluation of molecular integrals over Gaussian basis functions," *J Chem Phys*, vol. 65, p. 111, 1976.

[124] H. Friedrich, *Scattering Theory*. Springer, 2013.

[125] M. Abramowitz, *Handbook of Mathematical Functions, With Formulas, Graphs, and Mathematical Tables*. Dover Publications, Incorporated, 1974.

[126] L. S. Rodberg and R. M. Thaler, *The Qunatum Theory of Scattering*. Academic Press, Incorporated, 1970.

[127] G. Breit, E. U. Condon, and R. D. Present, "Scattering of Protons by Protons," *Physical Review*, vol. 50, pp. 825–845, 1936.

[128] A. F. Starace, *Fundamental Processes in Energetic Atomic Collisions*. Springer, 1982.

[129] I. G. Kaplan, B. Barbiellini, and A. Bansil, "Compton scattering beyond the impulse approximation," *Physical Review B*, vol. 68, p. 235104, 2003.

[130] C. M. Oana and A. I. Krylov, "Dyson orbitals for ionization from the ground and electronically excited states within equation-of-motion coupled-cluster formalism: Theory, implementation, and examples," *Journal of Chemical Physics*, vol. 127, no. 2007, 2007.

[131] E. P. Wigner, "Resonance Reactions and Anomalous Scattering," *Physical Review*, vol. 70, p. 15, 1946.

[132] H. Friedrich and D. Wintgen, "Interfering resonances and bound states in the continuum," *Physical Review A*, vol. 32, no. 6, pp. 3231–3242, 1985.

[133] A. U. Hazi, "Behavior of the eigenphase sum near a resonance," *Physical Review A*, vol. 19, no. 2, pp. 920–922, 1979.

[134] A. F. Starace, "Behaviour of Partial Cross Sections and Branching Ratios in the nNighborhood of a Resonance," *Phys Rev A*, vol. 16, p. 231, 1977.

[135] I. Sánchez and F. Martín, " Photoionization of He-like systems below the n=2 threshol," *Journal of Physics B*, vol. 4263, no. 23, pp. 4263–4274, 1990.

[136] I. Sánchez and F. Martín, "Photoionization of He above the n=2 threshold," *Physical Review A*, vol. 44, no. 11, pp. 7318–7334, 1991.

[137] I. Sanchez and F. Martín, "Photoionization of He above the N=2 threshold. II. Angular distribution of photoelectrons and asymmetry parameter," *Physical Review A*, vol. 45, no. 7, pp. 4468–4475, 1992.

[138] I. Sánchez and F. Martín, "Extensive L2 calculation of partial photoionization cross sections of He in the 4lnl resonance region," *Physical Review A*, vol. 48, no. 2, 1993.

[139] M. Cortés and F. Martín, "Photodetachment of H- with excitation to H(N=2)," *Physical Review A*, vol. 48, no. 2, p. 1227, 1993.

[140] I. Bray, D. A. Konovalov, and I. E. McCarthy, "Convergence of an L2 approach in the coupled-channel optical-potential method for e-H scattering," *Phys Rev A*, vol. 43, no. 3, pp. 1301–1305, 1991.

[141] a. T. Stelbovics, "discretisation of the Coulomb problem in an orthonormal Laguerre function basis," *Journal of Physics B: Atomic, Molecular and Optical Physics*, vol. 22, pp. L159–L163, 1999.

[142] A. Macias, F. Martin, A. Riera, and M. Yanez, "Simple discretization method for autoionization widths. III. Molecules," *Physical Review A*, vol. 36, no. 9, p. 4179, 1987.

[143] K. Kaufmann, W. Baumeister, and M. Jungen, "Universal Gaussian basis sets for an optimum representation of Rydberg and continuum wavefunctions," *Journal of Physics B: Atomic, Molecular and Optical Physics*, vol. 22, no. 14, pp. 2223–2240, 1989.

[144] I. Cacelli, "Performance of polynomial Gaussian functions in describing the molecular electronic continuum," *Journal of Physics B: Atomic, Molecular and Optical Physics*, vol. 30, no. 24, pp. 5643–5655, 1997.

[145] I. Cacelli, R. Moccia, and A. Rizzo, "Gaussian Type Orbitals basis sets for the calculation of continuum properties in molecules: The differential photoionization cross section of acetylene," *Chemical Physics*, vol. 252, no. 1-2, pp. 67–81, 2000.

[146] B. W. Shore, "Solving the radial Schroedinger equation by using cubic-spline basis functions," *J Chem Phys*, vol. 58, no. 9, pp. 3855–3866, 1973.

[147] C. F. Fischer and M. Idrees, "Spline algorithms for continuum functions," *Computers in Physics*, vol. 3, no. 3, pp. 53–58, 1989.

[148] C. F. Fischer and M. Idrees, "Spline methods for resonances in photoionizations cross sections," *J. Phys. B*, vol. 23, p. 679, 1990.

[149] C. F. Fischer and W. Guo, "Spline algorithms for the hartree-fock equation for the helium ground state," *Journal of Computational Physics*, vol. 90, no. 2, pp. 486–496, 1990.

[150] C. F. Fischer, W. Guo, and Z. Shen, "Spline methods for multiconfiguration Hartree Fock calculations," *International Journal of Quantum Chemistry*, vol. 42, no. 4, pp. 849–867, 1992.

[151] T. Brage, C. F. Fischer, and G. Miecznikt, "Positions and widths , and photodetachment and photo- ionization cross sections for H- and He," *J. Phys. B*, vol. 25, pp. 5289–5314, 1992.

[152] T. N. Chang and X. Tang, "Photoionization of two-electron atoms using a nonvariational configuration-interaction approach with discretized finite basis," *Physical Review A*, vol. 44, no. 1, pp. 232–238, 1991.

[153] N. Chang, "Photoionization from $1sns\ ^{1,3}S^e$ states of Helium," *Phys Rev A*, vol. 47, no. 6, p. 4849, 1993.

[154] N. Chang and F. Fischer, "He photoionization to the doubly excited (2pnd) and (sp,2n-)1P0 series," *Phys Rev A*, vol. 47, no. 4, pp. 3441–3443, 1993.

[155] N. Chang, "Widths of the doubly excited resoncances of two-electron atoms below the n=2 threshold," *Phys Rev A*, vol. 47, no. 1, pp. 1–4, 1993.

[156] H. Bachau and F. Martin, "Electric-field effects on the photodetachment of H^- below the N = 3 threshold.," *J. Phys. B*, vol. 29, p. 1451, 1996.

[157] H. Bachau and S. Stout, "The hydrogen atom in an external DC electric field : the discretization approach," *J. Phys. B*, vol. 32, p. 1169, 1999.

[158] D. Toffoli and P. Decleva, "A Multichannel Least-Squares B-Spline Approach to Molecular Photoionization: Theory, Implementation, and Applications within the Configuration-Interaction Singles Approximation," *Journal of Chemical Theory and Computation*, vol. 12, no. 10, pp. 4996–5008, 2016.

[159] C. de Boor, *A Practical Guide to Splines*. Springer, 1978.

[160] H. Bachau, E. Cormier, P. Decleva, J. E. Hansen, and F. Martín, "Applications of B -splines in atomic and molecular physics," *Reports on Progress in Physics*, vol. 64, no. 12, p. 1815, 2001.

[161] M. Ruberti, V. Averbukh, and P. Decleva, "B-spline algebraic diagrammatic construction: Application to photoionization cross-sections and high-order harmonic generation," *Journal of Chemical Physics*, vol. 141, no. 16, 2014.

[162] C. C. Marston and G. G. BalintKurti, "The Fourier grid Hamiltonian method for bound state eigenvalues and eigenfunctions," *The Journal of Chemical Physics*, vol. 91, no. 6, pp. 3571–3576, 1989.

[163] R. Kosloff and D. Kosloff, "A Fourier method solution for the time dependent Schrödinger equation: A study of the reaction $H+H_2^+$, $D+HD^+$ and $D+H_2^+$," *The Journal of Chemical Physics*, vol. 79, no. 4, pp. 1823–1833, 1983.

[164] R. Kosloff, "Time-dependent quantum-mechanical methods for molecular dynamics," *The Journal of Physical Chemistry*, vol. 92, no. 8, pp. 2087–2100, 1988.

[165] D. T. Colbert and W. H. Miller, "A novel discrete variable representation for quantum mechanical reactive scattering via the Sâmatrix Kohn method," *Journal of Chemical Physics*, vol. 96, no. 3, pp. 1982–1991, 1992.

[166] C. Leforestier, R. H. Bisseling, C. Cerjan, M. D. Feit, R. Friesner, a. Guldberg, a. Hammerich, G. Jolicard, W. Karrlein, H.-D. Meyer, N. Lipkin, O. Roncero, and R. Kosloff, "A comparison of different propagation schemes for the time dependent Schrödinger equation," *Journal of Computational Physics*, vol. 94, pp. 59–80, 1991.

[167] J. H. Shirley, "Solution of the schrödinger equation with a hamiltonian periodic in time," *Phys. Rev.*, vol. 138, pp. B979–B987, May 1965.

[168] U. Peskin and N. Moiseyev, "The solution of the time-dependent Schrodinger equation by the (t,t') method: Theory, computational algorithm and applications," *The Journal of Chemical Physics*, vol. 99, p. 4590, 1993.

[169] S. I. Chu and D. a. Telnov, "Beyond the Floquet theorem: Generalized Floquet formalisms and quasienergy methods for atomic and molecular multiphoton processes in intense laser fields," *Physics Reports*, vol. 390, no. 2004, pp. 1–131, 2004.

[170] V. Roudnev and B. D. Esry, "General theory of carrier-envelope phase effects," *Physical Review Letters*, vol. 99, no. November, pp. 1–4, 2007.

[171] K. Hanasaki and K. Takatsuka, "Unified treatment of field-induced and intrinsic nonadiabatic transitions with a generalized Floquet Hamiltonian method," *Physical Review A - Atomic, Molecular, and Optical Physics*, vol. 88, pp. 1–14, 2013.

[172] H. Koppel, W. Domcke, and L. Cederbaum, "Multimode Molecular-Dynamics Beyond The Born-Oppenheimer Approximation," *Adv. Chem. Phys.*, vol. 57, pp. 59–246, 1984.

[173] T. Pacher, L. S. Cederbaum, and H. Kppel, *Adiabatic and Quasidiabatic States in a Gauge Theoretical Framework*, vol. 84. John Wiley and Sons, 1993.

[174] M. Baer, *Beyond Born-Oppenheimer - Conical Intersections and Electronic Nonadiabatic Coupling Terms*. Wiley and Sons, 2006.

[175] W. Domcke, D. R. Yarkony, and H. Koppel, *Conical Intersection*. World Scientific Publishing, 2004.

[176] W. H. Press, *Numerical Recipes - The Art of Scientific Programming*. Cambridge University Press, 2007.

[177] C. A. Mead and D. G. Truhlar, "Conditions for the definition of a strictly diabatic electronic basis for molecular systems," *J. Chem. Phys.*, vol. 77, no. 12, pp. 6090–6098, 1982.

[178] R. Abrol and A. Kuppermann, "An optimal adiabatic-to-diabatic transformation of the 12A and 22A states of H3," *The Journal of Chemical Physics*, vol. 116, no. 3, pp. 1035–1062, 2002.

[179] J. B. Delos and W. R. Thorson, "Diabatic and adiabatic representations for atomic collision processes," *The Journal of Chemical Physics*, vol. 70, no. 4, pp. 1774–1790, 1979.

[180] A. Boutalib and F. X. Gadéa, "Ab initio adiabatic and diabatic potentialenergy curves of the LiH molecule," *The Journal of Chemical Physics*, vol. 97, no. 2, pp. 1144–1156, 1992.

[181] S. Matsika and D. R. Yarkony, "Spin-orbit coupling and conical intersections. IV. A perturbative determination of the electronic energies, derivative couplings, and a rigorous diabatic representation near a conical intersection. The general case," *Journal of Physical Chemistry B*, vol. 106, no. 33, pp. 8108–8116, 2002.

[182] M. Desouter-Lecomte, D. Dehareng, and J. C. Lorquet, "Constructing approximately diabatic states from LCAO-SCF-CI calculations," *The Journal of Chemical Physics*, vol. 86, no. 3, p. 1429, 1987.

[183] C. Galloy and J. C. Lorquet, "Nonadiabatic interaction in unimolecular decay. III. Selection and propensity rules for polyatomic molecules," *The Journal of Chemical Physics*, vol. 67, no. 1977, pp. 4672–4680, 1977.

[184] T. L. Redmon, "Perturbative determination of nonadiabatic coupling matrix elements," *Phys Rev A*, vol. 25, no. 5, p. 2453, 1982.

[185] D. R. Yarkony, "Conical Intersections: Diabolical and Often Misunderstood," *Accounts of Chemical Research*, vol. 31, no. 8, pp. 511–518, 1998.

[186] C. Mead, "The geometric phase in molecular systems," *Reviews of Modern Physics*, vol. 64, p. 51, 1992.

[187] R. S. Mulliken, "Molecular compounds and their spectra. ii," *Journal of the American Chemical Society*, vol. 74, no. 3, pp. 811–824, 1952.

[188] N. Hush, "Intervalence-transfer absorption. part 2. theoretical considerations and spectroscopic data," *Prog. Inorg. Chem*, vol. 8, no. 391, p. 12, 1967.

[189] H. J. Werner and W. Meyer, "MCSCF study of the avoided curve crossing of the two lowest $^1\Sigma^+$ states of LiF," *The Journal of Chemical Physics*, vol. 74, no. 10, pp. 5802–5807, 1981.

[190] E. S. Kryachko and D. R. Yarkony, "Diabatic Bases and Molecular Properties," *International Journal of Quantum Chemistry*, vol. 76, no. November 1998, p. 235, 2000.

[191] T. Pacher, L. S. Cederbaum, and H. Koppel, "Approximately diabatic states from block diagonalization of the electronic Hamiltonian," *The Journal of Chemical Physics*, vol. 89, no. 12, pp. 7367–7381, 1988.

[192] T. Pacher, H. Koppel, and L. S. Cederbaum, "Ab initio study of the twophoton boundbound electronic transitions of trans butadiene," *The Journal of Chemical Physics*, vol. 95, p. 6668, 1991.

[193] W. Domcke and C. Woywod, "Direct construction of diabatic states in the CASSCF approach. Application to the conical intersection of the 1A2 and 1B1 excited states of ozone," *Chemical Physics Letters*, vol. 216, no. 3-6, pp. 362–368, 1993.

[194] W. Domcke, C. Woywod, and M. Stengle, "Diabatic CASSCF orbitals and wavefunctions," *Chemical Physics Letters*, vol. 226, no. 3-4, pp. 257–262, 1994.

[195] K. Ruedenberg and G. J. Atchity, "A quantum chemical determination of diabatic states," *The Journal of Chemical Physics*, vol. 99, pp. 3799–3803, 1993.

[196] G. J. Atchity and K. Ruedenberg, "Determination of diabatic states through enforcement of configurational uniformity," *Theoretical Chemistry Accounts: Theory, Computation, and Modeling (Theoretica Chimica Acta)*, vol. 97, pp. 47–58, 1997.

[197] A. Troisi and G. Orlandi, "Construction of electronic diabatic states within a molecular orbital scheme," *Journal of Chemical Physics*, vol. 118, no. 12, pp. 5356–5363, 2003.

[198] A. Macias, F. Martin, A. Riera, and M. Yanez, "A practical solution to the unknown normalization problem," *International Journal of Quantum Chemistry*, vol. 33, no. 4, pp. 279–300, 1988.

[199] M. Zdeněk and D. G. Jimena, "Towards an accurate representation of the continuum in calculations of electron, positron and laser field interactions with molecules," *Journal of Physics: Conference Series*, vol. 490, no. 1, p. 12090, 2014.

[200] P. G. Burke and K. T. Taylor, "R-matrix theory of photoionization. Application to neon and argon," *Journal of Physics B: Atomic and Molecular Physics*, vol. 8, p. 2620, 1976.

[201] P. Lambropoulos, P. Maragakis, and J. Zhang, "Two-electron atoms in strong fields," *Physics Reports*, vol. 305, no. 5, pp. 203–293, 1998.

[202] L. a. a. Nikolopoulos and P. Lambropoulos, "Multichannel theory of two-photon single and double ionization of helium," *Journal of Physics B: Atomic, Molecular and Optical Physics*, vol. 34, no. 01, pp. 545–564, 2001.

[203] L. A. A. Nikolopoulos, "Electromagnetic transitions between states satisfying free-boundary conditions," *Physical Review A - Atomic, Molecular, and Optical Physics*, vol. 73, no. 4, pp. 1–10, 2006.

[204] I. Sánchez and F. Martín, "The doubly excited states of the H_2 molecule," *The Journal of Chemical Physics*, vol. 106, no. 18, pp. 7720–7730, 1997.

[205] I. Sánchez and F. Martín, "Representation of the electronic continuum of H2 with B -spline basis," *Journal of Physics B: Atomic, Molecular and Optical Physics*, vol. 30, pp. 679–692, 1997.

[206] O. A. Fojón, J. Fernández, A. Palacios, R. D. Rivarola, and F. Martín, "Interference effects in H2 photoionization at high energies," *Journal of Physics B: Atomic, Molecular and Optical Physics*, vol. 37, no. 15, pp. 3035–3042, 2004.

[207] I. Sánchez and F. Martín, "Dissociative photoionization of H_2 and D_2 by (3037)-eV photons via $^1\Pi_u$ states," *Physical Review A*, vol. 60, no. 3, pp. 2200–2206, 1999.

[208] J. J. Hopfield, "Absorption and Emission Spectra in the Region λ 600-1100," *Phys. Rev.*, vol. 35, no. 9, pp. 1133–1134, 1930.

[209] J. J. Hopfield, "Absorption and Emission Spectra in the Region λ 600-1100," *Phys. Rev.*, vol. 36, p. 789, 1930.

[210] A. C. Parr, D. L. Ederer, and B. E. Cole, "Tiply-Differential Photoelectron Studies of Molecular Autoionizations Profiles," *PRL*, vol. 46, p. 22, 1981.

[211] R. S. Mulliken, "Hopfield's Rydberg series and the ionization potential and heat of dissociation of N_2," *Physical Review*, vol. 46, no. 2, pp. 144–146, 1934.

[212] H. C. Tuckwell, "Calculation of the photoionization cross section of N_2 from first threshold at 500 AA," *Journal of Physics B: Atomic and Molecular Physics*, vol. 3, pp. 293–305, 1970.

[213] M. Raoult, H. Le Rouzo, G. Raseev, and L. H. Brion, "Ab initio approach to the multichannel quantum defect calculation of the electronic autoionisation in the Hopfield series of N_2," *Journal of Physics B: Atomic and Molecular Physics*, vol. 16, no. 24, p. 4601, 1983.

[214] C. Jungen, "Rydberg Series in the NO Spectrum: An Interpretation of Quantum Defects and Intensities in the s and d Series," *The Journal of Chemical Physics*, vol. 53, no. 11, p. 4168, 1970.

[215] R. R. Lucchese and R. W. Zurales, "Comparison of the random-phase approximation with the multichannel frozen-core Hartree-Fock approximation for the photoionization of N_2," *Physical Review A*, vol. 44, no. 1, pp. 291–303, 1991.

[216] S. Semenov, N. Cherepkov, G. Fecher, and G. Schönhense, "Generalization of the atomic random-phase-approximation method for diatomic molecules: N_2 photoionization cross-section calculations," *Physical Review A*, vol. 61, no. 3, p. 032704, 2000.

[217] M. Eckstein, C.-H. Yang, F. Frassetto, L. Poletto, G. Sansone, M. J. Vrakking, and O. Kornilov, "Direct Imaging of Transient Fano Resonances in N_2 Using Time-, Energy-, and Angular-Resolved Photoelectron Spectroscopy," *Physical Review Letters*, vol. 116, no. 16, p. 163003, 2016.

[218] M. Eckstein, N. Mayer, C.-H. Yang, G. Sansone, M. J. J. Vrakking, M. Ivanov, and O. Kornilov, "Interference stabilization of autoionizing states in molecular N_2 studied by time- and angular-resolved photoelectron spectroscopy," *arXiv*, vol. 1605.02632, p. 8, 2016.

[219] W. B. Peatman, B. Gotchev, P. Guertler, V. Seile, and E. E. Koch, "Transition probabilities at threshold for the photoionization of molecular nitrogen," *Jcp*, vol. 69, no. 1978, pp. 2089–2095, 1978.

[220] P. Morin, A. M.Y., I. Nenner, J. Delwiche, M. J. Hubin-franskin, and P. Lablanquie, "Measurements of Partial and Differential Photoionization Cross Sections of Helium and Diatomic Molecules," *Nuclear Instruments and Methods*, vol. 208, pp. 761–766, 1983.

[221] L. Journel, B. Rouvellou, D. Cubaynes, J. Bizau, F. Wuilleumier, M. Richter, P. Sladeczek, K.-H. Selbmann, P. Zimmermann, and H. Bergeron, "First observation of a Fano profile following one step autoionization into a double photoionization continuum," *Journal De Physique. IV : JP*, vol. 3, no. 6, 1993.

[222] T. C. Owen, "On the origin of titans atmosphere," *Planetary and Space Science*, vol. 48, no. 7, pp. 747 – 752, 2000.

[223] N. Teanby, P. Irwin, R. de Kok, C. Nixon, A. Coustenis, B. Bzard, S. Calcutt, N. Bowles, F. Flasar, L. Fletcher, C. Howett, and F. Taylor, "Latitudinal variations of HCN, HC_3N, and C_2N_2 in Titan's stratosphere derived from Cassini CIRS data," *Icarus*, vol. 181, no. 1, pp. 243 – 255, 2006.

[224] V. A. Krasnopolsky, "A photochemical model of titan's atmosphere and ionosphere," *Icarus*, vol. 201, no. 1, pp. 226 – 256, 2009.

[225] Z. Peng, T. Gautier, N. Carrasco, P. Pernot, A. Giuliani, A. Mahjoub, J.-J. Correia, A. Buch, Y. Bnilan, C. Szopa, and G. Cernogora, "Titan's atmosphere simulation experiment using continuum uv-vuv synchrotron radiation," *Journal of Geophysical Research: Planets*, vol. 118, no. 4, pp. 778–788, 2013.

[226] R. R. Meier, "Ultraviolet Spectroscopy and Remote Sensing of the Upper Atmosphere," *Space Science Reviews*, vol. 58, pp. 1–185, 1991.

[227] F. Lücking, A. Trabattoni, S. Anumula, G. Sansone, F. Calegari, M. Nisoli, T. Oksenhendler, and G. Tempea, "In situ measurement of nonlinear carrier-envelope phase changes in hollow fiber compression," *Opt. Lett.*, vol. 39, pp. 2302–2305, Apr 2014.

[228] I. Sola, E. Mével, L. Elouga, E. Constant, V. Strelkov, L. Poletto, P. Villoresi, E. Benedetti, J.-P. Caumes, S. Stagira, *et al.*, "Controlling attosecond electron dynamics by phase-stabilized polarization gating," *Nature Physics*, vol. 2, no. 5, pp. 319–322, 2006.

[229] Y. Mairesse and F. Quéré, "Frequency-resolved optical gating for complete reconstruction of attosecond bursts," *Phys. Rev. A*, vol. 71, p. 011401, Jan 2005.

[230] L. Poletto, S. Bonora, M. Pascolini, and P. Villoresi, "Instrumentation for analysis and utilization of extreme-ultraviolet and soft x-ray high-order harmonics," *Review of scientific instruments*, vol. 75, no. 11, pp. 4413–4418, 2004.

[231] O. Ghafur, W. Siu, P. Johnsson, M. F. Kling, M. Drescher, and M. Vrakking, "A velocity map imaging detector with an integrated gas injection system," *Review of Scientific Instruments*, vol. 80, no. 3, p. 033110, 2009.

[232] M. Feit, J. Fleck, and A. Steiger, "Solution of the schrdinger equation by a spectral method," *Journal of Computational Physics*, vol. 47, no. 3, pp. 412 – 433, 1982.

[233] M. Feit and J. Fleck Jr, "Wave packet dynamics and chaos in the hénon–heiles system," *The Journal of chemical physics*, vol. 80, no. 6, pp. 2578–2584, 1984.

[234] M. Feit and J. Fleck Jr, "Solution of the schrödinger equation by a spectral method ii: Vibrational energy levels of triatomic molecules," *The Journal of Chemical Physics*, vol. 78, no. 1, pp. 301–308, 1983.

[235] R. Kosloff, "Propagation methods for quantum molecular dynamics," *Annual review of physical chemistry*, vol. 45, no. 1, pp. 145–178, 1994.

[236] D. E. Manolopoulos, "Derivation and reflection properties of a transmission-free absorbing potential," *Journal of Chemical Physics*, vol. 117, no. 21, pp. 9552–9559, 2002.

[237] T. Aoto, K. Ito, Y. Hikosaka, A. Shibasaki, R. Hirayama, N. Yamamono, and E. Miyoshi, "Inner-valence states of n_2^+ and the dissociation dynamics studied by threshold photoelectron spectroscopy and configuration interaction calculation," *The Journal of chemical physics*, vol. 124, no. 23, p. 234306, 2006.

[238] J. Itatani, F. Quéré, G. L. Yudin, M. Y. Ivanov, F. Krausz, and P. B. Corkum, "Attosecond streak camera," *Phys. Rev. Lett.*, vol. 88, p. 173903, Apr 2002.

[239] M. Eckstein, C.-H. Yang, M. Kubin, F. Frassetto, L. Poletto, H.-H. Ritze, M. J. Vrakking, and O. Kornilov, "Dynamics of n_2 dissociation upon inner-valence ionization by wavelength-selected xuv pulses," *The journal of physical chemistry letters*, vol. 6, no. 3, pp. 419–425, 2015.

[240] V. P. Majety, A. Zielinski, and A. Scrinzi, "Photoionization of few electron systems: a hybrid coupled channels approach," *New Journal of Physics*, vol. 17, no. 6, p. 063002, 2015.

[241] I. Corral, J. Gonzalez-Vazquez, and F. Martin, "Potential energy surfaces of core-hole and shake-up states for dissociative ionization studies," *Journal of Chemical Theory and Computation*, vol. 13, no. 4, pp. 1723–1736, 2017.

[242] L. S. Cederbaum, J. Zobeley, and F. Tarantelli, "Giant intermolecular decay and fragmentation of clusters," *Phys. Rev. Lett.*, vol. 79, pp. 4778–4781, Dec 1997.

[243] T. Jahnke, "Interatomic and intermolecular coulombic decay: the coming of age story," *Journal of Physics B: Atomic, Molecular and Optical Physics*, vol. 48, no. 8, p. 082001, 2015.

[244] S. Scheit, V. Averbukh, H.-D. Meyer, N. Moiseyev, R. Santra, T. Sommerfeld, J. Zobeley, and L. Cederbaum, "On the interatomic coulombic decay in the ne dimer," *The Journal of chemical physics*, vol. 121, no. 17, pp. 8393–8398, 2004.